

12/27/95 (881)

DOE/METC-95/1018, Vol. 2  
(DE95009733)  
**CONF-9506162--Vol. 2**

---

# Proceedings of the Advanced Coal-Fired Power Systems '95 Review Meeting Volume II

---

Heather M. McDaniel  
Darren J. Mollot  
Venkat K. Venkataraman

June 1995



U.S. Department of Energy  
Office of Fossil Energy  
Morgantown Energy Technology Center  
Morgantown, West Virginia

DISTRIBUTION OF THIS DOCUMENT IS UNLIMITED

## **Disclaimer**

This report was prepared as an account of work sponsored by an agency of the United States Government. Neither the United States Government nor any agency thereof, nor any of their employees, makes any warranty, express or implied, or assumes any legal liability or responsibility for the accuracy, completeness, or usefulness of any information, apparatus, product, or process disclosed, or represents that its use would not infringe privately owned rights. Reference herein to any specific commercial product, process, or service by trade name, trademark, manufacturer, or otherwise does not necessarily constitute or imply its endorsement, recommendation, or favoring by the United States Government or any agency thereof. The views and opinions of authors expressed herein do not necessarily state or reflect those of the United States Government or any agency thereof.

This report has been reproduced directly from the best available copy.

Available to DOE and DOE contractors from the Office of Scientific and Technical Information, 175 Oak Ridge Turnpike, Oak Ridge, TN 37831; prices available at (615) 576-8401.

Available to the public from the National Technical Information Service, U.S. Department of Commerce, 5285 Port Royal Road, Springfield, VA 22161; phone orders accepted at (703) 487-4650.

# **Proceedings of the Advanced Coal-Fired Power Systems '95 Review Meeting Volume II**

## **Editors**

Heather M. McDaniel  
Darren J. Mollot  
Venkat K. Venkataraman

## **Sponsored by**

U.S. Department of Energy  
Office of Fossil Energy  
Morgantown Energy Technology Center  
P.O. Box 880  
Morgantown, WV 26507-0880  
(304) 285-4764  
(304) 285-4403/4469

June 27-29, 1995

MASTER

DISTRIBUTION OF THIS DOCUMENT IS UNLIMITED

*Dr*

1. The first part of the paper is a review of the literature on the effects of the 1997 Asian financial crisis on the Asian economies. It discusses the impact of the crisis on the real economy, the financial system, and the labor market. It also discusses the policy responses of the Asian governments and the international community.

2.



# Contents

## Volume I

---

### Session 1 — Perspectives on the Future of Power Generation Industry

1.1	And Deregulation Shall Lead Me to Lie Down in Green Pastures — Gary Weidinger .....	3
1.2	World Market: A Survey of Opportunities for Advanced Coal-Fired Systems — Neville A.H. Holt .....	4
1.3	METC Clean Coal Technology Status -- 1995 Update — Larry K. Carpenter .....	19

### Session 2 — Advanced Power Systems

2.1	Power Systems Development Facility Progress Report — Randall E. Rush, Howard L. Hendrix, Darrell L. Moore, Timothy E. Pinkston, P. Vimalchand, and John M. Wheeldon .....	23
2.2	Pilot Plant Becomes Demonstration Plant Design — Archie Robertson, James Van Hook, Frank Burkhard, Giovanni Carli, Rich Conn, Paul Crooker, Dave Kulcsar, Chongqing Lu, Anthony Mack, Aydemir Nehrozoglu, Mark Torpey, and Frank Zoldak .....	32
2.3	Gasification Product Improvement Facility Status — R. Don Carson, Vijay B. Dixit, Richard S. Sadowski, P. Thamaraichelvan, and H. Culberson .....	47
2.4	Externally Fired Combined Cycle Demonstration — Nelson J. Orozco, Stephen Young, Paul G. LaHaye, John Strom-Olsen, John L. Seger, and Helen Pickup .....	55
2.5	Advanced Gas Turbine Systems Program — Charles M. Zeh .....	65

## **Poster Session A — METC CRADA Opportunities**

<b>PA.1</b>	Dynamic Analysis of Process Reactors — Lawrence J. Shadle, Larry O. Lawson, and Stephen D. Noel .....	69
<b>PA.2</b>	CRADA Opportunities With METC's Gasification and Hot Gas Cleanup Facility — Edwin N. Galloway, John M. Rockey, and Mark S. Tucker .....	70
<b>PA.4</b>	CRADA Opportunities in Pressurized Combustion Research — Daniel J. Maloney, Thomas S. Norton, and Kent H. Casleton .....	71
<b>PA.5</b>	Pressure-Gain Combustion for Gas Turbines — Randall S. Gemmen, George A. Richards, and Michael C. Janus .....	79
<b>PA.6</b>	Hot-Gas Filter Testing With the Transport Reactor Demonstration Unit — Michael D. Mann, Michael L. Swanson, Robert O. Ness, and Jay S. Haley .....	87
<b>PA.7</b>	High-Temperature Gas Stream Cleanup Test Facility — John S. Ontko and Ta-Kuan Chiang .....	98
<b>PA.8</b>	Cooperative Research and Development Agreements at METC — J. Christopher Ludlow, Lisa A. Jarr, and Rodney J. Anderson .....	104
<b>PA.9</b>	High Pressure Optical Combustion Probe — Steven D. Woodruff and George A. Richards .....	105
<b>PA.10</b>	METC CFD Simulations of Hot Gas Filtration — Thomas J. O'Brien .....	107
<b>PA.11</b>	CRADA Opportunities in the Removal of Particulates From Hot-Gas Streams by Filtration — Duane H. Smith .....	108
<b>PA.12</b>	Dynamic Modeling of Power Systems — Michael E. Reed and Jay S. White .....	109

## **Session 3 — Hot Gas Particle Control**

<b>3.1</b>	Westinghouse Advanced Particle Filter System — Thomas E. Lippert, Gerald J. Bruck, Zal N. Sanjana, and Richard A. Newby .....	123
<b>3.2</b>	Lightweight Ceramic Filter Components: Evaluation and Application — Paul M. Eggerstedt .....	140

<b>3.3</b>	Status of Granular Bed Filter Development Program — Keith B. Wilson, John C. Haas, and Jeff Prudhomme .....	150
<b>3.4</b>	Pulsed Combustion and Hot Gas Cleanup Island — Ravi R. Chandran, Momtaz N. Mansour, S. Yavuzkurt, Gary H. Koopmann, and John L. Loth .....	158
<b>3.5</b>	Filter Component Assessment — Mary Anne Alvin, Thomas E. Lippert, Edward S. Diaz, and Eugene E. Smeltzer .....	160
<b>3.6</b>	Application of CFCC Technology to Hot Gas Filtration Applications — Scott Richlen .....	183

#### **Session 4 — Hot Gas Desulfurization**

<b>4.1</b>	Integrated Operation of a Pressurized Fixed Bed Gasifier, Hot Gas Desulfurization System and Turbine Simulator — Steve Bevan, David Najewicz, Raul E. Ayala, Alan Feitelberg, and Anthony Furman .....	187
<b>4.2</b>	Pilot Scale Experience on IGCC Hot Gas Cleanup — Reza Ghazanfari, Gabor Feher, Jukka Kontinen, Arto Lehtovaara, and Wahab Mojtahedi .....	202
<b>4.3</b>	Zinc Titanate Tests in Transport Reactor — Santosh K. Gangwal, William M. Campbell, Raghubir P. Gupta, and Gunnar B. Henningsen .....	215
<b>4.4</b>	Slipstream Testing of Hot-Gas Desulfurization With Sulfur Recovery — Santosh K. Gangwal and Jeffrey W. Portzer .....	220
<b>4.5</b>	Bench-Scale Testing of Fluidized-Bed Sorbents — ZT-4 — Santosh K. Gangwal and Raghubir P. Gupta .....	229
<b>4.6</b>	Pilot Plant Tests of Z-Sorb™ Sorbent — G.J. Greenwood, G.P. Khare, D.H. Kubicek, G.A. Delzer, and D.L. Kinsinger .....	241

#### **Session 5 — Fuel Gas Combustion**

<b>5.1</b>	Fuel Gas Combustion Research at METC — Thomas S. Norton .....	249
<b>5.2</b>	Performance of Low Btu Fuel Gas Turbine Combustors — Stephen Bevan, John H. Bowen, Alan S. Feitelberg, Stephen L. Hung, Michael A. Lacey, and Kenneth S. Manning .....	250

<b>5.3</b>	Development of a Topping Combustor for Advanced Concept Pressurized Fluidized-Bed Combustion Systems — William F. Domeracki, Thomas E. Dowdy, and Dennis Bachovchin .....	263
<b>5.4</b>	Development and Demonstration of a Solid Fuel-Fired Gas Turbine System — James G. Speight and Vijay K. Sethi .....	275

## **Poster Session B — Filters and Sorbents**

<b>PB.1</b>	Assessment of Ceramic Membrane Filters — Rajesh K. Ahluwalia, Howard K. Geyer, Kwan H. Im, Chao Zhu, David Shelleman, and Richard E. Tressler .....	279
<b>PB.2</b>	Carbon Formation and Metal Dusting in Hot-Gas Cleanup Systems of Coal Gasifiers — Roddie R. Judkins, Peter F. Tortorelli, Jackson H. DeVan, and Ian G. Wright .....	292
<b>PB.3</b>	Development of a Monolithic Ceramic Cross Flow Filter — David A. Larsen .....	302
<b>PB.4</b>	Properties of Ceramic Candle Filters — Duane H. Pontius and H. Stuart Starret .....	318
<b>PB.5</b>	Nitride-Bonded Silicon Carbide Composite Filter — Bruce N. Thomson and Stephen G. DiPietro .....	320
<b>PB.6</b>	3-D Woven, Mullite Matrix, Composite Filter — Jay E. Lane, Carol J. Painter, Kenneth C. Radford, and Jean-Francois LeCostaouec .....	329
<b>PB.7</b>	Hot Particulate Removal and Desulfurization Results From the METC Integrated Gasification and Hot Gas Cleanup Facility — John M. Rockey .....	340
<b>PB.8</b>	Simultaneous Hot Desulfurization and Improved Filtration in Coal Utilization Processes — Paul M. Eggerstedt .....	342
<b>PB.9a</b>	Liming Efficacy and Transport in Soil of a Dry PFBC By-Product — Warren A. Dick .....	356
<b>PB.9b</b>	Characterization and Laboratory Weathering Studies — Joel H. Beeghly, Warren A. Dick, R.K. Fowler, U.I. Soto, and J.M. Bigham .....	358

<b>PB.10</b>	Disposal of Fluidized-Bed Combustion Ash in an Underground Mine to Control Acid Mine Drainage and Subsidence — Paul F. Ziemkiewicz, D. Courtney Black, William J. Head, Donald D. Gray, Hema J. Siriwardane, and William A. Sack .....	360
<b>PB.11</b>	Use of FBC Ash to Stabilize Dairy Barn Feedlots, Minimize Nutrient Pollution, and Develop New Utilization Outlets — Ronald F. Korcak and William L. Stout .....	362
<b>PB.12</b>	Hot Coal Gas Desulfurization With Manganese-Based Sorbents — Malcolm T. Hepworth and Rachid Ben-Slimane .....	367
<b>PB.13</b>	High-Temperature H <sub>2</sub> S Removal Using Limestones — Elton J. Cairns and Scott Lynn .....	382
<b>PB.14</b>	A Long Life ZnO - TiO <sub>2</sub> Sorbent — Michael E. Karpuk, Robert J. Copeland, Mike Cesario, Margarita Dubovik, Dan Feinberg, and Brian Windecker .....	394
<b>PB.15</b>	Development of Advanced Hot-Gas Desulfurization Sorbents — K. Jothimurugesan, Adeyinka A. Adeyiga, and Santosh K. Gangwal .....	402
<b>PB.16</b>	Advanced Low-Temperature Sorbents — Raúl E. Ayala, Venkat S. Venkataramani, Javad Abbasian, and Andy H. Hill .....	407
<b>PB.17</b>	Spectral Methods Applied to Fluidized Bed Combustors — Robert C. Brown, Thomas S. Raines, and Theodore D. Thiede .....	417
<b>PB.18</b>	Fossil Fuel Conversion – Measurement and Modeling — Peter R. Solomon, L. Douglas Smoot, Michael A. Serio, B. Scott Brewster, David G. Hamblen, and Predrag T. Radulovic .....	425
<b>PB.19</b>	Development of Methods to Predict Agglomeration and Deposition in FBCs — Michael D. Mann, Ann K. Henderson, Michael L. Swanson, and Thomas A. Erickson .....	440
<b>PB.20</b>	Evaluation of Options for CO <sub>2</sub> Capture/Utilization/Disposal — David K. Schmalzer and Richard D. Doctor .....	448
<b>PB.21</b>	Hot-Gas Filter Ash Characterization — John P. Hurley, Tina M. Strobel, and Bruce A. Dockter .....	449

## Volume II

---

### Session 6A — Hot Gas Filter Issues

<b>6A.1</b>	Development and Testing of PRD-66 Hot Gas Filters — Jeffrey A. Chambers .....	467
<b>6A.2</b>	Filter Systems for IGCC Applications — Stephen Bevan, Robert Gieger, Nelson Sobel, and Dale Johnson .....	472
<b>6A.3</b>	Thermal and Chemical Stability of Ceramic Candle Filters — Mary Anne Alvin, Thomas E. Lippert, Edward S. Diaz, and Eugene E. Smeltzer .....	485
<b>6A.4</b>	Novel Oxide-Oxide Fiber Reinforced Hot Gas Filter Development — Richard A. Wagner .....	510
<b>6A.5</b>	Filter Cake Characterization Studies — Richard A. Newby, Eugene E. Smeltzer, Mary Anne Alvin, and Thomas E. Lippert .....	517
<b>6A.6</b>	Hot Gas Filtration Technical Issues — Duane H. Pontius .....	531

### Session 6B — Hazardous Air Pollutants (HAPS)

<b>6B.2</b>	Comparison of HAPs From Advanced and Conventional Power Systems: Tidd Versus Cardinal — Steven A. Benson, Thomas A. Erickson, and David W. Brekke .....	549
<b>6B.3</b>	Trace Metal Transformations in Gasification — Steven A. Benson, Thomas A. Erickson , Christopher J. Zygarlicke, Cathy A. O'Keefe, Karen A. Katrinak, Sean E. Allan, David J. Hassett, and William B. Hauserman .....	559
<b>6B.4</b>	Hazardous Air Pollutant Testing at the LGTI Coal Gasification Plant — Robert G. Wetherold, W. Al Williams, David P. Maxwell, and Robert M. Mann .....	573
<b>6B.5</b>	Development of Mercury and Chloride Monitors for Coal Gasifiers — William H. Buttermore, Glenn A. Norton, Colin D. Chriswell, Dave E. Eckels, and Rachel E. Peters .....	574

<b>6B.6</b>	On-Line Elemental Analysis of Fossil Fuel Process Streams by Inductively Coupled Plasma Spectrometry — William P. Chisholm .....	587
-------------	--	-----

## **Session 7A — Sorbent Development and Processes**

<b>7A.1</b>	Moving-Bed Sorbents — Raúl E. Ayala, Timothy Chuck, and Raghubir P. Gupta .....	591
<b>7A.2</b>	Spray-Dried Fluid-Bed Sorbent Tests – CMP-5 — Santosh K. Gangwal and Raghubir P. Gupta .....	601
<b>7A.3</b>	Desulfurization Sorbent Development Activities at METC — Ranjani V. Siriwardane .....	609
<b>7A.4</b>	Advanced Sulfur Control Concepts — Douglas P. Harrison, Alejandro Lopez-Ortiz, Julie D. White, and Frank R. Groves .....	610
<b>7A.5</b>	Advanced Sulfur Control Concepts — Santosh K. Gangwal, Brian S. Turk, and Raghubir P. Gupta .....	622
<b>7A.6</b>	Development of Disposable Sorbents for Chloride Removal From High-Temperature Coal-Derived Gases — Gopala N. Krishnan, B.J. Wood, A. Canizales, R. Gupta, S.D. Shelukar, and R. Ayala .....	631

## **Session 7B — Separation Technologies**

<b>7B.1</b>	Advanced Metal-Membrane Technology - Commercialization — David J. Edlund .....	645
<b>7B.2</b>	Separation of Hydrogen Using Thin Film Palladium-Ceramic Composite Membrane — Shamsuddin Ilias, Franklin G. King, Nan Su, and Uduak I. Udo-Aka .....	646
<b>7B.3</b>	A Calcium Oxide Sorbent Process for Bulk Separation of Carbon Dioxide — Douglas P. Harrison, Chun Han, and George Lee .....	655
<b>7B.4</b>	Thermal/Chemical Degradation of Inorganic Membrane Materials — Gopala N. Krishnan, Ashok S. Damle, Angel Sanjurjo, Bernard J. Wood, Kai-Hung Lau .....	667
<b>7B.5</b>	Electrochemical Polishing of Hydrogen Sulfide From Coal Synthesis Gas — E. Faith Gleason and Jack Winnick .....	678

## Appendices

Agenda .....	709
Meeting Participants .....	721
Author Index .....	747
Organization Index .....	750



---

## Session 6A

### *Hot Gas Filter Issues*

---



## 6A.1 Development and Testing of PRD-66 Hot Gas Filters

### Contract Information

Contract Number DE-AC21-94MC31214

Contractor DuPont Lanxide Composites Inc.  
1300 Marrows Road PO Box 6077  
Newark, DE 19714-6077  
(302) 456-6235 (telephone)  
(302) 456-6480 (FAX)

### Other Funding Sources

Contract Project Manager Jeffrey A. Chambers, Ph.D.

Principal Investigator Jeffrey A. Chambers, Ph.D.

METC Project Manager Theodore J. McMahon

Period of Performance September 29, 1994 to November 30, 1995

### Schedule and Milestones

#### FY 95 Program Schedule

---

	O	N	D	J	F	M	A	M	J	J	A	S
NEPA Info												
Test Plan												
Development, Qualification, & Testing												

---

### Objectives

The overall objective of this program is to develop and commercialize PRD-66 hot gas filters for application in pressurized fluidized bed combustors (PFBC) and Integrated Gas Combined Cycle (IGCC) power generation systems. The work is being carried out in phases with the following specific objectives:

1. Demonstrate acceptable mechanical, chemical, and filtration properties in exposure tests.
2. Produce and qualify selected prototype design filter elements in high temperature high pressure (HTHP) simulated PFBC exposure tests.
3. (Option) Generate a manufacturing plan to support commercial scale-up.

4. (Option) Recommend process equipment upgrades and produce 50 candle filters.

### Background Information

For several years prior to the initiation of this project, DuPont, DuPont Lanxide Composites Inc. (DLC) and Westinghouse Electric Corporation cooperated in the fabrication and early testing of hot gas candle filters based on the PRD-66 technology. The result of that collaboration was what will be referred to hereafter as the 'baseline' PRD-66 candle filter.

PRD-66 ceramic oxides are materials with a unique combination of high continuous use temperature and high thermal shock resistance in a

non-fiber reinforced material (Figure 1). To be sure, there are monolithic ceramics with higher continuous use temperature, but they tend to have poor thermal shock resistance. Certainly there are metals with better thermal shock resistance, but these metals tend to melt and/or oxidize at high

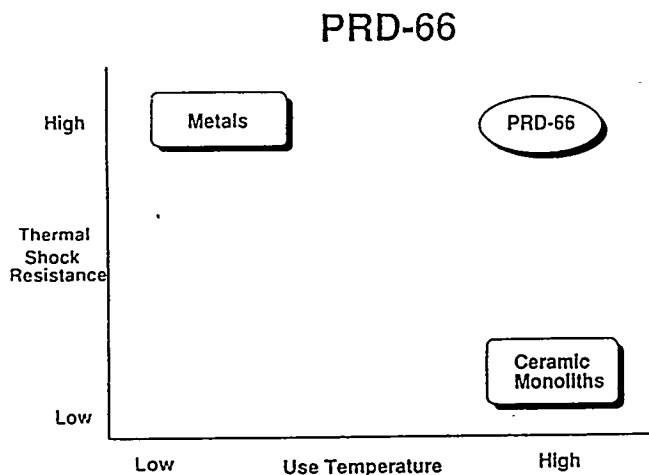


**Figure 1. Thermal Properties of PRD-66**

temperatures. PRD-66 is comprised of a layered, microcracked structure of an all-oxide chemical composition of silica, magnesia, and alumina (Figure 2). It consists of alternating layers in the crystal forms of corundum, mullite and cordierite, each layer being 50-100 microns thick. These layers repeat throughout the body of the filter. The all-oxide chemical composition is thought by

experts in the field to be favorable for survival in the coal combustion gas environment. The extensive network of microcracks and interfaces between the oxide layers is thought to provide the outstanding thermal shock resistance and damage tolerance of PRD-66, as any cracks that may form in the material do not progress very far before they encounter a crack or interface which helps reduce crack propagation energy.

PRD-66 is manufactured through a simple, patented process (Figure 3). A fiberglass yarn is coated with a slurry of alumina in water, and placed by high precision fiber handling techniques, in this case, filament winding, into the net shape of the filter. This preform is allowed to dry, then fired through a proprietary firing cycle. In this

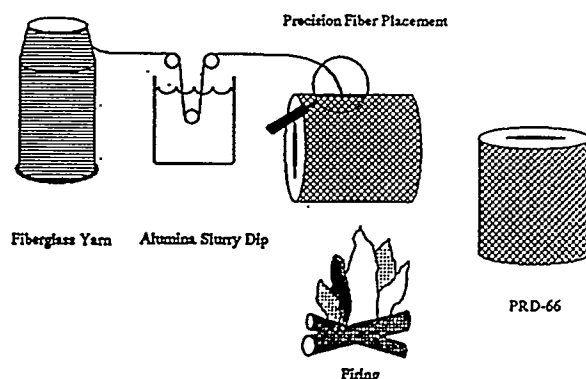


**Figure 3. PRD-66 Manufacturing Process**

firing process, the silica and magnesia in the fiberglass react with the alumina in the slurry to form mullite and cordierite. The surface of the material is unreacted alumina. It should be noted that the fiberglass is consumed in this chemical reaction, and the resulting product is not fiber reinforced.

The resulting ceramic material has a continuous use temperature of approximately 1200-1300°C in oxidizing atmospheres. In other applications, PRD-66 has survived numerous thermal shock cycles in excess of 1000°C/sec. It is believed that these thermal properties are in great excess of those experienced in this application. Through careful control of the filament winding process, DLC has been able to produce a filter body which is an

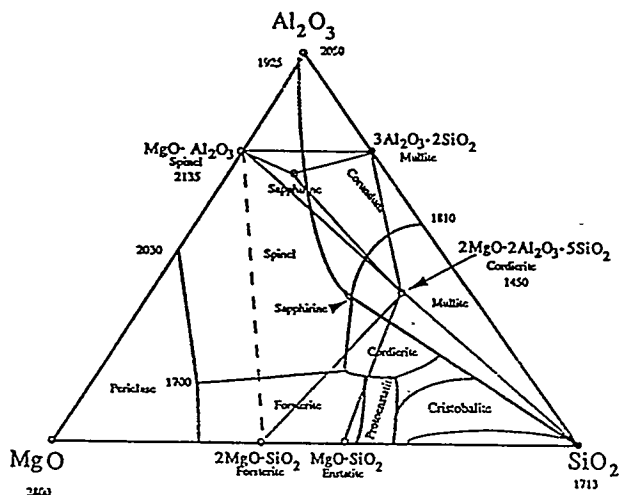


**Figure 2. PRD-66 Composition**

absolute bulk filter, as well as having a surface membrane which is a completely efficient particle filter. In the event that the surface filter should be damaged, the bulk filter would take over the filtration.

## Project Description

The project is being carried out in five tasks, two of which have been completed and the third is underway. Task 1 provided the management plan and the necessary NEPA information for the project. In Task 2, the test plan was written. Laboratory work began in Task 3, which consists of three subtasks. In Subtask 3.1, attempts at design improvements of the baseline candle filter were made. Among the design improvements sought in the project were increased strength of the flange area of the filter, and a reduced pressure drop filter. Full size candle filters incorporating these attempts at design improvements were fabricated. These filters would then be tested by our subcontractor, Westinghouse Corporation, to assure that the improved filters still met the fundamental requirements of acceptable permeability and filtration efficiency. After this testing, a decision on which improvements were successful will be made, and full sized candle filters incorporating the selected improvements will be made for testing in subsequent tasks. Also in Subtask 3.1, mechanical property tests suitable for monitoring progress toward stronger filters, and ultimately for process control, were surveyed. After choosing the best test, mechanical properties of the baseline filter would be obtained.

In Subtask 3.2, corrosion testing will be carried out on the improved candle filters at Westinghouse. In Subtask 3.3, HTHP testing simulating PFBC conditions will also be carried out. After exposure testing, mechanical properties will be measured to determine residual mechanical properties.

In Task 4, which is an option to be exercised at METC's discretion, basic manufacturing issues necessary for scale-up to commercial production will be investigated. These issues include raw ingredient quality, process economics, and manufacturing equipment reliability, among others. In Task 5, also an option, recommendations for process improvements will be made, and 50 filters will be manufactured.

## Results

As of this writing, the project is in the latter stages of Subtask 3.1. Tasks 1 and 2 were completed per the projected schedule. DLC has completed development of design improvements on both filter subelements and full sized filters, as described below. Sections of those filters have been tested for filtration and permeability by Westinghouse, and those results are presented below. Mechanical tests have been surveyed, and a preferred test has been selected and applied to understand the mechanical properties of the baseline PRD-66 hot gas filter.

### Reduced Pressure Drop Filter

The objective of this effort was to reduce the pressure drop of PRD-66 filters compared to the baseline filter, while maintaining good filtration, cake formation and release characteristics. As shown in Figure 4, those efforts have been successful. Through a series of process modifications, it was demonstrated that virtually all the pressure drop of the candle is developed by the surface membrane. Thus the task of reducing the overall backpressure was reduced to lowering the pressure drop of the membrane. Figure 4 shows that pressure drops could be lowered as much as 85%. In the very lowest pressure drop candles, problems developed with adhesion of the

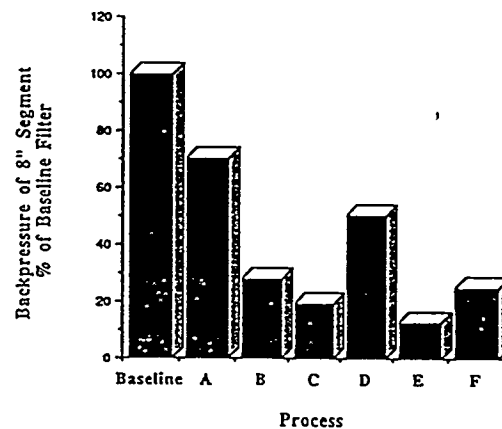


Figure 4. Pressure Drop vs. Process Iteration

membrane to the body of the candle filter, and it has been shown that a 'medium' level of pressure drop reduction can be obtained with a membrane that is strongly adhered. Full scale filters incorporating the lower pressure drop membrane have been manufactured.

## Strengthened Flanges

The objective of this effort was to increase the strength of the flange region of the filter while maintaining a graceful failure mode. It was deemed desirable to be able to control the location and degree of reinforcement. As shown in Figure 5, DLC was able to increase the strength of the filter body material by up to 50% relative to the baseline filter. We were also able to vary the degree of reinforcement over a relatively smooth curve. Within a reasonable degree of control, we were also able to provide a gradient of reinforcement from the strongest section to the filter body. Load deflection curves of o-ring sections showed graceful similar to the baseline material.

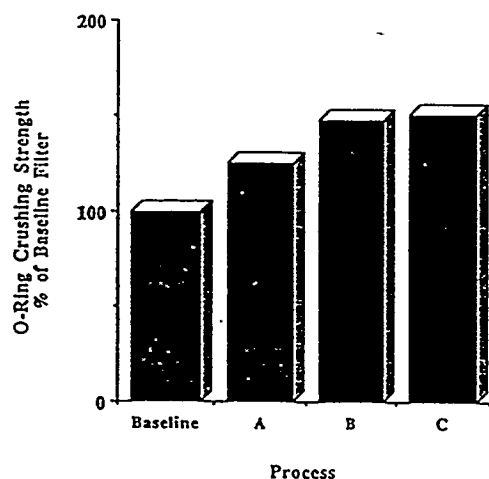


Figure 5. O-ring Crushing Strength vs. Process Iteration

## Mechanical Property Testing

The objective of this effort was to identify a mechanical property test which is precise and accurate for the PRD-66 material. In addition, it is desirable for such a test to minimize the effect of machining damage incurred in fashioning the test

specimen, and to be amenable for quality control in future production.

PRD-66 hot gas filters are made by a process which, at a fundamental level, produces only tubular shapes. It is impossible to manufacture a flat coupon which closely mimics the internal structure of a PRD-66 filter, and therefore only tests which are based on a cylindrical sample were considered. This limits the range to o-ring or c-ring tests. C-ring tests were evaluated, but cutting the 1 inch notch from the coupon incurred machining damage and additional cost. O-ring tests are ideal from that standpoint, with only two cuts required to sample a tubular product. Since o-ring tension tests require more complicated and costly fixtures, a simple o-ring compression test was most favored.

Figure 6 shows a load deflection curve typical of the o-ring compression tests carried out in this project. It shows a great deal of reloading and

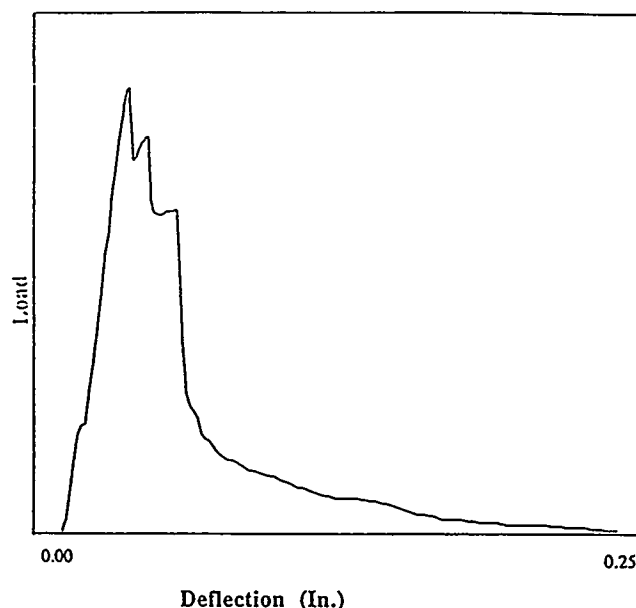
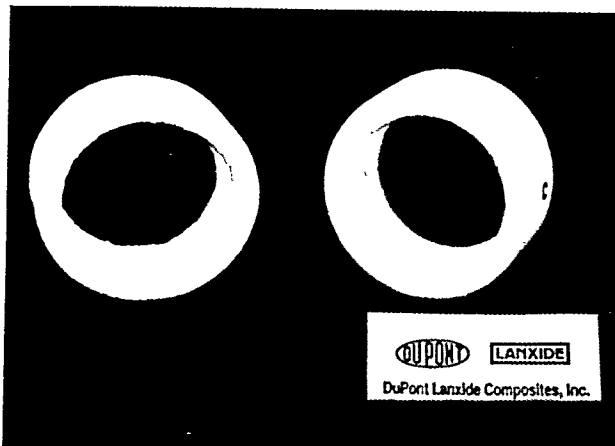


Figure 6. Load Displacement Curve of Typical PRD-66 Filter Section

strain tolerance after peak load. Tests carried out until essentially no load resistance was encountered often had deflections as high as 0.25 inches, or roughly the same as the wall thickness of the sample. In the 100 or so mechanical tests conducted in developing this o-ring section test, no sample displayed catastrophic failure, i.e., failure into two or more pieces. Figure 7 shows the test



**Figure 7. PRD-66 Filter Section Before (right) and After (left) O-ring Compression Test.**

specimen from Figure 6 after failure, displaying a permanent deflection of 0.25 inches, but still intact. Method plus product variability of the o-ring compression test was on the order of  $\pm 10\%$ , fairly remarkable for mechanical tests on porous ceramics. Other laboratories have also conducted o-ring and c-ring tests on PRD-66 filter samples and calculated different strengths. DLC's estimate is the most conservative. DLC hopes to reconcile the different testing results in the near future.

### **Filtration and Permeability Testing**

The objective of this effort is to verify that the design improvements developed in the work described above do not adversely impact the fundamental properties needed in a hot gas filter, permeability and filtration efficiency. To demonstrate this, 2 inch segments of full sized filters were tested on bench scale equipment at Westinghouse. While permeability results are not finalized, they appear to be acceptable. Filtration tests showed the filters to be of acceptable efficiency, with very smooth and uniform cake formation.

### **Future Work**

In the near future, DLC, Westinghouse and METC will reach a decision on which of the design improvements to incorporate into a final filter

design. A number of those filters will then be manufactured for corrosion and HTHP filtration testing at Westinghouse. Assuming those tests are successful, and METC exercises the optional portions of the contract, DLC will address manufacturing issues in Task 4, and begin commercial manufacturing of 50 filters in Task 5.

## 6A.2

## Filter Systems for IGCC Applications

### CONTRACT INFORMATION

**Contract Number** DE-AC2-87MC23170

**Contractor** General Electric Environmental Systems Inc.  
200 North Seventh Street  
Lebanon, PA 17042  
(717) 274-7077

**Other Funding Sources**

**Contractor Project Manager** Stephen Bevan

**Principal Investigators** Stephen Bevan (GEESI)  
Robert Gieger (Pall Corporation)  
Nelson Sobel (Pall Corporation)  
Dale Johnson (Dakota Gasification)

**METC Project Manager** Justin Beeson

**Period of Performance**

**Schedule and Milestones** September '94 to June '95

#### Program Schedule

	S	O	N	D	J	F	M	A	M	J	J	A
Field Testing												
Sample Analysis												
Topical Report												

### OBJECTIVES

The objectives of this program were to identify metallic filter medium to be utilized in the Integrated Gasification Combined Cycle process (IGCC). In IGCC processes utilizing high efficiency desulfurizing technology the traditional corrosion attack, sulphidation, is minimized so that metallic filters are viable alternatives over ceramic filters.

### BACKGROUND

#### Hot Gas Clean Up (HGCU)

Tampa Electric Company's Polk Power Station is being developed to demonstrate Integrated Gasification Combined Cycle technology. Hot Gas Clean Up (HGCU), a new technology, is being supplied by General Electric Environmental Systems, Inc. (GEESI).



Approximately 45,000lb/hr of raw syngas will be treated in several steps in HGCU, namely initial particulate removal, chloride removal, desulfurization and barrier filtration, see Figure 1. The HGCU system will deliver clean fuel for firing in the combustion turbine.

The initial step in the HGCU system is the

The sulfur laden syngas next contacts the mixed metal oxide sorbent in the absorber vessel where, in counter current flow to the sorbent, desulfurization takes place at 900°F and 400psi. The feed to the combustion turbine is thermodynamically superior since the heat of the syngas has been retained to a high degree as compared to conventional cold gas clean up systems.

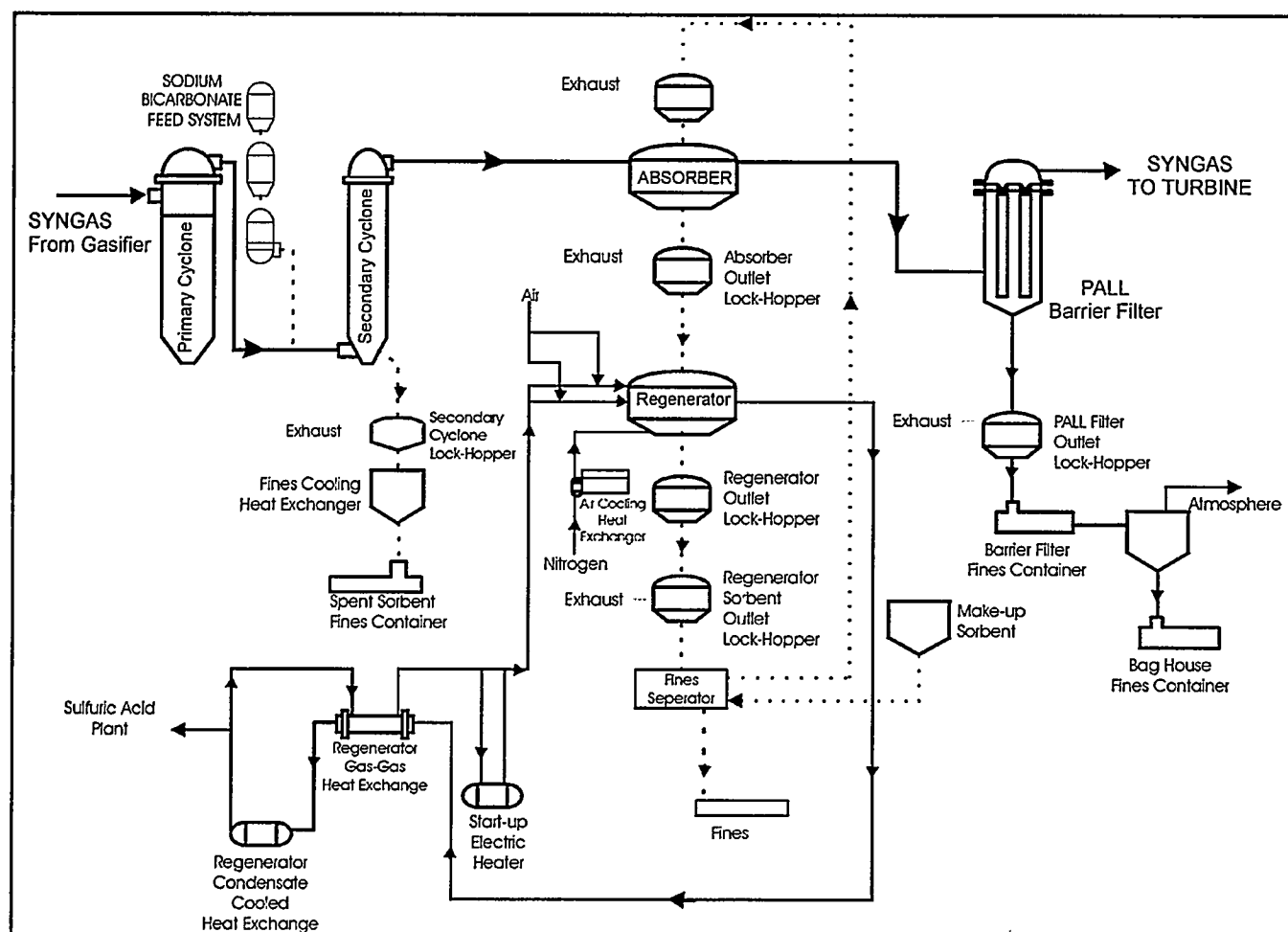


Figure 1. Simplified Hot Gas Clean Up System

removal of entrained particulate by use of high efficiency cyclone separation. Downstream of the primary cyclone, a circulating fluidized bed (CFB) cyclone is employed to remove chlorides from the fuel gas. This is accomplished by injecting sodium bicarbonate into the gas entering the CFB cyclone.

The sorbent bed in the absorber acts as a granular filter, removing large particulate matter in the syngas, which is not removed in the primary or CFB cyclones. A small quantity of entrained fines, 30ppm or less, are expected in the syngas exiting the absorber. These solids are removed in a barrier filter which will capture all sorbent dust and fines. The

high temperature barrier filter, employing in-situ cleaning, will reduce residual particulate by greater than 99.9% by weight. Clean syngas exiting the barrier filter is mixed with the balance of the syngas from conventional cold gas clean up system before being combusted in the combustion turbine.

### Description of Hot Gas Clean Up Barrier Filtration System

The Pall Gas Solid Separation (GSS) System is a self cleaning filtration system designed to remove virtually all particulate matter from gas streams. To achieve this, filter elements constructed with high efficiency filtration medium effectively retain the gas stream solids on the filter element's outside surface. This results in the formation of a solids cake which is dislodged from the surface by initiating a momentary reverse flow, blowback, through the filter element.

For the Tampa Electric project, a GSS System using jet pulse blowback technology to clean the elements was chosen. The reverse flow through each element is created by the momentary pulsing of a high pressure jet located above each filter element. This technology has effectively been used in many applications including high temperature, high pressure service. It is an efficient method for generating a reverse flow for effective in-situ element cleaning, while minimizing blowback gas consumption.

Figures 2a, 2b and 2c show the filter elements in a housing, collecting, then discharging the solids. The cake formed on the filter element has two distinct parts; a non-permanent cake which is dislodged during the cleaning operation, and a thin, permeable, permanent cake which adheres to the filter's surface even during blowback. The permanent cake is formed after several "conditioning" cycles, and becomes a finer filter than the filter medium itself. It is the permanent cake that

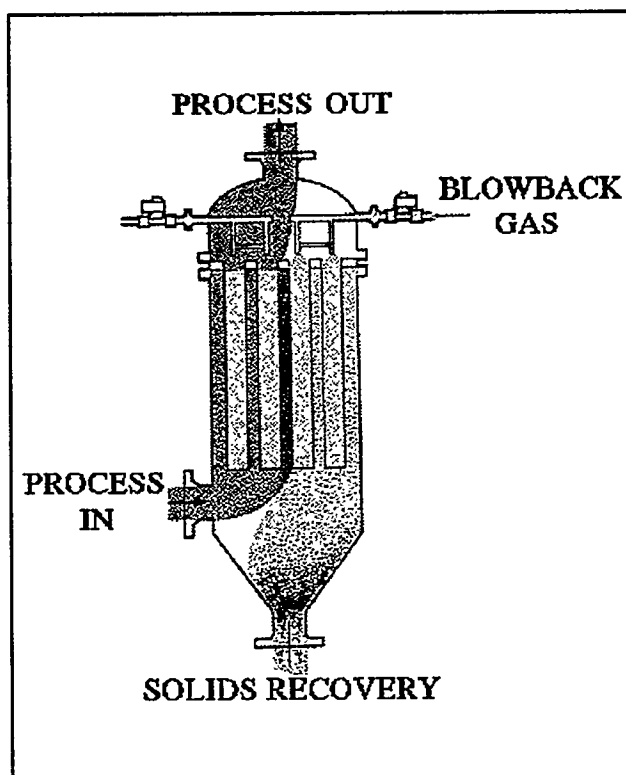


Figure 2a. Pall GSS System in Blowback Mode

gives the system the ability to remove virtually all particles including ones smaller than filter medium's removal capability.

The heart of the system is the filter medium used to collect the particles on the filter surface. The medium's filtration efficiency, uniformity,

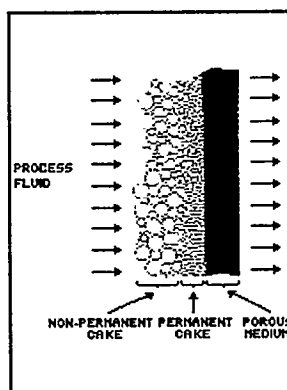


Figure 2b. Cake Formation

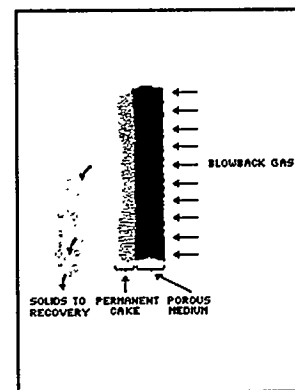


Figure 2c. Permanent Cake

permeability, voids volume, and surface characteristics are all important to establishing a permeable permanent cake. Pall produces a wide range of proprietary filter media, both metallic and non-metallic, that can be used in the GSS Systems. In-house laboratory blowback tests, using representative full scale system particulate, were used to confirm the medium selection for this project.

Figure 3 depicts the main components of the GSS System, which includes:

- Filter vessels designed to the ASME pressure vessel code.
- Tubesheet assembly to mount the filter elements and blowback gas distribution

- Gas receiver to store high pressure gas for the blowback pulse.
- Instrumentation and controls to monitor system operation.
- Miscellaneous valves and components.

The Filter housing is a 42 inch diameter externally insulated vessel, designed for 440 psig and 1000°F. The vessel's material of construction is 347 SStl and the tubesheet is 310 SStl. The system design considers many factors to ensure that performance specifications are met with reliable operating equipment. Among these factors is filter element construction, element support structure within the vessel, sealing mechanisms, ancillary equipment selection, etc. Heated blowback gas is used to avoid potential condensation and the

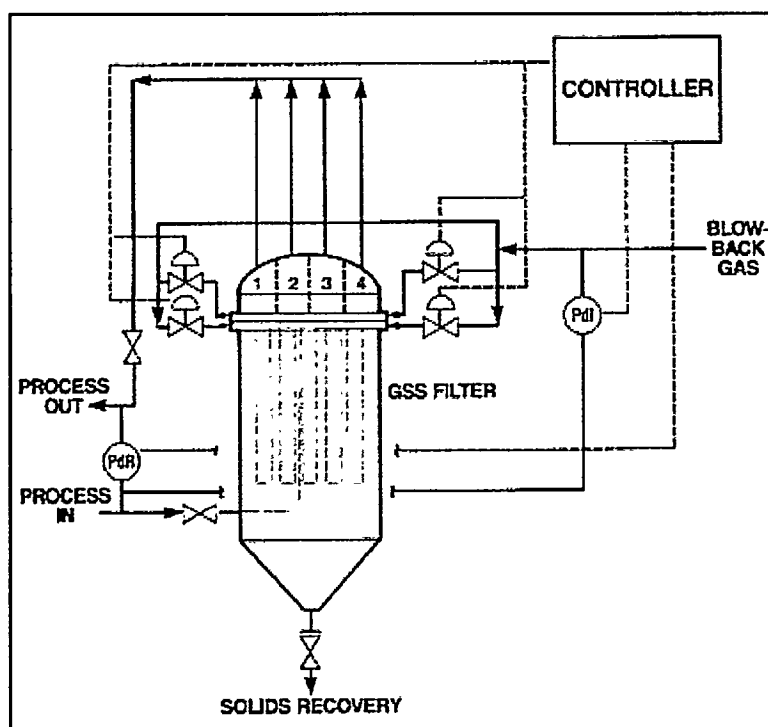


Figure 3. The Components of a Pall GSS Blowback System

- manifolds.
- Fast response valves to control the blowback gas flow.

associated corrosion that could occur within the filter vessel. If ceramic candles are used, heating the blowback gas precludes premature mechanical

failure caused by thermal cycling with ambient temperature blowback gas.

To increase system reliability, a fail safe fuse is included in the design. In essence, the fuse is a coarse grade, strong non-blowback filter element that is located at the outlet of each primary element. In the unlikely event of a primary element failure, the fuse will rapidly plug with particles, effectively removing the damaged element from service and preventing solids bypass. The loss of one element has a negligible effect on system performance, and under normal operation, the fuse gives very low resistance to flow and has no effect on filter blowback performance.

### Filter Media

For the Tampa Electric Project, two types of filter medium were considered; Vitropore™ silicon carbide and PSS® porous metal medium elements. Ceramic candles have traditionally been used in IGCC application because of their known corrosion resistance to the process conditions. The base material for Vitropore candles is silicon carbide grit which is bonded together with a proprietary sodium aluminosilicate bond system. The candle, shown in Figure 4, has a 10 mm thick coarse grit body for strength, and a thin outer membrane coating for filtration.

Although having excellent corrosion resistance, service problems have been reported with ceramic candles in this application due to element brittleness and sealing mechanisms. Since the GSS system is located downstream of chloride and sulfur removal equipment, it opens up the potential for using PSS metal medium elements. If metal media can withstand the reduced chloride and sulfur levels in the gas stream, the mechanical problems associated with ceramic candles would be solved. In addition, metal media filters typically results in lower cost filtration systems. A porous metal element assembly is shown in Figure 5.

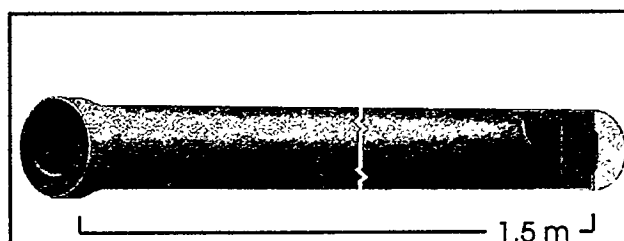


Figure 4. Vitropore Silicon Carbide Element

With regard to filter media corrosion, it should be noted that PSS medium is made from relatively small particles of the base material and sinter bonds produce material with about 45-60% void volume depending on the product. Since there

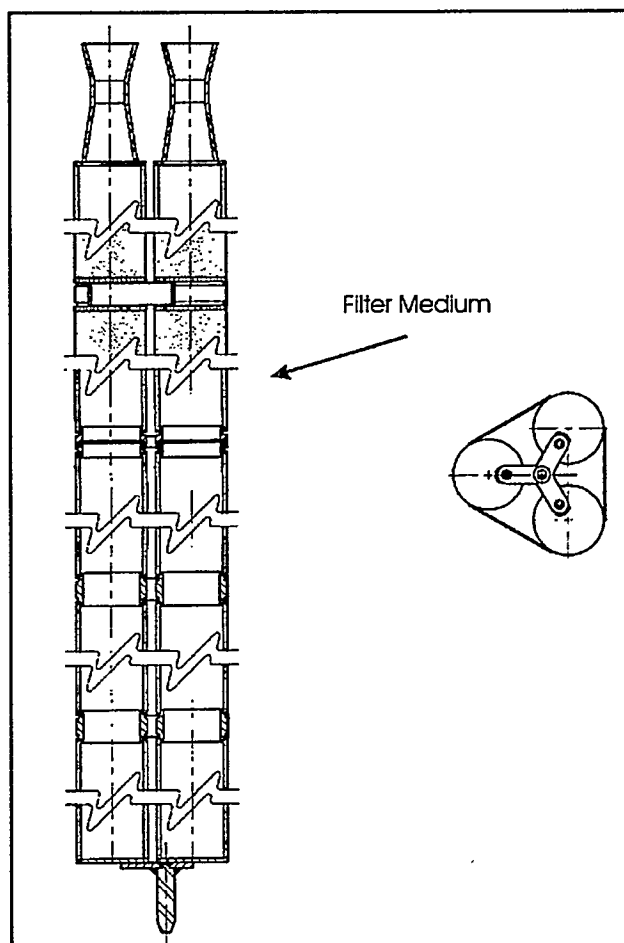


Figure 5. Pall PSS Element Triad Assembly

is an extremely high surface area within the medium pore structure, and the cross section of the bonds are small, corrosion rates need to be applied to the bond cross section and not to the overall medium thickness. As such, typical corrosion evaluations made for solid materials do not necessarily apply to filter media.

Iron aluminide materials have shown very good resistance to sulfidation, and are potentially viable candidates for future projects. Samples of non-commercially available medium were exposed in this test for purposes of gathering information. Pall has recently been awarded funding under a DOE PRDA for the development of iron aluminide medium. This product is expected to be very beneficial for IGCC applications, especially with high sulfur containing gases.

When the filter system design was started, the medium selection, Vitropore SiC ceramic, or PSS metal, was not finalized. To meet the overall project schedule, as well as to provide flexibility for future media developments, the system is designed to have interchangeable filter elements. All components in the system are designed to accommodate any of the filters that would be used.

## PROJECT DESCRIPTION

### Process Simulation

**Filter Media Evaluation Program at Dakota Gasification Company.** The filter media test system was developed by Dakota Gasification Co, Pall Corporation and GEESI to test several media samples simultaneously under process conditions which closely resemble conditions experienced in the HGCU system. The H<sub>2</sub>S content, moisture content and operating temperature were of particular importance. Table 1 shows the expected conditions of the HGCU system and the filter test system process set points.

The purified syngas exiting the rectisol system was chosen as the primary feedstock due to the similarities in composition and the lack of undesirable contaminants. The rectisol syngas is cool, dry and essentially sulfur free. Therefore, the filter test system required the addition of steam and H<sub>2</sub>S to achieve the appropriate composition and an electric heater was utilized to achieve the desired temperature.

**Table 1. HGCU and Test Systems Process Set Points**

Parameter	HGCU System	Test System
H <sub>2</sub> O	12 -18%	18%
H <sub>2</sub>	30%	52%
N <sub>2</sub>	8%	0.1%
CO	35%	15%
CO <sub>2</sub>	12%	1%
CH <sub>4</sub>	0.2%	13%
H <sub>2</sub> S	30 - 50ppm	30ppm
Temperature	800 - 1000°F	900°F
Pressure	300 - 400psig	300psig

Figure 6 is the simplified configuration of Dakota Gasification Company's filter system. Syngas and steam are metered and combined at the inlet of the electric heater. The heater and filter system are protected from overheating or insufficient steam flow with an interlock system. H<sub>2</sub>S is metered and introduced at the discharge of the electric heater. The H<sub>2</sub>S spiked hot gas is then introduced into the filter housing, which holds up to 30 test elements. The effluent from the filter housing is discharged to the flare system.

The filter test system was designed to safely

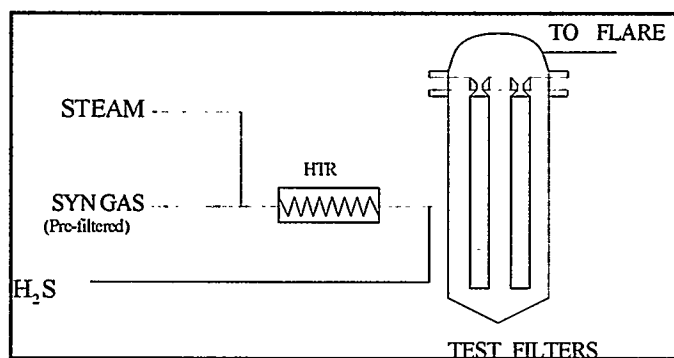


**Figure 6. Simplified Diagram of Simulated Test System**

perform the filter media evaluation at the desired test condition. The system was manually controlled and monitored. Dakota Gasification Company provided 24hr monitoring of the test system.

## EXPOSURE TEST METHOD

To obtain flow-through media test, 4" test elements were constructed from various alloys and supplied to General Electric Environmental Systems, Inc. by Pall Corp. The total test duration was for 153 days with elements being removed at 12, 26, 71 and 153 day intervals.

The test gas flows from the housing inlet, through the filter medium of each element, to the housing outlet. Flow distribution is controlled within the housing with orifices to ensure that each element sees adequate flow.

Test elements constructed from six alloys were supplied for exposure tests, see the list below:

- PSS 310SC (modified 310S alloy),
- PSS 310SC heat treated,
- PSS 310SC-high Cr,
- PSS 310SC-high Cr heat treated,
- PSS Hastelloy X,
- PSS Hastelloy X heat treated,

After exposure, the elements were thoroughly cleaned using DI water and alcohol. The threaded fitting was wire brushed to remove any residual anti-seize compound.

The samples were then subjected to the following analyses: **Weight Change**, the exposure samples were weighed prior to and after testing to monitor changes in weight of the samples( all weight loss was attributed to the medium); **Air Flow Permeability Test**, a constant gas flow (28scfm/ft<sup>2</sup>) is applied to the exposure sample. The sample represents a restriction to gas flow and the differential pressure is a measure of the sample's permeability at the given air flow; **Bubble-Point Test**, the sample is immersed in a test liquid which wets and saturates the filter pore structure. Gas pressure is applied to one side of the porous medium so that the wetting fluid is displaced by the gas. The gas pressure is slowly increased until the first steady stream of gas bubbles is observed from a point on the sample's surface; **Ductility**, was performed by compressing ring samples until an initial crack was observed. The percent change in outer diameter was calculated and is an indicator of ductility; **Tensile Strength**, tensile strength on samples was performed using a MTS 810 Material Testing System. **Chemical Analysis**, chemical analysis was performed with the following equipment:

- Oxygen and nitrogen: LECO TC-136.
- Carbon and sulfur: LECO CS-344

Samples of 0.1g were digested in acid and analyzed via a Beckman DCP Spectrophotometer; **Visual Examination**, samples were viewed utilizing a scanning electron microscope to detect fines entrained in the filter medium; **Microstructural Examination**, representative samples of exposed medium were epoxy impregnated, placed in a metallographic mount and polished. The samples were viewed and photographed in both the as-polished and etched condition.

## TEST RESULTS

Type 310SC SSII performed the best of all alloys exposed based on the data collected. The following sections outline these results.

### Weight Change

Figure 7 shows that the exposure to the environment has negligible effects on weight gain for 310SC SSII alloy.

### Air Flow Permeability Test

The 310SC samples showed small changes in air flow vs. delta P. This is primarily due to the element capturing particles in the gas stream. There was an average increase of ~10% after in-house cleaning using DI water and alcohol.

### Bubble-Point Test

Results from bubble-point testing show slight increases in bubble-point values. There was an average increase of ~ 3%. Some values fell within acceptable specifications used in QC process.

### Ductility

The 310SC samples tested retained an average of 65% of their original ductility. Experience has shown that ~25% is an acceptable

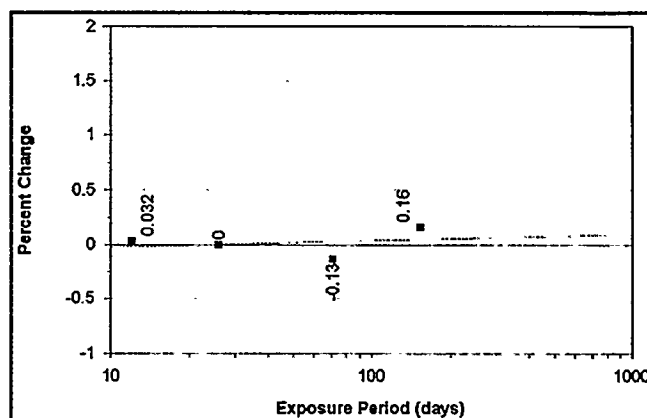


Figure 7. Percent Weight Change

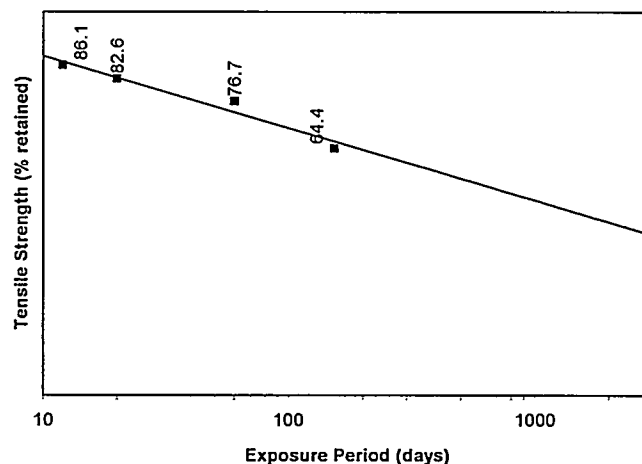
minimum value.

### Tensile Strength.

Figure 8 shows the tensile strength data for the samples. All but one sample retained tensile strength within allowable manufacturing ranges. The last sample returned was <5% out of manufacturing range. Overall, it does not appear as if tensile strength was adversely affected due to exposure.

### Chemical Analysis.

The results from chemical analyses show negligible increases/decreases for all elements tested. All samples show an increasing carbon pick up with increasing exposure time. The chemical composition of the gas at Dakota Gasification Co.



has a substantially higher methane content when compared to Tampa Electric Co. conditions, see Table 1. The carburizing component of TECO's environment is carbon monoxide and carbon dioxide. Methane is a stronger carburizing agent. It is expected that a carbon pick up will be less at Polk Station than at Dakota Gasification Co.

#### **Visual Examination.**

Exposed and unexposed samples were viewed for medium pore plugging. Photographs 1a and 1b are at low magnification (300X) and photographs 2a and 2b are at high magnification (1000X). It is evident that the pores of the medium are essentially free of fines entrainment. At the high magnification, the surface of the medium appears very similar to the unexposed state.

#### **Microstructural Examination**

Results of the analysis performed on representative samples of the medium show an even distribution of irregularly shaped particles and voids typical of sintered powder materials. The as-polished sample revealed a structure similar to unexposed material, see photographs 3a and 3b

Etching revealed a microstructure typical for 300 series stainless steel, see photographs 4a and 4b. Inspection for intergranular corrosion followed ASTM procedure A262-86. Results revealed no difference in structure between the new and exposed sample.

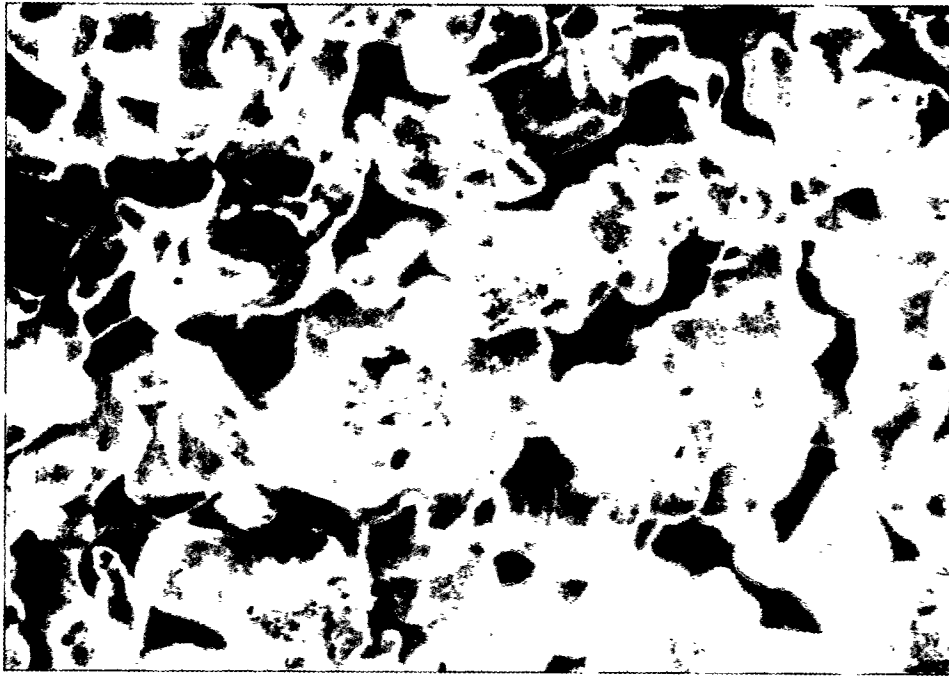
#### **CONCLUSIONS**

In the IGCC processes utilizing high efficiency chloride removal and desulfurizing technology the traditional corrosion attack, sulfidation, is minimized so that metallic filters are viable alternatives. Metallic filters offer better mechanical properties (ductility, less prone to shock/vibration crack propagation) and a more secure sealing mechanism (ease of welding).

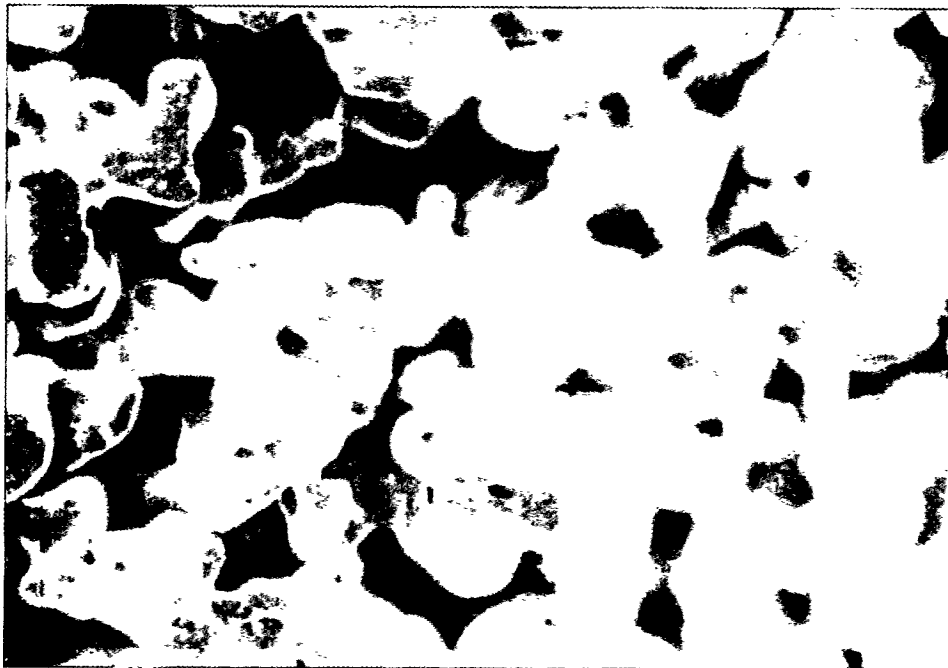
Pilot Scale exposure tests, utilizing 4" high x 2.375" diameter metallic filter elements of various metal alloys, were performed at Dakota Gasification Company. The filters were exposed for various time intervals (12, 26, 71 and 153 days) at 900°F and 30ppm H<sub>2</sub>S process equivalent. The returned samples were analyzed for performance properties (air flow vs. differential pressure and bubble point testing), mechanical properties (tensile strength, ductility and weight change) and chemical/structural properties (chemical composition, electron microscopy and microstructure).

Results from the investigation demonstrate that filter elements of PSS medium Type 310SC stainless steel showed good resistance to corrosion. It is concluded that a Pall Gas Solids Separation System utilizing metallic filter elements is a viable option and will be used in the GEESI Hot Gas Clean Up system.





**Photograph a. Unexposed 310SC media open pore structure (300X).**



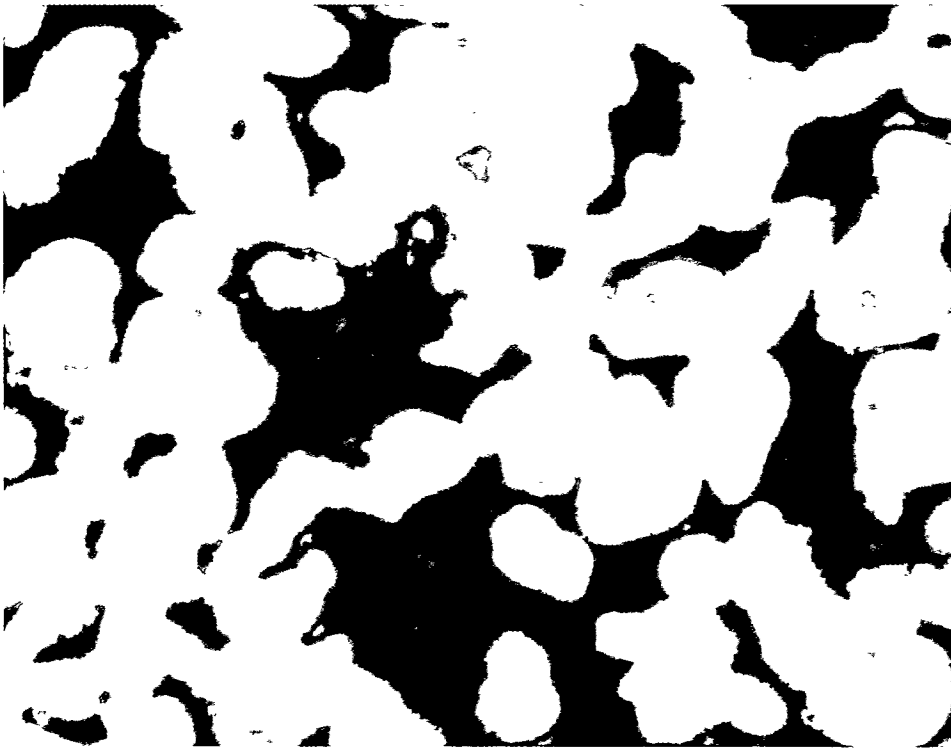
**Photograph 1b. Exposed 310SC media open pore structure (153 days, 300X).**



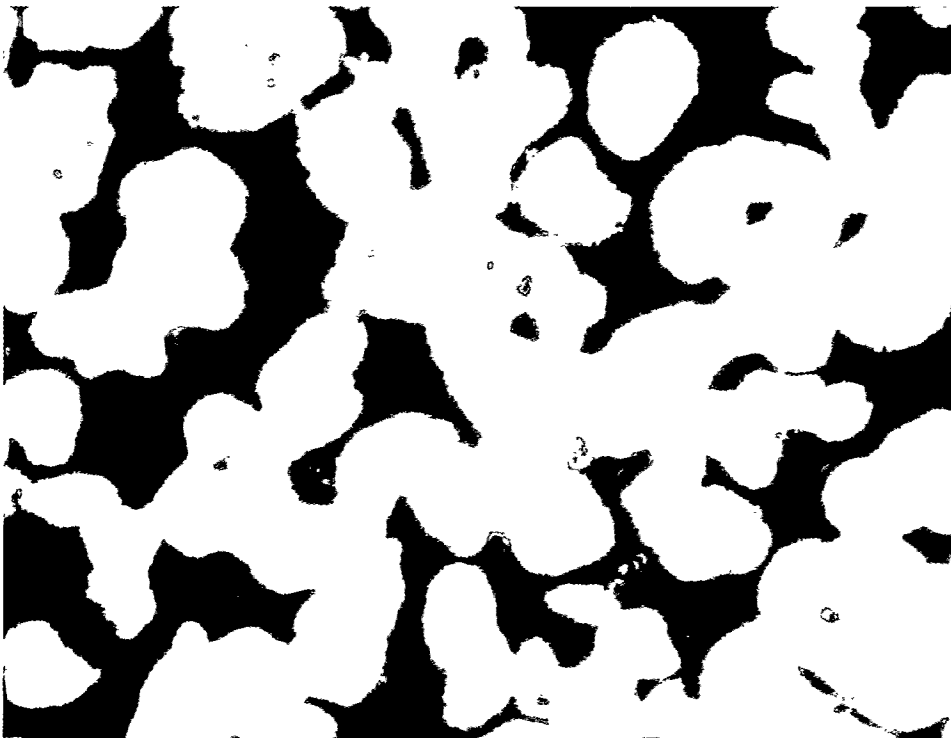
**Photograph 2a. Unexposed 310SC media open pore structure (1000X)**



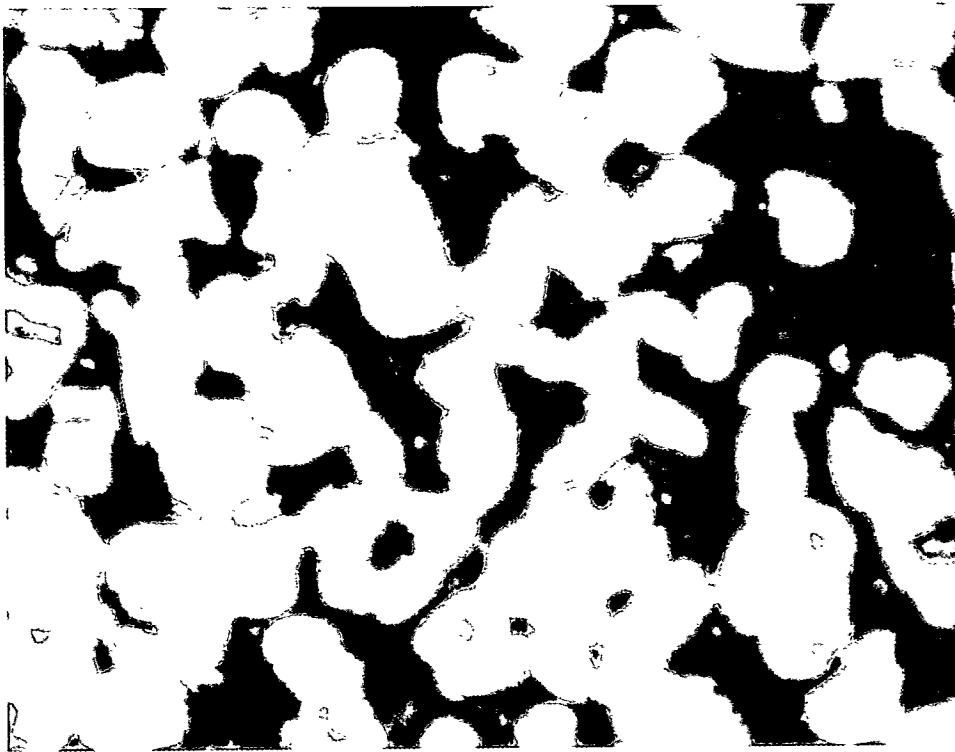
**Photograph 2b. Exposed 310SC media open pore structure (153 days, 1000X)**



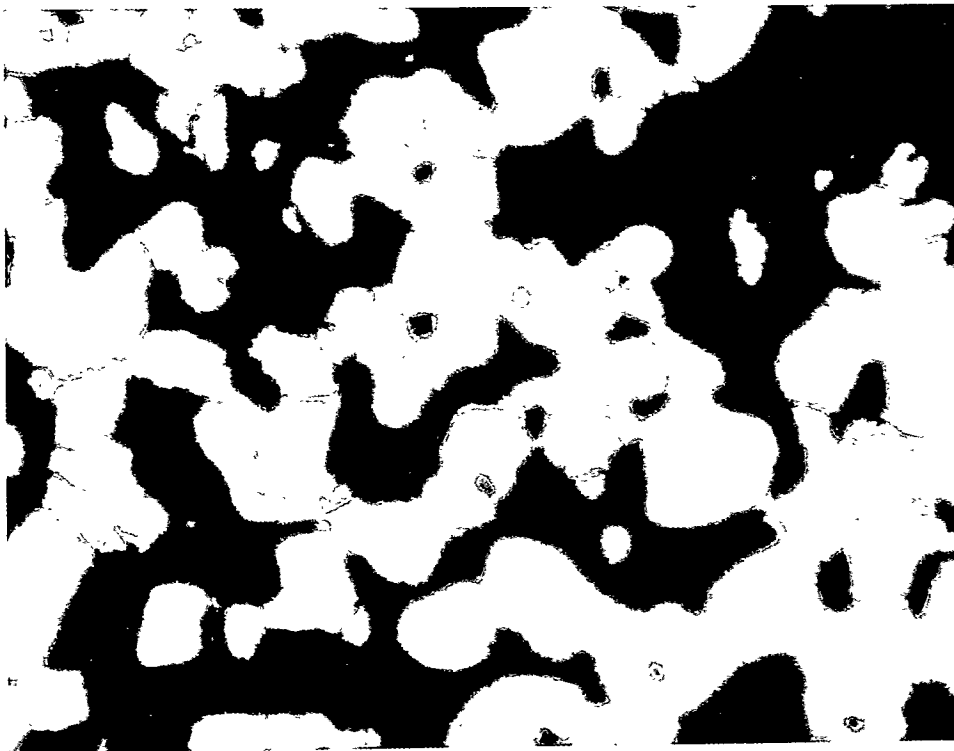
**Photograph 3a. Photomicrograph of unexposed 310SC in the polished condition (400X)**



**Photograph 3b. Photomicrograph of exposed 310SC in the polished condition (153 days, 400X)**



**Photograph 4a. Photomicrograph of unexposed 310SC in the etched condition (400X)**



**Photograph 4b. Photomicrograph of exposed 310SC in the etched condition (153 days, 400X)**

## 6A.3 Thermal and Chemical Stability of Ceramic Candle Filters

### CONTRACT INFORMATION

**Contract Number** DE-AC21-88MC25034  
DE-FC21-89MC26042

**Contractor** Westinghouse Electric Corporation  
Science & Technology Center  
1310 Beulah Road  
Pittsburgh, PA 15235-5098  
(412)256-2066 (Telephone)  
(412)256-2121 (Telefax)

**Contractor Project Manager** Mary Anne Alvin

**Principal Investigators** Mary Anne Alvin  
Thomas E. Lippert  
Edward S. Diaz  
Eugene E. Smeltzer

**METC Project Manager** Theodore J. McMahon

**Period of Performance** October 1, 1988 - October 31, 1995

**Schedule and Milestones**

#### FY 95 Program Schedule

TASK	S	O	N	D	J	F	M	A	M	J	J	A
Experimental Testing												
Field Analysis												
Model Development												
Final Report												

### OBJECTIVES

The objectives of this program are to identify the potential long-term thermal/chemical effects that advanced coal-based power generating

systems have on the stability of porous ceramic filter materials, as well as to assess the influence of these effects on filter operating performance and life.

## BACKGROUND INFORMATION

High temperature particulate removal systems have been designed and operated by Westinghouse for use in advanced coal-fired process applications. Typically monolithic, first generation, clay bonded silicon carbide candles were tested for a maximum of 1341 hours in the Ahlstrom pressurized circulating fluidized-bed combustion (PCFBC) pilot plant in Karhula, Finland, and for 5855 hours in the American Electric Power (AEP) pressurized fluidized-bed combustion (PFBC) Demonstration Plant in Brilliant, Ohio.<sup>(1)</sup> Testing was also conducted for periods of 716 hours utilizing the monolithic, first generation alumina/mullite candle filters at Ahlstrom, and for 2185 hours at AEP. When the filters were operated in the combustion gas environments at temperatures which exceeded 800°C, creep resulted within the clay bonded silicon carbide candle filter matrix, while the alumina/mullite filters demonstrated susceptibility to thermal fatigue and/or shock when exposed to severe thermal process transient conditions. Both the nonoxide and oxide-based candles experienced failure during plant shutdown when ash bridges formed between adjacent filter elements.

Several manufacturing changes have been undertaken by the various monolithic candle filter suppliers as a response to the issues encountered in the field. Prior to 1993, the Coors alumina/mullite candle filter was constructed with a blunt end cap which contained internal, relatively sharp corners.<sup>(2)</sup> Based on the stress analyses conducted by Adapco, the internal corners were suspected to act as stress risers and crack initiators during process operation.<sup>(3)</sup> As a result of the Adapco analyses, the Coors candle filter end cap was redesigned to contain a full radius, and the entire body was manufactured with a uniform wall thickness. Subsequently the redesigned candle filters were installed and operated in the Westinghouse Advanced Particulate Filtration

(W-APF) system at the AEP Demonstration Plant in Brilliant, Ohio.

Similarly Schumacher and Pall reformulated the binder composition and/or changed the grit size of their clay bonded silicon carbide filter matrices, producing not only stronger, but also higher temperature, creep resistant matrices (i.e., Schumacher Dia Schumalith FT20; Pall 326) for potential use in >800°C coal-fired process applications. To date, Schumacher Dia Schumalith FT20 filters have been successfully operated in the W-APF system at AEP. Based on recent materials evaluation conducted at Westinghouse, as well as at the various filter supplier test facilities, and preliminary HTHP testing at Westinghouse, both the Schumacher Dia Schumalith FT20 and Pall 326 filter elements are expected to demonstrate improved operating performance and extended life at 900°C in the PCFBC test facility in Karhula, Finland.

## PROJECT DESCRIPTION

Westinghouse has undertaken a two phase program to determine the possible long-term, high temperature influence that advanced coal-based power systems have on the stability of porous ceramic filter elements. During the past year, Westinghouse has utilized its high temperature, high pressure (HTHP) and bench-scale test facilities to replicate field operating conditions which induce creep and/or thermal fatigue in the clay bonded silicon carbide and alumina/mullite candle filters. These results serve as the basis for identifying critical operating and design parameters which are essential for the long-term viability of the filter matrices, and ultimately commercialization of the filter system. Westinghouse has also identified the axial and radial temperatures gradients that are generated through the porous ceramic candle filter wall during either pulse cleaning, or during exposure to simulated process

transient or thermal excursion events. The results of the bench-scale and HTHP testing, as well as recent field test material characterization results for the first generation, monolithic, porous ceramic filter elements are presented in this paper.

## RESULTS

### Thermal Transient Testing

**Accelerated Pulse Cycling.** In previous high temperature, high pressure (HTHP) thermal fatigue testing at Westinghouse, as-manufactured Coors alumina/mullite (i.e., redesigned end cap and uniform body/end cap wall thickness), Pall Vitropore 442T, and Schumacher Dia Schumalith F40 candle filters were shown to remain intact after being subjected to 10,000 accelerated pulse cleaning cycles.<sup>(4)</sup> Similarly several of the originally designed alumina/mullite candle filters which had experienced 227 and 716 hours of operation in the W-APF system in the Ahlstrom PCFBC test facility in Karhula, Finland, were included in the W-HTHP filter array. After exposure to 10,000 accelerated pulse cycles, the PCFBC-exposed filters also remained intact.

A reduction in strength along the ID surface of the alumina/mullite filter matrix was evident very early in the pulse cleaning sequence (i.e., 713-770 pulse cycles; Table 1). The strength of the matrix along the ID surface then stabilized, indicating that conditioning of the matrix had resulted. Post-test characterization indicated that a circumferential crack had formed at ~1-2 mm from the ID wall of the alumina/mullite candle after extended pulse cycling (Figure 1).

When the as-manufactured Pall Vitropore 442T candle was subjected to 10,000 accelerated pulse cycles, an initial reduction in the OD and ID high temperature strength resulted, followed by strengthening of the filter matrix. For the



**Figure 1. Cross-Sectioned Wall of the Thermally Fatigued Alumina/Mullite Candle Filter**

Schumacher Dia Schumalith F40 candle, the high temperature strength along the OD and ID surfaces was initially reduced, which subsequently stabilized with extended accelerated pulse cycling. Table 2 provides a summary of the resulting burst pressure, burst strength (i.e., ultimate hoop stress), elastic modulus, and Poissons ratio for each of the HTHP accelerated pulse cycled candle filters.

**Pulse Cycle Temperature Profile.** High speed, 0.004 inch Chromel Alumel Type K thermocouples manufactured by Watlow Gordon were used to monitor temperatures which resulted within and along the length of the filter body, as well as through the filter wall during pulse cycling. Each high speed thermocouple had a 5 mm exposed bare wire junction, and the remainder of the lead was protected by an 0.020 inch Inconel 600 sheath. Each thermocouple was delicately positioned into an 0.025 inch hole that had been drilled into the filter wall. The thermocouples were positioned along both the ID and OD

**Table 1. Strength Characterization of the W-HTHP Tested Accelerated Pulse Cycled Porous Ceramic Filter Materials**

Filter Identification Number	Test No.	Accelerated Pulse Cycles	Room Temp., Strength(a)		Hot Strength,(843 ° C)(a)	
			C-Ring Compression, psi	C-Ring Tension, psi	C-Ring Compression, psi	C-Ring Tension, psi
<u>ALUMINA/MULLITE FILTERS (1.5 m)</u>						
CC-012	--	---	2813±105	3719±395	2745±168	3356±266
CC-011	3	771	2441±162	2248±240	2679±161	2401±213
CC-001	1	10,000	2450±175	2661±125	2628±225	2339±251
CC-010	4	713	2394±131	2813±275	2661±232	2913±197
CC-002	2	10,000	2185±146	2286±165	2246±129	2368±232
<u>ALUMINA/MULLITE (CFBC-EXPOSED FILTERS, 1.5 m)</u>						
AC-128 RA (T3; 572 Hrs)*	--	---	2195±147	1512±181	2118±129**	1283±139**
AC-122 RB (M27; 227 Hrs)*	1	10,000	2380±117	2445±299	2652±196	1916±239
AC-135 RB (M26; 227 Hrs)*	2	10,000	2137± 97	2005±133	2354±246	1808±269
AC-274*** (B19; 716 Hrs)	--	---	2369±147	2469±503	2254±208**	1900±170**
AC-162*** (M32/M31; 716 Hrs)	1	10,000	2389±106	1766±188(b)	2617±152	1601±250
AC-206*** (M28/M32; 716 Hrs)	2	10,000	2474±120	1701±118	2565±150	1407±111
<u>SCHUMACHER DIA SCHUMALITH F40 CLAY BONDED SILICON CARBIDE</u>						
S2097/352C	--	---	1451± 83	1843±239	1450±100	2374±213
S2102/352C	3	771	1393±147	1574±381	1217±120	1344± 60
S2099/352C	1	10,000	1244± 57	1466±156	1204± 51	2202±345
S2104/352C	4	713	1497±127	1338± 93	1238± 80	1359± 76
S2103/352C	2	10,000	1242± 74	1142±125	1323±106	1610± 82
<u>PALL VITROPORE 442T CLAY BONDED SILICON CARBIDE</u>						
R4-148	--	---	2510±158	2654±256	2497±227	2730±238
R5-148	3	771	2804±191	2200±344	2266±160	1836±233
R4-161	1	10,000	2696±182	2236±195	2470±235	2207±264
R9-151	4	713	3272±226	2945±145	2607±273	2326±176
R8-151	2	10,000	2765±214	1905±120	2571±171	1922±252

(a) Nine C-rings per test; Cross-head speed of 0.05 in/min is consistently utilized during conduct of C-ring compressive or tensile testing.

\* Candles did not experience initial fuel ignition event in PCFBC testing.

\*\* Strength testing at 900 °C.

\*\*\* Candles experienced initial fuel ignition event in PCFBC testing.

(b) One C-ring broken during sample preparation. Dimensions still acceptable for strength testing.



**Table 2. Material Properties of the Accelerated Pulse Cycled Candle Filters**

Filter Identification Number	Pulse Cycles	Burst Pressure, psi	Burst Strength, psi	Elastic Modulus, psi x 10 <sup>6</sup>	Poissons Ratio
CC-012	---	1045	2843	5.55	0.11
CC-011	771	705	1914	4.35	0.17
CC-001	10,000	665	1822	5.61	0.21
CC-010	713	845	2292	6.10	0.22
CC-002	10,000	725	1992	4.49	0.16
S2097/352C	---	1125	1896	6.16	0.12
S2102/352C	771	1150	1951	5.45	0.12
S2099/352C	10,000	840	1413	5.51	0.09
S2104/352C	713	1130	1906	6.50	0.24
S2103/352C	10,000	865	1437	5.53	0.17
R4-148	---	830	2125	5.25	0.15
R5-148	771	715	1841	6.12	0.11
R4-161	10,000	670	1690	6.09	0.12
R9-151	713	1130	2896	7.25	0.13
R8-151	10,000	995	2524	6.70	0.14

surfaces of the 10 mm wall alumina/mullite filters, and at distances which were 2 mm and 6 mm from the ID wall. The thermocouples were positioned at various locations along the length of the filter elements (i.e., top, mid-section and bottom; and at ~17 inches and ~44 inches below the flange). A bead of ceramic adhesive was added along the sheathed section of each thermocouple lead wire (i.e., along the outside surface of the filter element), in order to maintain the position of the thermocouples during testing. In addition, a metal strap was placed around each set of thermocouples at the top, mid-section and bottom of the filter elements, in order to provide added security and stabilization (i.e., prevent pull-out) during filter assembly and testing.

The operating temperature and pressure of the W-HTHP filter array during accelerated pulse cycle testing was 1550°F (843°C) and 100 psig. The five candle filter array was subjected to pulse cycling every 2.5 minutes. The pulse cycle electrical "on-time" as controlled by a pulse solenoid valve was determined to be 0.17 sec/pulse. The pulse valve open-to-close time was 0.4 sec. The thermal duty of the pulse cleaning cycle that was delivered to the filter array was comparable to that utilized in the W-APF system at AEP.

At ~0.35 sec after pulse initiation, a maximum temperature drop of ~750°F was identified along the ID wall of the alumina/mullite filter at ~17 inches and at ~31 inches below the flange

(Figure 2). The actual temperature drop may have been greater than the recorded high speed thermocouple temperature response (i.e., masked by thermal radiation effects). As shown in Figure 2, the temperature directly below the flange decreased by 325°F during the pulse cleaning cycle. At ~44 inches below the flange, the temperature was indicated to decrease by 280°F, while at the bottom of the alumina/mullite candle near the radiused end cap, a temperature decrease of 525°F was observed. At each location, the greatest decrease in temperature resulted at ~0.35 sec after pulse initiation. The response of all five thermocouples along the ID wall of the alumina/ mullite candle filter completely or nearly completely recovered to their original temperature 5 seconds after pulsing was initiated.

During pulse cycling, the ID surface of the alumina/mullite filter experienced the greatest reduction in temperature in comparison to the remainder of the filter wall (Figure 3). A drop in temperature was not immediately evident at ~2 mm from the ID surface. Within 5 seconds after delivery of the pulse cleaning cycle, the ID surface reheated to 50°F below its original starting temperature, while with time, heat appeared to be transferred into the matrix (i.e., -20°F after 5 sec at 2 mm from the ID surface).

The high speed thermocouple response data clearly paralleled the stress models developed at Westinghouse which indicated that the deformation energy generated by thermal stress (i.e., pulse cycling) is absorbed at ~2 mm from the ID surface of the candle filter.<sup>(5)</sup> Similarly, the circumferential crack which formed at ~1-2 mm from the ID surface (Figure 1) was considered to reflect the location of highest stress which developed during extended accelerated pulse cycling.

**Thermal Shock Testing.** Testing also focused on calibrating the Westinghouse HTHP test facility in order to identify the temperature gradients which could be generated when increasing severity thermal excursions or transients were delivered to the candle filter array. As shown in Figure 4, a temperature drop of -17.5°F to -195°F was observed within the first five seconds after initiation of the transient (i.e., mild transient: -17.5°F resulted when 200 lb/hr air was introduced into the vessel after combustor flame-out; severe transient: -195°F resulted when 1500 lb/hr air was introduced into the vessel after combustor flame-out). Seven minutes after initiation of the transient, a temperature drop of -53°F to -870°F resulted along the OD surface of the candle filter.

When a newly manufactured, redesigned, radiused end cap Coors alumina/mullite candle filter and several AEP exposed Schumacher Dia Schumalith F40 candle filters were subjected to the increasing severity thermal transients, and subsequently subjected to four additional maximum severity thermal transients, all filters remained intact. Testing was repeated using an as-manufactured, radiused end cap alumina/mullite candle, traditional Pall Vitropore 442T and Schumacher Dia Schumalith F40 candle filters, as well as two aged alumina/mullite candles which had been operated in the Ahlstrom PCFBC test facility. The array was subjected to a series of increasing severity transients. All newly manufactured filters remained intact, while the aged alumina/mullite candles showed evidence of crack formations along the length of both filter elements. The OD and ID high temperature strengths of the intact as-manufactured filters were characterized, and were shown to have been reduced.

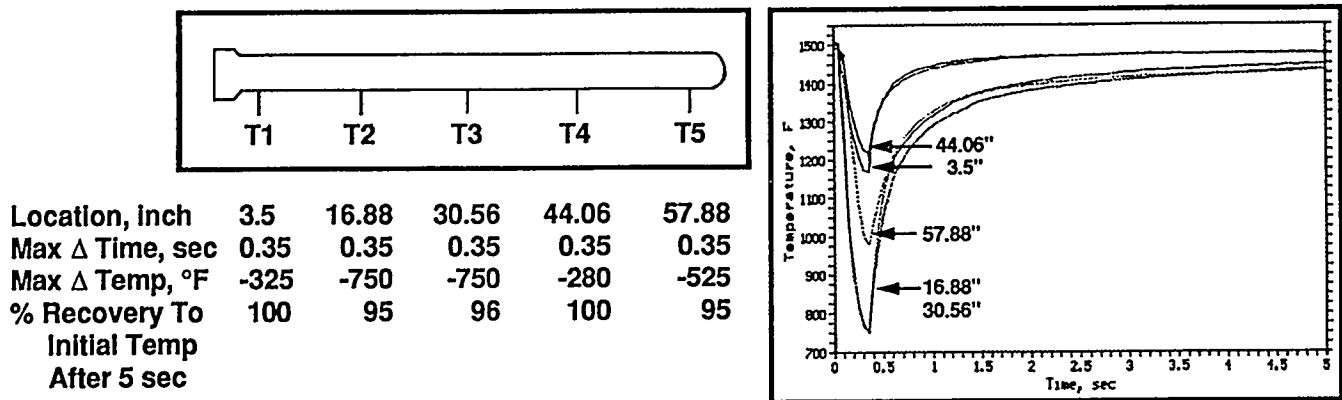


Figure 2. Axial Temperature Profile Along the ID Surface of the Alumina/Mullite Candle Filter as a Function of Time after Initiation of Pulse Cycling

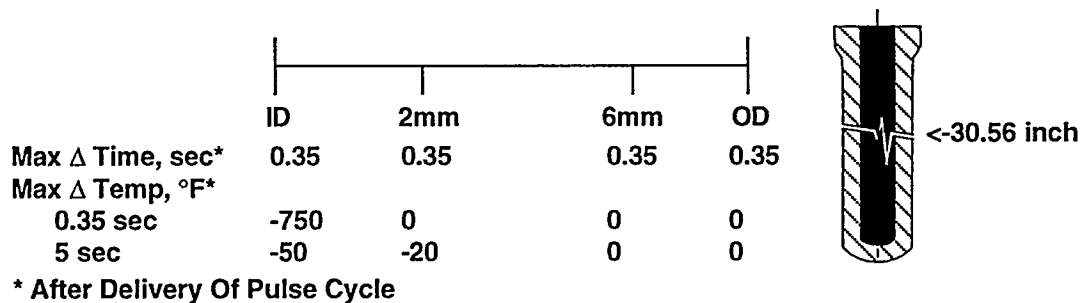
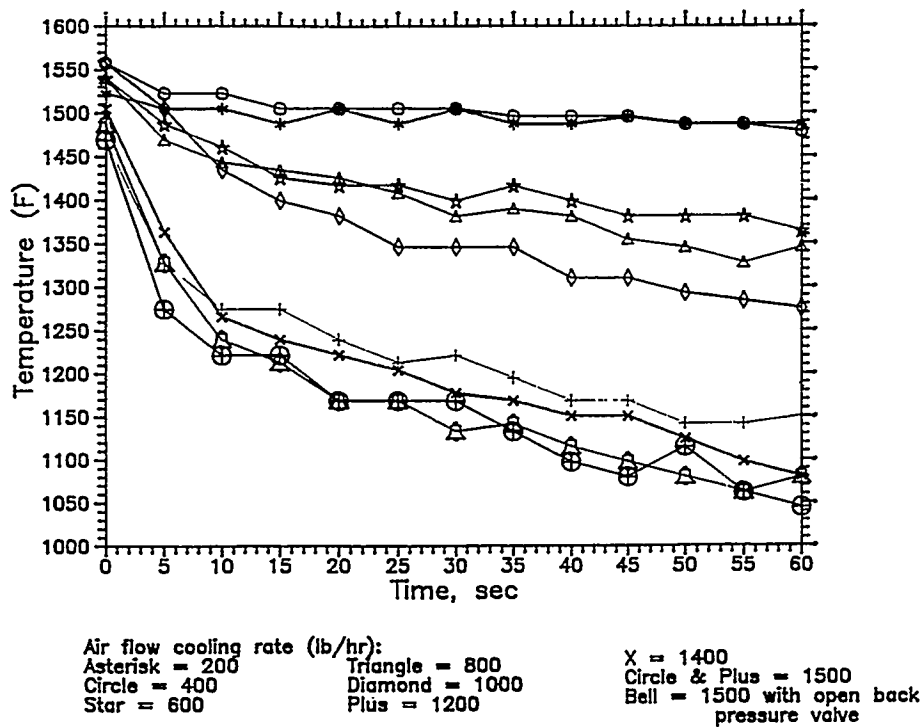


Figure 3. Radial Temperature Profile Through the Wall of the Alumina/Mullite Candle Filter During Pulse Cycling



**Figure 4. Candle Filter Outer Surface Temperature Profile as a Function of Time During Exposure to Increasing Severity Thermal Transients**

Since failure of the filter elements had not been encountered after subjecting the filter array to increasing severity transients, and subsequently four repetitive maximum severity transients, additional testing was conducted with a second set of filters which included a newly manufactured radiused end cap alumina/mullite filter, traditional Pall Vitropore 442T and Schumacher Dia Schumalith F40 candles, and PCFBC aged alumina/mullite candles. This array was subjected to twenty maximum severity thermal transients. Failure of the aged alumina/mullite filters resulted on disassembly of the filter array, while the as-manufactured filter elements were observed to remain intact. At this time it is unclear if failure resulted from the propagation of existing cracks which had been formed during earlier PCFBC testing, or was the result of microstructural phase changes that occurred during process aging of the filter matrix.

Three newly manufactured, radiused end cap alumina/mullite candle filters, which were equipped with high speed thermocouples, a

radiused end cap, 1705 hour, PFBC aged alumina/mullite candle, and an originally designed, 716 hour PCFBC exposed alumina/mullite candle filter were subsequently subjected to thermal transient testing in the W-HTHP system. In order to acquire the maximum amount of information while the delicate high speed thermocouples were functional, three thermal transients were delivered to the filter array. The least severe transient was induced by shutting off the combustor flame, and introducing air at a rate of 200 lb/hr into the vessel, while the moderate and severe thermal transients were accomplished by introducing 800 and 1500 lb/hr air, respectively, into the HTHP filter vessel.

After delivery of the maximum severity thermal transient and a subsequent pulse cycle, the pressure drop across the W-HTHP filter array decreased indicating that a breach in either the candles and/or gaskets had occurred. The facility was operated in this fashion for an additional five hours, prior to rapid cooling and disassembly of the filter array.

During disassembly, the 716 hour PCFBC aged alumina/mullite filter was observed to have failed. Numerous longitudinal sections of the failed candle, as well as the separated end cap were found in the ash hopper. The failed filter was replaced with a newly manufactured alumina/mullite candle, and the system was reheated to 1550°F (843°C). The entire time which had transpired between shutdown and reheat to temperature was 18 hours. Once at temperature, pulse cycling was reinitiated. After delivery of the first pulse, the pressure drop across the system again decreased, and testing was immediately terminated. Once the system had cooled and was disassembled, inspection of the array indicated that the 1705 hour PFBC aged alumina/mullite candle had failed. Unlike the first failure, an ~18 inch section of the failed filter with its end cap was found in the ash hopper. The failed PCFBC candle was removed, and a newly manufactured alumina/mullite candle was reinstalled in its position. The system was reassembled, and reheated to 1550°F (843°C), and testing resumed.

During continued testing, 100 pulse cycles and a maximum severity thermal transient (i.e., 1500 lb/hr) were delivered to the array. During the thermal transient, the vessel experienced a temperature drop of 778°F within the first 15 minutes after the transient had been initiated. After 15 minutes of cooling, the vessel was subjected to a rapid reheat. The time interval between initiation of the maximum severity thermal transient and reheat to 1550°F (843°C) was one hour and thirty-five minutes.

An additional series of 100 pulse cycles was delivered to the array (i.e., pulse cycle #551-651), and was followed by the maximum severity thermal transient, reheat, and dust feed sequence. No indication of dust passage into the effluent gas stream was evident. Testing continued in this fashion for ~48 hours during which time the array

experienced eight complete cycles of 100 pulse cleaning events, a maximum severity transient, and dust feed. After completing this segment of testing, a total of 1451 pulse cleaning cycles had been delivered to the filter array. During reheat and subsequent pulse cycling, failure within the array was once again experienced (i.e., pulse cycle #1471), and the system was shutdown after pulse cycle #1484. The entire vessel was again rapidly cooled and inspected. The newly manufactured candle which had been installed in the position which originally contained the 716 hour PCFBC failed alumina/mullite candle filter was observed to have failed. An ~18 inch section of the bottom of the filter element was found in the ash hopper. A newly manufactured, radiused end cap alumina/mullite candle was reinstalled into the failed filter position, and the unit was reassembled and reheated to 1550°F (843°C). Approximately 20 hours had transpired between shutdown, disassembly, inspection, reassembly, and reheat to temperature. An additional 67 pulse cleaning cycles were delivered to the filter array, followed by a maximum severity thermal transient. This sequence was then repeated, and dust was fed for 15 minutes to determine if the filters and/or gaskets remained intact. One hundred pulse cycles were then delivered to the array, followed by a maximum severity transient and rapid reheat to 1550°F (843°C), and 15 minutes of dust feed. Testing continued in this fashion for an additional eight cycles of 100 pulse cleaning events, a maximum severity thermal transient, reheat, and 15 minutes of dust feed. After completing this segment of testing, the array had experienced a total of 21 maximum severity thermal transients, and 2451 pulse cleaning cycles.

During the initial series of HTHP tests which were conducted at Westinghouse, consideration had been given to the fact that although the alumina/mullite filters had not failed during exposure to 20 maximum severity thermal transients, the candles had not been subjected to

pulse cycling which appeared to be needed to precipitate failure. By having conducted subsequent HTHP testing which combined maximum severity thermal transient testing with pulse cycling, we have addressed this concern, and have shown that five out of the six newly fabricated, radiused end cap, alumina/mullite candle filters survived the combined thermal fatigue/thermal shock transient sequence. The fact that one filter failed may statistically reflect the short, perhaps premature life which may be expected for a limited number of filter elements during field operation.

Since the alumina/mullite candle filters remained intact after completing 21 maximum severity thermal transients, and 2451 pulse cleaning cycles, exposure to the pulse cycling and maximum severity transient testing continued. One hundred pulse cleaning cycles were then delivered to the filter array, followed by a maximum severity transient. Five pulse cleaning cycles were then delivered to the array and subsequently followed by a maximum severity transient. This sequence was repeated four additional times, prior to dust feed. The array was then subjected to five additional maximum severity transients with five pulse cleaning cycles delivered between each transient event, prior to dust feed. Twenty pulse cleaning cycles were then delivered to the array, and followed by a maximum severity transient, twenty pulse cleaning cycles, and a maximum severity transient, and ultimately dust feed. This sequence was repeated twice. Twenty pulse cycles and a maximum severity transient were then delivered to the filter array with an extremely rapid reheat to 1550°F (843°C) in <1 hour. This sequence was repeated seven times.

Ten pulse cycles were then delivered to the array followed by an extreme transient where an additional pulse cycle was delivered to the array as the thermal transient was initiated (i.e., cooling along both OD and ID surfaces). This sequence

was repeated twice, followed by dust feed, and subsequently repeated two additional times.

Ten pulse cycles were delivered to the filter array, followed by a maximum severity transient, with pulse cycling continuing throughout the entire maximum severity transient. This sequence was repeated four additional times. Ten final pulse cycles were delivered to the array, followed by a maximum severity transient, with a single pulse cycle delivered at the beginning of the transient. Testing was terminated, and after cooling, the vessel was disassembled. After 60 maximum severity thermal transients and 3016 pulse cleaning cycles, all five alumina/mullite filters were observed to have remained intact. Crack formations were not visibly evident along any of the filter elements. Two of the five filters were selected and submitted for C-ring strength characterization. During C-ring sample preparation, the alumina/mullite filter matrix was further inspected for crack formations. Cracks were not identified.

As shown in Table 3, the bulk material strength of the alumina/mullite candle filters after exposure to the 60 maximum severity thermal transients, and 3016 pulse cleaning cycles was reduced. A greater loss of bulk material strength occurred along the ID surface of the filter elements (i.e., tensile testing).

The residual strength of the 60 maximum severity thermal transient, 3016 pulse cycled alumina/mullite filter matrix was generally lower than the resulting strength of the alumina/mullite filter element which had been subjected to either 771 or 10,000 accelerated pulse cleaning cycles (i.e., absence of maximum severity thermal transient exposure). This implied that the alumina/mullite candles experienced additional damage to the bulk matrix as a result of exposure to the maximum severity thermal transient conditions (i.e., enhanced crack propagation).

**Table 3. Strength Characterization of the Coors Alumina/Mullite Candle Filters After Exposure to Thermal Shock and Extended Accelerated Pulse Cycling**

Filter Identification Number	Test No.	Accelerated Pulse Cycles	Room Temp., Strength(a)		Hot Strength,(843 ° C)(a)		Burst Strength, psi
			C-Ring Compression, psi	C-Ring Tension, psi	C-Ring Compression, psi	C-Ring Tension, psi	
<u>ALUMINA/MULLITE FILTERS (1.5 m)</u>							
CC-012	--	---	2813±105	3719±395	2745±168	3356±266	2843
CC-000	2/95	3016/60 *	2211±110	2425±183	2281±242	2172±245	TBD
CC-060	2/95	3016/60 *	2262±156	2237±356	2380±159	2346±251	TBD
CC-011	3	771	2441±162	2248±240	2679±161	2401±213	1914
CC-001	1	10,000	2450±175	2661±125	2628±225	2339±251	1822
CC-010	4	713	2394±131	2813±275	2661±232	2913±197	2292
CC-002	2	10,000	2185±146	2286±165	2246±129	2368±232	1992

(a) Nine C-rings per test.

\* 60 Maximum Severity Thermal Transients; 3016 Accelerated Pulse Cycles.

TBD: To Be Determined.

#### **Thermal Transient Temperature Response.**

Table 4 provides a summary of the high speed thermocouple temperature response along both the ID and OD surfaces of the porous ceramic filter element as a function of time (i.e., 50, 300, and 900 sec) after simulated process transient initiation (i.e., 200 lb/hr, 800 lb/hr, and 1500 lb/hr). These data are reported at the top of the filter element immediately below the flange, at the mid-section of the candle, and near the closed end cap of the body. As shown in Table 4,

- Cooling was experienced along the OD surface of the filter element during a thermal transient (i.e., higher temperature along the ID wall).
- Higher temperatures resulted near the flange vs the end cap during exposure to

the mild and moderate severity thermal transients.

- A maximum temperature drop resulted along the mid-section of the filter element during exposure to a maximum severity thermal transient.

When the thermocouple response data were reviewed in terms of the axial temperature distribution along the outer surface of the filter element (Table 5), we see that,

- The matrix directly below the flange was cooled to a lesser extent than along the mid-section and/or end cap of the filter element during exposure to mild, moderate and/or maximum severity thermal transients.

**Table 4. High Speed Thermocouple Response Data Generated During  
Candle Filter Thermal Transient Testing**

Time After Transient	50 sec			300 sec			900 sec		
Wall Location	ID-OD	ID-OD	ID-OD	ID-OD	ID-OD	ID-OD	ID-OD	ID-OD	ID-OD
Transient Severity, lb/hr	200	800	1500	200	800	1500	200	800	1500
Candle Location, °F									
Top	1500-1495	1500-1450	1470-1390	1475-1465	1300-1250	1150-1100	1390-1380	975-950	700-700
Middle	1500-1475	1500-1400	1500-1275	1450-1425	1225-1100	975-900	1280-1250	800-750	550-520
Bottom	1500-1475	1500-1400	1500-1300	1425-1400	1240-1100	1025-825	1250-1210	805-750	550-500

- With continued exposure to the thermal transient condition, the temperature difference along the length of the filter body increased.

**Table 5. Outer Surface Axial Temperature Gradient Established Along the Length of the Candle Filter During Thermal Transient Testing**

Transient	Time		
	50 sec	300 sec	900 sec
200 lb/hr	Δ 20°F*	Δ 65°F	Δ 170°F
800 lb/hr	Δ 50°F	Δ 150°F	Δ 200°F
1500 lb/hr	Δ 90°F	Δ 275°F	Δ 200°F

\* Temperature Difference Between Flange and End Cap

During exposure to the thermal transient event, a temperature gradient was established through the filter wall. As shown in Table 6,

- Higher temperatures resulted along the ID wall in comparison to the OD surface.
- As the severity of the transient increased, a greater change in temperature initially existed across the filter wall.
- A greater change in temperature was initially experienced across the wall along the mid-section and end cap area of the filter body in comparison to the matrix directly below the filter element flange.

**Candle Failure Characteristics.** The alumina/mullite candle filter which had been exposed for 716 hours in the PCFBC gas environment failed after being subjected to five pulse cleaning cycles, and a mild, moderate, and maximum severity thermal transient in the 1550°F (843°C) Westinghouse HTHP test facility.



**Table 6. Temperature Gradients Established Through the Wall of the Alumina/Mullite Candle Filter During Thermal Transient Testing**

Time, sec	Area Below Flange		
	50	300	900
200 lb/hr	$\Delta$ 5°F*	$\Delta$ 10°F	$\Delta$ 10°F
800 lb/hr	$\Delta$ 50°F	$\Delta$ 50°F	$\Delta$ 25°F
1500 lb/hr	$\Delta$ 80°F	$\Delta$ 50°F	$\Delta$ 0°F

Time, sec	Mid-Section of Filter Element		
	50	300	900
200 lb/hr	$\Delta$ 25°F	$\Delta$ 25°F	$\Delta$ 30°F
800 lb/hr	$\Delta$ 100°F	$\Delta$ 125°F	$\Delta$ 50°F
1500 lb/hr	$\Delta$ 225°F	$\Delta$ 75°F	$\Delta$ 30°F

Time, sec	End Cap		
	50	300	900
200 lb/hr	$\Delta$ 25°F	$\Delta$ 25°F	$\Delta$ 40°F
800 lb/hr	$\Delta$ 100°F	$\Delta$ 140°F	$\Delta$ 55°F
1500 lb/hr	$\Delta$ 200°F	$\Delta$ 200°F	$\Delta$ 50°F

\* ID Temp - OD Temp.

Fracture occurred at ~32-34 inches below the flange of the PCFBC exposed filter element. The lower section of the filter element was observed to have fractured longitudinally, generating several 8-12 inch sections. Smaller fractured filter segments were also evident. What was most interesting was that the end cap of the filter had become completely separated from the remainder of the body (i.e., forming a "hockey puck"). Hackel lines were readily evident through the fractured wall. These lines, as well as the longitudinal fractures, and the length of the alumina/mullite filter body that remained in the

holder were comparable to what had previously been experienced in the field.

The 1705 hour PFBC aged alumina/mullite candle filter which failed after restart of the Westinghouse HTHP test facility failed at ~39-40 inches below the flange. Unlike the PCFBC aged candle, when the redesigned, radiused end cap filter failed, the lower section of the filter body fell into the ash hopper as an intact segment without evidence of longitudinal crack formations. Questions have been raised as to whether the radiused end cap was responsible for the absence of the longitudinal fracturing of the alumina/mullite filter matrix.

After the as-manufactured, alumina/mullite filter experienced eleven maximum severity thermal transients and 1466 pulse cleaning cycles, failure was observed to be similar to that encountered in the 1705 hour, PFBC aged, radiused end cap alumina/mullite filter element. Fracture occurred at ~27.5-29.5 inches below the flange, with the lower section of the filter body falling into the ash hopper as a complete 18-20 inch section. Approximately 10 inches of the candle that had been originally located between these two sections showed evidence of longitudinal cracking. When further inspected, the ~27.5-29.5 inch section of the filter body was observed to contain two 4-6 inch cracks radiating longitudinally (i.e., in the direction of the flange) from the fractured surface. Again the question was raised as to whether the redesigned radiused end cap limited longitudinal crack propagation in the alumina/mullite filter matrix.

HTHP testing that was conducted at Westinghouse indicated that

- Severe thermal transient conditions experienced in the field (i.e., process upset conditions) can be realistically simulated.

- Failure of the alumina/mullite filters can be simulated using aged filters, (i.e., Hackel lines; mid-body failure location).
- As-manufactured filters tend to be unaffected (i.e., remain intact) when subjected to thermal transient conditions. This was clearly demonstrated by the fact that after 60 maximum severity thermal transients and continued pulse cycling, five out of six candles did not experience failure. The thermal transient testing that the as-manufactured filters encountered in the Westinghouse HTHP test facility exceeded the severity of the thermal transients which were previously experienced in the Westinghouse APF system during field testing.<sup>(5)</sup>

Although the Westinghouse HTHP test facility can clearly demonstrate the filtration characteristics of a particular filter element (i.e.,  $\Delta p$ , particulate collection efficiency, flange sealing, dust cake removal, response to thermal transients and pulse cycling), testing appears to be limited to qualifying materials in terms of their natural aging or life. Limited aging may be accomplished during testing in the Westinghouse HTHP test facility, however, generating the response of the microstructure to the process gas environment which contains sulfur, chlorides, steam, etc., requires field exposure as a function of extended operating time. Currently these parameters are considered to have a significant impact on the response of the ceramic filter materials to service conditions, and to ultimately influence filter element life. Further HTHP testing of field-tested candles in on-going and future test programs is recommended.

**Comment.** The positions of the fractured surfaces that were generated during HTHP testing were virtually identical to those observed during

field or service operation. These fractures were generally at or below the mid-section of the filter element. The repeatable nature of this failure may correspond to the temperature profile generated along the ID wall at this location during pulse cycling. As previously discussed, the mid-section of the alumina/mullite filter experienced the greatest drop in temperature, followed by what appeared to be a sharp rise in temperature, and a subsequent decrease along the length of the filter body proceeding in the direction of the closed end cap. The temperature gradient may be responsible for enhanced thermal fatigue in this area. Similarly, the greatest difference in temperature between the top and bottom of the filter element was observed to be near the mid-section of the candle when the filter was subjected to maximum severity thermal transient conditions. By combining the thermal gradients, the compound effect in this area may support a region where maximum stress is encountered, and ultimately where failure along the alumina/mullite filter matrix is most likely to occur.

## Field Testing

Operation of the W-APF system at the AEP PFBC Tidd Demonstration Plant in Brilliant, Ohio, was conducted in five test campaigns. Schumacher Dia Schumalith F40 clay bonded silicon carbide candle filters were exposed to process operating temperatures ranging between 620 and 790°C for periods of 464.5, 1295, 1279, and 1705.8 hours in Test Segments #1 through #4, and between 760 and 845°C for 1110 hours in Test Segment #5 (Table 7). In Test Segment #4, eight Schumacher Dia Schumalith FT20, eight Coors alumina/mullite, and eight Pall Vitropore 442T candles were included in the 288 candle filter system, while 98 Coors alumina/mullite, and 153 Pall Vitropore 442T candles were installed in the W-APF in Test Segment #5. During conduct of Test Segments #4 and #5 at AEP, advanced, second generation filter

**Table 7. W-PFBC Hot Gas Filter Testing at AEP**

PFBC Test Segment	1	2	3	4	5
	10-92-12/92	7/93-9/93	1/94-4/94	7/94-10/94	1/95-3/95
Operating Time, Hrs.	464	1295	1279	1705	1110
Operating Temperature, °C	730-790	620-790	650-780	660-760	760-845
Number of Filter Elements					
Schumacher F40	384	384	384	258	5
Schumacher FT20	----	----	----	8	----
Pall Vitropore 442T	----	----	----	8	153
Coors Alumina/Mullite	----	----	----	8	98
3M CVI-SiC Composite	----	----	----	3	10
DuPont PRD-66	----	----	----	3	22

elements were also installed within various arrays. The following sections present a discussion of the currently available Test Segment #4 and #5 material characterization analyses for the Schumacher Dia Schumalith F40, Schumacher Dia Schumalith FT20, Pall Vitropore 442T, and Coors alumina/mullite matrices. Materials characterization analyses for the advanced, second generation filters are presented elsewhere.<sup>(6)</sup>

#### **Schumacher Dia Schumalith F40.**

Schumacher Dia Schumalith F40 surveillance candles successfully achieved 5855 hours of operation in the W-APF system at Tidd. The residual bulk strength of the Schumacher Dia Schumalith F40 matrix was determined via room temperature and process temperature C-ring compressive and tensile testing using 15 mm samples that were cut with a diamond wheel from the PFBC exposed filter elements. As shown in Figure 5, the bulk strength of the Schumacher Dia Schumalith F40 matrix decreased during the initial 1000-2000 hours of PFBC operation. With continued operation, however, the bulk strength of the Schumacher Dia Schumalith F40 matrix

remained constant. The residual or "conditioned" strength was considered to result from the complete or nearly complete crystallization of the binder phase that encapsulated the silicon carbide grains, as well as the bond posts or ligament surfaces (Figure 6).

In order to ascertain whether the Schumacher Dia Schumalith F40 filter matrix experienced creep during operation in the PFBC environment, the overall length of the surveillance filter elements were measured after the various test campaigns, and compared to their initial, as-manufactured lengths. After 5855 hours of operation in the W-APF at AEP, the 1.5 m elements were observed to have elongated by 5-7 mm. Cracks, as a result of high temperature creep, were not evident along the external surface of the filter elements particularly within and/or below the densified section of the flange.

During operation of the W-APF in the initial test segments, failure of the Schumacher Dia Schumalith F40 filter elements had previously occurred at the base of the flange, primarily during cooldown after ash bridging extensively deposited

- PFBC -

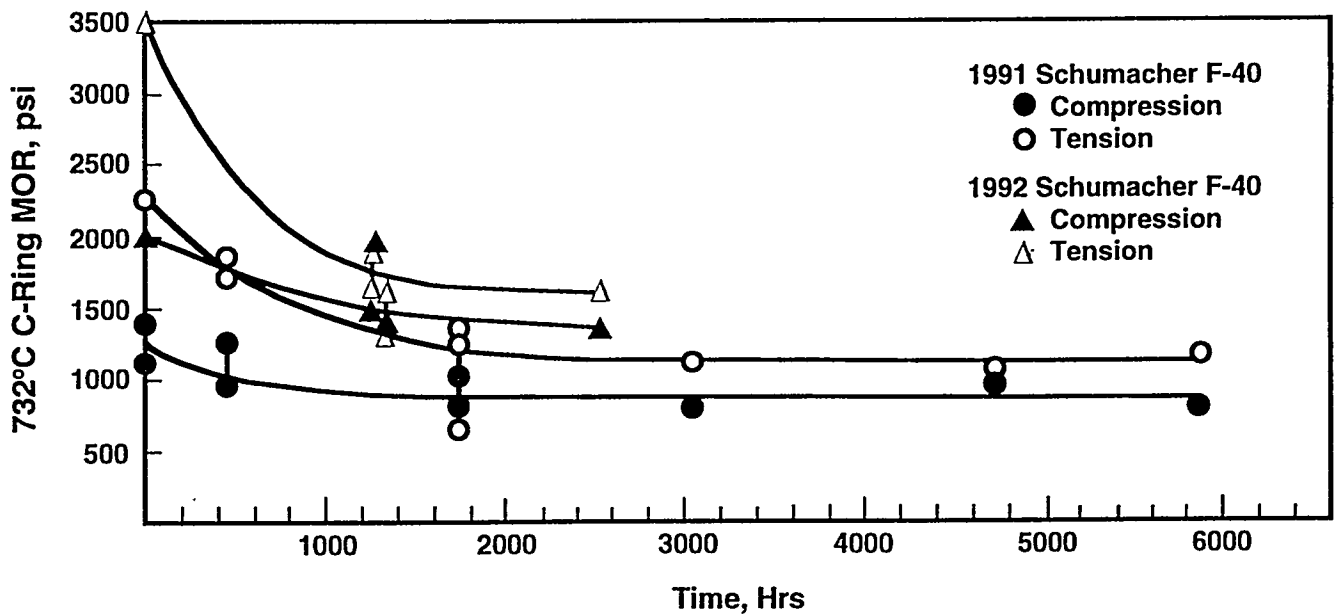
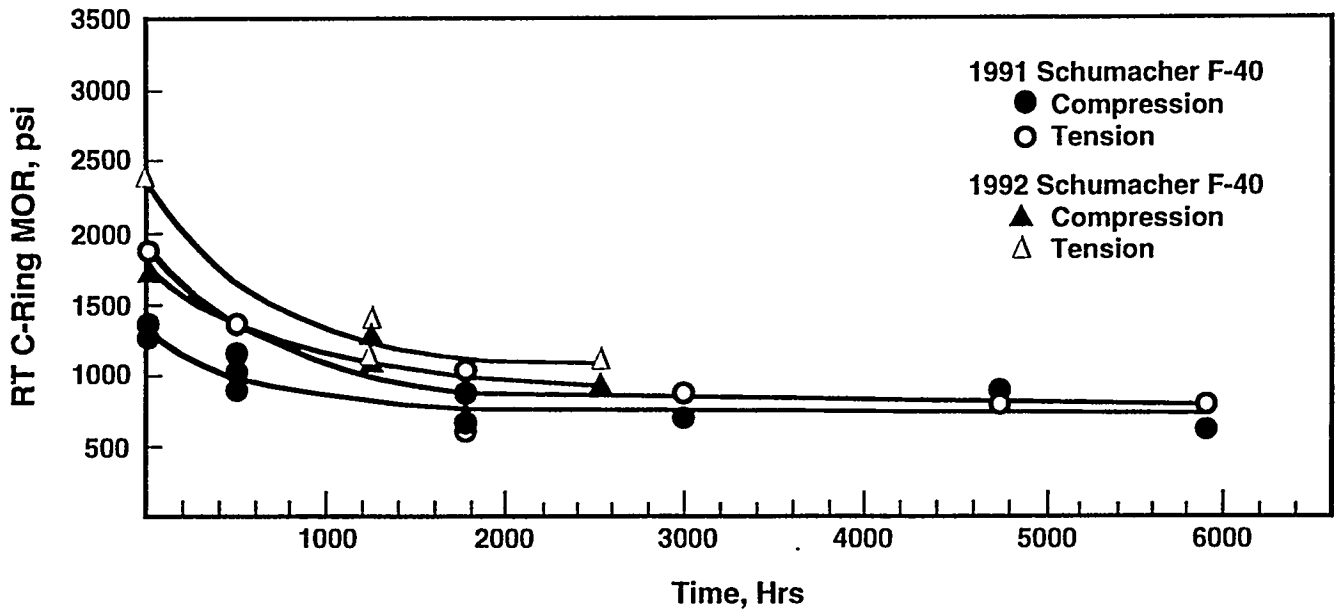
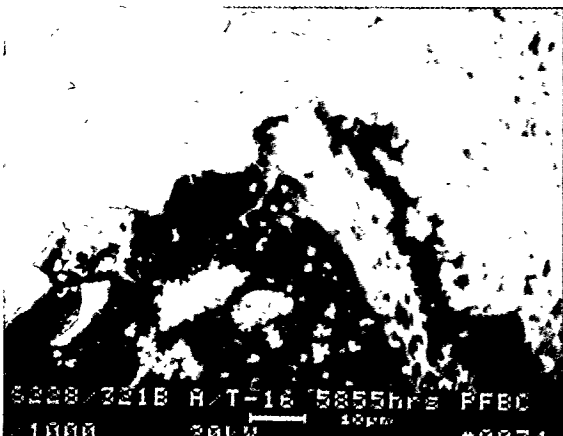


Figure 5. Residual Strength of the Schumacher Dia Schumalith F40 Candle Filters During Operation in the W-APF at AEP

(a)



(b)



(c)



**Figure 6. Micrographs Illustrating Crystallization of the Binder Phase in the Schumacher Dia Schumalith F40 Filter Matrix After 5855 Hours of Operation in the W-APF at AEP**  
(a) Support Matrix  
(b) Binder Coated Grain  
(c) Cross-Sectioned Binder Phase

finer between adjacent filter elements, and/or the plenum support pipe and dust sheds. Failure of the Schumacher Dia Schumalith F40 filter matrix also resulted when a densified plug of fines was embedded within the ID bore of the filter element. The difference between the thermal coefficient of expansion of the ash, ceramic, and/or metal structure was considered to be responsible when failure of the Schumacher Dia Schumalith F40 clay bonded silicon carbide filters occurred at AEP.

**Schumacher Dia Schumalith FT20.** Eight improved, high temperature, creep resistant Schumacher Dia Schumalith FT20 clay bonded silicon carbide candles were installed and operated in the W-APF system in Test Segment #4 at AEP. The initial bulk strength of the Schumacher Dia Schumalith FT20 matrix was stronger than the 1991 Schumacher Dia Schumalith F40 filter production lot which had been used throughout the entire AEP test program. The as-manufactured bulk strength of the Schumacher Dia Schumalith FT20 matrix was, however, comparable to the 1992 Schumacher Dia Schumalith F40 filter production lot.

As shown in Table 8, the residual bulk strength of the Schumacher Dia Schumalith FT20 matrix after 1705 hours of successful operation in the W-APF at AEP was comparable to that of the initial bulk strength of the filter matrix. Scanning electron microscopy/energy dispersive x-ray analyses (SEM/EDAX) are currently being performed to discern whether changes within the morphology of the binder phase that encapsulates the silicon carbide grains have occurred.

**Pall Vitropore 442T.** During operation at AEP in Test Segment #4, eight Pall Vitropore 442T filter elements were installed and operated in

**Table 8. Residual Strengths of the Porous Monolithic Candle Filters After Operation in the W-APF at AEP**

Filter Matrix	Candle Filter Location	Test Segment No.	Operating Time, Hrs	C-Ring Testing			
				Room Temperature Strength, psi		High Temperature (732°C) Strength, psi	
				Compression	Tension	Compression	Tension
Schumacher Dia Schumalith F40 - 1991 Production Lot							
S153/317B	---	---	---	1300±213	1907±111	1416±127	2328±228
S504/322B	B/T-1	1	464	1120±123		1226±116	
S436/321B	B/M-1	1	464	1096±116		1172±134	
S193/318B	B/B-1	1	464	1147±119		1245±108	
S065/314B	A/B-6	1	464	940± 60		1056±131	
S106/317B	B/B-45	1	464	1180±98		1230±127	
S324/319B	B/B-9	1	464	1083±148	1438±108	1137±101	1778±246
S109/317B	B/B-41	1	464	1140±120	1424±162	1132±112	1873±174
S215/378B	B/M-22	1,2	1760	908±72	1117±91	1064±72	1418±122
S447/322B	A/T-22	1,2	1760	794±50	709±71	1028±94	973±121
S455/322B	B/T-22	1,2	1760	793±58	711±89	989±77	885±54
S523/322B	C/T-22	1,2	1760	793±39	1016±134	968±96	1252±241
S418/321B	B/T-16	1,2,3	3038	720±57	944±172	890±65	1284±199
S422/322B	B/B-16	1,2,3,4	4734	870±145	816±112	1031±105	1139±160
S228/318B	A/T-16	1,2,3,4,5	5855	592±56	763±87	777±57	1208±99
						891±52 (a)	966±47 (a)
Schumacher Dia Schumalith FT20							
S199/315E	---	---	---	2296±261	2268±167	3034±148	2708±360
S039/312E	C/M-15	4	1705	2283±184	2370±238	3041±238	3102±272
Pall Vitropore 442T							
R2-325	---	---	---	2857±186	2574±177	3430±221	3029±149
R5-325	B/M-20	4	1705	2311±231	2034±139	2453±187	2138±180
R2-360	C/T-1	5	1110	2569±132	2277±156	2721±138	2201±212
						2454±214 (a)	2115±238 (a)
Coor Alumina/Mullite							
DC-013	---	---	---	2575±182	2721±415	3107±276	3353±231
DC-003	B/M-16	4	1705	2475±189	2903±289	2738±161	3291±246
DC-056	A/T-1	5	1110	2079±140	2392±130	2368±93	2636±238
						2512±107 (a)	2717±167 (a)
DC-068	A/T-1	5	1110	1958±68	2544±214	1800±135	2542±196
						2079±85 (a)	2659±109 (a)

(a) High Temperature Strength Testing Conducted At 843°C.

the W-APF system. All eight filter elements were successfully operated for a period of 1705 hours. As shown in Table 8, a loss of bulk material strength resulted in the Pall Vitropore 442T filter matrix (i.e., 19% room temperature and 29% process temperature compressive strength; 21% room temperature and 29% process temperature tensile strength).

Three of the Test Segment #4 Pall Vitropore 442T filter elements were reinstalled in the W-APF, and were successfully operated for a period of 1110 hours in Test Segment #5. Post-test inspection indicated that the Pall Vitropore 442T filters elongated by 17-20 mm after 2815 hours of operation at AEP. Cracks as a result of high temperature creep were not evident along the elongated Pall Vitropore 442T candle filter body, particularly in the area of the filter directly below the flange.

During operation in Test Segment #5, 150 newly manufactured Pall Vitropore 442T candle filter elements were installed in the W-APF system. All candles remained intact after 1110 hours of operation. Post-test characterization of seventeen elements indicated that the filters elongated by 0-4 mm. Since the filter elements were identically manufactured for both test segments at AEP, the limited elongation of the clay bonded silicon carbide filter matrix after 1110 hours of operation in the 760-845°C, PFBC environment in test Segment #5 vs 17-20 mm elongation after 1705 hours of operation in the 660-760°C, PFBC environment implied that aging or a lag time was required to initiate high temperature creep within the binder containing Pall Vitropore 442T filter matrix. Currently SEM/EDAX analyses are being conducted to discern whether phase and/or morphology changes have occurred within the 1110 hour, PFBC exposed, Pall Vitropore 442T filter matrix.

**Alumina/Mullite.** Eight Coors alumina/mullite filters were installed in the W-APF system during conduct of Test Segment #4 at AEP. All Coors alumina/mullite filter elements remained intact after 1705 hours of operation in the 660-760°C PFBC gas environment. The residual bulk strength of the 1705 hour PFBC-exposed Coors alumina/mullite filter matrix was comparable to that of the as-manufactured Coors filter matrix (Table 8).

Three of the Test Segment #4 Coors alumina/mullite filters were installed in the W-APF system prior to initiating Test Segment #5. Post-test inspection indicated that all three of the Coors alumina/mullite filters remained intact, achieving 2815 hours of successful operation. Materials characterization of the 2815 hour, PFBC exposed, Coors alumina/mullite filter matrix is currently being conducted.

In addition, 95 newly manufactured Coors alumina/mullite filters were installed in the W-APF system during conduct of Test Segment #5 at AEP. After 1110 hours of PFBC operation at temperatures of 760-845°C, two of the 95 filters had failed, while the remaining 93 Coors alumina/mullite filters remained intact. One of the Coors alumina/mullite filters failed directly below the flange, while the second filter fractured at approximately 1000 mm below the flange. The circumferential fracture of the mid-body failed Coors alumina/mullite filter was similar to the fracture patterns generated during HTHP thermal transient testing at Westinghouse vs the longitudinal fractures experienced in the matrix during operation in the Ahlstrom PCFBC test facility in Karhula, Finland. The difference between the nearly circumferential vs longitudinal fracture may reflect the response of the matrix to the lower operating temperatures and/or the redesigned end cap and uniform wall thickness that

was utilized to produce candle filters for use at AEP and at Westinghouse.

Characterization of the residual bulk strength of the 1110 hour, PFBC-exposed, Coors alumina/mullite filter elements indicated that the Coors alumina/mullite matrix tended to lose strength during operation in the 760-845°C, oxidizing environment (i.e., 22% room temperature and 33% process temperature compressive strength; 9% room temperature and 23% process temperature tensile strength). These data perhaps imply a sensitivity of the Coors alumina/mullite matrix to process operating temperature which may either induce or accelerate phase changes, or enhance crack propagation properties along the ID surface and/or through the 10 mm filter wall. SEM/EDAX analyses of the 1110 hour, PFBC exposed, Coors alumina/mullite filter matrix are currently being conducted.

Post-test inspection of the W-APF arrays indicated that one of the Coors alumina/mullite filters had a hairline crack at ~8 inches from the end cap of the filter element. After removal of the element from its filter holder, ash was evident within the ID bore of the candle. Although the hairline crack was visibly evident, tracking of fines across the 10 mm candle filter wall was not apparent. Fracture of the Coors alumina/mullite matrix was considered to have occurred when a densified plug of fines was embedded within the ID bore of the filter element. The difference in thermal coefficient of expansion of the ash and the porous ceramic filter was considered to be responsible for crack initiation within the alumina/mullite filter body.

**Comment.** Table 9 provides a summary of the burst pressure, hoop stress, elastic modulus, and Poissons ratio for various, first generation, monolithic filter elements which were operated in the W-APF system at AEP. What has clearly been

demonstrated was that the Schumacher Dia Schumalith F40 matrix experienced numerous phase changes and a loss of bulk material strength, but attained a "conditioned" strength of 600-800 psi which was acceptable for extended operation in the PFBC environment. Although the Coors alumina/mullite filter matrix experienced a loss of bulk strength in Test Segment #5, and the Pall Vitropore 442T filter elements experienced elongation in Test Segment #4, and loss of bulk material strength in Test Segments #4 and #5, virtually no change in bulk strength was evident for the improved, high temperature, creep resistant Schumacher Dia Schumalith FT20 filter matrix after 1705 hours of operation at AEP.

### Creep Testing

**As-Manufactured Filter Materials.** In the PCFBC environment at the Ahlstrom test facility in Karhula, Finland, elongation and catastrophic failure of the clay bonded silicon carbide Pall Vitropore 442T candle filter elements resulted after 500-1341 hours of operation at temperatures of 830°C. Examination of the flange area and fractured sections indicated that the clay bonded silicon carbide, Pall Vitropore 442T filter matrix experienced creep crack growth as the principal failure mechanism.

As a result, Westinghouse initiated a test effort which subjected the clay bonded silicon carbide filter materials to high temperature creep testing utilizing a four-point bend fixture. Test samples were 76 mm x 6.4 mm (3 in x 0.25 in) bend bars which were removed from the candle filters. The bend bars were subjected to temperatures of 1550°F for 300 hours with an applied load of 500 or 700 psi. Figure 7 illustrates that creep under these conditions resulted in the coarse matrix of the Schumacher Dia Schumalith F40 filter body, as well as in the Pall Vitropore 442T filters. Both of these materials contain of a clay binder which



**Table 9. Material Properties of the Porous Monolithic Candle Filters After Operation in the W-APF at AEP**

Filter Element	Operating Hours	Test Facility	Location	Burst Pressure, psi	Ultimate Hoop Stress, psi	Elastic Modulus, psi x 10 <sup>6</sup>	Poissons Ratio
Schumacher Dia Schumalith F40 - 1991 Production Lot							
S455/322B	1760	PFBC	B/T-22				
S418/321B	3038	PFBC	B/T-16	540	914	3.78	0.19
S422/322B	4734	PFBC	B/B-16	495	845	4.24	0.18
Schumacher Dia Schumalith F40 - 1992 Production Lot							
S528/315C	2574	PFBC	B/B-16	695	1168	5.26	0.38
S452/315C	1296	PFBC	B/B-22				0.14
S291/314C	1278	PFBC	B/T-17	710	1191	6.26	
Schumacher Dia Schumalith F40 -1993 Production Lot							
S1788/348C	-----	-----	-----	1370	2267	5.89	0.25
S2187/355C	-----	-----	-----	1140	1893	6.26	0.31
S2134/355C	1268	PFBC	B/B-22	740	1243	4.7	0.42
S1742/348C	1705	PFBC	B/T-22	780	1312	5.99	0.18
S2129/355C	2973	PFBC	B/B-18	1010	1705	7.28	0.25
Schumacher Dia Schumalith FT20							
S199/315E	-----	-----	-----	665	1703	7.3	0.17
S039/312E	1705	PFBC	C/M-15	555	1426	6.93	0.16
Pall Vitropore 442T - Production Lot No. 1							
R2-110	514	PCFBC	B15	725	1925	6.67	0.18
R2-118	1026	PCFBC	B38	626	1602	5.28	0.18
Pall Vitropore 442T - Production Lot No. 2							
R7-133	-----	-----	-----	513	1307	5.93	0.14
R7-134	514	PCFBC	B6	630	1594	5.92	0.14
Pall Vitropore 442T - Production Lot No. 3							
R4-148	-----	-----	-----	830	2125	5.25	0.15
R5-140	1026	PCFBC	B88	575	1452	4.83	0.16
R2-151	1026	PCFBC	B19	590	1493	4.49	0.17
Pall Vitropore 442T - 1994 Production Lot Replacement							
R2-325	-----	-----	-----	970	2499	6.52	0.19
R5-325	1705	PFBC	B/M-20	310	771	5.66	0.15
Coors Alumina/Mullite							
DC-013	-----	-----	-----	860	2317	5.7	0.23
DC-003	1705	PFBC	B/M-16	835	2319	5.76	0.23

# Bending Creep 500 psi, 1550 F

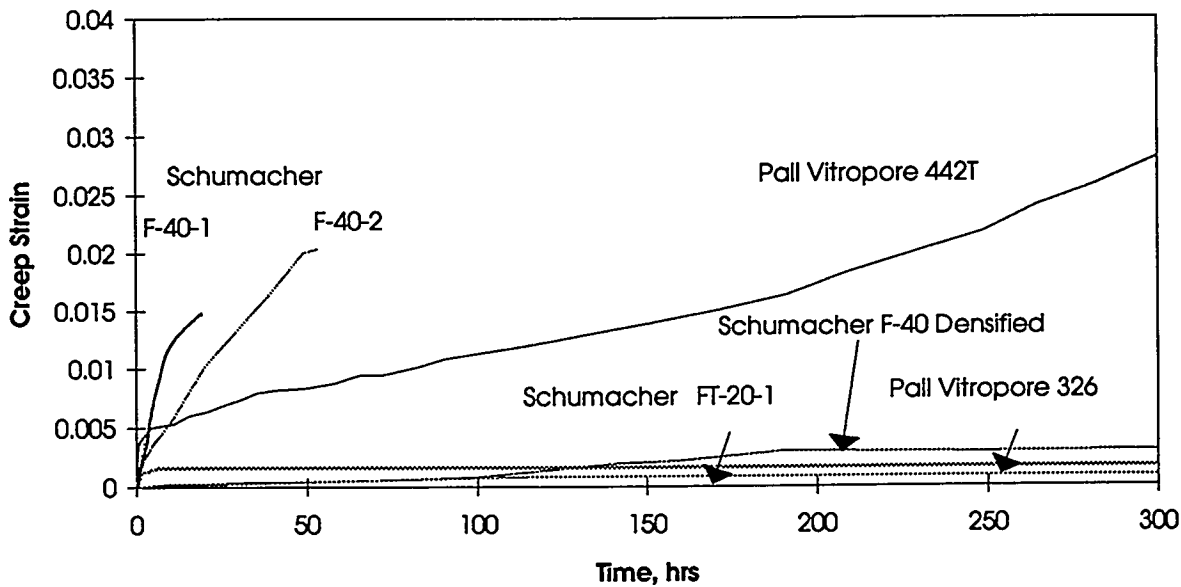


**Figure 7. High Temperature Creep of the As-Manufactured Clay Bonded Silicon Carbide Candle Filter Materials**

bonds adjacent silicon carbide grains to each other. At high temperature, the binder tends to soften, and under an applied load, both matrices experience creep.

Further efforts were also conducted using sections of material that were removed from the densified flange section of the clay bonded silicon carbide Schumacher Dia Schumalith F40 filter element. High temperature creep of the dense F40 matrix was shown to be limited in comparison to the coarse Schumacher Dia Schumalith F40 or the Pall Vitropore 442T matrix. An interesting observation which was made was that the smaller the silicon carbide grain size which was used to manufacture the filter matrix (i.e., the greater number of ligament bond posts per unit volume), the higher the strength of the filter material, and the lower the high temperature creep.

Schumacher reformulated the binder phase of its Dia Schumalith F40 filter matrix, retained its traditional fibrous aluminosilicate membrane layer, but constructed the matrix with finer grit silicon

carbide, producing what was considered by Schumacher to be a stronger, higher temperature, creep resistance filter matrix. When the Schumacher Dia Schumalith FT20 matrix was subjected to high temperature four-point bend creep testing at Westinghouse, the matrix demonstrated excellent creep resistance under the 500-700 psi applied load at temperatures of 1550°F. Since the Schumalith Dia Schumalith FT20 filter was constructed with a uniform body (i.e., absence of the dense/coarse flange transition section as in the Dia Schumalith F40 candle filter body), Westinghouse felt that selection and use of this filter would be acceptable at Tidd, and eight Schumacher Dia Schumalith FT20 filter elements were installed in the W-APF at AEP in Test Segment #4. These filter were successfully operated for 1705 hours at nominal temperatures of 732°C.

Recently Pall has produced an improved creep resistance binder silicon carbide filter matrix. As shown in Figure 7, high temperature creep of the Pall 326 matrix is comparable to that of the

Schumacher Dia Schumalith FT20, as well as the densified Schumacher Dia Schumalith F40 matrix.

Additional high temperature creep testing which was conducted using the Coors P-100A-1 alumina/mullite filter matrix indicated that the oxide-based filter material did not exhibit creep characteristics at 1550°F under applied loads of either 500 or 700 psi. This was attributed to the absence of the clay binder or a significant amorphous phase content in the filter matrix.

**Field-Tested Filter Materials.** High temperature creep testing was also conducted on bend bars removed from the Schumacher Dia Schumalith F40 filter matrix which experienced 3038 hours of operation in the PFBC environment at AEP, and from the Pall Vitropore 442T filter matrix which experienced 1341 hours of test operation in the PCFBC environment at Karhula, Finland (Figures 8 and 9). Although both filters were operated at different temperatures in the field, bend bars from each matrix were subjected to creep testing at 1550°F. Crystallization of the binder phase in the Schumacher Dia Schumalith F40 filter matrix occurred after 3038 hours of operation at Tidd which appeared to reduce creep in the filter matrix. Conversely operation of the Pall Vitropore 442T filter matrix at temperatures of 830°C at Karhula may not have only initiated crystallization of the binder, but due to the high temperature, oxidation may also have been induced along the surface of the silicon carbide grains which increased the concentration of SiO<sub>2</sub> (i.e., non-crystallized, amorphous glass) at the binder/grain interface. The presence of SiO<sub>2</sub> at the binder/grain interface may have subsequently enhanced creep of the Pall Vitropore 442T matrix under load in comparison to the as-manufactured filter matrix. Further effort will be needed to support the above scenario.

## FUTURE WORK

- Complete materials characterization of the porous ceramic filter coupons that were exposed for ~10,000 hours above the AEP combustor freeboard area.
- Submit the Final Report for this program.

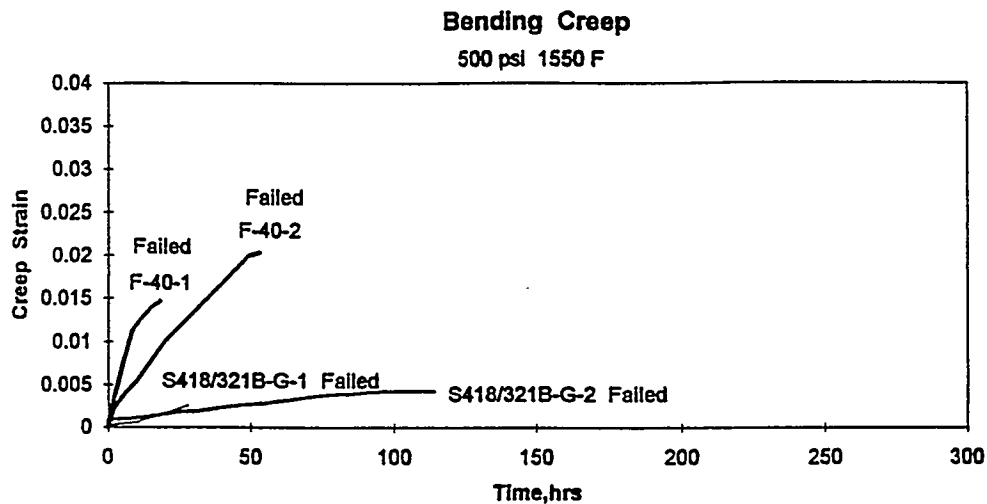
## ACKNOWLEDGMENTS

We wish to acknowledge Mr. Theodore J. McMahon, Mr. Norman Holcombe, and Ms. Diane Hooie at DOE/METC for their guidance and support throughout the entire test program, as well as Mr. Mike Mudd and Mr. John Hoffman at AEP, for their continued support.

We also wish to acknowledge the efforts of Mr. Bob Walko for performing the destructive strength testing, Mr. Art Fellers, Mr. George Schneider, Mr. Joe Condle, Mr. Tony Gasparovic, and Mr. John Meyer for participating in the HTHP test program, and Mr. Tom Mullen for performing the analytical microscopy efforts.

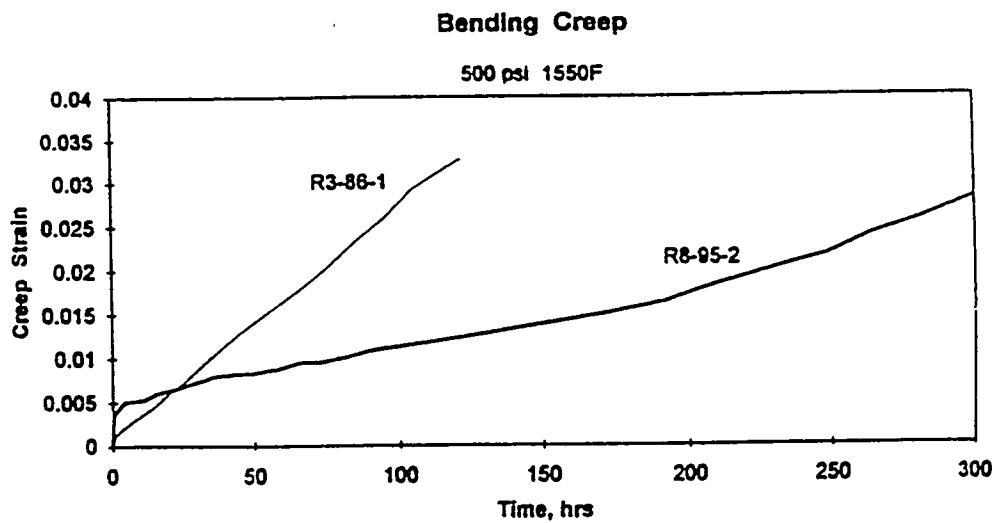
## REFERENCES

1. T. E. Lippert, G. J. Bruck, Z. Sanjana, and R. A. Newby, "Westinghouse Advanced Particle Filter System," *Proceedings of Advanced Coal-Fired Power Systems '95 Review Meeting*, June 27-29, 1995, Morgantown, WV.
2. M. A. Alvin and T. E. Lippert, "Mechanical Analysis of a Cross Flow Filter," Final Report, Westinghouse Science and Technology Center, DOE/METC Contract No. DE-AC21-86MC23252, January 31, 1995.



F40: As-Manufactured  
S418/321B: 3,038 Hours PFBC (732 °C)

**Figure 8. High Temperature Creep of the As-Manufactured and Field-Tested Schumacher Dia Schumalith F40 Filter Matrices**



R8-95: As-Manufactured  
R3-86: 1,341 Hours PCFBC (830 °C)

**Figure 9. High Temperature Creep of the As-Manufactured and Field-Tested Pall Vitropore 442T Filter Matrices**

3. W. R. Wheeler, "Failure Modes Assessment of Ceramic Candle Filters," Adapco, Report No. 19-04-001, October 19, 1993.
4. M. A. Alvin, R. E. Tressler, T. E. Lippert, E. S. Diaz, and E. E. Smeltzer, "Durability of Ceramic Filters," *Proceedings of Coal-Fired Power Systems 94 -- Advances in IGCC and PFBC Review Meeting*, June 21-23, 1994, Morgantown, WV.
5. T. E. Lippert, G. J. Bruck, Z. N. Sanjana, and R. A. Newby, "Westinghouse Advanced Particle Filter Systems," *Proceedings of Coal-Fired Power Systems 94 - Advances in IGCC and PFBC Contractors Review Meeting*, June 21-23, 1994, Morgantown, WV.
6. M. A. Alvin, T. E. Lippert, E. S. Diaz, and E. E. Smeltzer, "Filter Component Assessment," *Proceedings of Advanced Coal-Fired Power Systems '95 Review Meeting*, June 27-29, 1995, Morgantown, WV.

## Novel Oxide-Oxide Fiber Reinforced Hot Gas Filter Development

<b>Contract Number</b>	DE-AC21-94MC31212
<b>Contractor</b>	Babcock & Wilcox P. O. Box 11165 Lynchburg, VA 24506-1165 (804)522-5697 (telephone) (804)522-6980 (telefax)
<b>Other Funding Sources</b>	B&W Fossil Power, B&W ERI, and B&W Research and Development Divisions
<b>Contractor Project Manager</b>	Richard A. Wagner
<b>Principal Investigator</b>	Richard A. Wagner
<b>METC Project Manager</b>	Theodore J. McMahon
<b>Period of Performance</b>	September 29, 1994 to May 29, 1996
<b>Schedule and Milestones</b>	

[illegible]

## OBJECTIVES

The objective of this program is to fabricate and test oxide fiber reinforced composite hot gas filter elements for advanced power generation systems.

## BACKGROUND INFORMATION

Pressurized fluid bed combustion (PFBC) and integrated gasification combined cycle (IGCC) systems are among the advanced coal-based energy cycles being considered for low cost, clean power generation. Hot gas filters are required to remove particulates from the high temperature turbine inlet stream in order to protect turbine components from excessive erosive wear and to meet clean air requirements.

The level of mechanical durability exhibited by the currently available filters in field tests indicates that more rugged filters are required to meet the demands of large power generation systems. Furthermore, long term corrosion resistance of currently available filters has yet to be demonstrated in PFBC systems.

The essential requirements of a composite material designed to meet the program objective for a toughened hot gas filter include the following:

- o stable continuous fiber
- o rigid porous matrix
- o engineered fiber-matrix interface
- o cost effectiveness

Based on properties, availability, and cost, Mitsui's ALMAX alumina fiber and 3M's NEXTEL 610 alumina fiber were selected as the oxide reinforcement fibers. In order to

meet the economic goals of the program it is essential that the cost and amount of continuous fiber be minimized. A four axis filament winder will be used to fabricate filter preforms in a variety of fiber architectures.

Carbon was used as the initial fiber coating because it was known to be resistant to the processing chemicals. The coating was produced by pyrolysis of the resin based sizings on the continuous fibers.

The matrix of the composite filter is comprised of chopped ceramic fiber. Saffil fiber was used for all compositions in this program.

## PROJECT DESCRIPTION

The key to achieving the goal of this program is to apply the composite technology developed under the DOE Continuous Fiber Ceramic Composite (CFCC) program to the special requirements of a toughened hot gas filter. Figure 1 illustrates the roles of the various contributors to this program.

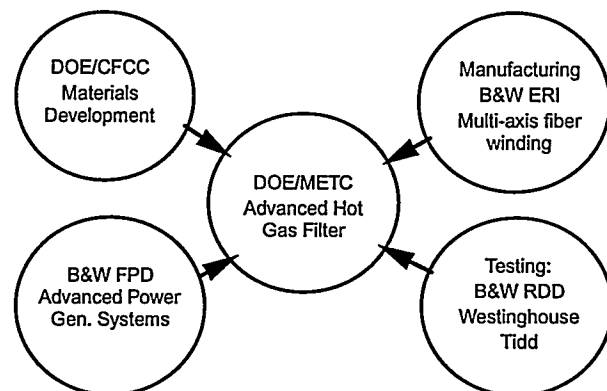


**Figure 1.** Organization of Advanced Hot Gas Filter Program

In addition to the DOE/CFCC materials development support, two Babcock & Wilcox operating divisions play key roles in the development and commercialization of an advanced hot gas filter. The B&W ERI division's expertise in filament winding has been utilized in the fabrication of program samples and would also be the ultimate manufacturing facility for commercial filter element production. B&W's Fossil Power Division (FPD) experience in the design of advanced power systems including hot gas filter systems provides valuable guidance to this program. FPD would utilize the composite filter elements produced by B&W ERI in the B&W Advanced Ceramic Tube Filter system.

In Phase I, porous composite fabrication technology developed under the CFCC program was transferred to the B&W ERI facility. A porous oxide-oxide composite system has been selected based on the predicted chemical stability in advanced combustion environments. A modified filament winding process was used to fabricate porous composite preforms containing either Nextel 610 alumina fibers or ALMAX alumina fibers as reinforcements. The compositions given in Table 1 were fabricated in the form of 12 inch tubes and tested. For compositions C1 and C2, the continuous fibers were pyrolyzed at 1600 °F in nitrogen to convert the fiber sizing as supplied by 3M and Mitsui to a carbon coating. Compressive C-ring tests performed at room temperature and 1600 °F were used as a preliminary characterization of the mechanical properties of candidate filter element compositions. Permeability measurements were performed at room temperature. Bond phase microstructure and fiber degradation was evaluated by SEM examination of fracture and polished sections. The results of these tests will be

used to guide the fabrication of sub-scale filter elements that will be evaluated in a coal combustion exposure test.

In Phase II, the manufacturing process will be developed to fabricate full scale filter elements for testing in a PFBC environment.

## RELATED WORK

In addition to the CFCC program, B&W R&DD funded a preliminary exposure test at the Tidd PFBC and subsequent test specimen characterization. Two separate exposure tests were performed on two sets of developmental composite filter samples. These preliminary samples contained considerably more binder phase than the samples produced under this program. The samples were contained in stainless steel wire mesh pouches and suspended from the horizontal evaporator legs in the freeboard region of the Tidd PFBC. The first exposure began on September 22, 1994 and continued for 690 coal-firing hours. A second set of samples was installed on November 20, 1994 and received an exposure of 1850 coal-firing hours. The effects of the test exposures were determined by comparing the compressive C-ring strength before and after testing. In addition, polished sections will be examined to evaluate the degree of reaction with the constituents of the fluid bed and combustion atmosphere.

In order to guide the filter process development, B&W R&DD in conjunction with B&W-ERI and B&W-FPD performed a preliminary review of the materials and manufacturing costs associated with the filter processes being developed. It is clear from these studies that low cost raw materials and fabrication methods will be required for commercialization. The selection of the continuous fiber is particularly important



because it represents a substantial fraction of the total filter cost.

## RESULTS

The lighter weight filament wound composite samples have bulk densities in the range 0.8 to 0.9 g/cc compared to 1.4 to 1.9 g/cc for monolithic filter materials. Because the fabrication process used in this program is not limited to thick wall structures in order to achieve adequate handling strength during processing, very light weight filters are possible. The combined effect of the lower filter density and the thinner tube walls results in significant potential weight savings in the filter system.

A summary of the test results for this program is given in Table 2. Examples of the room temperature and elevated temperature fracture behavior of compositions C1, C2, and C3 are shown in Figures 2, 3, and 4, respectively. Figure 2 also includes the room temperature fracture behavior of a monolithic cordierite filter material. The observed brittle fracture is typical of monolithic ceramic materials. In comparison to the monolithic material, composition C1 exhibited relatively non-brittle stress-strain behavior at room temperature. At 1600 °F however, the fractures tended to be more brittle. The more brittle fracture behavior of composition C3 at room temperature is attributed to the lack of a coating on the continuous fibers. During the bonding operation, the continuous fibers were attacked by the bonding chemicals which degraded the fiber properties. This composition was included in the test matrix because the lack of a coating simplified the processing. It is clear that an improved fiber coating system is needed to protect the continuous fibers at

elevated temperatures. A new fiber coating method currently under development in the CFCC program will be transitioned into this program for the subscale filter fabrication task.

The permeability results for compositions C1, C2, and C3 are also included in Table 2. Compositions C1 and C3 are at or very close to the pressure drop goal of 5 inches of water at a face velocity of 10 ft/min. It is expected that composition C2 can be easily modified to meet this goal.

### Tidd Exposure Results

The results of compressive C-ring tests on the Tidd PFBC exposure samples are given in Table 3. At room temperature, these samples exhibited brittle fracture behavior as a result of the high binder phase content. The permeability of these samples was also very low as a result of this level of binder phase. Following the Tidd PFBC exposure, the fractures tended to be more non-brittle. Polished sections and fracture surfaces will be examined to determine the reason for the change in fracture mode.

## FUTURE WORK

In the next work phase, 12" long sub-scale filter tubes will be fabricated and tested. The evaluation of these samples will include a static exposure test in a coal combustion environment. The results of pre-test and post-test property measurements will be used to guide the decision to proceed with Phase II and the fabrication and testing of full-scale filter elements.

**Table 1. Candidate filter compositions.**

	C1	C2	C3	C4
continuous fiber	ALMAX	NEXTEL 610	ALMAX	NEXTEL 610
continuous/ matrix fiber	1:1	1:1	2:1	1:1
continuous fiber coating	carbon	carbon	none	none
continuous fiber architecture	45° helical	45° helical	45° helical	45° helical

**Table 2. Property summary of composite hot gas filter materials.**

	C1	C2	C3	C4
continuous fiber (%)	34	36	51	nd*
Saffil (%)	35	35	28	nd
binder (%)	30	28	21	nd
pressure drop (in. H <sub>2</sub> O @10 ft/min)	4.1	9.8	5.7	nd
C-ring (rt) (psi)	1651	1477	2100	nd
Tangent mod. (rt) (msi)	0.64	0.51	0.84	nd
C-ring (1600F) (psi)	1139	1249	1716	nd
Tangent mod. (1600F) (msi)	0.36	0.49	0.80	nd

\* = not determined

**Table 3. C-ring strength of composite samples from Tidd PFBC exposure test.**

	9	20	21	22
continuous fiber	NEXTEL 610	NEXTEL 610	ALMAX	ALMAX
exposure time, (hours)	690	1849	1849	1849
C-ring, pre-test (psi)	3843	2318	5654	4107
C-ring, post-test (psi)	1616	1495	2213	2054
percent retained	42	64	54	50

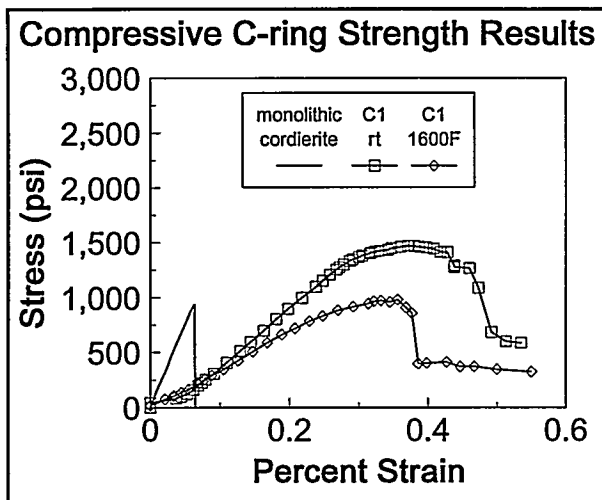


**Figure 2.** Comparison of the stress-strain results for composition C1 (at room temperature and 1600 °F) and a monolithic cordierite filter material.

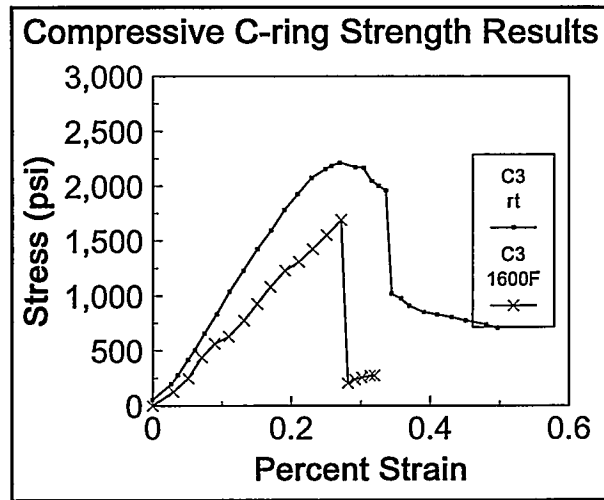


**Figure 4.** Stress-strain behavior of composition C3 at room temperature and 1600 °F.

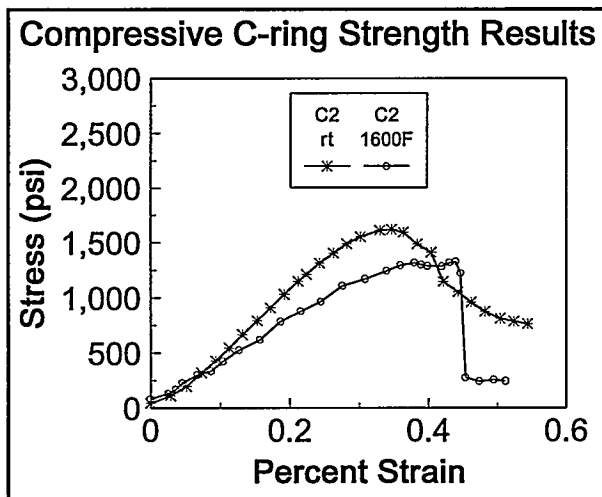


**Figure 3.** Stress-strain behavior of composition C2 at room temperature and 1600 °F.

**CONTRACT INFORMATION**

**Contract Number** DE-AC21-87MC24257

**Contractor** Westinghouse Electric Corporation  
Science & Technology  
Pittsburgh, PA 15235  
(412)256-2210  
(412)256-2121 (FAX)

**Contractor Program Manager** Richard A. Newby

**Principal Investigators** Eugene E. Smeltzer  
Mary Anne Alvin  
Thomas E. Lippert

**METC Project Manager** Heather M. McDaniel

**Period of Performance** September 30, 1987 to May 30, 1995

**Schedule and Milestones**

**FY95 Program Schedule**

	S	O	N	D	J	F	M	A	M	J	J	A	S
<u>Phase III</u>													
Testing													
Evaluation													
Final Report													

**OBJECTIVES**

The Westinghouse Electric Corporation, Science & Technology Center is developing an Integrated Low Emissions Cleanup (ILEC)

concept for high-temperature gas cleaning to meet environmental standards, as well as to provide gas turbine protection. The ILEC system is a ceramic barrier hot gas filter (HGF) that removes particulate while simultaneously contributing to

the control of sulfur, alkali, and potentially other contaminants in high-temperature, high-pressure fuel gases, or combustion gases. The gas-phase contaminant removal is performed by sorbent particles injected into the HGF.

The overall objective of this program is to demonstrate, at a bench scale, the technical feasibility of the ILEC concept for multi-contaminant control, and to provide test data applicable to the design of subsequent field tests. The program has conducted ceramic barrier filter testing under simulated PFBC conditions to resolve issues relating to filter cake permeability, pulse cleaning, and filter cake additive performance. ILEC testing has also been performed to assess the potential for in-filter sulfur and alkali removal.

## BACKGROUND INFORMATION

Westinghouse hot gas filter (HGF) field testing has recently been completed at three major PFBC installations (Lippert and Newby, 1995): the American Electric Power, Tidd Plant, Bubbling-PFBC, Advanced Particle Filter (APF); the Foster Wheeler Development Corporation (FWDC) Phase 2, circulating-PFBC, HGF; and the Ahlstrom-Pyropower, circulating-PFBC pilot plant, HGF. The characteristics of these HGF facilities are summarized in Table 1. These facilities have provided critical data supporting the design of new HGF systems associated with several PFBC development and demonstration facilities:

- Foster Wheeler Development Corporation (FWDC), Phase 3, Advanced-PFBC subscale test program (Livingston, NJ),
- Southern Company Services, PCD test program (Wilsonville, Alabama),

- Foster Wheeler, Advanced-PFBC pilot program (Wilsonville, Alabama),
- Pyropower circulating-PFBC, DMEC-1, Clean Coal Technology Program,
- Air Products, Advanced-PFBC, FREMP, Clean Coal Technology Program.

Test observations made at the three PFBC, HGF facilities are summarized in Table 2. Issues with filter cake permeability, ash bridging, and ash bulk flow can arise in PFBC, depending on the nature of the fly ash and the HGF operating conditions. The Tidd APF tests, with test periods using an efficient precleaning cyclone; a spoiled, precleaning cyclone; and, most recently, eliminating the precleaning cyclone, has established that the ash bridging occurrence is induced by very fine particle sizes in the filter cake at higher temperatures, and is essentially eliminated when the precleaning cyclone is removed. The circulating-PFBC facilities had only recycle cyclones and hard filter cakes and ash bridging were observed only during periods of extreme temperatures.

The occurrence of "hard" filter cakes and ash bridging, particularly at the Tidd APF, has led to conjecture as to the phenomena leading to this behavior, and the ILEC program has attempted to identify the key phenomena. It is also important to note that significant SO<sub>2</sub> removal has been consistently measured across the Tidd APF (Radian, 1995) and is consistent with the high conversion of Ca and Mg to sulfates found in the filter cakes at all three HGF facilities. The content of alkali in the filter outlet gas is an issue to turbine protection when the HGF operates at temperatures greater than about 1400°F based on alkali sampling conducted at the FWDC Advanced-PFBC facility.

**Table 1. Westinghouse PFBC, HGF System Characteristics**

	AEP Tidd, APF Bubbling-PFBC Brilliant, OH			FW Phase 2 Circ-PFBC Livingston, NJ	Ahlstrom Pilot Circ-PFBC Karhula, Finland
Facility Size (MW <sub>e</sub> ):	30			1.2	10
Gas Flow (acfm):	7600			300	3070
Pressure (psig):	135			100-200	160
Fuels/Sorbents:	Pgh #8/Plum Run Dolomite			3 Variations	7 Variations
Hours of Test Operation - Max. Continuous: - Cumulative:	600 5800			72 800	280 2050
Preclean Cyclone:	Yes	Spoiled	None	None	None
Number Candles:	384	288-384	288	14-22	128
Face Velocity (fpm):	6.5	4.5-8.7	8.9	2-8	3-8
Temperature (°F):	1150- 1450	1200- 1400	1400- 1550	1450-1700	1300-1650

**Table 2. Westinghouse PFBC, HGF Filter Cake Observations**

	AEP Tidd, APF Brilliant, OH			FWDC Phase 2 Livingston, NJ	Ahlstrom Pilot Karhula, Finland
Preclean Cyclone:	Yes	Spoiled	None	None	None
Fly Ash Size: (mean, $\mu\text{m}$ )	1-3	5-7	25-30	5-25	12-22
Dust Loading: (1000 ppmw)	0.5-1	3-4	15-20	2-30	4-18
Permeability: ( $10^{-10}$ lb/ft)	.2-.6	1-2	5-6	2-5	2-6
Pulse Frequency: (1/hr)	1-2	2-4	4	0.5-3	1-3
Occurrence of Bridging and Hard Cake:	Temp > 1400°F	Less Severe	Very Little	Temp > 1600°F	Very Little
Vessel Drainage Performance:	Poor	Little Problem	Good	Periods of Poor	Good

## PROJECT DESCRIPTION

The ILEC development program consisted of three phases:

- Phase I - Laboratory-Scale Testing
- Phase II - Bench-Scale Equipment Design and Fabrication
- Phase III - Bench-Scale Testing

Phases I and II had been previously completed and a report issued (Newby, et al., 1990). Included was an evaluation of alternative ILEC concepts. The ILEC feasibility testing, Phase III, has been recently completed. The Phase III test program has focused on PFBC filter cake issues, as well as sulfur and alkali removal. Five test series have been conducted:

1. Cake Permeability Tests
2. Additive Tests
3. Cake Pulse Removal Tests
4. Sulfur Removal Tests
5. Alkali Removal Tests

The first series of tests were highly controlled tests measuring changes in filter cake permeability primarily as a function of temperature and PFBC fly ash source. The results of these tests were previously reported (Newby, et al., 1994). Test series two examined the performance of various filter cake additives and the additive application procedures. The third series of tests were directed toward measuring the impact of temperature, PFBC fly ash source, and pulse intensity on pulse cleaning effectiveness. Test sets four and five have characterized the potential for sulfur removal and alkali removal within the HGF. These final test series have also noted the influence of the injected sorbents on the filter cake behavior.

## RESULTS

### Bench-Scale Facility Description

A natural gas-fired, bench-scale, high-pressure, high temperature, ceramic barrier filter test facility was used to study ILEC performance under simulated PFBC conditions. The objective of the bench-scale simulation was to produce a gas having pressure, temperature, gas composition ( $\text{SO}_2$ , alkali content, and particulate content), and fly ash particulate characteristics similar to actual coal-fired PFBC. An assembly drawing of the facility is shown in Figure 1. A horizontal, natural gas combustor is attached to the filter pressure vessel inlet nozzle. The combustor is a carbon steel, refractory-lined, pipe with an internal, high-alloy steel liner. The burner has been designed to operate entirely on natural gas, or with coal and natural gas combinations. PFBC fly ashes, sulfur sorbents, alkali sorbents, or additives may be injected into the secondary zone of the combustor as required by the specific test. Sulfur and alkali contaminants may also be injected into the filter gas through the combustor.

The uncooled tubesheet, with a 31-inch plate diameter, has been designed with commercial candle holder features that included fail-safe/regenerator devices. The tubesheet, capable of holding up to 19 candles, supported four ceramic candle filter elements in this program, each 1.5 meter in length. The inlet gas enters the vessel horizontally, near the level of the base of the candles, with no baffle to deflect the inlet jet. The four candles are located so that direct impaction by the inlet gas stream is avoided. The four candles are pulse cleaned simultaneously. The outlet piping section incorporates gas sampling for particulate content, alkali content, sulfur content, and other gas species of interest, such as  $\text{CO}_2$ , as well as instrumentation to measure total gas flow and temperature.



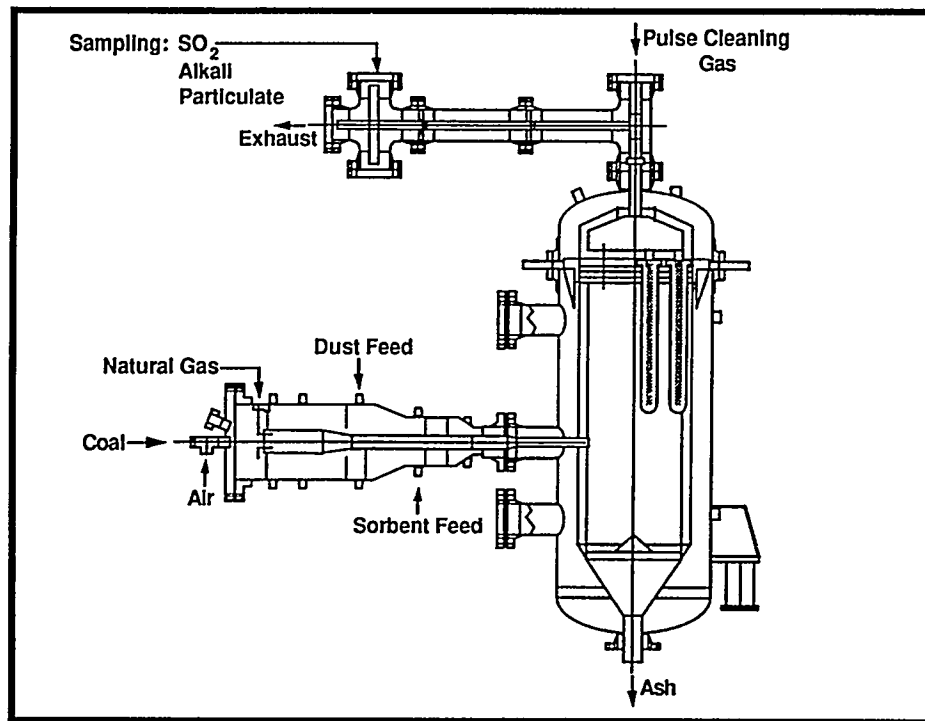


**Figure 1. Bench-Scale Test Facility Assembly Drawing**

Almost all of the tests were conducted under the following nominal conditions:

- Face velocity: 7 ft/min,
- Pressure: 100 psig.

Key measurements made during the tests were:

- Inlet gas and fly ash mass flow rates,
- Gas inlet and outlet temperature,
- Tubesheet pressure drop,
- Outlet gas mass flow rate, particulate, CO<sub>2</sub>, SO<sub>2</sub>, and alkali vapor content.

### Filter Cake Permeability Test Results

The testing identified the key phenomena relating to PFBC filter cake behavior as "sintering" of the filter cake calcium constituents induced by SO<sub>2</sub> and CO<sub>2</sub> in the gas (Newby, et al., 1994). The test results are consistent with PFBC field test

trends, and direct comparison of the bench-scale test permeabilities and PFBC field test permeabilities are shown in Table 3. The bench-scale permeabilities were generally greater than the PFBC field test permeabilities, and this may be because 1) the CO<sub>2</sub> and SO<sub>2</sub> partial-pressures are lower in the bench-scale tests than in the PFBC field tests, and 2) the PFBC fly ashes tested were re-entrained particles, previously exposed to the filter environment in field units. The primary cyclone drain material from Tidd had a permeability higher than the PFBC field permeability, possibly because it was not previously exposed to the HGF environment.

Conclusions reached in the Test Series 1 program were:

- Bench-scale filter cake trends are consistent with field unit data trends, although the cake permeability values are higher in the bench-scale tests than in the field tests;

**Table 3. Bench-Scale and PFBC Field Filter Cake Permeabilities**

	Bench-Scale Mass Permeability (10 <sup>-10</sup> lb/ft)	Field Mass Permeability (10 <sup>-10</sup> lb/ft)
Tidd Fly Ash		
Efficient Cyclone <sup>a</sup> :	1.6	0.2 - 0.6
Spoiled Cyclone <sup>b</sup> :	3.2	1 - 2
Primary Cyclone Drain <sup>c</sup> :	4.4	—
No Cyclone:	6.1	5 - 6
Karhula <sup>d</sup> :	3.3 - 8	2 - 6
Grimethorpe Red <sup>e</sup> :	1.0	—
FWDC (TRC5) <sup>f</sup> :	8.5	2 - 5

- a: AEP, Tidd bubbling-PFBC fly ash collected from filter during initial test period through Run 11  
b: AEP, Tidd bubbling-PFBC fly ash collected from filter following testing with partially-spoiled primary cyclone  
c: AEP, Tidd bubbling-PFBC fly ash drained from primary cyclone mixed with APF drain  
d: Ahlstrom, Karhula, Finland circulating-PFBC pilot filter fly ash  
e: Grimethorpe Red fly ash collected from Grimethorpe bubbling-PFBC filter during Run 129  
f: FWDC Circulating-PFBC fly ash collected from the filter vessel during Test Run TRC5 using FREMP feed stocks

- PFBC filter cake permeability is largely controlled by limestone constituents in the fly ash;
- Adverse filter cake behavior is a result of sintering induced by CO<sub>2</sub> and SO<sub>2</sub> in the gas;
- Increased filter cake sintering results from:
  - higher CO<sub>2</sub> and SO<sub>2</sub> pressures,
  - higher temperatures,
  - finer fly ash particles,
  - calcitic limestone vs dolomitic limestone;

permeability and have been of two types: additive premixed with PFBC fly ash, and additive applied as a precoat on the filter elements. The tested additive characteristics are listed in Table 4. The five additive tests summarized in Table 5 were performed.

The results show that the use of pulverized dolomite, Test 2.1, benefitted the Tidd fly ash permeability significantly. The filter cake permeability was increased about 50%, even though only 10 wt%, or about 5 volume percent, additive was used. It is expected that the tendency for cake sintering and bridging would also be reduced with this additive.

### Additive Test Results

The additive tests performed have focused on the influence of additives on the filter cake

Test 2.2 precoat the candle elements with Neutralite, a commercial baghouse filter aid. Neutralite was fed for 4 days to obtain a standard filter cake pressure drop of about 40" H<sub>2</sub>O. A

**Table 4. Additive Characteristics**

Additive	Supplier	Composition	Particle Size
Dolomite	Espoma garden lime	21 wt% Ca 12 wt% Mg	92% -325 mesh 99.9% -200 mesh
Neutralite	BHA commercial bag house aid	aluminum silicate (proprietary)	Very fine
Kaolin	Thiele Kaolin Co.	hydrous aluminum silicate	100% -325 mesh 56% <2 $\mu\text{m}$

**Table 5. Additive Test Results**

Test	Fly Ash	Additive	Results/Change in Mass Permeability (lb/ft X $10^{-10}$ )
2.1	Tidd fine; (Preclean cyclone)	10 wt% pulverized dolomite	Permeability increased from 1.6 to 2.7
2.2	None	Neutralite precoat	5/8" - thick precoat generated
2.3	Grimethorpe Red	On Neutralite precoat	Permeability decreased from 1.0 to 0.9
2.4	Grimethorpe Red	5 wt% Neutralite	Permeability decreased from 1.0 to 0.4
2.5	Grimethorpe Red	10 wt% kaolin	Permeability increased from 1.0 to 1.1

cake having relatively high permeability resulted, and temperature variations were performed for two days. A large reduction in the filter cake permeability as the temperature increased was observed on the first day. The Neutralite filter cake permeability was measured to be slightly lower on the second day, but was still a relatively high value.

The next test, Test 2.3, built a cake of fly ash, Grimethorpe Red, on the Neutralite precoat to see if a measurable impact on the cake permeability resulted. The results showed that the cake permeability was slightly lower than it had been in earlier tests having no precoat. Following this test, the vessel was opened for inspection and it was found that the Neutralite precoat was very thick (about 5/8") and was a hard, stable layer that

needed to be cut out in sections. A thinner precoat should be used, and the stable layer could provide some protection to the candle if no detrimental reactions occurred with the candle materials. Such a stable precoat might provide an aid to pulse cleaning. Further assessment of the precoat concept should be considered.

The next test, Test 2.4, built a cake of Grimethorpe Red fly ash mixed with 5 wt% Neutralite, and resulted in a cake permeability much lower than previously measured with Grimethorpe Red. Neutralite would not appear to be a useful cake permeability aid. A further series of continuous pulse cleanings and cake buildups showed a significant deterioration in the baseline pressure drop, further exposing the poor performance of Neutralite as a direct additive. Neutralite might be a useful aid to reduce re-entrainment with some filter cakes having low cohesion.

The final additive test performed, Test 2.5, used a mixture of 10 wt% Kaolin with Grimethorpe Red fly ash. The results showed little influence of the Kaolin on the Grimethorpe Red cake permeability compared to prior tests without the additive. In general, the practicality of additive use is uncertain based on the testing. The dolomite additive positive results might combine with the possibility for additional sulfur removal to make it a feasible candidate.

### Pulse Cleaning Test Results

Pulse cleaning performance was characterized by building filter cakes at a specified temperature, and measuring the recovery of the baseline pressure drop over a range of pulse cleaning intensities. Two PFBC fly ashes were tested, Tidd fine fly ash, and Karhula PFBC fly ash. The solenoid valve opening and closing characteristic

were fixed at near optimum values in all of the testing. The test conditions are listed in Table 6.

**Table 6. Filter Cake Pulse Cleaning Test Conditions**

Face Velocity: 7 ft/min Pressure: 100 psig			
Test	Fly Ash	Temperature (°F)	Maximum Relative Pulse Tank Pressure (atm)
3.11 3.12 3.13	Tidd Fine	1300 1450 1550	26
3.21 3.22 3.23	Karhula	1300 1450 1550	26
3.31 3.32 3.33	Tidd Fine	1300 1450 1550	61
3.41 3.42 3.43	Karhula	1300 1450 1550	61

The pulse intensities measured in all of the tests are plotted in Figure 2, for Tidd fine fly ash, and in Figure 3, Karhula fly ash, against the relative tank pressure. The pulse intensity is defined as the maximum pressure reached in the filter plenum during the pulse event minus the background pressure (100 psig). The relative tank pressure is defined as the pulse gas tank pressure applied at the start of the pulse minus the background pressure. The pulse intensity rises almost linearly as the relative tank pressure increases, but it also appears that the intensity is slightly higher as the temperature is increased.

## PULSE CLEANING TESTS

Tidd Fine Fly Ash (Tests 3.11 - 3.13)

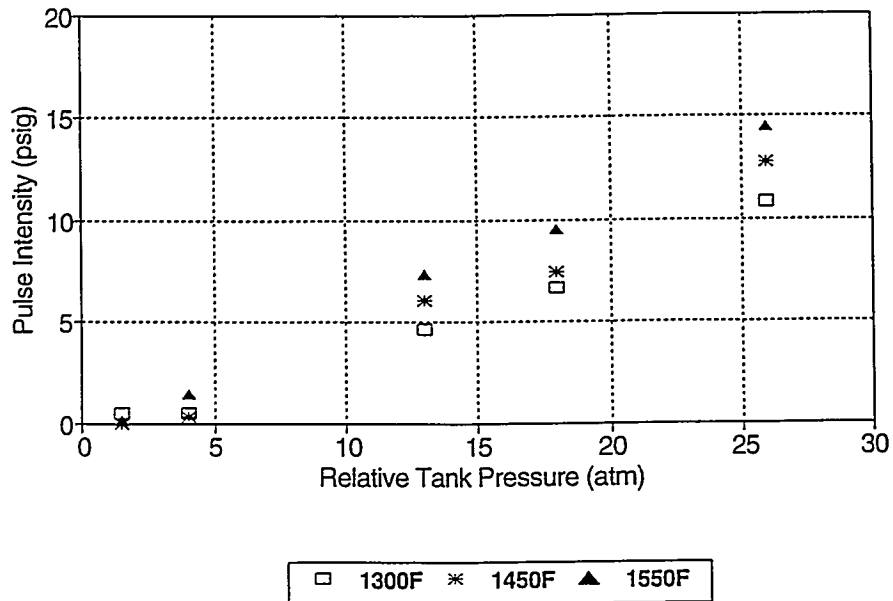


Figure 2. Pulse Intensity vs. Relative Tank Pressure (Tidd Fine)

## PULSE CLEANING TESTS

Karhula Fly Ash (Tests 3.21 - 3.23)

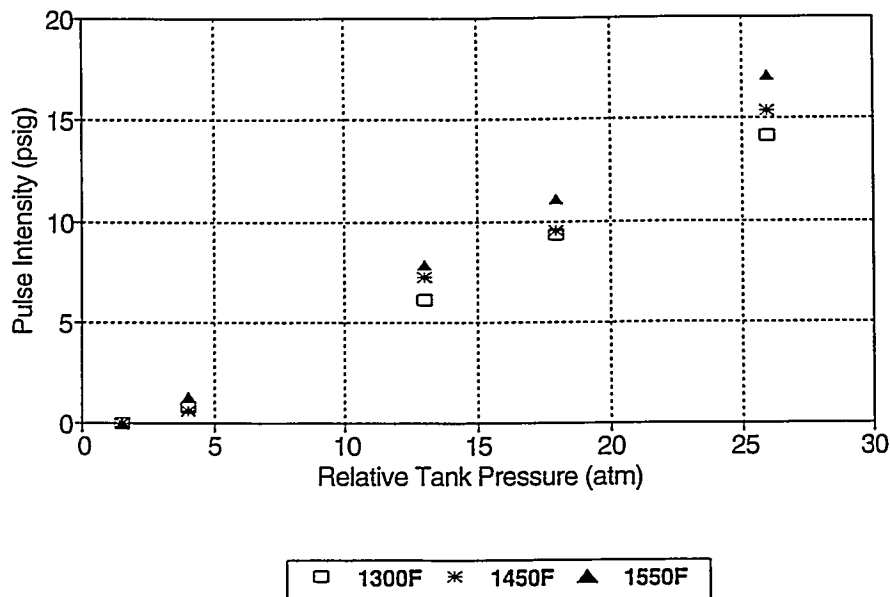


Figure 3. Pulse Intensity vs. Relative Tank Pressure (Karhula)

This probably results because the filter cake and "residue" permeabilities have decreased as the temperature was increased.

In Figure 4, for Tidd fine fly ash, the pulse intensity and the "baseline minus the clean system pressure drop" is plotted against the cumulative, hot operating hours in the tests. The three sets of data at 1300°F, 1450°F, and 1550°F are shown. The "baseline pressure drop" is the tubesheet pressure drop following the pulse cleaning event. The quantity plotted, "baseline minus clean DP" is equal to the sum of the filter cake pressure drop and the "residue" pressure drop. A lower value of this quantity means a more effective pulse cleaning was performed. At each temperature, as the pulse intensity was decreased a clear increase in the baseline minus clean DP quantity resulted. As the temperature increased, the baseline minus clean DP quantity was higher at the same pulse intensity. For example, at 1300°F a pulse intensity of 5 psi resulted in a baseline minus clean DP quantity of about 0.5" H<sub>2</sub>O, while at 1450°F the same 5 psi pulse intensity resulted in a baseline minus clean DP quantity of about 3 psi, and at 1550°F the same 5 psi pulse intensity resulted in a baseline minus clean DP quantity of about 7 psi.

Figure 5, for Karhula PFBC fly ash, plots similar data, showing the tank relative pressure and the "baseline minus the clean system pressure drop" plotted against the cumulative, hot operating hours in the tests. Even though the Karhula fly ash has a significantly higher permeability than the Tidd fine fly ash, with also much less sensitivity to temperature, a significant influence of temperature and time on the pulse cleaning effectiveness was observed, and is shown in the figure.

There are two factors that have contributed simultaneously to these results. First, higher temperature results in lower cake permeability and

greater residue accumulation, so that a lower pulse gas quantity yields the same measured pulse intensity. Secondly, the tests were performed in the order of ascending temperatures, so that as the temperatures increased the cumulative test time also increased. This second factor resulted in more opportunity for residue accumulation on the candles, or within the candle surface pores, as time, and temperature progressed. In any case, the results imply that, with both the Tidd fine fly ash and the Karhula fly ash, a steady accumulation of residue might occur that cannot be effectively cleaned even at the highest pulse intensity conditions used in these tests.

Test Series 3.3 and 3.4 were conducted to observe the benefits of a higher pulse source pressure on the pulse cleaning performance. The Tidd fine fly ash was used in Test 3.3, and the Karhula ash in Test 3.4. Both tests used a tank relative pressure of 61 atm, and both resulted in a pulse intensity of about 35 psi. The results imply that with the Tidd fine ash, a continued buildup of residue occurred on the candles that increased as the temperature increased, while this temperature sensitivity was not shown for the Karhula ash. A significant residue resistance remains on the candles even with this high pulse intensity, but is a normal filter element conditioning and would not lead to adverse behavior.

### **Sulfur Removal Test Results**

An objective of this testing was to determine the influence of SO<sub>2</sub> on the filter cake permeability, since SO<sub>2</sub> induces filter cake sintering. The testing was also conducted to measure the SO<sub>2</sub> removal performance of PFBC fly ashes and calcium-based sorbents. The SO<sub>2</sub> removal activity was measured for fly ashes and sorbent when they were injected as entrained,

# PULSE CLEANING TESTS

Tidd Fine Fly Ash (Tests 3.11 - 3.13)

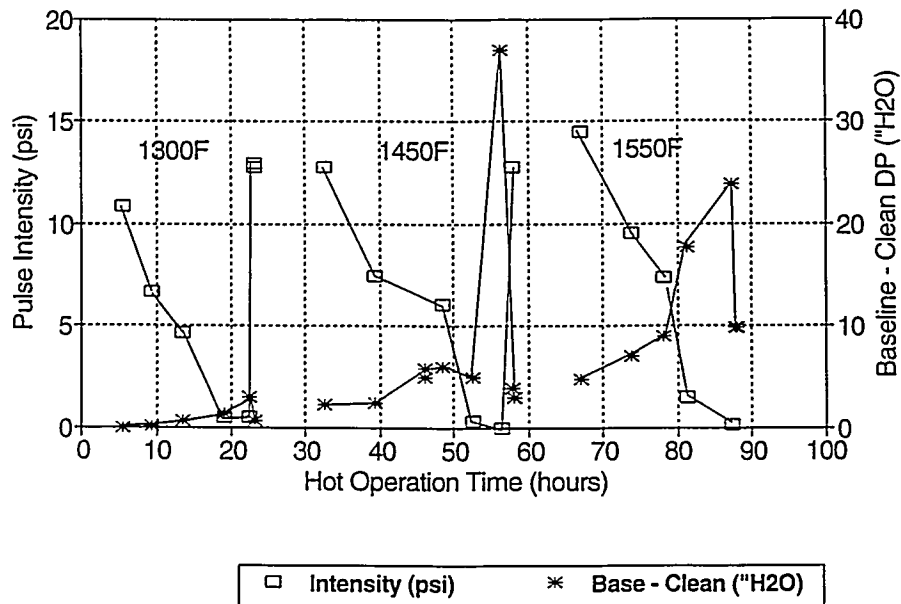


Figure 4. Pulse Intensity and Baseline-Clean  $\Delta P$  vs. Time (Tidd Fine)

# PULSE CLEANING TESTS

Karhula Fly Ash (Tests 3.21-3.23)

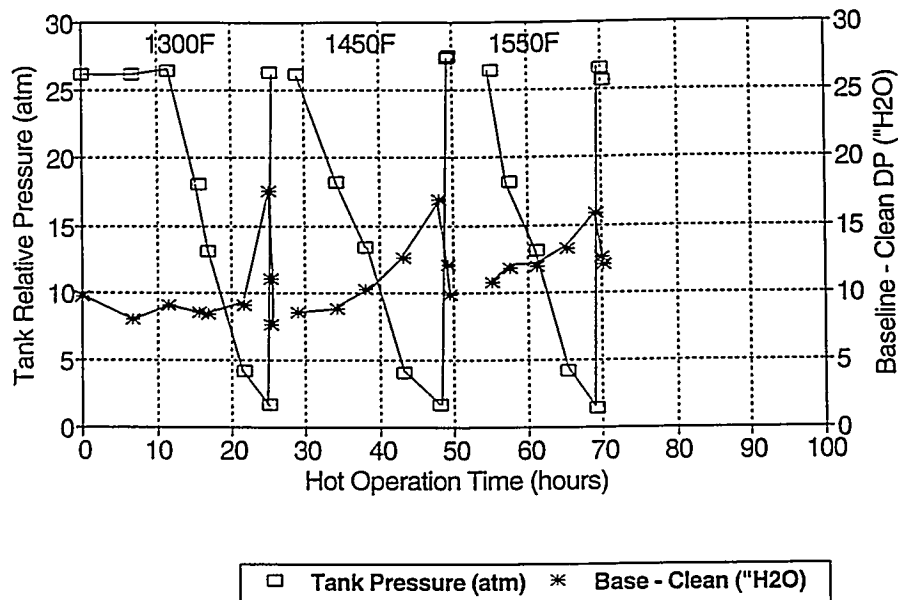


Figure 5. Tank Relative Pressure and Baseline-Clean  $\Delta P$  vs. Time (Karhula)

dispersed particulate or as predeposited filter cakes. The test parameters were:

- Fly ash type: Tidd, spoiled cyclone; and Karhula
- Sorbent type: -325 mesh dolomite alone or mixed with PFBC fly ash
- Temperature: 1450-1550°F
- Pressure: 100 and 150 psig

Two types of SO<sub>2</sub> removal tests were performed. The first procedure was a test of the influence of SO<sub>2</sub> on the cake permeability and on the ability of the filter cake to remove sulfur:

1. Test Initiation: Raise gas inlet temperature to prescribed level (1450 - 1550°F) following normal heatup procedure.
2. Build a filter cake on the candles until cake pressure drop (tubesheet minus baseline) of prescribed value (20 to 30" H<sub>2</sub>O) is reached -- fly ash flow is discontinued at this point.
3. Inject premixed SO<sub>2</sub>-gas into the vessel inlet gas, at levels of about 200 ppmv, continuing long enough to exhaust 1 to 4 gas bottles of SO<sub>2</sub>-gas.
4. Pulse clean the candles with several vigorous pulses at the completion of the test.

The second procedure was a test of the particulate (PFBC fly ash and/or sorbent) to remove SO<sub>2</sub> while being fed in the suspended state and while building a filter cake.

The conditions and results of eight tests are summarized in Table 7. The sulfur removal tests included SO<sub>2</sub> calibration runs. Only one test of the

transient entrained sorbent performance was conducted (Test 4.4), and the rest of the tests were predeposited filter cake tests. All of the tests were performed at 1550°F and a pressure of 100 psig, except Test 4.7 (1450°F and 150 psig). In the Table, the "free calcium/sulfur ratio" is the estimated molar ratio of calcium carbonate fed during the test divided by the total sulfur fed during the test. The "sulfur removal" is the estimated percent retention of sulfur in the HGF. There were uncertainties in the tests as a result of a relatively high background SO<sub>2</sub> level that existed.

No significant differences in filter cake behavior or SO<sub>2</sub> removal performance were observed during the transient entrained sorbent test (Test 4.4) or at the lower temperature/ higher pressure conditions (Test 4.7) relative to comparable tests. In Test 4.2, Karhula ash was deposited on the candles the first test day and was left overnight before being subjected to SO<sub>2</sub> exposure. The filter cake pressure drop was observed to increase overnight from 55" H<sub>2</sub>O to 67" H<sub>2</sub>O, leading to a large reduction in the calculated cake permeability. The filter cake permeability is not reported in the continuous feed test of Test 4.4 because it was a transient test and not expected to give an accurate filter cake permeability value.

While the sulfur removal measurements had a large uncertainty because of a high background SO<sub>2</sub> indicated by the SO<sub>2</sub> monitoring system, the results do provide representative and significant trends:

- The inclusion of SO<sub>2</sub> in the filter inlet gas had a very small impact on the filter cake permeability with the two PFBC fly ashes, as well as with the dolomite. The permeability appears to drop only slightly during the SO<sub>2</sub>-gas injection periods.



**Table 7. SO<sub>2</sub> Removal Test Results**

Fixed Conditions: Face Velocity 7 ft/min  
SO<sub>2</sub> Feed Level about 200 ppmv

Test	Fly Ash/Sorbent	Free-Calcium/ Sulfur Ratio	Cake Mass Permeability (lb/ft, 10 <sup>-10</sup> )	Sulfur Removal (%)
4.1 (Cake test)	Tidd spoiled cyclone	small	5.3	none
4.2 (Cake test)	Karhula	1 - 2	3.3	80
4.3 (Cake test)	Dolomite	25.7	5.7	60 - 80
4.4 (Feed test)	Dolomite	2.3	—	60 - 80
4.5 (Cake test)	Tidd cyclone/ dolomite (50%)	3.1	5.6	80
4.6 (Cake test)	Karhula/ dolomite (50%)	2.2	3.5	95
4.7 (Cake test)	Dolomite	1.0	4.6	95
4.8 (Cake test)	Dolomite	1.0	4.4	98

- The Tidd fly ash, from the spoiled cyclone testing on the Tidd APF, showed little ability to capture sulfur, while the Karhula fly ash had significant sulfur capture capability. This may be because the Karhula ash was less sulfated than the Tidd ash.
  - The PFBC fly ash-sorbent mixtures and the sorbent alone showed significant sulfur capture ability, greater than 90% at moderate calcium-to-sulfur ratios.
  - No indication of hard filter cake formation, or deposits that would initiate filter bridging, was found on observation of the filter elements after testing, even for the tests with dolomite alone. This is probably because the dolomite fed was of relatively coarse particle size.
- These trends indicate that relatively coarse (-325 mesh) sorbent injection for in-filter sulfur removal would be very efficient and would not result in adverse filter cake formation. It is expected that injection of much finer sorbent particles (mean size 5 µm or less) into the filter would be expected to

result in a high degree of filter cake sintering. The fact that SO<sub>2</sub> exposure did not result in sintered filter cakes when using the PFBC fly ashes probably is due to 1) the previous exposure and sulfation of these fly ashes in PFBC field HGF units, and 2) their relatively coarse particle size.

## Alkali Removal Tests

Alkali removal tests were performed by injecting PFBC fly ashes and alkali sorbent (emathlite powder) premixed with micro-pulverized sodium chloride, following procedures similar to those used in the sulfur removal testing. Alkali was sampled at two locations using an extractive, condensing probe. The first location was downstream of the filter exit pipe, where particle, and SO<sub>2</sub> sampling was performed. The temperature was too low at this location and was expected to result in significant alkali vapor condensation within the piping prior to extraction. The second location was directly from within the vessel head, with minimal temperature loss occurring. The probe extracted gas during the entire alkali salt feeding period.

The objectives of the testing were to observe the filter cake permeability to see if difficult filter cakes were generated at temperatures where the reacted emathlite may become relatively soft, and to measure the alkali removal performance. All of the tests were at the following conditions:

- Face velocity: 7 ft/min,
- Pressure: 100 psig,
- Temperature: 1550°F.

Test periods for calibration of the alkali probe and for determination of alkali background reading were also conducted. The test types conducted were:

- Emathlite filter cake permeability without alkali exposure
- Alkali background determination
- Alkali probe calibration
- Emathlite alkali removal during feeding
- Emathlite and PFBC fly ash alkali removal

The tests listed were performed, and probe samples were analyzed for condensate water-soluble sodium. Complete analytical results and test conclusions are not yet available. No indication of adverse filter cake behavior was observed in the tests. Uncertainties in the results arise from the possibility of alkali vapor condensation, alkali vapor reactions with the metal internals in the filter vessel, and incomplete vaporization of the injected alkali salt.

## REFERENCES

- Lippert, T. E. and R. A. Newby, 1995 Development and Commercialization of Hot Gas Filters for Power Generation Applications, to be published in *Proceedings of the 1995 Turbo Expo Conference*, Houston, TX.
- Newby, R. A., et al., 1990, Integrated Low Emissions Cleanup System for Direct Coal Fueled Turbines, Phase I, Final Report to DOE under Contract No. DEAC21-87MC24257, (DOE/MC/24257--2927).
- Newby, R. A., T. E. Lippert, M. A. Alvin, D. M. Bachovchin, and E. E. Smeltzer, 1994, PFBC Dust Cake Studies, In *Proceedings of Coal-Fired Power Systems 94 -- Advances in IGCC and PFBC*, Morgantown, WV, June 1994.
- Radian Corporation, A Study of Hazardous Air Pollutants at the Tidd PFBC Demonstration Plant, Report to American Electric Power Corporation, October 1994 (DCN 94-633-021-03).

**CONTRACT INFORMATION**

**Contract Number** DE-AC21-89MC26239

**Contractor** Southern Research Institute  
P. O. Box 55305  
Birmingham, Alabama 35255-5305  
(205) 581-2268

**Contractor Project Manager** Duane H. Pontius

**Principal Investigator** Duane H. Pontius

**METC Project Manager** Thomas P. Dorchak

**Period of Performance** August 23, 1989 to August 22, 1994

**Schedule and Milestone****FY95 Program Schedule**

	S	O	N	D	J	F	M	A	M	J	J	A
Particle Characterization												
Material Assessment												

**OBJECTIVES**

The primary objective of this research has been to provide an understanding of factors pertinent to the development of an effective filtration system for removing particles from high-temperature, high-pressure gas streams in advanced power generation systems under development by the Department of Energy. Information used to define the filtration system issues was compiled from the Morgantown Energy Technology Center (METC) Contractors Conferences, specific tasks assigned to Southern Research Institute, meetings with METC

personnel and contractors, and other conferences and workshops organized by METC.

**BACKGROUND INFORMATION**

Effective hot gas filtration is an enabling technology for advanced power systems that are now under development to improve the efficiency of thermal to electrical energy conversion of coal burning power stations. In conventional coal-fired power systems thermal energy is extracted from the combustion products in the boiler, economizer and air preheater, leaving a flue gas to be expelled from

the plant. To satisfy environmental requirements, the gas is cleaned, usually with an electrostatic precipitator or a fabric filter, before it is released to the stack. The gas cleaning operation is carried out at temperatures typically in the range of 120°C to 180°C. Modern hot-side precipitators (so called because they are installed upstream of air preheaters) operate at a somewhat higher temperature, but still within the stable range of a fairly wide range of materials.

The challenge of hot-gas cleanup arises from the requirement to remove contaminants from gases at temperatures of 600°C and possibly much higher. In both PFBC and IGCC systems hot gases from the reaction process (combustion or gasification) are applied directly to steam turbines, which requires that they be substantially free of particulate material. In general, higher thermal efficiency in these kinds of systems requires higher filtration temperature.

Above 840°C the limitations of conventional materials become apparent. Most metals become affected by corrosion and loss of strength. Although ceramics are less subject to such deterioration, they are not invulnerable to degradation by thermal and mechanical effects.

Initial research and pilot scale installations have shown that there are some potential problem areas. Thick ash deposits have formed, bridging from passive surfaces to the filter material and between filter candles. A great number of ceramic filters have broken in various experimental and demonstration devices, especially during the long-term testing of the candle filter system at the Tidd station, American Electric Power's 70 Mwe PFBC Demonstration Plant located at Brilliant, Ohio. Similarly, there have been failures, although not as regularly, in Ahlstrom Pyropower's Circulating Pressurized Fluidized Bed Combustion System in Karhula,

Finland, in other pilot plants, and in tests of small discs or "patches" of filtration materials.

Although ceramic candle filters remain among the most promising candidates for Hot Gas Cleanup (HGCU) systems, there are still some significant problems with both durability of the candles and long-term buildup of dust deposits. These problems can be addressed by identifying and developing new filter materials and by developing design criteria and other means to avoid the formation of excessive dust accumulation.

## PARTICULATE CHARACTERISTICS

The behavior of fine particles suspended in a gas stream depends upon their size, shape and density. These physical quantities also determine, to a large extent, the nature of a dust cake formed in the process of filtering the particles from the gas. If the shape of a particle is complex, it may be difficult to define a single number to represent its geometric size. However, the geometric or physical dimensions of aerosol particles are not especially important in themselves. The more important consideration is the way that the size and shape affect the aerodynamic forces that develop when they are in motion relative to a gas stream or affecting flow through a dust cake on a filter.

Some devices that are used to determine the sizes of suspended particles do so by classifying them as a function of their movement relative to a fluid. Cascade impactors and sedigraphs are typical of such instruments. Particle sizes are determined by relating their aerodynamic behavior to that of spherical particles. These kinds of measurements define the *Stokes diameter* or *aerodynamic diameter*, depending upon the assumption of the particle density.

As a general rule, a particle with an irregular shape and a large surface area has a greater aerodynamic resistance than a spherical particle with the same mass and density. The irregularly shaped particle will therefore appear smaller than the corresponding spherical particle in any kind of aerodynamic classifier.

### Effects on Filtration Processes

The shapes and sizes of particles in a dust cake figure prominently in determining the porosity and the permeability of the dust cake. The porosity depends strongly upon the cohesiveness of the particles, and the permeability depends upon both the porosity and the aerodynamic drag of the particles.

A particle that is spherical or nearly so can touch a neighboring particle at only one point. One can slide or roll on the surface of another to adjust position in response to external forces. Jagged or angular particles can touch each other at more than one point, and their shapes tend to prevent relative motion among them. Consequently, setting aside questions of surface stickiness for the moment, spherical particles tend to be less cohesive compared to those of less regular geometry.

The porosity of a dust cake correlates directly with the cohesivity of the particles. If the cohesivity is high, particles tend to stick where they first make contact, rather than working their way down into a more compact arrangement.

Intuitively, one expects permeability of a dust cake to correlate with porosity, but the particle size distribution and morphology play an important part, irrespective of the porosity. To illustrate this principle, consider two regions of equal volume, one filled with close-packed spheres  $10\text{ }\mu\text{m}$  in diameter and the other filled with close-packed spheres  $1\text{ }\mu\text{m}$  in diameter. The

porosity is exactly the same for both cases, but the space with the larger spheres has a small number of large pores, which will present a smaller resistance to gas flow than will the larger number of small pores in the other case.

### Conventional Fly Ash

A very common design for coal combustion is the pulverized-coal boiler, in which particles of coal are burned while suspended in air. Inert material, such as  $\text{SiO}_2$  and  $\text{Al}_2\text{O}_3$  in the coal remains as ash after the carbon and other combustible materials have burned off.

In conventional boilers the temperature is normally above the fusion point of the ash. The melted droplets of ash solidify into small spherical particles. An example of such a fly ash is shown in Figure 1. In many cases such fly ash may have surface asperities or other slight irregularities, but the shape is generally spherical.

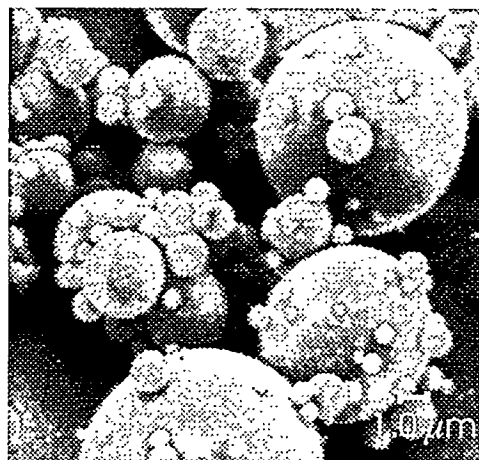


**Figure 1. Fly ash from a pulverized-coal-fired boiler**

### Gasifier Char

A gasifier produces gas from coal by heating it in an oxygen-poor gas under pressure. The char produced in this kind of process contains

unreacted carbon as well as the normal ash components found in conventional fly ash. Since gasification is usually carried out at temperatures well below the fusion point of the ash, no melting occurs, and the particles are merely the remains of the inert inclusions in the coal, mixed with the unreacted carbon.

Figure 2 is a SEM photograph of a gasifier char. The particles appear to be jagged fragments of ash and carboniferous material. The rough shape and fine size of these particles indicates a very cohesive powder. This material would be expected to form a very porous dust cake, and one that might be difficult to remove from a filter.

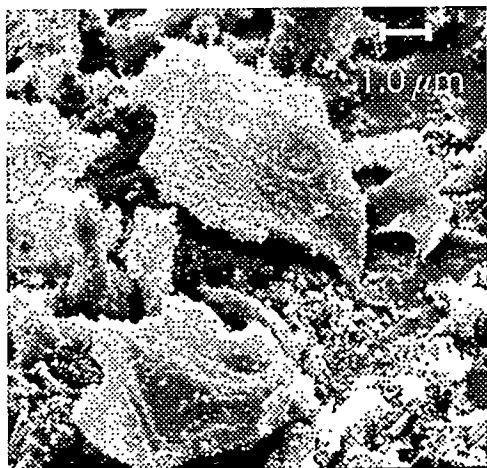


Figure 2. Gasifier char

### PFBC Ash

In a pressurized fluidized-bed combustor (PFBC), the temperature is somewhat lower than in a conventional boiler, and is often lower than the fusion temperature of the ash. As a result, the ash particles are formed from unmelted remnants of the fuel, which results in rough, irregularly-shaped particles.

One of the useful features of fluidized-bed combustion is that a sorbent may be mixed in with the fuel in the bed for sulfur removal. Some

of the sorbent, reacted or not, can be entrained in the exhaust gas. The particulate material in the process stream therefore contains not only ash, but components Ca, Mg and captured sulfur, especially in the form of soluble sulfates.

Figure 3 is an SEM photograph of an ash taken from the advanced particulate filter at the Tidd plant. As noted above, the absence of melting produces the angular or jagged particle shapes.

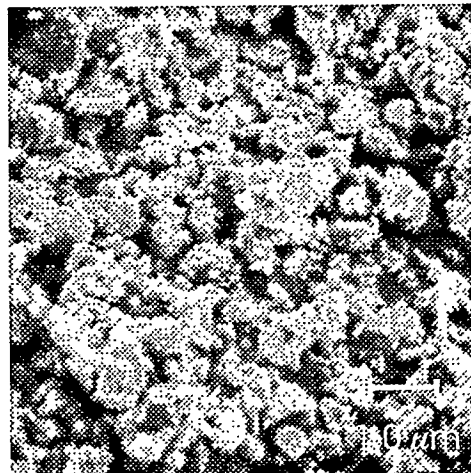
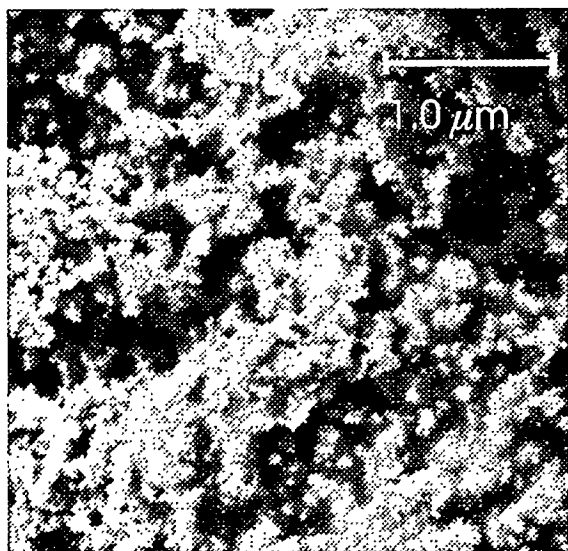


Figure 3. PFBC ash

In measurements of ash characteristics from various sources and under a number of conditions, we have noted that freshly deposited ash tends to have a high porosity — typically 85 to 90%. When exposed to temperatures in the range of 650 to 840 °C they gradually become consolidated, transforming into much stronger structures with porosity as low as 69%.

Various analyses and reviews of the literature indicate that the mechanism responsible for the extreme consolidation of the ash is a physical rearrangement of the particles attributable to the surface tension of melted or partially melted alkali-aluminosilicate mixtures formed at the contact points between adjacent particles. This conclusion is supported by the SEM picture shown in Figure 4.



**Figure 4. PFBC ash, sintered**

#### **Detailed studies of PFBC Ash**

Much of the PFBC ash represented in our data base was taken from the advanced filter system at the Tidd plant. While none of these were taken by isokinetic sampling in the gas stream, we were able to take samples directly from clearly identified regions of the dust cake, and from fixed, non-filtering areas (passive deposits).

Because the most freshly deposited portions of the filter cakes and passively deposited ash collected during the site visits were very fragile, a number of these samples were encapsulated in low-viscosity epoxy at the plant. This procedure allowed detailed measurements of the porosity of these deposits as well as preservation of the samples for further analyses.

When thick filter cakes were allowed to form on the candle surfaces, they consolidated as a result of eutectic formation, and they also tended to compact under the force of filtering pressure drop. The compaction was greatest in the layer closest to the filtering surface and progressively

less pronounced in the outer layers.

Measurements of the porosity of filter cakes removed from Tidd in September 1993 verified the existence of a gradient in the porosity of the filter cake. Porosity gradually increased from about 72% in the 0.1 inch of cake closest to the candle, to about 85% for the 30 to 40% of the cake most recently deposited. These compacted filter cakes had comparatively high mechanical strength and high resistance to gas flow. Laboratory data showed that the tensile strength of a fully consolidated filter cake nodule can exceed 12.5 psi, which is at least two orders of magnitude greater than that of a fresh ash deposit.

An SEM microprobe was used to examine agglomerates of ash obtained from the filter vessel in May 1994. This device performs elemental analyses on selected 1  $\mu\text{m}$  diameter hemispherical regions. There was little consistency from region to region in the various specimens that were examined. Each particle observed appeared to be a special case. Some particles were almost completely iron, others were very high in calcium or magnesium.

Aluminosilicate particles were also common. The shapes and sizes of the particles also varied considerably. Some particles showed evidence of having been melted and resolidified. Such particles, to the extent that it was possible to determine, were enriched in magnesium because of the formation of  $\text{MgSO}_4$ . The bonds between particles showed some enhanced levels of Mg, accompanied by such other species as Ti, Al, Ca, and S.

Although conclusions are hard to verify because of the limitations of the technique and the heterogeneity of the samples, particles rich in Mg and S apparently softened during combustion and/or collection and residence in the filter vessel. The presence of significant

amounts of Mg and S in the ash particles may have enhanced the chances for eutectic formation between particles.

### *Size Distribution*

During the test program at Tidd, problems with ash bridging and the development of thick passively deposited material were explained in terms of the small mean particle size and the concomitant high cohesivity. It was recognized that it might be advantageous to change the characteristics of the cyclone upstream of the filter to produce a larger particle size

distribution. Even though the total mass loading would increase substantially, the reduction in cohesivity would allow more effective cleaning. during the last few operational periods, the cyclones were derated and finally bypassed completely to achieve a more advantageous particle size distribution.

Information describing the bulk ash samples was derived from determinations of size distribution, chemical analyses, and uncompacted bulk porosity measurements. The most enlightening descriptions of size distributions were obtained with a combination

**Table 1**  
**Sieve Analyses of Tidd Ashes**

location, date	% weight		
	diam > 45 $\mu\text{m}$	45 $\mu\text{m}$ > diam > 15 $\mu\text{m}$	diam < 15 $\mu\text{m}$
Tube sheet, Oct. 1994	4.03	17.3	78.6
Ash shed, Oct. 1994	0.64	3.84	95.5
Tube sheet, May 1995	28.9	50.7	20.4
Filter cake, May 1995	30.1	34.3	35.6
Tube sheet, May 1995	44.8	33.3	21.9

of sieving and sedigraphic analyses. Before derating and eventually bypassing the cyclone upstream of the APF, the ash particles collected at various places in the filter vessel were very fine, with MMD's (mass mean diameters) around 3 to 5  $\mu\text{m}$ . As efforts to increase the size of the ash entering the APF by derating the cyclone progressed, somewhat larger MMD's were observed. However, the major changes in the size distributions of the ashes collected in the APF did not occur until the last period of operation, during which the cyclone was completely bypassed.

Sieve analyses were performed on ashes collected in October 1994, after derated cyclone operation, and May 1995, after operation with the cyclone completely bypassed. The data in Table 1 show that bypassing the cyclone between October 1994 and May 1995 significantly increased the size distributions of ash collected in the APF. The sieving process used on these five ashes separated a portion of the original ashes into three size fractions: particle diameters greater than 45  $\mu\text{m}$ , particle diameters greater than 15  $\mu\text{m}$ , but smaller than 45  $\mu\text{m}$ , and ash particles with diameters less than



15  $\mu\text{m}$ . (The sieving process caused this last, smallest fraction to be discarded along with the isopropanol used to wash the particles through the 45  $\mu\text{m}$  and 15  $\mu\text{m}$  sieves.)

In Figure 5, the size distribution data for these five samples obtained with the sieves have been combined with size distribution data obtained with a sedigraph. These data clearly show the increase in particle size induced by bypassing the cyclone.

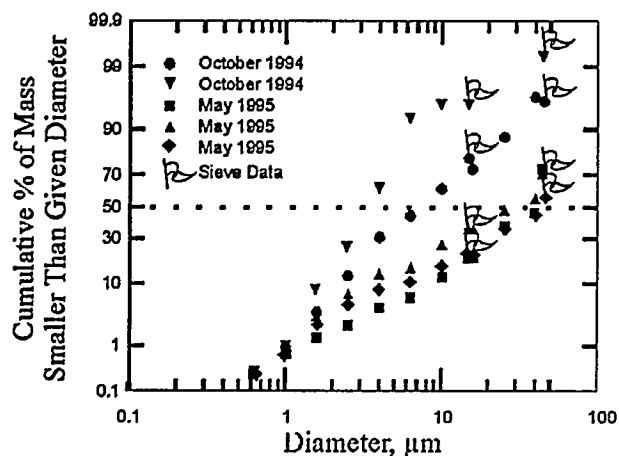


**Figure 5. Size distribution of ash obtained from the Tidd pilot plant**

The ash corresponding to the last row in Table 1 behaved much more like a free-flowing powder than the other samples collected on the same site visit. This free flowing ash exhibited the largest particle size distribution of those ashes that were analyzed. When this ash was removed from the tube sheet, it was loose and fluffy, unlike the other ash samples that were consolidated into nodules and deposits. This type of difference is common with fine powders. Powders normally become more free flowing as their particle size distribution becomes coarser.

Chemical analyses of this free flowing ash and one of the nodular ashes were performed to determine if differences other than particle size might account for the tendency of the coarser ash to behave like a free-flowing powder. Chemical analyses of these two ashes and the size-separated portions generated from them during sieving are summarized in Table 2.

These analyses demonstrated that the larger ash particles contain more Mg, Ca,  $\text{SO}_3$ , and have higher LOI values. The smaller particles are richer in Al, Na, K, Fe, Ti, and Si. These results suggest that the larger ash particles are derived mainly from the sorbent used in the combustion process, while the smaller particles are derived mainly from the coal. Because of the differences in the chemistry of the different size fractions of these ashes, it is possible that the increased flowability of the tube sheet ash represented in Table 2 may be attributable to chemical differences as well as differences in size distribution.

Standard mineral analyses of two bulk hopper ash samples and two filter cake ash samples (Table 3) showed that, like other Tidd ashes that have been analyzed, the primary elemental constituents of these ash samples were calcium, magnesium, aluminum, silicon and sulfur. Most of the calcium and magnesium in the ash in these samples is derived from use of limestone and/or dolomite in the fluidized bed. The other major constituents of the ash are derived from the coal. These chemical comparisons of hopper ashes and filter cake ashes have also helped to identify the mechanisms controlling the consolidation of ash deposits in the APF.

**Table 2**  
**Chemical Analyses of Tidd Ashes Collected in May, 1995, % wt.**

constituent	nodular ash (filter cake)			free flowing ash (tube sheet)		
	All Sizes	d > 45 $\mu\text{m}$	15 < d < 45	All Sizes	d > 45 $\mu\text{m}$	15 < d < 45
Li <sub>2</sub> O	0.01	0.01	0.01	0.01	0.01	0.01
Na <sub>2</sub> O	0.29	0.16	0.23	0.27	0.13	0.20
K <sub>2</sub> O	1.3	0.83	1.3	1.2	0.77	1.1
MgO	8.3	11.3	8.5	13.2	16.5	13.5
CaO	14.1	18.1	15.0	20.5	24.7	21.0
Fe <sub>2</sub> O <sub>3</sub>	7.1	4.8	7.5	8.0	6.2	9.9
Al <sub>2</sub> O <sub>3</sub>	11.7	7.5	10.8	10.8	7.2	9.5
SiO <sub>2</sub>	26.1	17.6	26.0	25.1	19.6	25.6
TiO <sub>2</sub>	1.2	0.41	0.46	1.1	0.33	0.49
P <sub>2</sub> O <sub>5</sub>	0.15	0.12	0.14	0.14	0.10	0.14
SO <sub>3</sub>	30.1	38.5	28.5	19.5	22.9	17.4
LOI	13.5	19.6	15.3	1.5	2.4	1.1
soluble SO <sub>4</sub> <sup>=</sup>	29.7	36.0	29.8	22.4	26.3	20.6

**Table 3**  
**Chemical Analyses of Tidd Ashes Collected in 1993, % wt.**

constituent	hopper ashes		filter cake ashes	
Na <sub>2</sub> O	0.30	0.31	0.30	0.27
K <sub>2</sub> O	1.6	1.42	1.73	1.77
MgO	9.9	9.63	8.77	7.96
CaO	15.3	15.48	14.16	13.67
Fe <sub>2</sub> O <sub>3</sub>	5.3	6.49	4.79	5.63
Al <sub>2</sub> O <sub>3</sub>	13.4	11.80	13.01	13.63
SiO <sub>2</sub>	19.2	21.29	23.03	22.89
TiO <sub>2</sub>	0.50	0.56	0.61	0.07
P <sub>2</sub> O <sub>5</sub>	0.08	0.12	0.11	0.10
SO <sub>3</sub>	33.6	31.10	31.06	31.38
LOI	1.5	2.96	1.45	1.84
soluble SO <sub>4</sub> <sup>=</sup>	48.3	--	--	40.2

### *Mechanisms Controlling the Consolidation of Ash Deposits*

Studies of the buildup of boiler tube deposits in conventional pulverized-coal fired boilers describe a mechanism which may account for the apparent consolidation of the Tidd ash deposits. Many of the ash particles collected in HGCU filter assemblies are derived directly from coal particles. These ash particles often contain a large percentage of aluminosilicate compounds. The other main source of ash particles is the sorbent used in the PFBC process. Sorbent-derived ash particles contain relatively large amounts of magnesium, calcium, or both. Once these two types of ash particles come in contact with each other in the agglomerates formed in the filter vessel, the aluminosilicate compounds in the coal fly ash tend to react with alkali and alkaline metals in the sorbent ash particles to form eutectics that melt at relatively low temperatures<sup>1</sup>. The progress of these reactions is supported by the intimate contact of the ash particles in the agglomerate and by long-term exposure of the ash particles to the temperatures in the filter vessel.

Most of the research into the formation of these eutectics has examined the formation of calcium aluminosilicate compounds (e.g.  $2\text{Ca}\cdot\text{Al}_2\text{O}_3\cdot\text{SiO}_2$  or  $\text{CaO}\cdot\text{Al}_2\text{O}_3\cdot 2\text{SiO}_2$ ). Although pure forms of these compounds do not melt at the temperatures encountered in HGCU filter vessels (pure  $2\text{Ca}\cdot\text{Al}_2\text{O}_3\cdot\text{SiO}_2$  and  $\text{CaO}\cdot\text{Al}_2\text{O}_3\cdot 2\text{SiO}_2$  melt at around 2800 °F), impurities that would almost certainly be present in these compounds because of the heterogeneous nature of coal fly ash particles would lower their melting points. It is likely that this reduction in melting points could

combine with long-term exposure to the temperatures in the filter vessel to create relatively soft, sticky layers on the surfaces of the ash particles<sup>2,3</sup>. As the viscosity of the outer layer of the ash particles decreases, the bonds between the particles become stronger. Also, the surface tension of the near-liquid layer on the particles tends to pull adjacent ash particles closer together, thereby eventually consolidating the structure of the entire ash agglomerate. This mechanism may be further enhanced by the relatively small size of the ash particles in the agglomerate.

Chemical reactions, such as the formation of calcium sulfate and/or magnesium sulfate on the surfaces of incompletely reacted sorbent particles in the agglomerate, may increase the strength of interparticle bonds and contribute to another mechanism for eutectic formation. Sulfate salts which form on the surfaces of the ash and sorbent particles result primarily from the reaction of gaseous  $\text{SO}_2$  with solid calcium oxide and/or magnesium oxide. Pure calcium sulfate melts at around 2600°F, and pure magnesium sulfate decomposes at around 2000°F. Therefore it is possible, even with the effects that impurities have on melting points, that these salts do not melt in the filter vessel. Because these sulfate salts may remain in the solid state, they could act as solid bridges between adjacent particles. Such salt bridges can increase particle bonding strengths by several orders of magnitude<sup>4</sup>. Because filter cake ash contacts much more flue gas than does passively deposited ash, this type of reaction would be accentuated in the filter cake.

However, passive ash deposits can remain in the filter vessel for extended periods since there is no effective means for their periodic on-line removal. Therefore this type of reaction may also occur to a significant extent in these passive deposits.

Additionally sodium, although present in only small amounts in the sorbent and coal fly ash particles, may react with sulfur compounds in the flue gas to form sodium sulfate. Although the melting point of sodium sulfate is over 1600 °F, it may form eutectic mixtures with calcium sulfate, thereby lowering the melting point of the eutectic mixture into the range of temperatures encountered in barrier filters. (A parallel reaction may also occur with sodium sulfate and magnesium sulfate.) Once this eutectic mixture is formed, it could then act to consolidate the ash agglomerate in the same way as does the calcium aluminosilicate eutectic mixture described above. The same consolidating mechanism would apply to any other eutectic mixture that melted or significantly softened at the temperatures within the filter vessel.

A review of the chemical analyses of hopper and filter cake ashes from Tidd was performed to assess whether additional material that might be condensed out of the flue gas or adsorbed onto the collected particles could account for the apparent consolidation of the various agglomerates of ash present in the filter vessel. The data show that the degree of consolidation of these agglomerates cannot be accounted for by condensation and/or adsorption of materials from the flue gas. The mechanism responsible for the extreme consolidation of these agglomerates of ash is most likely a physical rearrangement of the ash particles due to the surface tension of melted or partially melted

alkali-aluminosilicate eutectic mixture(s) that form at the contact points between adjacent particles after long-term exposure to the temperatures in the APF.

As can be seen in the SEM photograph of an aggregate of ash removed from the Tidd APF in October 1994 (Figure 4), the primary ash particles are nearly completely imbedded in a pervasive amorphous mass. Based on various observations of the behavior of these aggregates, it is apparent that the amorphous mass in which the particles are embedded is derived directly from the primary coal ash particles and sorbent particles originally deposited on the surface of the aggregate. The first observation that supports this contention is based on the difference between the porosity of newly-deposited regions of ash aggregates (85% or higher) and the porosity of portions of the aggregates that have been exposed to the temperatures in the APF for extended periods (around 74%). In other words, the newly-deposited regions of the agglomerates are no more than 15% solid, whereas the solid content of older portions is at least 26%. This means that as the aggregates age in the APF, either the amount of mass has been nearly doubled from some source other than the primary particles (condensation or adsorption from the flue gas), or the primary particles have rearranged themselves to occupy about 58% of their original total volume.

If the flue gas contributed large amounts of mass to the aggregate through condensation or adsorption, the chemical constituents of this added mass would be limited to compounds that could exist as a vapor at the normal operating conditions of the APF. Although many compounds could satisfy these requirements,

some of the major constituents found in the fly ash do not. Three major constituents that will not be found in a gaseous state in the APF are iron, aluminum and silicon. When we compare the mineral analyses of Tidd APF hopper ashes with mineral analyses of aged Tidd filter cake ashes (see Table 3), the iron, aluminum, and silicon contents of the two types of samples are very similar. Since the amounts of these three non-volatile elements are not significantly lower in filter cake ash than in hopper ash, it is apparent that essentially all of the mass of the filter cake is attributable to the original ash particles, and not to any significant deposition of gas-phase constituents from the flue gas.

By examining the SEM photograph of an aggregate of ash taken from the ash shedding cone below the middle plenum at Tidd (Figure 4), it is apparent that a significant portion of the mass of the ash particles has been transformed into the amorphous material mentioned above. The physical appearance of the amorphous mass is clearly distinct from the appearance of the small ash particles.

## **CERAMIC FILTER MATERIALS**

### **General Ceramic Material Issues**

Beyond the fundamental questions of filtration efficiency and pressure drop, the principal material issues for ceramic candle filters are mechanical strength and toughness, ability to withstand thermal stresses, and behavior in the high temperature filtration environment for long periods of time—up to 20,000 hr.

In general the mechanical loads on a ceramic candle under normal operating conditions are relatively low. A filter must support its own weight and that of an accumulated dust cake. In addition, it must sustain vibration-induced loads

that may occur in the system. Calculations, supported by in-situ measurements made by Westinghouse in the Tidd facility show that these vibrational loads are low, ranging up to a maximum of a few hundred psi on a conventional silicon carbide filter.

Mechanical strength requirements, except for process upsets that cause rapid temperature excursions, depend primarily on handling stresses. These kinds of loads are difficult to define or estimate; however, a tensile strength on the order of 7 MPa (1000 psi) appears intuitively to be a reasonable lower bound. Bridging between candles or other components by a dust cake generates bending loads at operating temperatures, and it is possible that such loads can increase as temperature is reduced to ambient, as occurs during shutdown.

The usual measures of a material's capability to sustain loads at high temperature is creep strength, or creep strain rate. Some ceramics do not show creep but do have time-dependent strength. This behavior is called delayed fracture, or static fatigue, and it is caused by slow crack growth in the material. The life of clay-bonded ceramics at temperatures above about 760 °C will be limited by creep; whereas for an alumina mullite ceramic, static fatigue may be the life-limiting property at temperatures of 900 °C and above.

The long-term effects of the gas chemistry at the operating temperature ultimately determines the durability of a specific ceramic filter. Binders or sintering aids used in ceramic materials may become soft or reactive at elevated temperatures. Chemical reactions can occur involving the constituents of the ceramic and those of the gas. New compounds formed by such reactions do not, as a general rule, correspond to improvements in the mechanical characteristics of the original material, so such

changes should normally be interpreted as degradation of the material. Since oxidizing and reducing atmospheres have different effects on various materials, it should not be expected that a single material would be suitable for all HGCU applications.

The critical material properties are tensile strength retention and tensile creep, or microcrack stability. These properties must be determined on materials previously exposed to the operating environment or measured under the conditions of normal operation. Projections of a material's ability to survive for a long time in the operational environment requires either long-term data under operational conditions or limited data supported by information on the micro- and macrostructures, chemical makeup, and other basic properties that can be used to develop predictive models.

### Thermal Stress

The highest stresses that occur in a candle during normal operation are thermal stresses, which occur during pulse cleaning, startup, shutdown, and any other thermal transients. In general the thermal stresses caused by cleaning pulses are the most severe. Although the exact conditions that occur during pulse cleaning are not known, the consensus among observers, supported indirectly by data, calculations, and inspection of used candles, is that the comparatively cool gas of the back pulse cools the inside surface of the candle rapidly, so that a steep temperature gradient is generated in the filter. This initial zone of cooled material appears to be confined to a layer 1 to 3 mm thick on the inner surface of the filter, as illustrated in Figure 6. For this situation the stress can be reasonably approximated by

$$s = \frac{1}{1 - \nu} E \alpha (\Delta T)$$

in which:

$\sigma$  = hoop stress at the ID

$\nu$  = Poisson's ratio of the filter material

$E$  = elastic modulus of the filter material

$\alpha$  = coefficient of thermal expansion of the filter material

$\Delta T$  = temperature difference ( $T_0 - T_a$ ) in

Figure 5

For a material with linear tensile stress-strain curve, in which  $\sigma = E\varepsilon$ , and  $\varepsilon$  is the strain, the above equation may be written

$$e = \frac{1}{1 - \nu} \alpha (\Delta T)$$

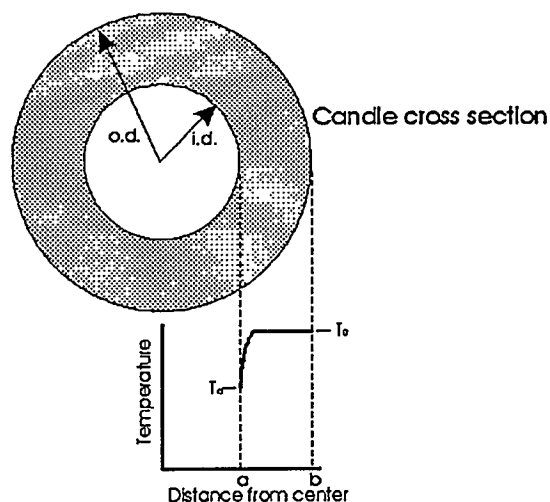
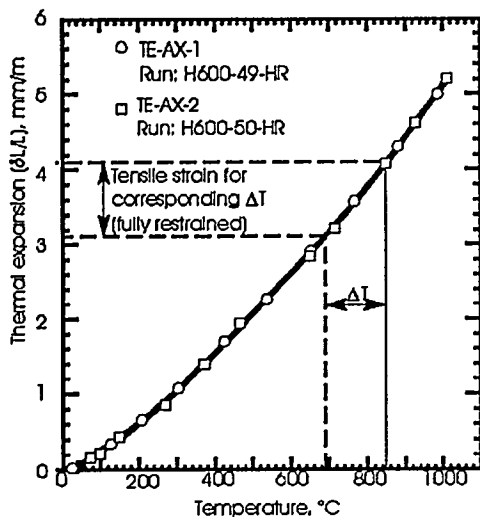


Figure 6. Temperature across a section of a candle filter

Calculations using measured values for the coefficient of thermal expansion and tensile strain to failure for monolithic filter materials show that transient, radial temperature differences of the order of 100 °C can cause microcracking in currently available ceramic filter elements. Slightly greater steady-state temperature differences can be sustained.

The above equation shows that the critical properties are coefficient of thermal expansion, tensile strain to failure, and some measure of the material's ability to resist cracking. For most monolithic ceramic materials, the tensile strains

to failure are low, so that microcracking is almost inevitable unless transient temperature differences can be kept below 100°C. Figure 7 illustrates the relationship between thermal expansion and mechanical strain for Coors alumina mullite, based on measurements of expansion as a function of temperature.



**Figure 7. Thermal stress in a monolithic alumina-mullite candle**

If microcracks do not propagate on the initial or subsequent loading, then the filter will not fail catastrophically, and it may be able to operate for many normal operational cycles. Depending upon the extent of microcracking that has occurred and its effects on the integrity of the candles, one may consider the element to be either "conditioned" or "damaged". A suitable measure of toughness could be useful in defining this somewhat subjective distinction; however, there are no generally accepted measures of toughness for ceramic materials that can be used in this context.

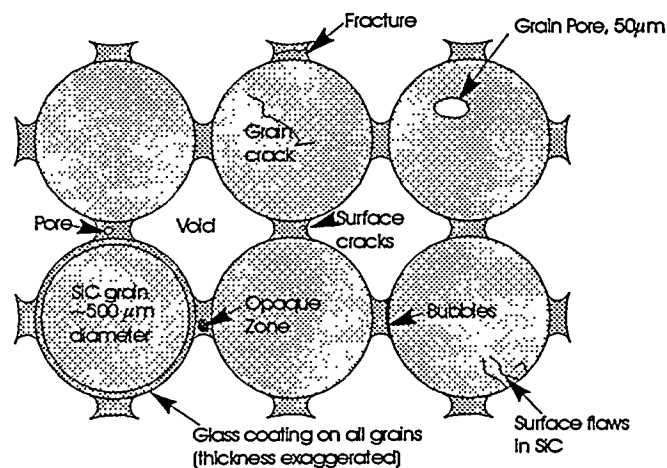
Since filters for PFBC's are expected to be required to operate at temperatures ranging upward from 650 °C to at least 870 °C, the high temperature mechanical responses of ceramic materials are important. Tensile strength, thermal

expansion, and tensile creep are probably the most important of these properties. These properties can also be affected by other characteristics of the operating environment. Since the gas may be either oxidizing or reducing; while sodium and/or sulfur compounds as well as other chemical species may be present, the material properties relative to these conditions need to be known.

### Clay-Bonded Silicon Carbide Filter Materials

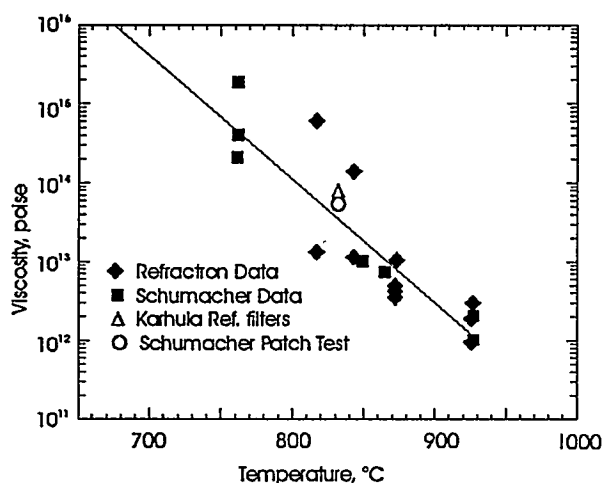
Clay-bonded silicon carbide materials are constructed of silicon carbide particles held together by a glass binder. The SiC particles for a typical candle filter material are irregularly shaped, with a nearly monodisperse size distribution. The sizes of the spaces between the particles are, generally, of the same order of magnitude as the dimensions of the particles themselves.

Figure 8 illustrates a simple conceptual model that has been used to qualitatively define the roles of the particles and the binder in the overall response of clay-bonded SiC materials.



**Figure 8. Model of a clay-bonded SiC filter material**

Using this approach with series and parallel models developed from observations of the microstructure and calibrated in terms of bulk properties, we have developed a basic understanding of the observed behavior. We have also made lifetime predictions which generally agree with observations in the operating filters at Tidd and Karhula. Figure 9 is a plot of measured viscosity versus temperature developed using the model approach discussed above. Data points are shown on the illustration for various ceramic materials developed from laboratory tests of mechanical properties. These samples were selected from materials used in the patch tests run on an atmospheric fluidized-bed combustor at Iowa State University, and from elongations measured on candles taken from the hot gas filter at Karhula.



**Figure 9. Viscosity as a function of temperature for a clay-bonded ceramic filter material**

Considering the diverse sources of data and the simplicity of the model, the results are quite consistent. The line drawn through the data points agrees with curves developed for glass viscosity. Figure 10 compares the viscosity of a Refractron clay-bonded ceramic filter with that of some industrial glasses. Since these data fall in

the middle of the glass data, the results support the conclusion that the glass binder controls this physical quantity in clay-bonded ceramic materials.

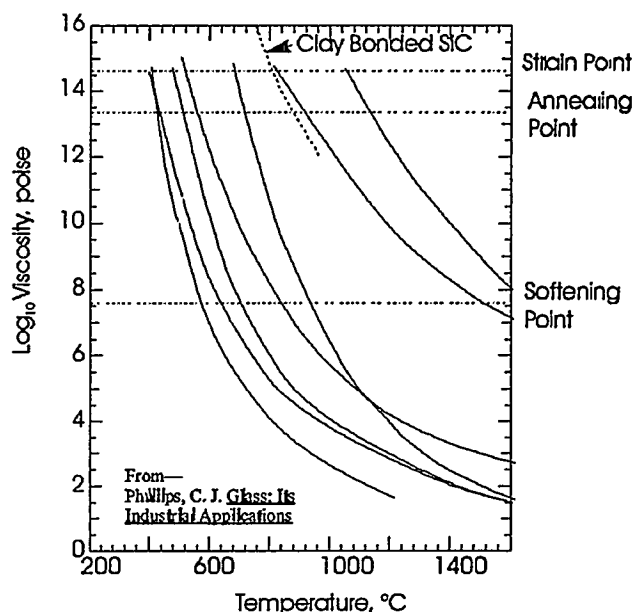


**Figure 10. Viscosity of various glasses compared with that of a clay-bonded SiC**

This result implies, or at least strongly suggests, that clay-bonded ceramic filters, as currently manufactured, cannot operate at temperatures above 760 °C (1400 F) for long periods of time. Even though the normal operating loads are relatively small, the viscosity of the binder is sufficiently low at temperatures above ~760 °C that the material will creep under its own weight. Improving these materials will require basic changes in the properties of the binder materials. Some limited improvements in the material may be possible by making the internal load paths more complicated, as for example with a broader particle size distribution. However, the only way to get a substantial improvement at high temperature is to change the binder material. For lower temperature performance, as in gasifier operation, the general construction of a clay-bonded material offers some advantages over



monolithic ceramics. Specifically, fracture typically occurs by failure of glass bridges rather than by failure of SiC particles. Thus there is no contiguous fracture path. As each glass bridge fails the crack terminates when it reaches a boundary with void space or with SiC. Inherent stress concentrations within the macrostructure of the material are low, so that cracks require a continuous source of energy to propagate. Although microcracks are likely to be generated during pulse cleaning, they are not likely to propagate unless there is another source of energy, such as that resulting from a process upset that generates a thermal or mechanical transient. The basic microstructure of a clay-bonded material thus has an advantage in toughness over monolithic ceramics. Nevertheless, because the glass holds the material together, in environments that diminish the properties of the glass binder the overall properties of the material will accordingly diminish.

### **Monolithic Ceramic Material**

An alumina mullite material manufactured by Coors is typical of a monolithic ceramic. Its properties and behavior are significantly different from those of such clay-bonded materials as those made by Schumacher and Refractron. This monolithic material is more sensitive to thermal stress failure, but less likely to creep or to degrade by exposure to a HGCU environment.

Observation of failed surfaces of candles taken from Karhula show evidence of extensive microcracking in all directions on the inner surfaces of the candles, which can be visualized as crazed surfaces. The spacing of microcracks depends on the stress states and the properties of the material. A detailed study of the crack patterns would provide indirect measurements of the magnitude and distribution of the stresses generated during pulse cleaning. Essentially the

microcracks weaken the material and provide an extensive array of stress concentrations, which act as sites for fracture initiation for loads applied later. The fracture resistance against such loads can be significantly lower than in a new candle.

Degradation of mechanical properties in terms of time and conditions of exposure has not yet been quantified for an alumina-mullite ceramic. Some tests have been run on exposed material, but the results are confounded by microcracks that have formed. A definitive test series to separate loss of strength by effects of simple exposure to the working environment from losses attributable to microcracks has not been carried out. There is apparently a general inference that the alumina-mullite material holds up better in a PFBC than does clay-bonded SiC, but this conjecture has not been confirmed by controlled experiments.

In contrast to the results found in measurements on clay-bonded ceramics, high-temperature creep has not been observed in alumina-mullite materials at temperatures up to 870 °C. There has been no evidence of creep found in used filter elements or patch test specimens, although some suggestions of slow crack growth failure have been inferred for temperatures of 900 °C and above. Tensile creep specimens that had not shown evidence of creep up to 870 °C failed at low stresses after only brief heating to 900 °C and 925 °C. Failure had initiated at small (75  $\mu\text{m}$ ) notches in the specimens, which suggests that stress concentration is a factor.

The alumina-mullite macrostructure has not been studied as extensively in this program as has that of clay-bonded materials described previously, so no information has been available to develop a model or to calculate results that might explain these high-temperature failures. The data are limited and require verification, but similar behavior has been observed elsewhere. Stress-

strain curves measured at 925 °C exhibit some non-linear behavior, but much less than has been measured for clay-bonded materials.

## ACKNOWLEDGMENTS

Substantial contributions to this work were provided by several engineers at Southern Research Institute. Mr. Todd Snyder has been instrumental in developing the particulate data base and its interpretation, Mr. Stuart Starrett directed the studies related to the thermal and mechanical properties of ceramic filter materials, Mr. Coultas Pears assisted with the development of an elementary model of sintered ceramic materials, and Dr. Grady Nichols helped in the interpretation and evaluation of experimental results. We would also like to acknowledge the advice and encouragement of our METC Project Manager, Mr. Thomas Dorchak.

## REFERENCES

1. O' Gorman, J.V. and P.L. Walker, Jr. Thermal behavior of mineral fractions separated from selected American coals," *Fuel* **52**, 71 (1973).
2. Wibberley, L.J. and T.F. Wall. "Alkali-ash reactions and deposit formation in pulverized-coal-fired boilers: experimental aspects of sodium silicate formation and the formation of deposits," *Fuel* **61**, 93 (1982).
3. Helble, J.J., S. Srinivasachar, and A.A. Boni. "Factors influencing the transformation of minerals during pulverized coal combustion," *Prog. Energy Combust. Sci.* **16**, 267 (1990).
4. Spain, J. D. and H. S. Starrett. "Physical, Mechanical and Thermal Properties of Schumacher SiC Filter Material," *SRI-MME-94-253*, March, 1994.
5. Spain, J. D. and H. S. Starrett. "Physical, Mechanical and Thermal Properties of Refractron SiC Filter Material," *SRI-MME-94-301*, March, 1994.
6. Spain, J. D. and H. S. Starrett. "Physical, Mechanical and Thermal Properties of Coors Alumina Mullite Filter Material," *SRI-MME-94-480*, March, 1994.
7. Pears. C. D. "A Model for the Response of Schumacher Glass-Bonded Silicon Carbide," *SRI Technical Note, SRI-MME-94-239*, March 25, 1994
8. Pears. C. D. "A Model for the Response of Refractron Glass-Bonded Silicon Carbide," *SRI Technical Note, SRI-MME-94-870*, March 25, 1994
9. Spain, J. D. and H. S. Starrett. "Creep of Schumacher, Refractron, and Coors Ceramic Filter Materials," *SRI Technical Note SRI-ENG-94-480*, March, 1994.

---

## Session 6B

### *Hazardous Air Pollutants (HAPS)*

---



## 6B.2 Comparison of HAPs From Advanced and Conventional Power Systems: Tidd Versus Cardinal

### CONTRACT INFORMATION

<b>Contract Number</b>	DE-AC21-92MC28016
<b>Contractor</b>	Energy & Environmental Research Center University of North Dakota 15 North 23rd Street Grand Forks, ND 58203
<b>Other Funding Sources</b>	None
<b>Contractor Project Manager</b>	Steven A. Benson
<b>Principal Investigators</b>	Thomas A. Erickson David W. Brekke
<b>METC Project Manager</b>	Norm Holcombe
<b>Period of Performance</b>	August 1992 to October 1995

### FY95-96 Program Schedule

	O	N	D	J	F	M	A	M	J	J	A	S
Task 1 Technical Review of Available Data	_____											
Task 2 Presentation of Available Data			_____									
Task 3 Assessment of Control Options					_____							
Task 4 Reporting	_____											

## OBJECTIVES

The goal of this project is to evaluate available hazardous air pollutant (HAP) emissions data from advanced power systems and compare those data with data from conventional systems. The specific objectives of this program are to 1) perform a technical review and assessment of the data accumulated on the fate of trace metals and other HAPs in advanced coal power systems and compare them to data on emissions from conventional pulverized coal power plants and 2) assess the effectiveness of conventional and innovative control technologies relative to potential regulation requirements.

## BACKGROUND INFORMATION

The Clean Air Act Amendments (CAAA) of 1990 identified 189 substances as air toxics or HAPs. Under the CAAA, the U.S. Environmental Protection Agency (EPA) must regulate emissions of these HAP at their sources, including advanced power systems used for the production of electricity. The EPA will also gain more authority for regulating emissions of these air toxics under the CAAA. The EPA will define those sources that require regulation and limit their emissions according to regulatory directives.

This project is an addition to an existing U.S. Department of Energy (DOE) program entitled Trace Element Emissions (TEE), which is being conducted by the Energy & Environmental Research Center (EERC). The purpose of this additional work is to examine and evaluate the HAPs emissions data currently available from full-scale and demonstration units employing advanced power or hot-gas cleanup systems. The majority of the HAPs

data are already available, and the results of recent sampling at advanced system sites need to be analyzed and condensed. Advanced systems employ a variety of sulfur capture methods and particulate filtration concepts that are expected to interact differently with trace elements and organic compounds. The effectiveness of conventional and innovative control technologies in advanced systems needs to be evaluated to determine the differences between the various desulfurization and filtration concepts. The data will be analyzed for trends associated with collection systems and operating conditions.

## PROJECT DESCRIPTION

To accomplish the above-mentioned goal and objectives related to this work, a three-task approach has been adopted: Task 1 – Technical Review of Available Data, Task 2 – Presentation of Available Data, and Task 3 – Assessment of Control Options. Each of these tasks is discussed in more detail below.

### Task 1 – Technical Review of Available Data

The purpose of this first task is to locate and technically review the existing data from advanced power systems. Data will be evaluated for their technical merit to determine if the sampling, sample recovery, measurements, and data interpretation methodologies are appropriate and consistent. The review process is divided into four areas: Acquisition of data reports, review of sampling appropriateness and adequacy, review of analytical appropriateness and adequacy, and review of data manipulation and statistical procedures.

The acquisition of data reports includes the search for and retrieval of reports and other forms of information relating to the emission of HAPs for both advanced and conventional power systems. Though the work is concentrated on advanced systems, conventional systems are also being reviewed for comparison purposes, since most regulations are expected to be based on conventional systems.

The review of both sampling and analytical procedures is done to ensure that comparisons between different information sources are appropriate. The review includes the evaluation of equipment testing, field and laboratory blanks, standards, and spikes, if performed. When information is lacking or is obviously erroneous, it is either qualified when reported or replaced with a better estimate. Similarly, the methods used for manipulating and reporting the data will be reviewed, and a single technique for data presentation will be chosen.

### **Task 2 – Presentation of Available Data**

The second task is designed to place all of the pertinent data into an easily accessible format for additional manipulation and comparisons, perform the comparisons, and present the resultant information in an easy-to-use format. The presentation of information includes the manipulation and comparisons of data within a single system as well as for multiple systems. A relational database and/or spreadsheets are used for storage of the information and for processing of the data.

### **Task 3 – Assessment of Control Options**

This task compares specific advanced power system and gas cleanup technologies for the ability to meet potential regulatory requirements for the emission of HAPs.

Comparisons of these technologies are made based on the data reports and assumptions of how each would operate under similar conditions. Comparisons between advanced and conventional coal conversion systems are also made. The assessment is being accomplished in four areas: Review of proposed/potential EPA regulations, HAPs emission characteristics from advanced power systems, assessment of pollutants in solid residues, and review of control technologies and potential control technologies.

The current status of EPA regulations that may pertain to advanced power systems is being explored. EPA regulations regarding coal utilization, waste incineration, and other forms of fossil fuel use are being reviewed. Potential regulations are being anticipated based on regulations currently in place, CAAA literature, and other sources.

HAPs emissions as a function of control technology are being correlated for all of the different data sets reviewed. In addition, results from the advanced power systems are being compared with existing data from conventional power systems to determine the differences between their potential impacts on the environment.

Although HAPs in solid residues have not drawn as much attention as air emissions, they are, nonetheless, potentially detrimental to the environment. The potential environmental risks of solid residues and their impact on the environment are being assessed based on existing data in the reports.

After the control technologies from these reports have been evaluated for their effectiveness on HAPs emissions, they will be compared with other control technologies for

which data are available but which are not part of the advanced power systems development effort at this time. Based on the characteristics of the HAPs emitted, other control technologies will be researched for their potential benefits to advanced power systems.

### **Deliverables**

The primary deliverable from this work will be a detailed report presenting all of the information collected under the scope of the work, including 1) a review of the sampling procedures currently used in advanced power systems, 2) a review of the analytical techniques used in characterizing samples from advanced power systems, 3) an assessment of the impact of advanced power systems on the environment, 4) an assessment of the impact of high-temperature gas cleanup systems on HAPs emissions, and 5) recommendations for future work under the DOE program to mitigate HAPs. This topical report will be entitled "Assessment of Hazardous Air Pollutants for Advanced Power Systems."

### **RESULTS**

The work performed on this project to date has centered around the evaluation of data from the Tidd pressurized fluid-bed combustor (PFBC) and advanced particulate filter (APF), the General Electric (GE) hot-gas cleanup unit (HGCU), and information from conventional systems. A brief description of these systems, including their location, furnace type, fuel type, control technologies type and temperature, and any SO<sub>2</sub> and NO<sub>x</sub> control systems, is shown in Table 1. Three sets of results are summarized below: Comparison of Tidd PFBC and Cardinal pulverized coal (pc)-fired combustor, comparison of Tidd APF and electrostatic

precipitator (ESP) with Cardinal ESP, and summary of conventional and advanced power system collection efficiencies and emission factors.

### **Comparison of Tidd PFBC and Cardinal pc-Fired Combustor**

Trace element partitioning from the Tidd PFBC system has been compared to the Cardinal pc-fired plant, which is located adjacent to it. The ratio of the mass of a given trace element in the exiting flue gas to that leaving the system in the bottom ash for both systems is shown in Figure 1. The flue gas ash is measured at the inlet of the APF for the Tidd Station and at the inlet to the ESP for the Cardinal Station. These two plants burn the same Pittsburgh No. 8 coal, although there is a significant length of time between the two sampling events over which time the coal samples may vary, making comparisons fairly easy. The partitioning that occurs within the power system boiler directly affects the amount of any metal reaching the gas cleanup site and potentially impacts the amount emitted from the total system. For all trace elements except mercury, the PFBC system at Tidd released fewer trace elements into the flue gas stream (entering the APF) than the Cardinal Station (entering the ESP). For mercury, both systems released essentially 100% into the flue gas, and none remained with the bottom ash of the systems. Figure 2 shows the amount of trace elements exiting in the Tidd PFBC flue gas that are in the vapor state. Cl, F, and Hg are primarily in the vapor state, and Cu, Mo, Ni, and Se contain greater than 10% of their mass in the vapor state. The remaining elements were primarily present as particulate.



**Table 1. Operational Information and System Design for Conventional and Advanced Systems**

Plant Location	Plant Yates Unit No. 1 (1)	Cardinal Plant Unit No. 1 (2)	Boswell Energy Center Unit No. 2 (3)	Baldwin Power Station Unit No. 2 (4)	Coal Creek Station Unit No. 1 (5)	Niles Station Unit No. 2 (6)	Niles/ SNOX (7)	Springerville Generating Station Unit No. 2 (8)	Bailey Station Units No. 7 and 8 (9)	Plant Tidd ESP Unit (10)	Plant Tidd APF Unit (11)
Furnace Type	Tangentially fired, dry bottom	Brilliant, OH	Cohasset, MN	Baldwin, IL	Underwood, ND	Niles, OH	Niles, OH	Springerville, AZ	Chesterton, IN	Brilliant, OH	Schenectady, NY
Fuel	Illinois No. 5, Illinois No. 6 bituminous blend	Opposed wall-fired, dry bottom	Front-fired, dry bottom	Cyclone-fired	Tangentially fired, divided, dry bottom	Cyclone-fired	Cyclone-fired	Tangentially fired, dry bottom	Cyclone-fired	Pressurized fluidized-bed combustor	Pressurized fixed-bed gasifier
Particulate Control	ESP	ESP	Baghouse	ESP	ESP	ESP	Baghouse	Baghouse	ESP	APF	Primary and secondary cyclones
Particulate Control Operating Temperature	280°F	300°F	350°F	335°F	320°F	300°F	390°F	180°F	310°F	400°F	1350°F
SO <sub>2</sub> Control	Jet bubbling reactor (JBR)	None	None	None	Wet flue gas desulfurization	None	Wet gas sulfuric acid (WSA)-SNOX	Spray dryer absorbers	Advanced flue gas desulfurization (AFGD)	None	HGCU
NO <sub>x</sub> Control	Tangentially fired	None	None	None	Tangentially fired/overfire air	None	WSA-SNOX	Tangentially fired/overfire air	None	None	None

- 1 Radian Corporation. "A Study of Toxic Emissions from a Coal-Fired Power Plant Utilizing an ESP While Demonstrating the ICCT CT-121 FGD Project," Final Report for DOE Contract No. DE-AC22-93PC93252; June 1994.
- 2 Energy and Environmental Research Corporation. "Assessment of Toxic Emissions from a Coal-Fired Power Plant Utilizing an ESP," Final Report for DOE Contract No. DE-AC22-93PC93252; December 1994.
- 3 Weston. "Toxics Assessment Report, Minnesota Power Company, Boswell Energy Center - Unit 2," Final Report for DOE Contract No. DE-AC22-93PC93255; July 1994.
- 4 Weston. "Toxics Assessment Report, Illinois Power Company, Baldwin Power Station - Unit 2," Final Report for DOE Contract No. DE-AC22-93PC93255; July 1994.
- 5 Battelle. "A Study of Toxic Emissions from a Coal-Fired Power Plant Utilizing an ESP/Wet FGD System," Final Report for DOE Contract No. DE-AC22-93PC93251; July 1994.
- 6 Battelle. "A Study of Toxic Emissions from a Coal-Fired Power Plant - Niles Station Boiler No. 2," Final Report for DOE Contract No. DE-AC22-93PC93251; June 1994.
- 7 Battelle. "A Study of Toxic Emissions from a Coal-Fired Power Plant Utilizing the SNOX Innovative Clean Coal Technology Demonstration," Final Report for DOE Contract No. DE-AC22-93PC93251; July 1994.
- 8 Southern Research Institute. "Springerville Generating Station Unit No. 2," Final Report for DOE Contract No. DE-AC22-93PC93254; August 1994.
- 9 Southern Research Institute. "Bailey Station Units 7 and 8 and AFGD ICCT Project," Final Report for DOE Contract No. DE-AC22-93PC93254; September 1994.
- 10 Radian Co. "A Study of Hazardous Air Pollutants at the Tidd PFBC Demonstration Plant," Draft Report for DOE Contract No. 94-633-021-02; September 1994.
- 11 Radian Co. "Trace Element Determinations During Integrated Operation of a Pressurized Fixed Bed Gasifier, Hot Gas Desulfurization System, and Gas Turbine Simulator," Final Report for DOE Contract No. 94-643-011-01; July 1994.

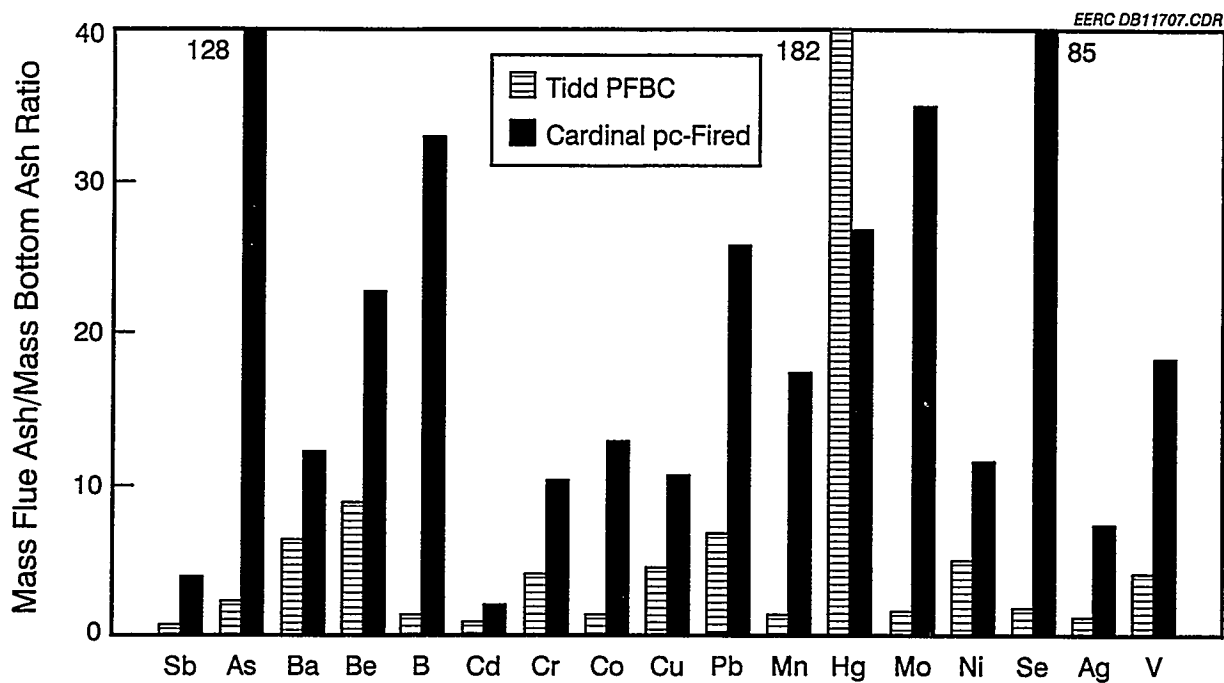


**Figure 1. Comparison of the Partitioning of Trace Elements into the Bottom Ash and Flue Gas for the Tidd PFBC and Cardinal pc-Fired System**

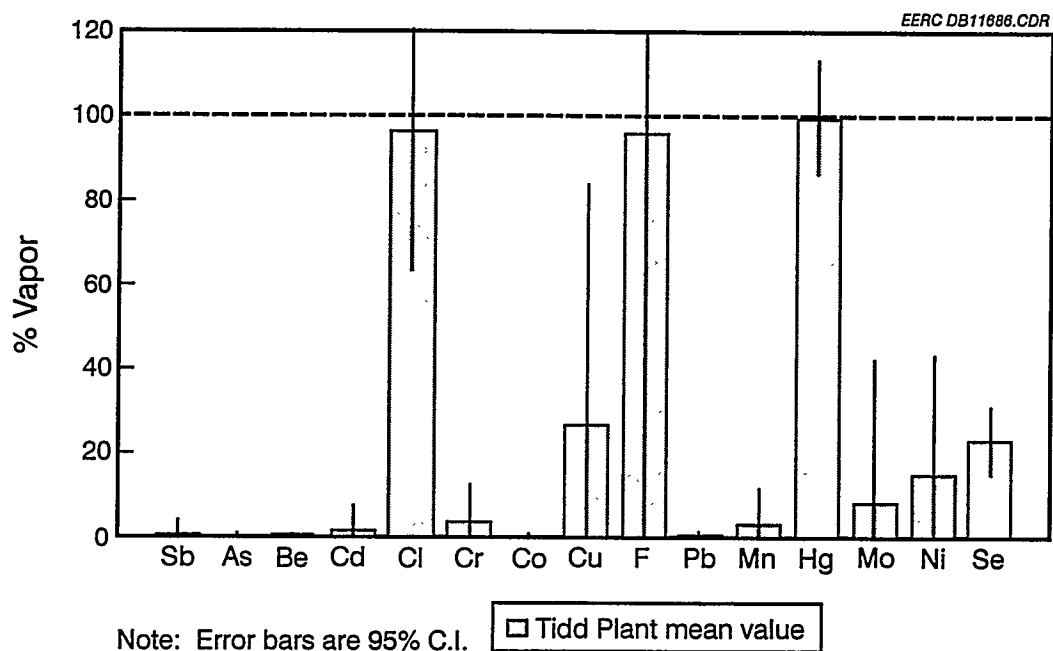


**Figure 2. Amount of Trace Elements Present in the Vapor State Exiting with the Flue Gas in the Tidd PFBC**

## Comparison of Tidd APF and ESP with Cardinal ESP

The efficiency of removing trace elements from flue gases using advanced and conventional control technologies for the Tidd and Cardinal systems is shown in Figure 3. As stated earlier, these two systems burn a similar Pittsburgh No. 8 coal, which allows for easier comparison. The Tidd system has an APF and an ESP, which are both shown on the graph. The APF shows a higher collection efficiency than the Tidd ESP for all trace elements except As, Cr, Mo, Ni, and Se. As noted in the contractor's report, there is an apparent error in the Ni, Cr, and Mo values of the APF due to contamination from a sampling probe. This results in a lower calculated collection efficiency for Cr, Ni, and Mo in the Tidd APF system. The APF shows a higher or equivalent collection efficiency than the Cardinal ESP except for Sb, Cr, Co, Hg, Mo, and Ni. In general, the Tidd APF was very effective (99.5%) in collecting the material that passed through it; however, the higher operating temperatures allow some elements to remain in the vapor state. Figure 4 shows the amount of each trace element leaving the Tidd APF and Tidd ESP that are present in the vapor state. Most of the trace elements escaping through the APF are in the vapor state, while a significant number escape through the ESP as particulate.

## Summary of Conventional and Advanced Power System Collection Efficiencies and Emission Factors

The collection efficiencies and emission factors from the nine conventional plants, as presented in the individual reports, were compared with the emission factors for the APF and HGCU. Since insufficient information was available to calculate the emission factors from the HGCU in its original system configuration, it was decided to calculate the emission factors

assuming it was placed after the Tidd PFBC, similar to the location of the APF.

The collection efficiencies for Hg, Se, and all CAAA trace elements are shown in Figure 5 for the average ESP, baghouse, FGD/other, APF, and HGCU. Hg and Se are recognized as the two most difficult trace elements to capture because of their presence in the vapor state at the temperature of collection in conventional systems (300°–400°F). Since advanced systems operate at much higher temperatures (1000°–1400°F), there would be no expected increase in capture due to particle entrapment. The general order of increasing capture of Hg and Se for the five control technologies is as follows:

ESP < APF < FGD/other < HGCU  
< Baghouse

The Tidd APF, because of the extreme temperatures, does not collect as much of the Hg and Se as the HGCU or baghouse systems. The HGCU appears to have an absorptive capability with both Hg and Se, even at the higher temperatures. It is possible that the Hg and Se are either physically or chemically captured during the capture of sulfur by the zinc titanate sorbent.

The total collection efficiency for all trace elements on the CAAA list is also shown in Figure 5 for conventional ESPs, baghouses, and FGD/other. The general order of capture for total CAAA trace elements for the five control technologies is as follows:

HGCU < ESP < Baghouse < FGD/Other  
< APF

The APF controls the total trace elements very well, since the majority of them are present as particulate, even at the higher temperatures of the APF. The HGCU performed poorly as a

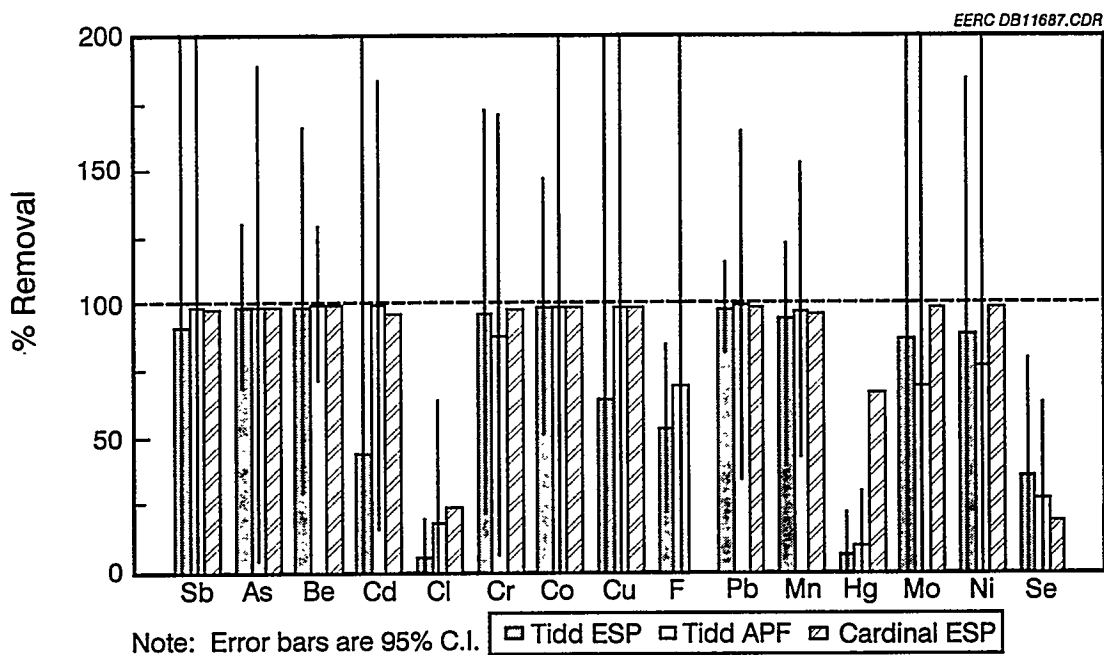


**Figure 3. Control Efficiency of Tidd APF, Tidd ESP, and Cardinal ESP**

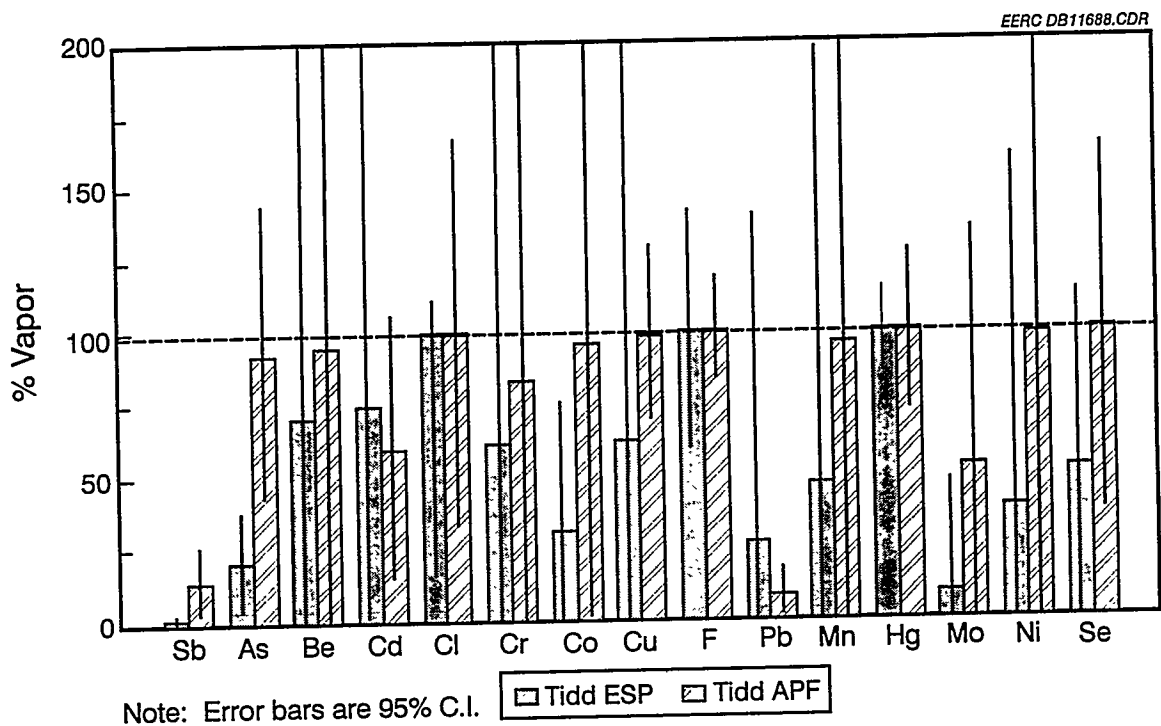


**Figure 4. Amount of Trace Elements Present in the Vapor State Exiting with the Flue Gas in the Tidd APF and Tidd ESP**

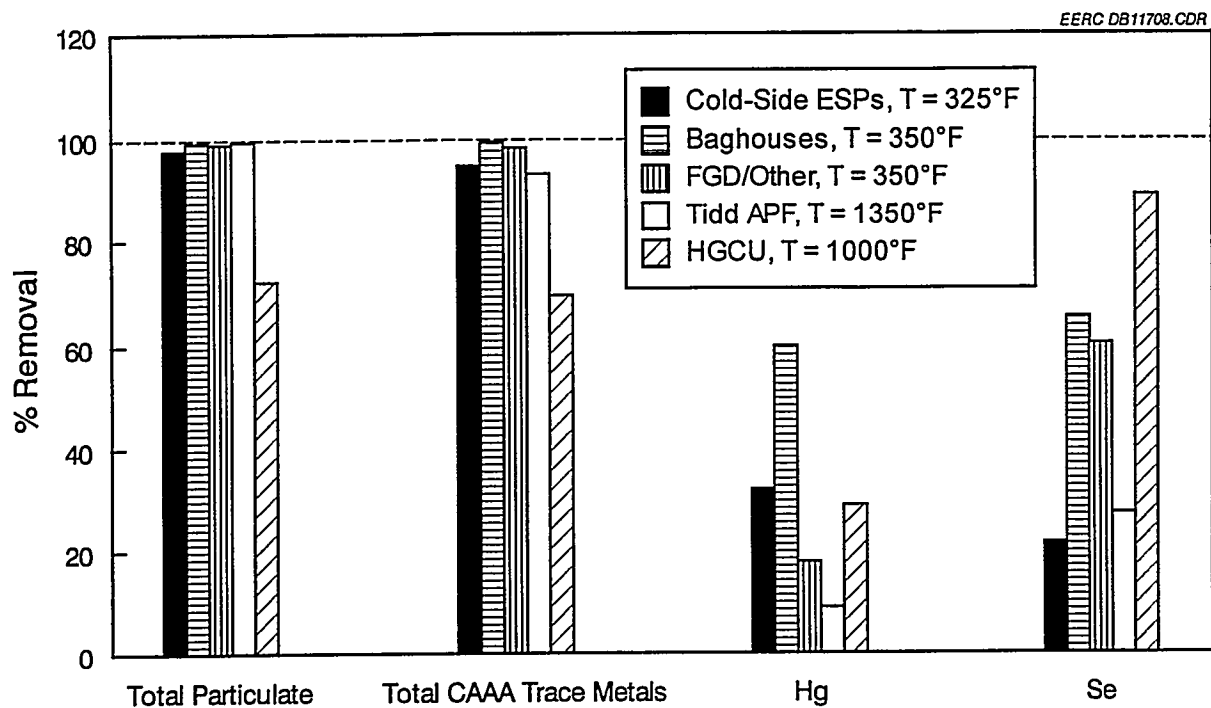


**Figure 5. Control Efficiencies for Conventional and Advanced Control Technologies**

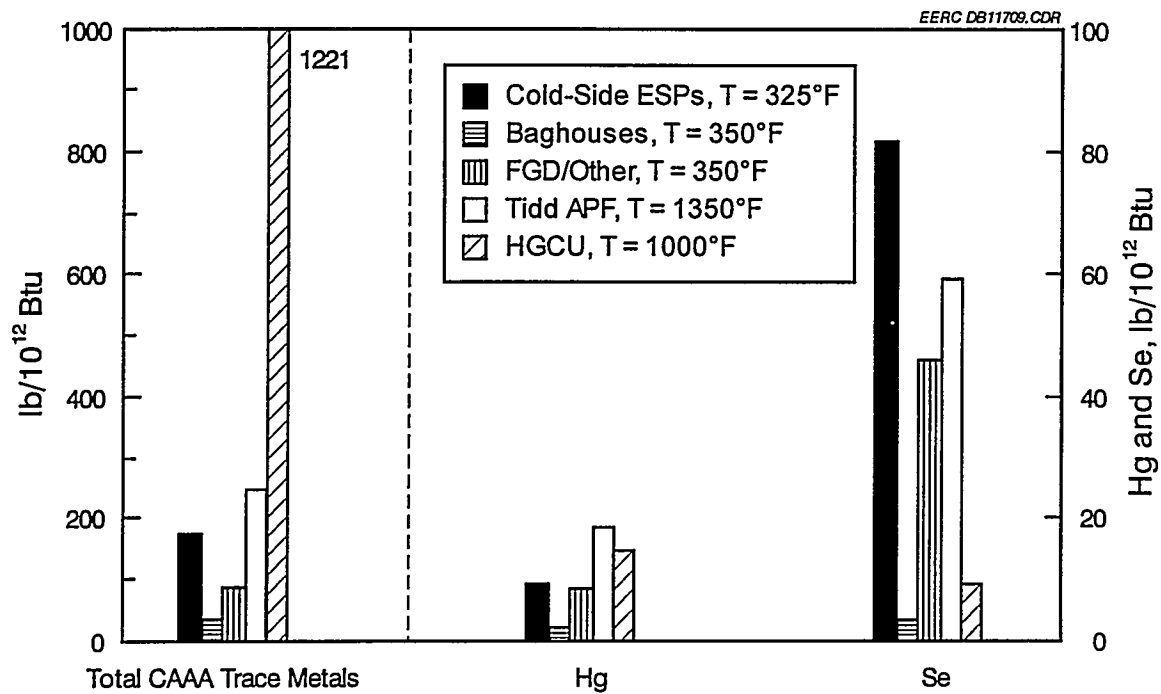


**Figure 6. Emission Factors for Conventional and Advanced Control Technologies**

particulate control device, even though it performed well for Hg and Se.

Emission factors are summarized for the total CAAA trace elements as well as Hg and Se separately in Figure 6. The results demonstrate that all of the plants studied have fairly low emission factors for total CAAA trace elements on average. It is important to note that the amount of trace elements emitted into the atmosphere is largely a function of the amount present in the coal initially. Therefore, comparisons with different coals are difficult, at best. The Tidd APF, however, shows a higher Hg and Se emission than the others. Although the total is small when compared to other technologies, the political awareness of Hg, regardless of the amount, is important.

## **FUTURE WORK**

The future efforts of this project include

- 1) inclusion of entrained gasifier data in the study,
- 2) investigation of potential solid residue regulations, and research in current and new control technologies for advanced systems. Data from the Texaco Coolwater and Louisiana Gasification Technology, Inc., systems are being studied. Potential utilization and disposal requirements for advanced power systems will be explored with reference to existing and future regulations. The potential to enhance trace element capture through enhancement of current control technologies or development of new technologies will also be explored.

**6B.3****Trace Metal Transformations in Gasification****CONTRACT INFORMATION**

**Contract Number** DE-AC21-92MC28016

**Contractor** Energy & Environmental Research Center  
University of North Dakota  
PO Box 9018  
Grand Forks, ND 58202-9018  
(701) 777-5000

**Other Funding Sources** None

**Contractor Project Manager** Steven A. Benson

**Principal Investigators** Thomas A. Erickson  
Christopher J. Zygarlicke  
Cathy A. O'Keefe  
Karen A. Katrinak  
Sean E. Allan  
David J. Hassett  
William B. Hauserman

**METC Project Manager** Dr. Norman T. Holcombe

**Period of Performance** August 1, 1992, to September 30, 1995

**Schedule and Milestones**

**FY96 Program Schedule**

	S	O	N	D	J	F	M	A	M	J	J	A
Partitioning	_____											
Modeling	_____											
Verification												
Reporting												

\* Project Review Meetings

## OBJECTIVES

The Energy & Environmental Research Center (EERC) is carrying out an investigation that will provide methods to predict the fate of selected trace elements in integrated gasification combined cycle (IGCC) and integrated gasification fuel cell (IGFC) systems to aid in the development of methods to control the emission of trace elements determined to be air toxics. The goal of this project is to identify the effects of critical chemical and physical transformations associated with trace element behavior in IGCC and IGFC systems. The trace elements included in this project are arsenic, chromium, cadmium, mercury, nickel, selenium, and lead. The research seeks to identify and fill, experimentally and/or theoretically, data gaps that currently exist on the fate and composition of trace elements. The specific objectives are to 1) review the existing literature to identify the type and quantity of trace elements from coal gasification systems, 2) perform laboratory-scale experimentation and computer modeling to enable prediction of trace element emissions, and 3) identify methods to control trace element emissions.

## BACKGROUND INFORMATION

Trace element emissions pose a potential problem to two emerging coal gasification electric power-generating systems: IGCC and IGFC. The potential problems associated with trace elements are the release of substances that are considered air toxics and the degradation of fuel cell efficiency due to contamination with minor elements. In order to develop effective technologies to control trace element emissions within anticipated regulatory requirements and to ensure the efficient operation of fuel cells,

the type and quantity of trace elements emitted from coal gasification-based systems must be determined as a function of system, system conditions, and coal composition.

The fate of trace elements in coals used in IGCC and IGFC systems is closely tied to how the trace elements are associated in the coal and the gasification conditions. Trace elements in coals are associated in several forms, including organic associations, such as salts of carboxylic acid groups and organic coordination complexes, and mineral associations, such as sulfides, sulfates, silicates, phosphates, and carbonates. During gasification, these inorganic elements are partitioned into gases, liquids, and solids. The transformation of these trace elements into the various states and phases depends upon the fundamental characteristics of the elements and their association with minerals and coal particles. Minerals that are not directly associated with coal particles experience a different process environment than minerals that are intimately associated with coal particles during gasification.

In order to predict the form of the inorganic species during gasification, it is essential that detailed information on the distribution of major mineral phases and organically associated inorganic elements be determined. This information is critical since the transformations and interactions during utilization impact the partitioning of trace elements. The primary transformations that occur to major and minor trace species during coal conversion are illustrated in Figure 1. Modeling the transformations using thermochemical equilibrium calculations combined with various chemical and physical constraints to reach equilibrium can be effectively used to estimate the distribution of gas, liquid, and solid components as a function of gasification conditions.



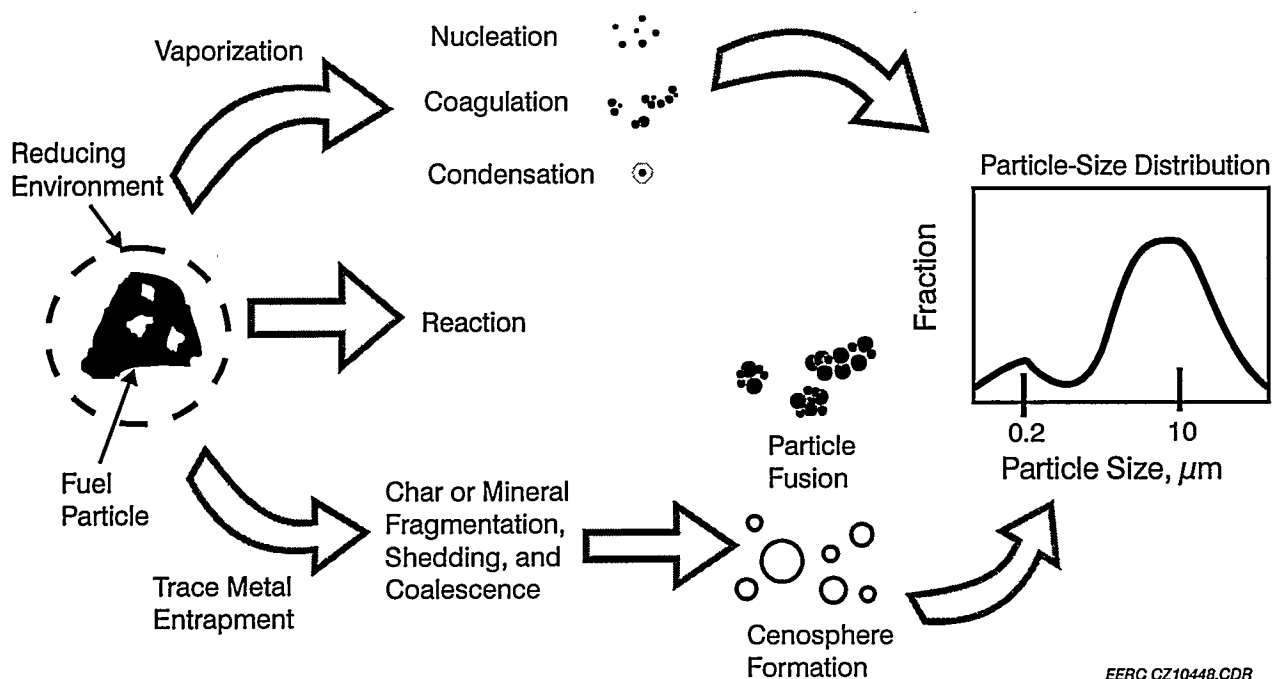


**Figure 1. Trace Metal Transformations and Partitioning**

## PROJECT DESCRIPTION

The approach of this project is to identify and model important physical and chemical transformation mechanisms of the trace elements during gasification as a function of coal compositions (trace element abundance and association) and gasification conditions. Identification of the reactions and transformations, coupled with accurate modeling of trace element behavior, is providing essential information for the identification of the form of the inorganic species. Gasification conditions—such as reducing and oxidizing

atmospheres, gas-phase composition, pressure, and temperature—influence the partitioning of the air toxics between various gases, liquids, and solid inorganic components as a function of location in the gasifier. This information will be used to identify the most effective control technology by predicting the form of the trace element as a function of operational conditions. The model will be used to predict the initial partitioning of the metals in the gasifier and their form downstream of the gasifier in the gas cleanup systems.

This project has four work categories: partitioning experiments and analysis, modeling, identification of control technologies, and model testing and verification. The partitioning experiments and analysis have concentrated on the operation of closely controlled experimental equipment to produce the appropriate samples and the analysis/characterization of those samples by state-of-the-art analytical techniques.

A pressurized drop-tube furnace (PDTF) was utilized for the experiments. Testing has been conducted for three coals under the following conditions: 1000°–1500°C, 50–200 psi, and 0.5–2.0 O/C ratio. The samples produced in the PDTF have been analyzed using inductively coupled plasma spectroscopy, atomic absorption, x-ray fluorescence (XRF), scanning electron microscopy (SEM), and various other techniques.

The modeling work has concentrated on the modification of two existing codes at the EERC: ash transformations (ATRAN) and thermochemical equilibrium analysis of coals and ashes (TEACH). Both codes are being modified to include specific algorithms associated with trace element behavior. The resultant model is a consolidation of the aforementioned codes into a single program capable of predicting the size, composition, and phase of the inorganic species at a given temperature and pressure. An operational shell is being developed to incorporate the two codes.

The identification of control technologies will be incorporated into the project after most of the testing and modeling are complete, at which time multiple scenarios can be addressed using the data and models. The model testing and verification will consist of testing the

model and assumptions on the transport reactor scaleup facility located at the EERC.

## RESULTS

The levels of the metals found in the coals are summarized in Table 1. The associations of the metals with minerals and organic portions of the coal were described in detail at the last conference (Benson and others, 1994). Table 2 summarizes the generalized associations found for the metals.

### Partitioning of Trace Metals

The partitioning of trace metals was ascertained by determining the fraction in which the different trace metal species were collected. Metals that are not vaporized during gasification remain in the residual ash and are collected in the size fraction greater than 1  $\mu\text{m}$ . Metals that are vaporized but condense in the system are collected in the submicron fraction. Metals such as Se and Hg, which may not condense in the system but remain in a vapor state, will escape the multicyclone system and will be collected in the impinger train. Several runs were made in the PDTF varying pressure, gas temperature, and O/C ratio.

Comparison of the average percentages of each element in the collection devices shows that a substantial portion, 40% or more, of the total amount of the trace elements is recovered in the coarse ash of the first cyclone (Figures 2 and 3). The trace elements have remained with the larger ash particles, have recondensed, or have been captured on the ash. Cr, Ni, (Figure 3), and, surprisingly, Hg (Figure 2) partition with the coarse ash, with an average of more than 65% remaining in the  $>3\text{-}\mu\text{m}$  fraction of collected sample, and the balance

**Table 1. Abundance of Trace Metals in Coals Tested ( $\mu\text{g/g}$ , dry coal basis)**

	Illinois No. 6	Sufco Utah	Pittsburgh No. 8
Arsenic	1.5	0.66	7.80
Cadmium	0.33	0.048	0.10
Chromium	26.0	26.9	18.8
Lead	2.84	0.86	3.87
Mercury	0.067	0.033	0.082
Nickel	15.1	8.35	14.9
Selenium	3.03	1.05	1.41

**Table 2. Trace Metal Associations**

Element	Associations
As	Pyrite, other sulfides, arsenates
Cd	Sulfides, clays
Cr	Clays, organic compounds
Hg	Pyrite, other sulfides
Ni	Pyrite, clays, organic compounds
Pb	Pyrite, other sulfides, clays
Se	Pyrite, other sulfides, organic compounds, sulfate

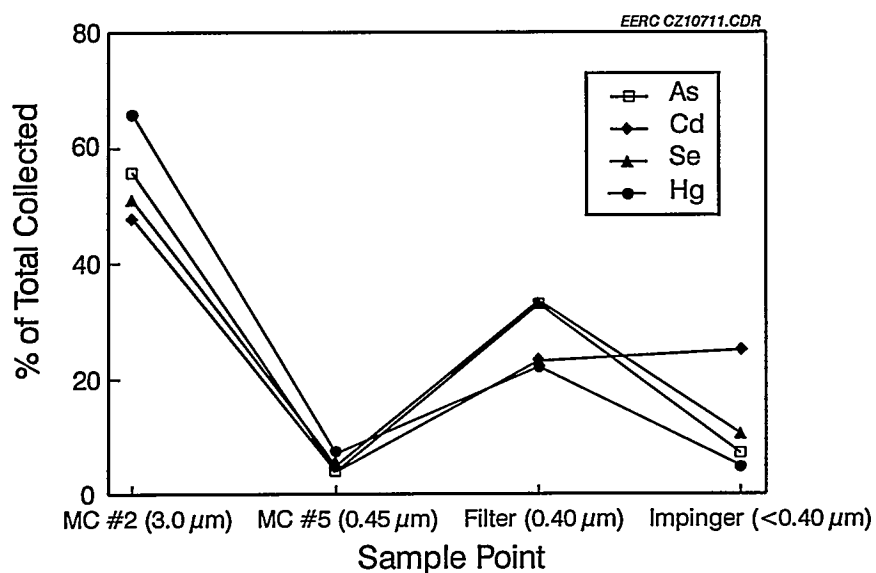


**Figure 2. Average Percentages of As, Cd, Se, and Hg Collected in Size Fractions of the Sampling Train**

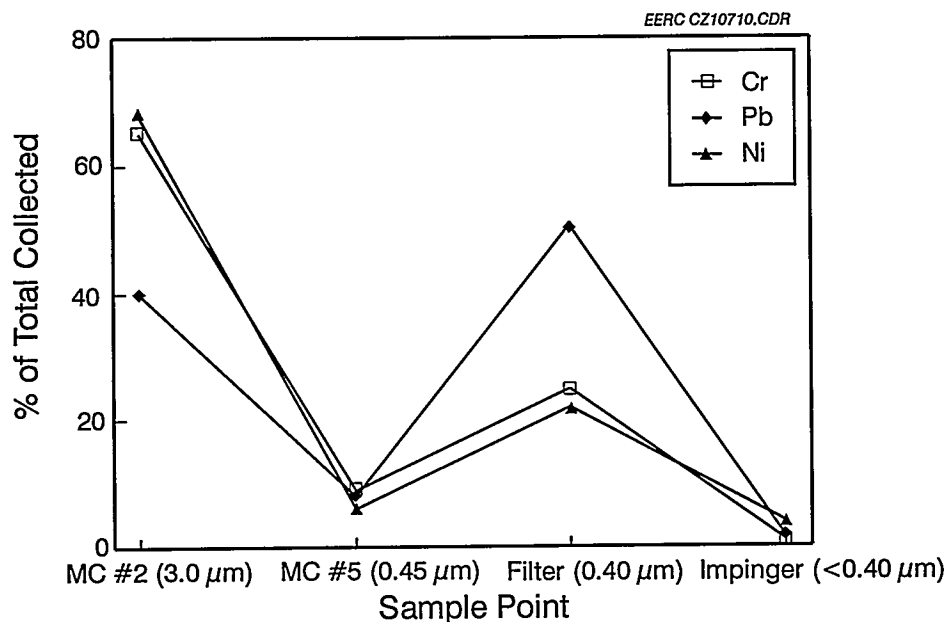


**Figure 3. Average Percentages of Ni, Cr, and Pb Collected in Size Fractions of the Sampling Train**

appearing in the 1–3- $\mu\text{m}$  fraction or the <0.4- $\mu\text{m}$  filter fraction. Very little Cr and Ni pass through the filter into the impingers (Figure 3), which is probably an indication that they are nonvolatile species, such as refractory oxides. The behavior of Hg is more complex. Although much of the Hg is collected in the cyclones and filter, under certain test conditions up to 30% of the Hg is in a volatile form passing through the filter into the impingers. Pb partitions primarily in the 1–3- $\mu\text{m}$  ash fraction and the <0.4- $\mu\text{m}$  filter, probably as a very fine oxide fume (Figure 3). Generally, little Pb passes through the filter into the impingers. Along with Hg, the trace elements As, Cd, and Se showed appreciable quantities in the impingers. Cd in particular appears to be exceptionally volatile or in the form of a very fine fume, with approximately 25% of that recovered present in the impingers (Figure 2).

In general, it can be summarized that Hg, As, Cd, and Se appear to be the most volatile, simply because a greater portion of the mass of these elements is in what would be considered condensed volatile size fractions. Here we are assuming that the trace metals in these fractions, since they are associated with particulate that is essentially less than 0.45  $\mu\text{m}$ , were in a vapor phase until capture. In contrast, Ni and Cr, along with Pb to a certain degree, concentrate primarily with the larger-sized particulate and are classified more as nonvolatile or vaporized species, with Pb showing consistently more mass in the 1–3- $\mu\text{m}$  range than Ni and Cr. Caution must be taken in making these types of assumptions, because some of these trace metal species may be condensing onto the particulate already trapped in the multicyclones or on the filter. For example, elemental Hg and Hg chloride are known to be captured on activated carbon, coal char, and fly ash. Of special concern in

these results is the amount of unburned carbon present in the ash samples. Because the PDTF tests were all run under reducing conditions, unburned carbon was found to varying degrees in nearly every size fraction of product ash collected. It is possible that some of the trace metals have not been released from their original coal host minerals or particles. Several ash grains from the largest cyclone were analyzed using WDS and yielded only Ni and Hg in iron-sulfur-rich particles and Cr in aluminosilicate particles. When this information is compared with Table 2, it could be inferred that trace metal-bearing pyrite and clay mineral aluminosilicates may not have yielded the trace metals contained within them to a vapor or fine aerosol form before they were quenched in the multicyclone. Ideally, the PDTF test runs should have 100% carbon conversion, which would ensure a minimum of carbon carryover and would maximize the release of trace metals into true postflame forms.

The effects of pressure were not clear from the data collected; however, some trends were noted for O/C and temperature effects. Figures 4 and 5 illustrate the effect of O/C ratio on the abundance of As, Cd, Se, and Hg in the assumed vapor phase at 1500° and 1000°C initial gasification temperatures, respectively. The results indicate a general decrease in As, Cd, and Hg with increasing O/C ratio and a slight increase in Se with increasing O/C ratio. A possible explanation for these results is that more oxidized forms of As, Cd, and Hg are less volatile, whereas the oxidized form or species of Se is more volatile. The lower volatility of reduced Se relative to the oxide form has been discussed by Dismukes (1994).

The effect of initial gasification temperature on the abundance of trace metals in the gas phase is depicted in Figure 6. At a constant pressure of 50 psi and an O/C ratio of 2.0, increasing the gas temperature causes the abundance of As, Cd, Se, Hg, and Pb to increase. The effects of carbon burnout, which also tends toward greater values with increasing temperature, may be overshadowing the temperature effect somewhat. Figure 7 illustrates a temperature effect by showing that the concentrations in the vapor phase of two of the more volatile elements, Hg and Se, increase with increasing temperature at constant carbon burnout.

### Predicting Trace Metals Behavior

**Model Design.** A computer model, TraceTran, to predict the evolution of major, minor, and trace elements during coal combustion and gasification has been created (Erickson and Benson, 1993), based on the algorithm shown in Figure 8.

The first task of the model is to determine the associations of the major, minor, and trace elements in the coal prior to utilization. The association of the elements prior to utilization will affect their phase, size, and composition distribution in the residual ash and gas streams. The three primary inorganic associations are water, organic, and mineral. Water-associated constituents are generally in the form of sulfates or chlorides present in the moisture of a coal particle. The organically associated constituents are generally found as the salts of carboxylic acid groups attached to the carbon matrix and as oxygen replacement (such as organic sulfur). The mineral

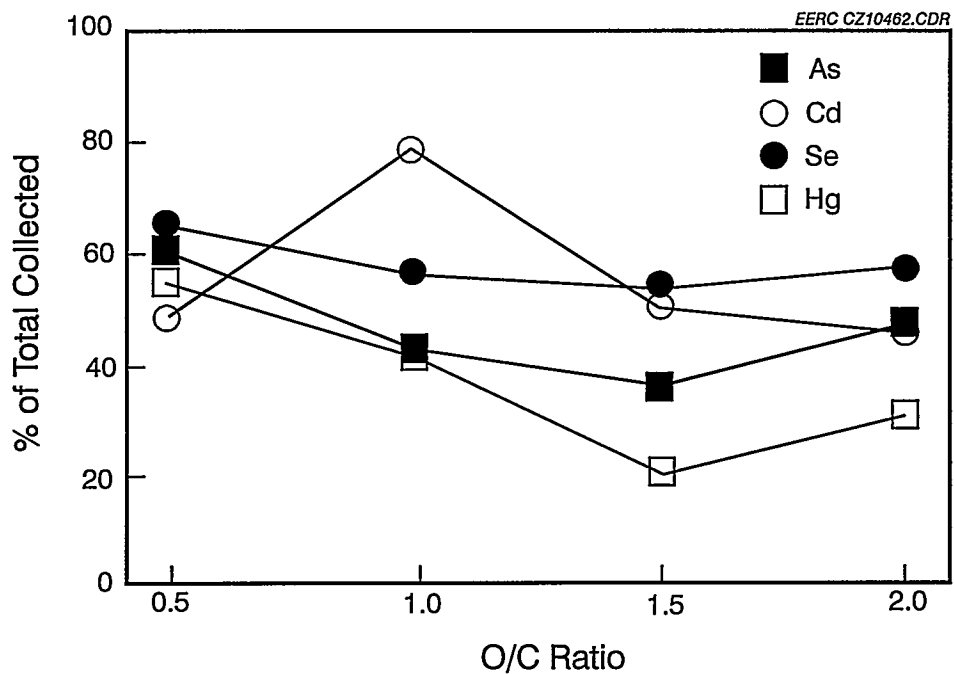


Figure 4. Trace Metal Distribution vs. O/C Ratio for Illinois No. 6

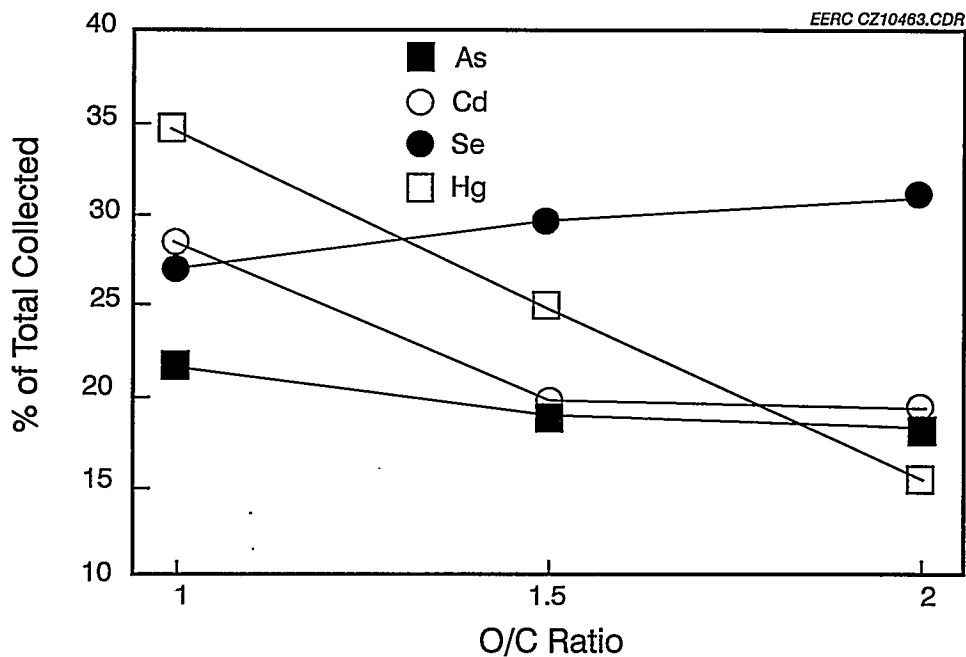
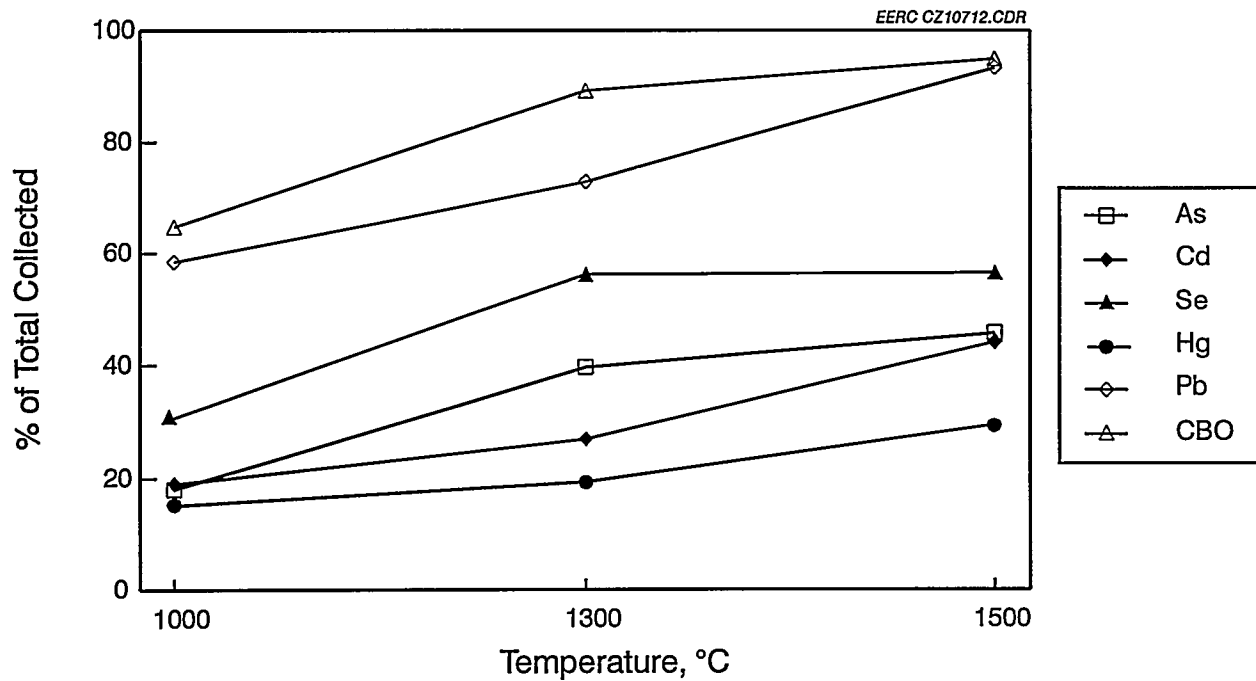
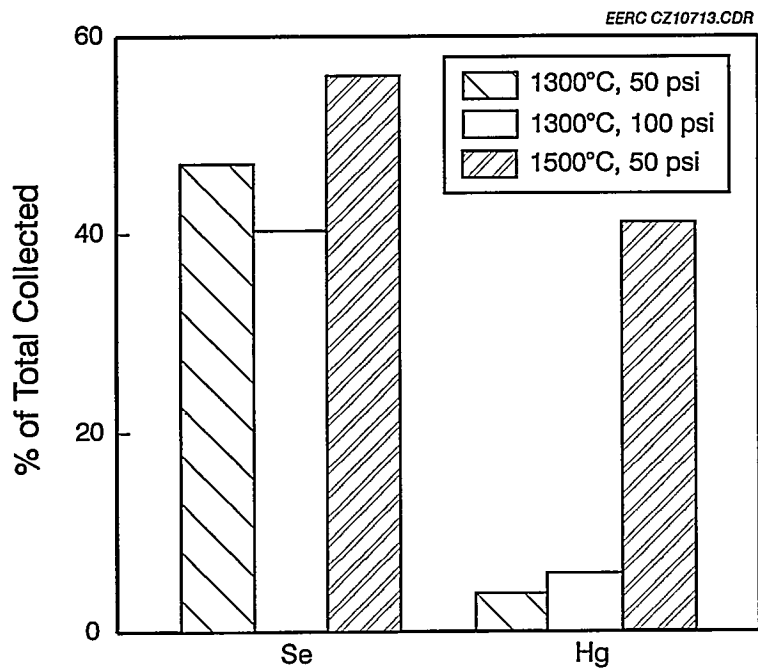


Figure 5. Trace Metal Distribution vs. O/C Ratio at 1500°C



**Figure 6. Trace Metal Distribution vs. O/C Ratio at 1000°C**



**Figure 7. Concentrations in the Vapor Phase of Hg and Se with Increasing Temperature at Constant Pressure and Carbon Burnout**

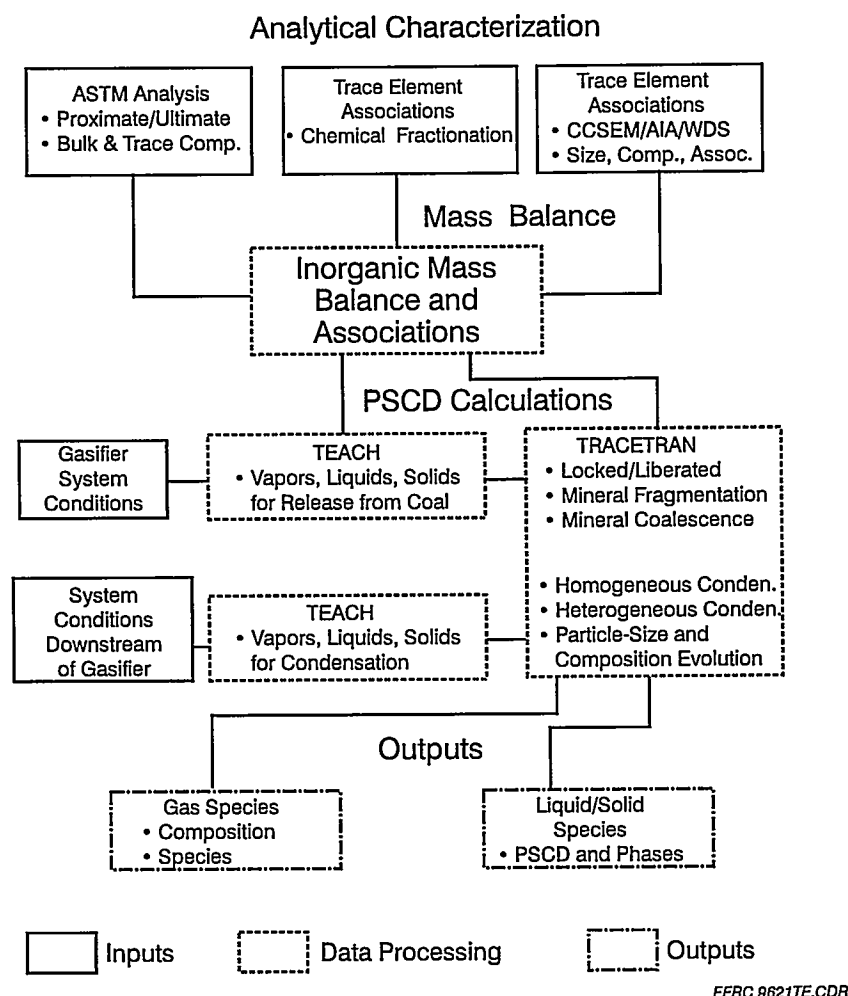


**Figure 8. Trace Element Emissions Model Algorithm**

associations are elements that comprise discrete minerals in the coal (such as clays, carbonates, and sulfides).

Because of the complexity of the interaction of inorganics during coal gasification, the mineral associations are further divided into mineral type, trace, minor, and major element content, size, and juxtaposition. Juxtaposition refers to the association of the minerals with the coal matrix and with other minerals. A locked mineral is intimately associated in the coal particle, while a

liberated mineral is external to the carbon matrix. The detailed mineral classification is very important because different minerals behave differently. For instance, carbonates will commonly release  $\text{CO}_2$ , resulting in a greater potential for mineral fragmentation, depending on the system conditions. Clays that contain high levels of moisture may fragment initially because of the release of  $\text{H}_2\text{O}$  from their porous structures. Silicates are much less prone to fragmentation because they lack any of the previously discussed components.



Many of the mineral particles encountered in coal utilization contain trace and minor components. To predict the transformations of the trace and minor elements effectively, their distribution among the minerals is required. Whether a mineral is locked within the coal matrix or external to the coal can also have a large impact on its transformations. Locked minerals will be much more likely to coalesce with other minerals and organically associated constituents than are the liberated minerals. The liberated particles will also experience a slightly different gas environment during coal gasification, since they are not in intimate contact with the highly reducing, exothermic reaction of the carbon matrix.

Once a mass balance is performed around the coal input data, it is necessary to determine which of the inorganic components will be vaporized during the initial conversion process. These calculations are performed with the use of a thermochemical equilibrium program created at the EERC. This code has been upgraded to include some of the appropriate trace element phases, and the ability to include more phases is being considered through the use of additional thermochemical equilibrium programs. With the exclusion of the vaporized species, the remaining constituents are processed through algorithms for mineral fragmentation, coalescence of both minerals and organically associated species, and the shedding of resulting particles. Examples of data obtained from the thermochemical equilibrium portion of the code are illustrated in Figures 9, 10, and 11.

The fragmentation, coalescence, and shedding algorithms have been developed with the aid of data from full-scale systems and

data generated in pilot- and laboratory-scale facilities. These algorithms are designed using data on various frequency distributions for each of the minerals and physical processes. The organically associated species that do not readily volatilize will also undergo coalescence with mineral particles as a function of the surface area of the minerals during coalescence. A portion of the organically associated species also homogeneously coalesces. The liberated minerals undergo fragmentation, but do not appreciably coalesce with other minerals because of their lack of intimate contact with the coal.

The state of the volatile species at the desired downstream conditions will then be determined, again using the TEACH code. The quantity of species that will condense prior to the given conditions is calculated from the TEACH data. The species will then be both homogeneously and heterogeneously condensed. Heterogeneous condensation is based on the surface area of the existing particles. The resultant particulate and vapor-phase species will be compiled and manipulated into various composition and size distributions at the user's discretion. These distributions can be used to determine effective control technologies for a specific coal or to locate a coal compatible to a specific control technology.

Although the emphasis of this model is to aid in the control of trace element emissions, only minor attention has been given at this time to the engineering mechanisms of the control technologies within a system. Once this model has been fully tested and verified, the next logical step will be to incorporate engineering models that mimic the control technologies. Figure 12 shows an example of the overall model applied to a pressurized

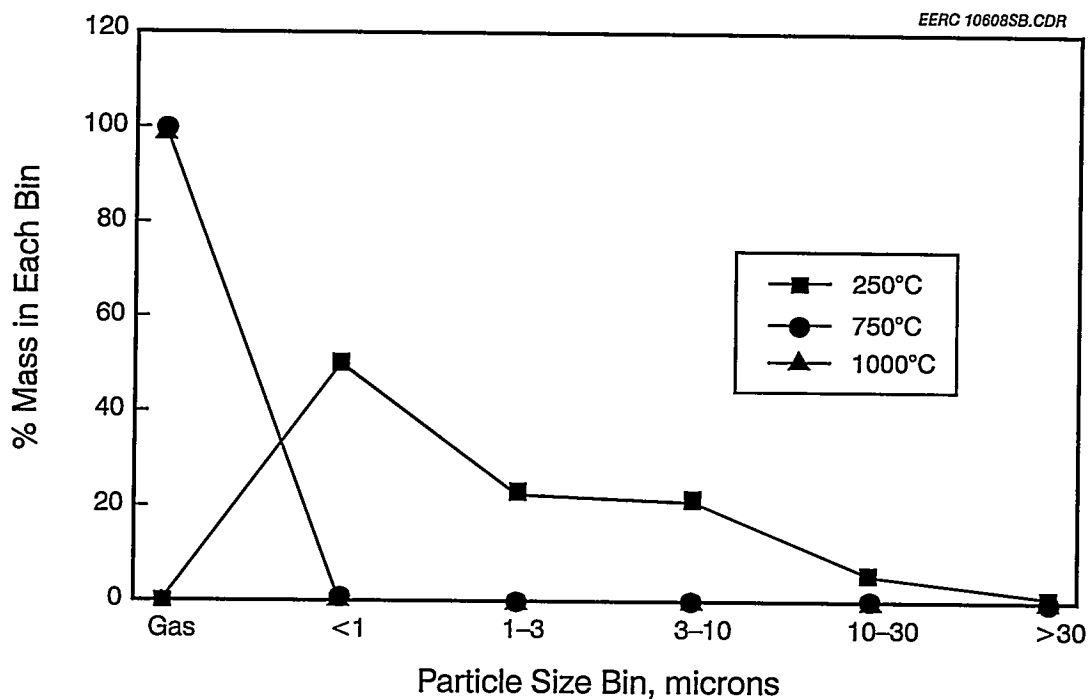


Figure 9. Illinois No. 6: TraceTran Predictions – Arsenic Particle-Size Distribution

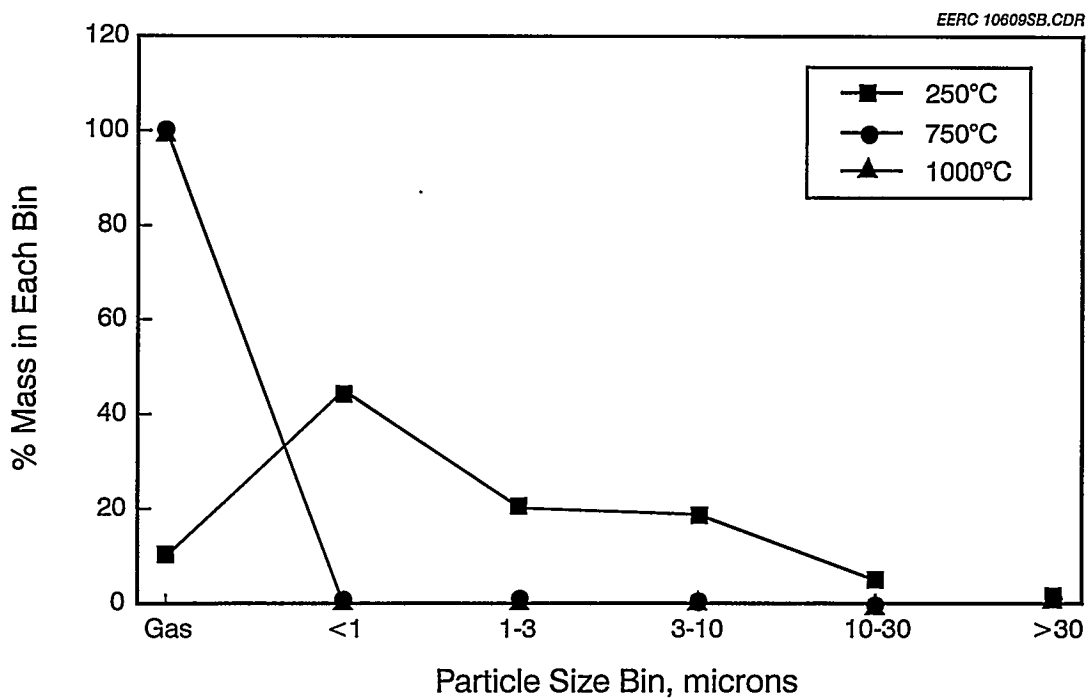


Figure 10. Illinois No. 6: TraceTran Predictions – Cadmium Particle-Size Distribution

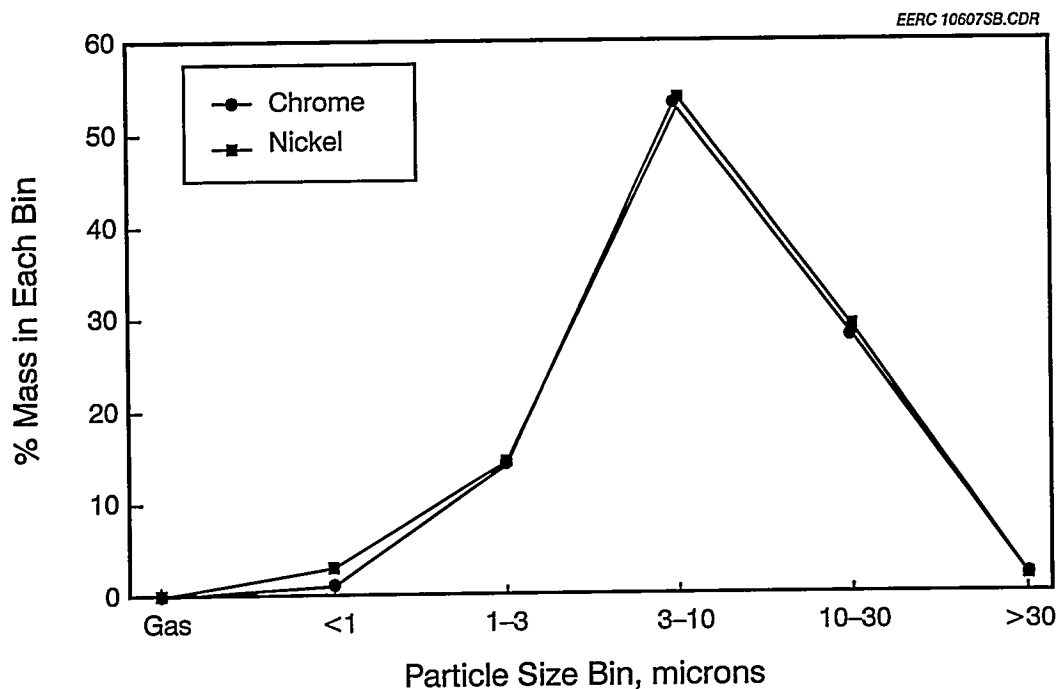


Figure 11. Illinois No. 6 TraceTran Predictions – Particle-Size Distribution, 750°C

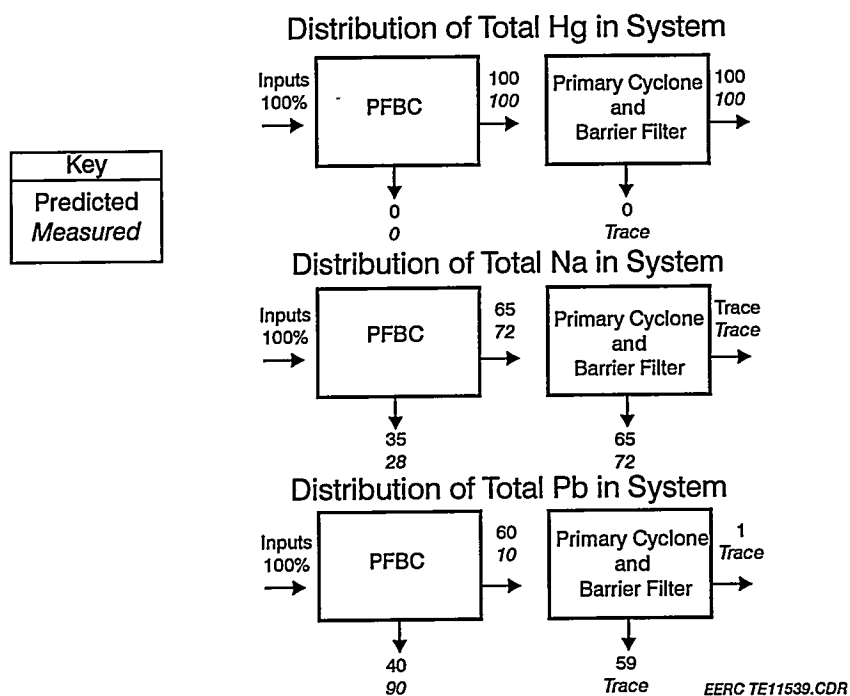


Figure 12. Trace Metal Distributions Predicted and Measured for a Pressurized Fluid-Bed Combustor

fluid-bed combustor for selected elements and the measured element distributions from full-scale sampling. A series of "crude" engineering algorithms were used for bed fluidization, cyclone efficiency, and filter performance. As expected, the model predicts well for Hg and Na, which are found largely in the vapor state, but performs only marginally for the mostly particulate lead (primarily because of the lack of robust engineering models).

Erickson, T.A.; Benson, S.A., 1993.  
Trace Element Emissions from Gasification Systems. Presented at the 205th American Chemical Society Meeting, Denver, CO, March 28–April 2, 1993.

## FUTURE WORK

Future work will involve the following:

- Completing the integration of the TraceTran computer code.
- Verifying the predictive capability of TraceTran using data obtained from larger-scale systems.

## REFERENCES

Benson, S.A.; Erickson, T.A.; Steadman, E.N.; Zygarlicke, C.J.; Hauserman, W.B.; and Hassett, D.J. 1994. Presented at Coal-Fired Power Systems 93—Advances in IGCC and PFBC Contractors' Review Meeting, DE-AC21-92MC28016.

Dismukes, E.B. 1994. Trace Element Control in Electrostatic Precipitators and Fabric Filters, In Trace Element Transformations in Coal-Fired Power Systems, Special Issue of *Fuel Processing Technology*; Benson, S.A.; Steadman, E.N.; Mehta, A.K.; and Schmidt, C.E.; Eds.; Vol. 39, Nos. 1–3, pp 403–416, August 1994.

## **Hazardous Air Pollutant Testing at the LGTI Coal Gasification Plant**

Robert G. Wetherold  
W. Al Williams  
David P. Maxwell  
Robert M. Mann  
Radian Corporation

### **ABSTRACT**

A comprehensive hazardous air pollutant test program was conducted in November 1994 at the Louisiana Gasification Technology, Inc. (LGTI), plant in Plaquemine, Louisiana. This program was sponsored by DOE/PETC, the Electric Power Research Institute (EPRI), and Destec Energy. In May of 1995, additional testing of the hot syngas stream was conducted at the LGTI facility under this same program. DOE/METC provided additional technical support for the hot gas testing effort. In this paper, the sampling and analytical methods used during the November and May test program are summarized. The hot gas testing is described in greater detail. In particular, the hot gas sampling probe and probe insertion/withdrawal system are discussed. The sampling probe was designed to collect particulate and extract gas samples at process temperature and pressure. The design of the probe system is described, and the operating procedures are summarized. The operation of the probe during the testing is discussed, and photographs of the testing are provided. In addition to the summaries and descriptions of the test methodologies, selected preliminary emissions results of the November sampling are included in the paper.

**6B.5****Development of Mercury and Chloride  
Monitors for Coal Gasifiers****CONTRACT INFORMATION**

**Contract Number** W-7405-Eng-82 (Ames)  
93MC30024.000 (METC)

**Contractor** Ames Laboratory  
Iowa State University  
Ames, Iowa 50011

**Contractor Project Manager** William H. Buttermore

**Principal Investigators** Glenn A. Norton  
Colin D. Chriswell

**Contributing Authors** Dave E. Eckels  
Rachel E. Peters  
William H. Buttermore

**METC Project Manager** Margaret A. Kotzalas

**Period of Performance** October 1, 1994 - continuing

**Schedule and Milestones**

**FY95 Program Schedule**

---

	O	N	D	J	F	M	A	M	J	J	A	S	O
Evaluate Permeation Tube Calibrator													
Evaluate Hg Detectors in the Laboratory													
Study NH <sub>3</sub> Removal With Reduction Tube													
Test HCl Detector Based on IR													
Study IMS and Colorimetric Analyzers for HCl													

---

## OBJECTIVES

Ames Laboratory will develop an integrated sampling and analysis system suitable for on-line monitoring of mercury (Hg) and hydrogen chloride (HCl) in advanced coal-based gasifiers. The objectives of this project are to 1) summarize current technology for monitoring Hg and HCl in gaseous effluents, 2) identify analytical techniques for such determinations in high-temperature, high-pressure gases from coal-based systems for producing electrical power, 3) evaluate promising analytical approaches, and 4) produce reliable on-line monitors which are adaptable to plant-scale diagnostics and process control.

## BACKGROUND INFORMATION

The capability to continuously monitor and effectively control critical effluents must be developed in order to implement new clean coal technologies. Although Hg and HCl concentrations in hot, high-pressure gases from power producing systems are of environmental and technological concern, instruments suitable for determining Hg and HCl in those environments have not yet been sufficiently developed and tested. On-line analysis is more complex for such systems than for more conventional coal-based power producing systems because of the high temperatures (up to 500°C) and pressures (up to 300 psi) involved. In addition, the different gas compositions in emerging coal-based power producing systems relative to those present in conventional combustors can pose special analytical problems. Concentrations of Hg are anticipated to be in the range of 2 - 200 ppb<sub>w</sub> in the raw gas. Concentrations of HCl are anticipated to be in the range of 50 - 500 ppm in the raw gas and less than 1 ppm after the flue gas is treated (1-3).

## PROJECT DESCRIPTION

In previous work (4), commercially available instrumentation suitable for monitoring Hg and HCl in coal gasifiers was reviewed. Also, pertinent literature was assessed to obtain additional information on methods which could potentially be used. For Hg, the techniques selected for further consideration were atomic absorption and atomic fluorescence. For HCl, non-dispersive infrared absorption, a dry colorimetric procedure, and ion mobility spectroscopy were selected for testing in the laboratory.

After the analytical methods to be used for on-line analysis of Hg and HCl have been tested in the laboratory, they will be adapted for application to monitoring hot pressurized gases from coal gasifiers. Additional work will involve developing suitable gas conditioning and sample introduction systems. That work may be as important as the development of the analytical detectors themselves. After the laboratory studies have been completed, prototype instruments will be tested and evaluated in the field.

## RESULTS

### Mercury Studies

A Thermo Separation Products Model 3200 cold vapor atomic absorption (AA) detector and a Tekran Model 2500 cold vapor atomic fluorescence (AF) detector were received and evaluated in our laboratories. This evaluation included examining parameters such as dynamic range, detection limits, precision, baseline noise and drift, and general utility of the instruments for on-line monitoring applications.

In order to assess detector response, known amounts of vapor phase elemental Hg ranging from 3 to 50,000 picograms (pg) were collected with gas-tight syringes by withdrawing Hg-saturated air above a pool of Hg in an Erlenmeyer flask fitted with a septum. By knowing the temperature and pressure within the flask, the Hg concentration in the air above the Hg pool was calculated from known Hg vapor pressure parameters. The Hg vapor was then manually injected into the carrier gas stream entering the detector. For comparative purposes, a series of injections was performed with the AF detector in which Hg vapor was collected from the flask containing an Ar atmosphere rather than air, thereby eliminating any potential quenching effects from the air being injected along with the Hg.

For the AA work, the carrier gas was either Ar or zero air. Research grade (99.9995% minimum purity) Ar was always used in the AF instrument to provide a continuous purge of the optical path. Research grade Ar was also generally used as the carrier gas for the AF tests. However, a series of tests was performed with the AF detector in which a variety of gases other than Ar were used for the carrier gas. These gases, which included CH<sub>4</sub>, CO, CO<sub>2</sub>, H<sub>2</sub>, and N<sub>2</sub>, were used to study fluorescence quenching effects to determine whether it might be possible to pass conditioned sample gases directly into the detection cell for analysis. It should be noted that the AF instrument is not intended to be operated with carrier gases other than Ar, and that passing other gases through the detector is an aberration from specified procedures in the instrument manual. Because molecular gases can quench the fluorescence signal, the instrument is intended to be used with a gold trap for collecting and preconcentrating the Hg, followed by thermally evolving the amalgamated Hg in an Ar atmosphere.

In addition to manual injections of Hg vapor, a VICI Metronics Model 340 Dynacalibrator with elemental Hg permeation tubes was used to provide a continuous flow of gases containing known Hg concentrations in the range of 0.1 to 1000 ppb<sub>w</sub> in air. All of the AA tests were performed using zero air as the carrier gas, except for one series of tests in which Ar was used as the carrier gas to allow better comparisons with data obtained by AF. Because of fluorescence quenching effects from molecular gases, Ar was used as the carrier gas for all tests using permeation tubes with the AF detector.

All data were collected on a strip chart recorder. The Hg responses were then obtained by measuring peak heights on the recorder output. For a given injection volume, three to six injections were made. When the permeation tubes were used, three sequential signals at each Hg concentration were recorded. Averages and relative standard deviations (RSDs) were then calculated from those data.

Results of the tests with the AA and AF detectors, a comparison of those two analytical techniques for monitoring Hg in coal gasification effluents, and work related to the accuracy of the permeation tube calibrator are discussed separately below.

**Atomic Absorption.** For the AA tests, baseline drift was less than  $1 \times 10^{-4}$  AU/hr. An AU reading of  $1 \times 10^{-4}$  is equivalent to a Hg concentration of about 0.5 ppb<sub>w</sub> in air or an injection of several pg Hg. Minimal baseline noise was observed, even for flows up to 1000 mL/min. However, changes in the gas flow rate into the detector for gas flows ranging from 200 to 1000 mL/min caused significant changes in baseline absorption values. The magnitude of change in baseline absorption values for a flow rate adjustment of about 200 mL/min was typically equivalent to a signal that would be



observed from a Hg concentration of 1 ppb<sub>w</sub> or less in a gas stream.

Results from Hg injections indicated that the detector could easily detect less than 3 pg Hg. A detection limit of 0.3 pg was calculated by comparing the peak height to the magnitude of the background noise for a 3-pg injection. The instrument response was linear in the range of 3 to 50,000 pg. The RSDs were typically  $\pm 1$ -5% for injections of 25 pg or more and were typically  $\pm 10$ -15% for injections of lesser amounts.

Results of tests with the permeation tube calibrator indicated that the dynamic range was excellent and spanned at least four orders of magnitude (from 0.1 to 1000 ppb<sub>w</sub>) in Hg concentration. A typical signal for a Hg concentration of 0.5 ppb<sub>w</sub> is shown in Figure 1. As can be seen, an excellent signal is obtained at that concentration. When a 0.1 ppb<sub>w</sub> (0.01 ppb<sub>v</sub>) Hg stream, which is near the minimum detectable concentration, was passed through the detector, a distinct signal was observed. For Hg concentrations ranging from 0.1 to 1000 ppb<sub>w</sub>, RSDs for the sequential measurements at a given concentration were  $\pm 5$ % or better. For concentrations above 10 ppb<sub>w</sub>, RSDs did not exceed  $\pm 2$ %.

**Atomic Fluorescence.** The baseline drift for the AF unit was typically on the order of 0.5 mV/hr. A signal of 0.5 mV is roughly equivalent to the signal produced from injecting about 1 pg Hg. Flow rate changes for gas flows in the range of 10-1000 mL/min generally did not affect the baseline signal level or baseline noise.

Excellent peaks were observed for 3-pg injections of Hg. A detection limit of 0.1 pg was calculated by comparing the peak height with the magnitude of the baseline noise. The RSDs were  $\leq 5$ % for injections of 25-5,000 pg and 5-25% for injections of 2-25 pg.

The AF instrument response to Hg injections was nearly linear over at least two orders of

magnitude (from 3 to 300 pg), although a significant degree of non-linearity was observed over a wider range. The non-linearity may be a result of quenching effects related to the increased amounts of air associated with the increasing amount of Hg injected into the detector. It could also be partially due to the fact that peak heights rather than peak areas were used to measure instrument responses.

When studying quenching effects from molecular carrier gases, a 20-30% decrease in instrument sensitivity was noted after the use of CO. Instrument sensitivity was not recovered even after purging the sample cell for up to 24 hours with Ar. However, it was later observed that the sample cell had numerous black specks of unknown origin. When the specks were removed by washing the sample cell, the instrument was restored to its original sensitivity. Although this complicated assessing the magnitude of quenching effects, conclusions could still be drawn from the data. No quenching effects were observed for CH<sub>4</sub>, but quenching effects were substantial for N<sub>2</sub> and were severe for CO<sub>2</sub>, CO, and H<sub>2</sub>. For Hg injections of 500 pg or less, the decrease in signal strength was roughly 75% for N<sub>2</sub> and was 99% or more for CO<sub>2</sub>, CO, and H<sub>2</sub>.

When the permeation tube calibrator was used, the detector could easily see an emission of about 20 pg/min of Hg into an Ar stream flowing at 170 mL/min. In Figure 2, results obtained using the permeation tubes are shown and compared to data obtained under identical conditions using AA with the Hg-containing Ar carrier stream. Unlike the Hg injections, nearly identical linearity was observed for AA and AF when the permeation tube calibrator was used. The use of the calibrator eliminated several experimental concerns, including peak broadening, quantifying peaks by peak heights, variable injection times, and quenching effects from air in the injected volumes.

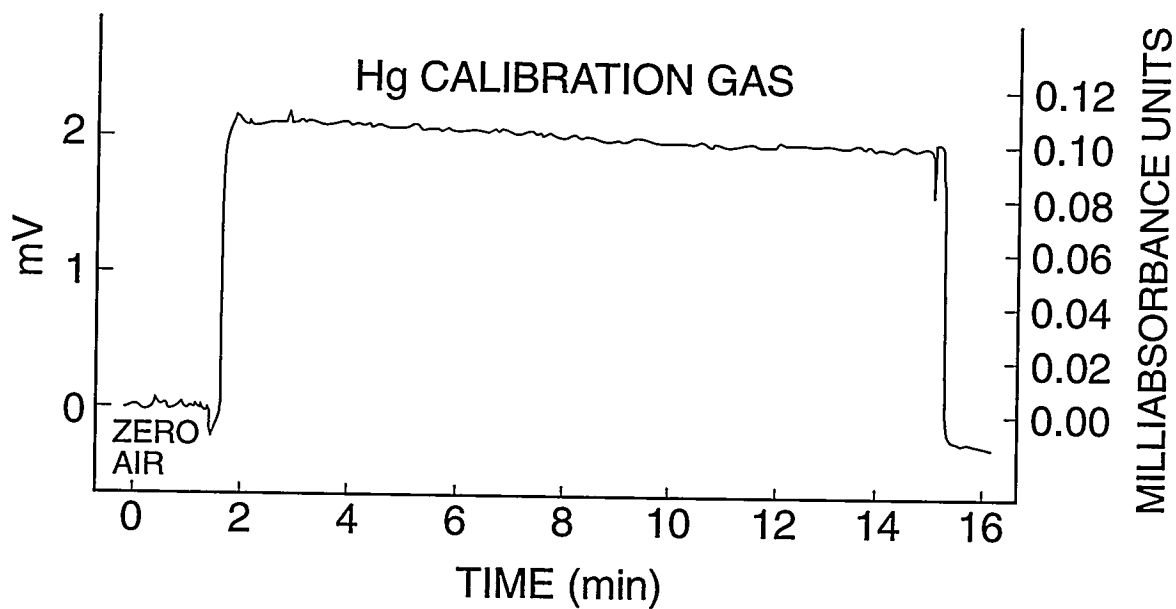


Figure 1. AA Signal Observed for 0.5 ppb<sub>w</sub> Hg in Air

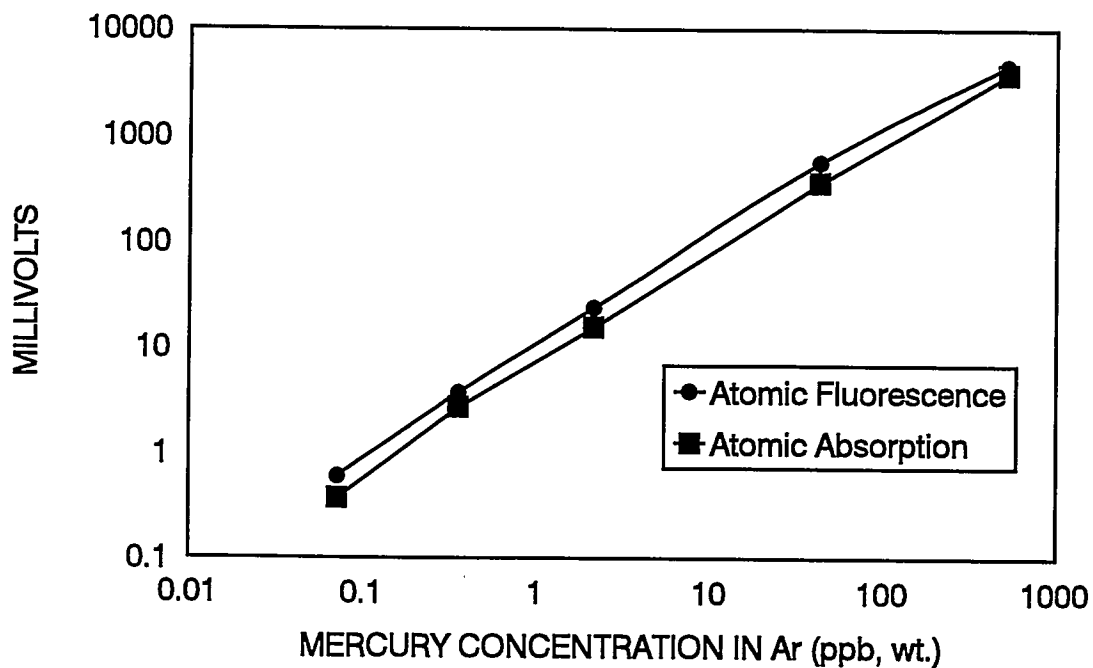


Figure 2. AA and AF Calibration Curves Obtained with a Permeation Tube Calibrator

**Instrument Selection.** We have carefully considered the AA and AF detectors for possible use in an on-line Hg monitor for coal gasifiers. Both detectors are compact, have minimal baseline noise, exhibit comparable precision, and require Hg to be in the elemental form for detection. In addition, they each offer rapid analysis, high sensitivity, low cost, and simplicity.

Because concentrations of Hg in gasifier effluents are anticipated to range from 2 to 200 ppb<sub>w</sub>, both techniques should have sufficient sensitivity to measure total vapor phase Hg after all of the Hg has been converted to the elemental form for detection. Although the sensitivity of the AF unit appears to be somewhat better than that of the AA detector, there was less than a factor of two difference based on results from Hg injections and results obtained with the permeation tube calibrator.

The AF unit exhibited less baseline drift than the AA unit, although the amount of drift in the AA baseline was still acceptable in view of the Hg concentrations anticipated in gasifier streams. Unlike the AA unit, the AF baseline was not significantly affected by flow rate changes. Thus, at low Hg concentrations, small changes in flow rate during sampling would be less problematic.

As a result of the high sensitivity of the AF unit, the possibility existed that extensively conditioned effluent gases could be directly analyzed by passing those gases through the AF detector cell in spite of quenching effects. The gold amalgamation step would be eliminated along with the need for high purity Ar. Unfortunately, the extent of quenching from most of the major gases in a gasifier stream precludes the possibility of direct analysis at the anticipated Hg concentrations. The potential for passing conditioned effluent gases directly into the absorption cell is therefore an advantage to using

AA. Also, AA does not have the requirement for a high purity Ar carrier gas.

For many coals, it appears that the AA unit has a low enough detection limit that stream dilution (e.g., 10:1) could be used to lower the dew point of water in the sample gas to room temperature prior to passing the gases into the detection cell. However, if higher dilution ratios are needed, the detection limit may not be adequate. In this event, it may become necessary to capture the Hg by gold amalgamation for preconcentration prior to thermally evolving the Hg into a suitable dry carrier gas for detection by AA.

After weighing numerous considerations, we have decided to pursue the use of AA for an on-line Hg monitor. With AA, it may still be possible to pass conditioned gases into the detection cell without the additional step of gold amalgamation. However, for direct gas analysis, extensive gas conditioning may be required. In particular, coal tars will have to be eliminated. Also, it will be necessary to correct for or remove interfering compounds, such as H<sub>2</sub>S and hydrocarbons.

**Calibrator Accuracy.** Checks on equipment vendors and proper instrument operation are an integral part of our research. This type of supporting work related to instrument development is crucial since it ultimately relates to the accuracy and reliability of our intended end product (i.e., on-line chemical monitors). In view of this, the operation of the Hg permeation tube calibrator was checked by bubbling Hg-containing gases from the calibrator into nitric acid absorbing solutions. The absorbing solutions were analyzed by conventional cold vapor atomic absorption spectroscopy. Recoveries of Hg were about 80%, which are very good in view of the uncertainties in the Hg emission rates (typically  $\pm 15$ -25% for uncertified tubes), gas flow rate, Hg collection

efficiencies, and Hg analysis by AA. When more precise instrument calibration is desired in later stages of this project, certified permeation tubes with reported Hg emission uncertainties of  $\pm 10\%$  or better will be used.

Despite good Hg recoveries in our initial tests, subsequent work indicated that many of the permeation tubes did not meet the vendor's specifications listed on the tubes. This was discovered after sending one of the uncertified permeation tubes to the vendor for certification. Although the uncertified tube was reportedly accurate to within 25%, the certified value for that tube was only within 50% of the uncertified value. The vendor has since revised the emission rates and uncertainties for the uncertified Hg permeation tubes we had previously purchased.

## Hydrogen Chloride Studies

**Gas Filter Correlation IR.** We received a Thermo Environmental Instruments Model 15 Gas Filter Correlation IR (GFCIR) HCl analyzer on loan and evaluated the monitor in our laboratories. The sample cell for this instrument can operate up to about 50°C. Tests were performed at room temperature with HCl calibration gas (3000 ppm<sub>v</sub>) in a nitrogen balance. Instrument readings were very stable and the calibration curve was linear in the range of about 50 to 3000 ppm<sub>v</sub> HCl. At lower concentrations, particularly below 25 ppm<sub>v</sub>, erratic responses were noted. It was suspected that memory effects due to sorption/desorption with sample line walls (noted even with Teflon lines) and dilution errors were at least partially to blame. Baseline fluctuations were minimal and were equivalent to the signal from only about 0.2 ppm HCl or less.

In addition to the above tests, a VICI Metronics Model 340 Dynacalibrator with HCl permeation tubes was used to provide a gas stream with HCl concentrations ranging from 0.2

to 2 ppm<sub>v</sub>. The instrument response showed good linearity from about 0.5 to 2 ppm<sub>v</sub>, as shown in Figure 3. Long equilibration times and pronounced memory effects were noted when passing low concentrations of HCl through the sample lines and flow meters. This could explain why many users of GFCIR for HCl have reported problems in differentiating between different concentrations of HCl below 10 ppm.

Tests were also performed to study the severity of the known interference from CH<sub>4</sub>. For these experiments, CH<sub>4</sub> was blended with a stream of N<sub>2</sub> containing 100 ppm HCl. The CH<sub>4</sub> concentration in the gas stream was varied from 0 to 12% and the increase in the instrument reading (in ppm) was recorded for each CH<sub>4</sub> concentration used. Results indicated that 300-400 ppm CH<sub>4</sub> gives a response equivalent to 1 ppm HCl. This has important implications on the analysis of gasifier streams using GFCIR. Concentrations of CH<sub>4</sub> can be as high as 15% in effluents from coal gasification. The equivalent HCl reading for this level of CH<sub>4</sub> is on the order of 400 ppm. Thus, if no CH<sub>4</sub> is removed prior to gas analysis, the magnitude of the error in the HCl concentration can be higher than the HCl concentration itself. Consequently, most of the CH<sub>4</sub> will need to be removed prior to analysis if GFCIR is used. Depending on the relative concentrations of CH<sub>4</sub> and HCl in the gasifier effluents, 75% to nearly 100% of the CH<sub>4</sub> will need to be removed prior to the HCl determination. Removing the CH<sub>4</sub> by oxidation is one approach that could be utilized.

In addition to our laboratory studies, personnel from several different companies who had both laboratory and field experience with the Model 15 GFCIR analyzer were contacted. They reported in discussions with us that the instrument generally works well. However, several of the instrument users noted that the analytical uncertainty is significant in the 1-10 ppm range and recommended "dampening" the

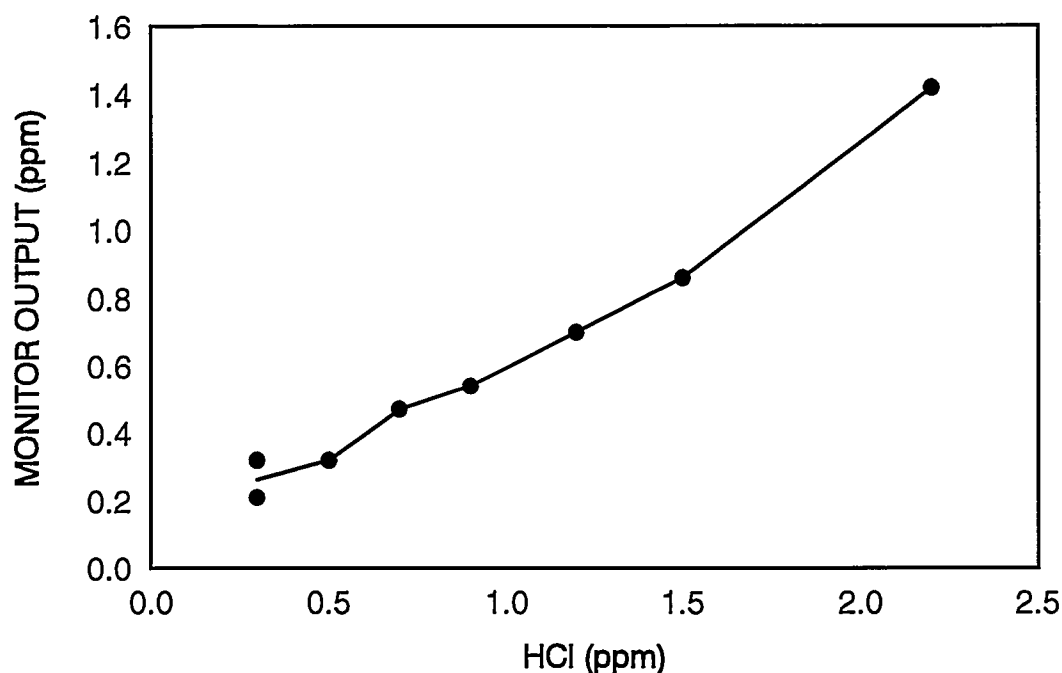


**Figure 3. Calibration Curve for GFCIR Monitor Using Permeation Tubes**

signal by taking 60-second averages. Baseline drift was also reported to be significant, which sometimes made it difficult to differentiate between 1 and 10 ppm.

**Ion Mobility Spectroscopy.** The use of ion mobility spectroscopy (IMS) for process gas monitoring was discussed with several researchers experienced in the laboratory and field determination of HF or HCl by IMS. The IMS technology is still considered to be emerging and there are numerous uncertainties involved with its use. Advantages of IMS include high sensitivity and few occurrences of false positives (5). Problems encountered include large baseline drift, sensitivity to changes in temperature and pressure of sample gas, matrix dependency, and narrow dynamic range (about two orders of magnitude). We are currently attempting to arrange the loan of an IMS system to evaluate in the laboratory.

**Colorimetric Method.** An analyzer using the colorimetric "dot" method was tested in the field by other researchers about seven years ago at a MSW incinerator. Accuracy problems were encountered and it was suspected that those problems involved different levels of humidity between the sample and calibration gases. We contacted the manufacturer of the colorimetric analyzer to discuss the accuracy problems that had been encountered earlier. Technical experts with the company informed us that the relative humidity at room temperature of the gas delivered to the analyzer needs to be between 25 and 70%. HCl readings are too low if humidity levels are outside of that range. It was also noted that the sample gas temperature at the detector inlet must be at or below 50°C. They believe that their instrument will work for our application and that sample delivery will be the most difficult part. We are currently pursuing the loan of one of their process gas analyzers for evaluation in our laboratories.

**Problems with Ammonia.** In previous work, a laboratory apparatus containing Teflon and stainless steel (types 304 and 316) components was designed and constructed to blend, heat, and deliver gases to simulate gasifier streams (6). Good HCl recoveries were obtained by passing an HCl gas mixture (3000 ppm<sub>v</sub> in nitrogen) through the testing apparatus using both heated (180-200°C) and unheated gases with flows of 100-550 mL/min.

In our recent work, tests were performed in which HCl gas was mixed with other gas components (including CH<sub>4</sub>, CO, CO<sub>2</sub>, COS, H<sub>2</sub>, H<sub>2</sub>S, NH<sub>3</sub>, and HCN) and passed through the testing apparatus. The gases were heated to about 200°C and did not contain added moisture. Good recoveries were obtained in the absence of NH<sub>3</sub>. However, difficulties were encountered in obtaining acceptable HCl recoveries in the presence of NH<sub>3</sub> due to the formation of solid NH<sub>4</sub>Cl in sections of the sample line that were at room temperature. The formation of NH<sub>4</sub>Cl has important sample delivery and analytical implications. For sample delivery, losses of chloride during sample transport must be avoided. Based on the vapor pressure of NH<sub>4</sub>Cl as a function of temperature, it is evident that NH<sub>4</sub>Cl can be kept in the vapor phase by proper heating of the sample line. However, since most of the HCl monitors to be evaluated are low-temperature (<100°C) analyzers and require the chloride to be present as HCl rather than NH<sub>4</sub>Cl, the presence of NH<sub>3</sub> gases in the sample stream presents a problem.

Because it may be necessary to remove NH<sub>3</sub> gas prior to determining HCl in coal gasifier streams, tests were performed with a reduction tube consisting of a heated quartz tube containing about 100 mL of granular (minus 20 mesh) copper. Components of the reduction tube were purchased from Perkin Elmer, who manufactures the tubes for use in their CHN analyzers. Semiquantitative tests were performed using

color-indicating paper for NH<sub>3</sub> by passing 5% (molar) NH<sub>3</sub> in a nitrogen balance through the reduction tube at a flow rate of about 25 mL/min. Results of these tests indicated that the reduction tube needs to be at a temperature of about 800-900°C in order to effectively remove the NH<sub>3</sub> under the concentrations and flows employed. However, additional semiquantitative tests indicated that the removal of NH<sub>3</sub> decreased as the flow rate was increased beyond 25 mL/min.

To help quantify the decrease in NH<sub>3</sub> removal efficiency with increased flow rate, NH<sub>3</sub> concentrations exiting the reduction tube were measured using a Sensidyne gas sampling pump with color-indicating NH<sub>3</sub> detector tubes (accurate to within  $\pm 25\%$ ). For these tests, 5% (molar) NH<sub>3</sub> in a nitrogen balance gas was passed through the reduction tube at about 950°C. For gas flows of 25 and 45 mL/min, final NH<sub>3</sub> concentrations were 200 and 600 ppm, respectively. This corresponds to a NH<sub>3</sub> removal efficiency of nearly 100% at 25 mL/min and about 99% at 45 mL/min.

Another series of tests was performed in which higher flow rates and lower initial NH<sub>3</sub> concentrations were used. When 5% NH<sub>3</sub> flowed through the tube at 100 and 500 mL/min, NH<sub>3</sub> removal efficiencies at 950°C were  $\geq 99\%$  and 90-95%, respectively. When 1% NH<sub>3</sub> was used, NH<sub>3</sub> removal efficiencies were 100% and 95% at flow rates of 500 and 1000 mL/min, respectively.

Tests were also performed to determine whether anticipated concentrations of HCl in a gasifier can pass through the hot reduction tube without being affected. This was studied by passing a 300 ppm HCl stream in a N<sub>2</sub> balance through the reduction tube, which had been previously exposed to NH<sub>3</sub>, as the temperature was increased from ambient to 950°C. Results of these tests and results from NH<sub>3</sub> removal tests obtained previously are depicted in Figure 4. The reduction tube appears to effectively remove NH<sub>3</sub> only at temperatures at which the analyte (HCl)

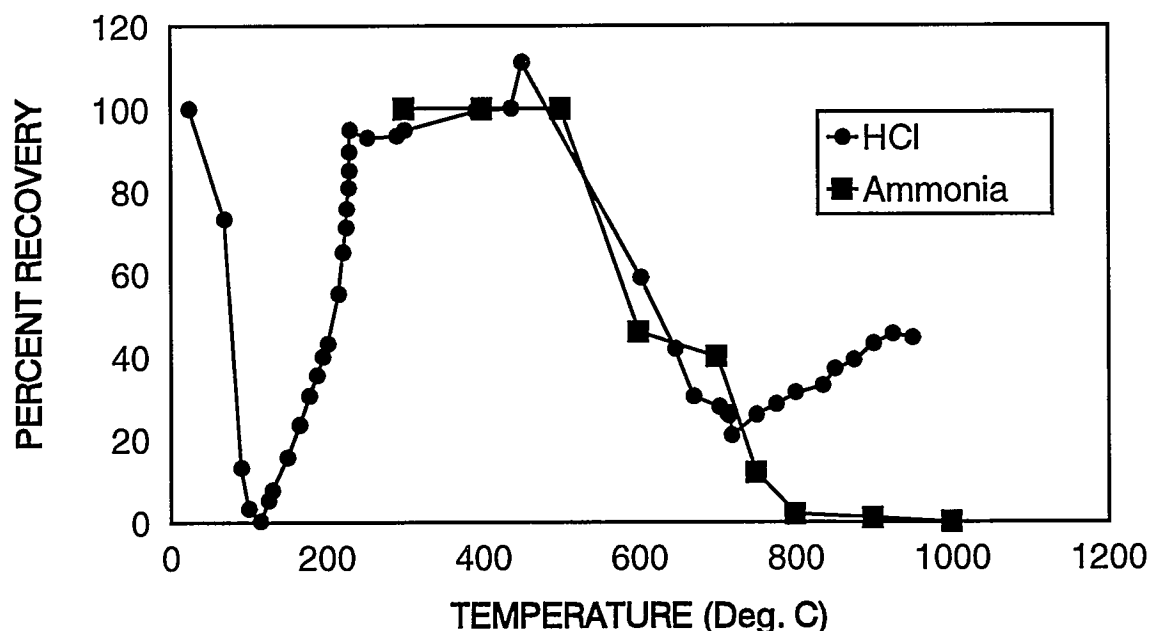


Figure 4. Percent Recovery of  $\text{NH}_3$  and HCl Versus Temperature

does not pass through the tube without loss. Also,  $\text{NH}_3$  is not permanently removed by the copper. At temperatures above  $600^\circ\text{C}$ , the decrease in HCl concentration is apparently due to the formation of  $\text{NH}_4\text{Cl}$ . The presence of  $\text{NH}_3$  is due to previous tests involving  $\text{NH}_3$  streams. Thus, this approach for removing  $\text{NH}_3$  does not appear to be promising. Consequently, alternate approaches for  $\text{NH}_3$  removal, including oxidation, are currently being considered.

**Calibrator Accuracy.** Verification of the HCl concentration output from the calibrator is important for evaluating HCl analyzers and for performing accurate calibration of those analyzers. Consequently, numerous experiments were performed to test the correct operation of the calibrator and to check the accuracy of permeation tubes supplied by the manufacturer. The permeation tubes used in our studies are filled with an azeotropic 20.2% solution of hydrochloric acid.

Calibration gases from the permeation tube calibrator were bubbled into a series of collection solutions for several days. The solutions were then analyzed titrimetrically and by ion chromatography to determine the amount of chloride collected. In addition, calibration gases were passed directly from the calibrator into a Teflon gas sampling bag. The gas in the bag was analyzed for HCl using a Sensidyne gas sampling pump with color-indicating HCl detector tubes (accurate to within  $\pm 25\%$ ). As a final test, the calibration gases in the permeation chamber were analyzed directly with the Sensidyne sampling pump and detector tubes. The total mass loss rates from the permeation tubes were also checked to determine whether they were within the range specified by the vendor (i.e.,  $\pm 15\%$ ). This was done by performing gravimetric analyses on the tubes after using the tubes in the heated permeation chamber for several days. All of the above tests were performed with two

different permeation tubes with nominal emission rates of 2500 and 6000 ng/min of 20.2% HCl.

Results of the gravimetric analyses indicated that the total emission rates were within the uncertainty listed for the tubes. The HCl concentration determined by analyzing the gases directly using the Sensidyne pump and detector tubes was about 50% of the nominal value. Results of the analyses of the collection solutions by titration and ion chromatography indicated that the solutions contained only about 20% of the HCl expected based on the nominal HCl emission rates from the permeation tubes. It is unlikely that all of the different collection and analytical techniques are erring on the low side. Consequently, we suspect the HCl concentration of the gases from the calibrator are lower than expected.

The equipment vendor has confidence in the accuracy of their equipment. However, their experimental verification of proper HCl emissions from the tubes are based on gravimetric determinations of the permeation tubes to check mass loss rates. They have not determined HCl concentrations of gases emitted from the calibrator. Although the permeation tubes are filled with an azeotropic solution of hydrochloric acid, the emitted vapors from the tubes may have a lower HCl concentration. Also, it is possible that there are some HCl "wall losses" during transport of the calibration gases.

### Gas Conditioning

In order to monitor Hg and HCl in actual gasifier streams, it is likely that the dew point of the gas stream will need to be decreased substantially by removing much of the water or by dilution. Potential methods for removing moisture from gasifier streams without affecting Hg or HCl concentrations are being evaluated.

Common approaches for moisture removal prior to analysis of effluent gases include the use

of condensers, desiccants, and selective permeable membranes. Condensers and desiccants are unsuitable for our purposes because of loss of analytes that would occur during gas conditioning. There is disagreement among the experts as to whether HCl would be retained by permeable membranes, and little information is available on the effects of those membranes on Hg vapor. The applicability of using permeable membranes to condition our sample gases requires experimental verification. Another possible gas conditioning approach for moisture removal is to use a special chemically selective membrane, such as Nafion, which reportedly has a higher moisture removal rate than permeation membranes and reportedly does not retain significant amounts of Hg or HCl.

### FUTURE WORK

For Hg, problems associated with the use of AA will be investigated. The primary problem anticipated is the presence of interfering compounds (e.g., aromatic hydrocarbons and sulfur compounds) in actual gasifier streams. Future work will focus on studying approaches for either removing interfering compounds through gas conditioning or for performing suitable spectral background corrections during analysis of the gasifier streams. The best approach for use in an on-line analyzer for coal gasifiers will then be selected. Also, because AA analysis requires the Hg to be present as elemental Hg, approaches for converting Hg compounds (e.g., methyl mercury) to the elemental state will be investigated.

For HCl, the analytical method to be used for the on-line monitor will be selected. Studies on the delivery of known amounts of HCl will continue. In particular, the use and accuracy of permeation tubes and permeation tube calibration systems will continue to be investigated.



Methods for removing or destroying  $\text{NH}_3$  in the sample gas prior to HCl analysis will be considered and tested.

For both Hg and HCl, subsequent testing will include determining the effects of gas temperature, pressure, and composition (including moisture content) on detection limits, dynamic range, precision, and accuracy. The effects of sample line composition will also be considered. Modifications to existing commercial instruments will be made in order to adapt those systems for use with gasifier streams.

The severity of interferences from compounds such as  $\text{H}_2\text{S}$ , HF, and selected hydrocarbons on Hg and HCl determinations will continue to be investigated. In addition, suitable sample handling systems will be developed. Gas conditioning steps which may be required include temperature and pressure adjustments, filtering particulate matter, and removing moisture and interfering gases. The amount and type of gas conditioning will be largely dependent on the analytical methodology employed. The effects of any necessary sample conditioning steps (e.g., moisture removal) on analyte concentrations will be examined. Ultimately, prototype integrated analytical systems which appear to be acceptable based on results of laboratory studies will be tested in the field.

## ACKNOWLEDGEMENTS

We thank Laura Clifford for her research assistance in this study. We also thank Frank Schaedlich, President of Tekran Incorporated, for the loan of an atomic fluorescence Hg detector and for helpful discussions. In addition, thanks are due to Thermo Environmental Instruments for the loan of an HCl analyzer based on GFCIR and to Steve Schelwat of WESLINE Company for helping to arrange that loan. This work was performed with funds provided by the U.S.

Department of Energy through the Morgantown Energy Technology Center. Ames Laboratory is operated for the U.S. D.O.E. by Iowa State University under Contract No. W-7405-Eng-82.

## REFERENCES

1. G. N. Krishnan, G. T. Tong, B. J. Wood, and N. Korens, "High Temperature Coal Gas Chloride Cleanup for Molten Carbonate Fuel Cell Applications," Final Report, DOE/MC/21167-2080 (DE87001041), November 1986, pp. 57-60.
2. G. L. Anderson, F. O. Berry, B. D. Harmon, R. M. Laurens, and R. Biljetina, "Development of a Hot Gas Cleanup System for Integrated Coal Gasification/Molten Carbonate Fuel Cell Power Plants," Final Report, DOE/MC/19403-1816 (DE86001589), October 1985, p. A-4.
3. T. Grindley and T. H. Gardner, "Trace Contaminants in Fixed-Bed Gasifier Gas," in Proc. Twelfth Annual Gasification and Gas Stream Cleanup Systems Contractors Review Meeting, Volume II, DOE/METC-92/6128, Vol. 2 (DE93000229), September 1992, pp. 479-497.
4. G. A. Norton, C. D. Chriswell, D. E. Eckels, and W. H. Buttermore, "On-Line Monitoring of Mercury and Hydrogen Chloride in Hot Gases from Coal Gasifiers," in Proc. Coal-Fired Power Systems 93 -- Advances in IGCC and PFBC Review Meeting, DOE/METC-93/6131 (DE93000289), June 1993, pp. 276-283.
5. V. Harris, "Field Validation of the Portable Ion Mobility Hydrogen Fluoride Continuous Emissions Monitoring Systems," presented

at Stationary Source Sampling & Analysis  
for Air Pollutants, XIX, Engineering  
Foundation Conference, San Diego, CA,  
March 26-31, 1995.

6. G. A. Norton, C. D. Chriswell, D. E. Eckels,  
and R. E. Peters, "Chloride and Mercury  
Monitors for Air Toxics Measurements," in  
Proc. Coal-Fired Power Systems 94 --  
Advances in IGCC and PFBC Review  
Meeting, Morgantown, WV, June 21-23,  
1994, 492-497.

## 6B.6

# On-Line Elemental Analysis of Fossil Fuel Process Streams by Inductively Coupled Plasma Spectrometry

William P. Chisholm  
Morgantown Energy Technology Center

## ABSTRACT

METC is continuing development of a real-time, multi-element plasma based spectrometer system for application to high temperature and high pressure fossil fuel process streams. Two versions are under consideration for development. One is an Inductively Coupled Plasma system that has been described previously, and the other is a high power microwave system. The ICP torch operates on a mixture of argon and helium with a conventional annular swirl flow plasma gas, no auxiliary gas, and a conventional sample stream injection through the base of the plasma plume. A new, demountable torch design comprising three ceramic sections allows bolts passing the length of the torch to compress a double O-ring seal. This improves the reliability of the torch.

The microwave system will use the same data acquisition and reduction components as the ICP system; only the plasma source itself is different. It will operate with a 750-Watt, 2.45 gigahertz microwave generator. The plasma discharge will be contained within a narrow quartz tube one quarter wavelength from a shorted waveguide termination.

The plasma source will be observed via fiber optics and a battery of computer controlled monochromators. To extract more information from the raw spectral data, a neural net computer program is being developed. This program will calculate analyte concentrations from data that includes analyte and interferant spectral emission intensity. Matrix effects and spectral overlaps can be treated more effectively by this method than by conventional spectral analysis.



---

# Session 7A

## *Sorbent Development and Processes*

---



## 7A.1

## Moving-Bed Sorbents

### CONTRACT INFORMATION

**Contract Number** DE-AC21-88MC25003

**Contractor** GE Corporate Research and Development  
P.O. Box 8  
Schenectady, NY 12301  
(518) 387-5850 (telephone)  
(518) 387-7258 (telefax)

**Contractor Project Manager** Raúl E. Ayala

**Principal Investigators** Raúl E. Ayala,  
Timothy Chuck, GE Corporate R&D  
Raghubir P. Gupta, Research Triangle Institute

**METC Project Manager** Daniel Cicero

**Period of Performance** September 21, 1988 to June 30, 1995

### Schedule and Milestones

#### FY95 Program Schedule

	S	O	N	D	J	F	M	A	M	J	J	A	S
Sorbent Preparation													
Bench-Scale Mods. and Testing													
Bench-Scale Analysis													
Topical Report													

### OBJECTIVES

The objective of the option 3 program within this contract is to develop chemically reactive and mechanically durable mixed-metal oxide sorbent formulations that are suitable for moving-bed, high-temperature, desulfurization of coal gas. One optimum formulation is to be evaluated in a pressurized 50-cycle bench-scale test. Work on zinc ferrite formulations was performed under the base program (Ayala, 1991). Work on zinc titanate formulations was initiated under the option 2 program (Ayala,

1993) and is continued under the present option 3 program along with testing of other mixed-metal oxides.

### BACKGROUND INFORMATION

GE is developing a moving-bed, high-temperature desulfurization system for integrated gasification combined-cycle (IGCC) power systems in which zinc-based regenerable sorbents are currently being used as desulfurization sorbents (Bevan et al., 1994). Zinc titanate and other zinc-based oxides are being considered as sorbents for use in the Clean

Coal Technology Demonstration Program at Tampa Electric Co.'s Polk Power Station. A key to success in the development of high-temperature desulfurization systems is the matching of sorbent properties for the selected process operating conditions, namely, sustainable desulfurization kinetics, sulfur capacity, and mechanical durability over multiple cycles.

Mixed-metal oxide sorbents have been studied quite extensively in the past, including various types of zinc titanates (e.g.,  $\text{Zn}_2\text{TiO}_4$  and  $\text{Zn}_2\text{Ti}_3\text{O}_8$ ) (Ayala et al., 1994; Gangwal and Gupta, 1993) or as combinations of other metal oxides such as nickel, copper, manganese, cobalt, tin, and others; see for instance (Gasper-Galvin et al., 1994; Hepworth, 1994; Karpuk, 1994). Proprietary zinc-based sorbents, such as Phillips Petroleum Company's Z-Sorb<sup>TM</sup> III sorbent and METC sorbents, have also been tested (Everitt, 1994; Gangwal et al., 1994; Siriwardane et al., 1994). The reactions occurring during desulfurization of coal gases and regeneration of the sulfided sorbents have been described before in many sources; see for instance, (Gangwal and Gupta, 1993).

## PROJECT DESCRIPTION

Program participants are: GE Corporate Research and Development (GE-CRD, prime contractor), GE Environmental Systems, Inc., (GEESI, subcontractor), and Research Triangle Institute (RTI, subcontractor). United Catalysts, Inc. (UCI) and Phillips Petroleum Company (PPC), acting as vendors, provided the sorbent samples for testing.

As mentioned in previous papers (Ayala et al., 1994; Ayala et al., 1993), sorbents developed for moving-bed systems must comply with a minimum of chemical and mechanical

durability performance characteristics in order to be considered acceptable for long-term operation. Among the desired properties, a sorbent must have:

- High chemical reactivity, as measured by the global rate of sulfur absorption (including gas-phase mass transfer, pore diffusion, and intrinsic reaction rates) [Westerterp, 1984] and the total sulfur loading on the sorbent.
- High mechanical strength, as measured by the pellet crush strength and the attrition resistance.
- Suitable pellet morphology, as given by pellet size and shape to promote good bulk flowability and reasonable porosity to increase reactivity.

## RESULTS

During the current reporting year ('94-'95), the bench-scale reactor system at GE-CRD was upgraded to conduct tests of sorbents at pressure (up to 10 atm). Previously, the system operated only at 1 atm in both absorption and regeneration modes. Both Z-Sorb<sup>TM</sup> III sorbent and zinc titanate have been considered in laboratory testing in the past 12 months. A 50-cycle bench test was planned using Z-Sorb<sup>TM</sup> III sorbent given that it had been shown to be more attrition resistant during side-by-side (1 atm) tests against zinc titanate sorbents (Ayala et al., 1994). Tests on zinc titanate have focused on understanding regeneration schemes during pressurized operation and making zinc titanate more attrition resistant when sulfates are present.

### Z-Sorb<sup>TM</sup> Sorbent Results

Preparation methods for Z-Sorb<sup>TM</sup> sorbent formulations are considered proprietary



to PPC, and only analyses that describe performance in hot gas desulfurization will be presented here.

Table 1 shows the properties of the Z-Sorb<sup>TM</sup> III sorbent formulation used in this study. These properties correspond to the GE designation "Z-Sorb E", which distinguishes it among various Z-Sorb<sup>TM</sup> III sorbent formulations provided in previous years that differed primarily in pellet size and reactivity (see, for instance, Ayala et al., 1994).

**Table 1.- Physical Properties of Z-Sorb<sup>TM</sup> III Sorbent**

	Z-SORB E
Pellet Length, mm	6.4
Pellet Diam., mm	4.3
Pellet Mass, mg	114
Crush Strength, lb/pellet	10.2
(ASTM) Attrition Loss*, %	1.6
Bulk Density, lb/ft <sup>3</sup>	~60

\* Attrition losses of the fresh sorbent at the GE-CRD Pilot Plant are typically a factor of 10 lower.

Samples of Z-Sorb<sup>TM</sup> III sorbent, prepared as 4-mm ellipsoidal pellets by PPC, were used for the bench tests using wet regeneration (2% H<sub>2</sub>O) and dry regeneration procedures. Wet regeneration tests were terminated early (after 12 cycles) due to loss of sorbent capacity that was assumed to be a combination of steam regeneration and sulfate formation effects arising from use of 20% oxygen in the final step of the second

regeneration. This regeneration step was abandoned thereafter; hence the data did not allow proper analysis of each process parameter separately. Only results corresponding to the dry regeneration tests will be presented here.

During dry regeneration multicycle tests, absorption was conducted in an 800 ml sorbent bed at 5 atm and 538 °C (1000 °F), with a simplified gas composition similar to that of an oxygen-blown gasifier with high H<sub>2</sub>S (39% CO, 10% CO<sub>2</sub>, 30% H<sub>2</sub>, 20% H<sub>2</sub>O, 1% H<sub>2</sub>S). Space velocity was 1000 scc/cc•hr (25 °C, 1 atm). Regeneration was conducted also at 5 atm, 538 °C (1000 °F), maintaining the peak bed temperature below 732 °C (1350 °F); gas composition was 0-4% O<sub>2</sub> in nitrogen. A final step in regeneration included depressurization of the reactor to 1 atm under nitrogen at 732 °C (1350 °F) to decompose zinc sulfates formed during regeneration. No SO<sub>2</sub> was added to the regeneration gas (which would have simulated recycled SO<sub>2</sub> in pilot plant operation). The direction of flow of gases was the same in both absorption and regeneration.

Figure 1 shows the results of ten cycles of bench testing of Z-Sorb<sup>TM</sup> sorbent at the GE-CRD reactor unit using a dry regeneration scheme. The first cycle shows a higher sulfur bed capacity than cycles two to seven. This is a result of the sulfidation of nickel during the first cycle that increases the overall sulfur capacity of the bed. After nickel is sulfided, the bed desulfurization capacity is a result of zinc-only desulfurization. Cycle ten shows a loss in bed capacity with respect to cycles two to five, which would be a concern if a stable operation is to be maintained.

Small samples were taken from the reactor bed after 5 cycles to conduct single-pellet TGA chemical reactivity tests. Figure 2 shows the thermogravimetric analyzer (TGA) chemical reactivity of pellets after the fifth and tenth cycles. The weight gained by the pellet is proportional to the sulfur loading in the pellet. The first forty minutes are exposure to pure nitrogen (30 minutes) and clean (i.e., no  $H_2S$ ) simulated coal gas (10 minutes).  $H_2S$  is introduced 40 minutes after start. Pellet weights are stable under  $N_2$ , and a small weight loss is observed when clean simulated coal gas is introduced, suggesting decomposition of small amounts of sulfate. Fresh pellets did not exhibit this weight loss upon exposure to coal gas. These reactivity tests were performed under a standard GE procedure using a simulated coal gas having 3%  $H_2S$  at 538 °C (1000 °F). The

high  $H_2S$  concentration is used to expedite the testing, such that pellet saturation with sulfur occurs in two to three hours. Full sulfidation of Z-Sorb™ III sorbent pellets corresponds to a weight gain of approximately 10%. For the samples after the fifth cycle, the results suggest that the samples that were sulfided heavily at each cycle (i.e., the gas inlet location) did not suffer loss in reactivity (given by the slope of the curve) and capacity (given by the final weight of the pellet), while those at the gas outlet location, where the pellets are partially sulfided, did. These results follow similar trends observed in pilot plant tests. For the gas outlet samples, reactivity is higher very early in the test (during the external sulfidation of the pellets), but decreases with time; capacity after two hours of sulfidation was about 60 to 65% of that of fresh pellets.

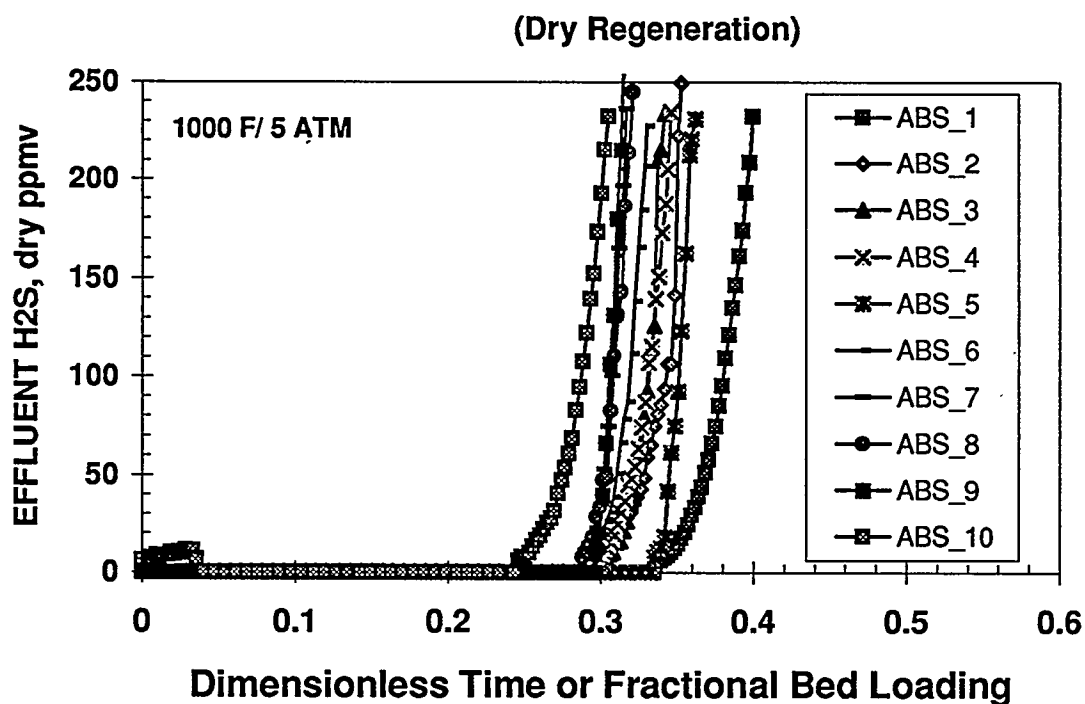


Figure 1.- Absorption Breakthrough Curves for Z-Sorb™ III Sorbent

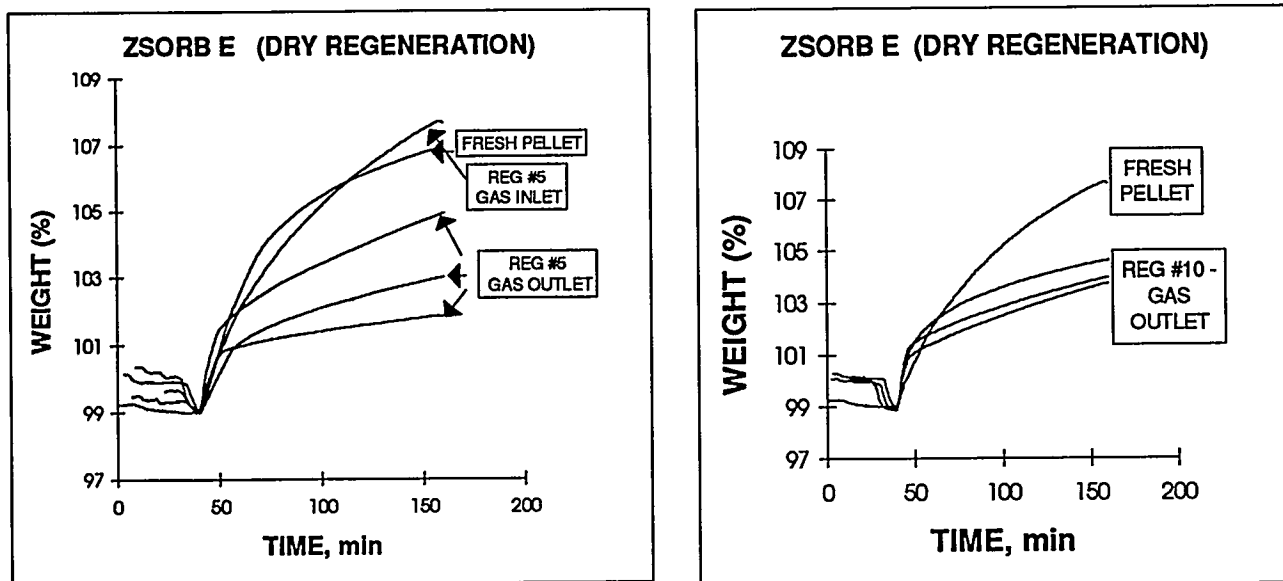


Figure 2.- TGA chemical reactivity of Z-Sorb™ III sorbent samples after 5 and 10 cycles

Design conditions for sorbent performance at Tampa Electric Co.'s moving-bed system require a sulfur loading of 6 lb/ft<sup>3</sup> on any sorbent. For Z-Sorb™ III sorbent, this requirement translates into 50% of theoretical sulfur loading or 5% weight gain under TGA testing. There is loss in reactivity and capacity in the gas outlet samples, as indicated by TGA tests, when exposed to laboratory conditions of simulated coal gases (no steam during regeneration, no tars during absorption, and no exposure to sodium-containing halogen-removal sorbents, as in pilot plant tests).

Further tests are needed to isolate the major cause of degradation and determine whether the problems encountered are surmountable. Currently, Phillips Petroleum Co. is working on a more resistant Z-Sorb IV sorbent formulation which will be available in the near future for testing.

Another operating scheme tested in the laboratory was the feasibility of decomposing sulfates during regeneration. Figure 3 shows the last step in the regeneration sequence where the sorbent is at 1350 °F under nitrogen at 5 atm. Some SO<sub>2</sub> is evolved as a result of sulfate decomposition. By depressurizing the reactor to 1 atm, still under N<sub>2</sub>, the sulfate decomposition is further accelerated, as given by the sudden burst of additional SO<sub>2</sub> evolved. This step is beneficial because less residual sulfate in the sorbent is carried to the absorption step, where it converts to SO<sub>2</sub> and H<sub>2</sub>S, thus resulting in lower overall desulfurization efficiency.

The effect of sulfate decomposition and subsequent  $\text{SO}_2$  evolution can be explained from thermodynamic principles. Figure 4 shows the phase stability diagram for the ternary system Zn-S-O at two temperatures 550 °C (1022 °F) and 732 °C (1350 °F). A typical regeneration gas composition at 550 °C and 1-7 atm of pressure in the presence of  $\text{O}_2$  and  $\text{SO}_2$  is shown by the point marked X. This point falls in the region of stable formation of  $\text{ZnO} \cdot 2\text{ZnSO}_4$  (zinc oxysulfate). As the temperature is increased to 732 °C, the pressure reduced to 1 atm, and the gas composition changed to  $\text{N}_2$  only, the system moves to point O, where the zinc oxysulfate is

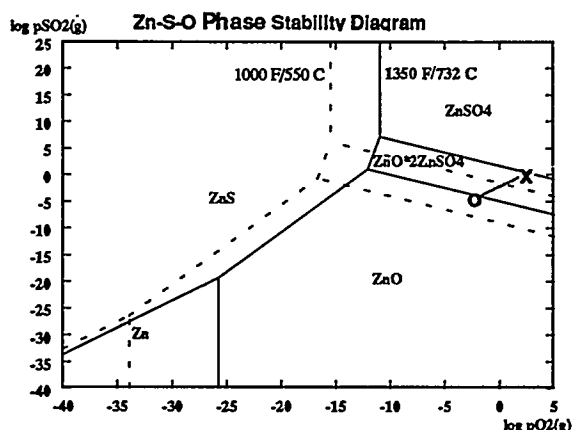


Figure 4.- Phase stability diagram for the system Zn-S-O at 550 °C and 732 °C

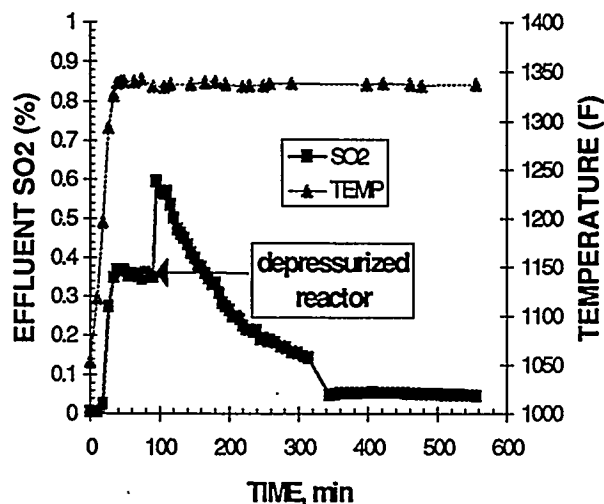


Figure 3.-  $\text{SO}_2$  evolution during regeneration at 5 atm and 1 atm

unstable and decomposes into zinc oxide. This operation mode is achieved during lockhopper operation in the moving-bed process, thus preventing carryover of sulfate into the absorption step.

### Zinc Titanate Sorbent Results

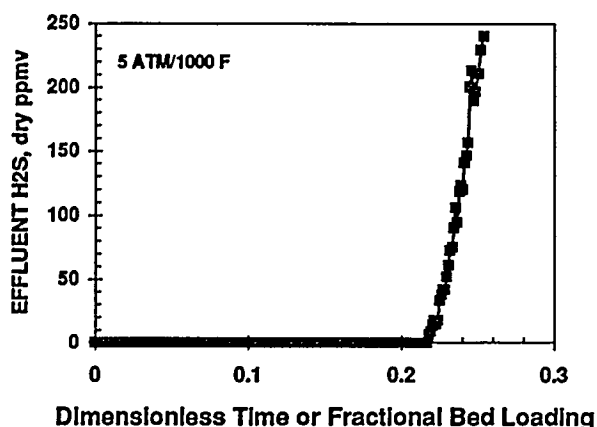
Zinc titanate sorbent formulations were also tested at pressure in the laboratory as an alternate sorbent; the objective of the zinc titanate testing is to characterize the sulfate formation kinetics during pressurized regeneration and be able to strengthen the pellet structure against sulfate-induced attrition. Tests at pressure are designed to provide additional data on the sorbent performance at conditions similar to those to be encountered at the Tampa Electric Co.'s Polk Station, where regeneration will be conducted at up to 7 atmospheres of pressure.

Table 2 shows the physical properties of T-2535M zinc titanate sorbent prepared by UCI. Preparation methods for UCI's zinc titanate sorbents have been described before (Ayala, 1993). T-2535M2 zinc titanate is the GE designation for second batch of formulation T-2535M having approximately 2.5%  $\text{MoO}_3$  as pore modifier and 3% bentonite binder. It was produced in 1993 as a large batch (6,000 lb) for use in the GE moving-bed pilot plant in Schenectady, New York.

**Table 2.- Physical Properties of Zinc Titanate Sorbent**

	T-2535M2
Pellet Length, mm	6.1
Pellet Diam., mm	4.9
Pellet Mass, mg	214
Crush Strength, lb/pellet	17.1
ASTM Attrition Resistance, %	98.5
Bulk Density, lb/ft <sup>3</sup>	~100

Bench-scale reactor tests on T-2535M zinc titanate have been re-initiated to determine its performance under pressurized regeneration in the laboratory. Figure 5 shows the breakthrough curve for T-2535M as a function of dimensionless time, or average bed sulfur loading. The outlet H<sub>2</sub>S prior to breakthrough was measured at less than 10 ppmv. For the size



**Figure 5.- Bench reactor testing of T-2535M zinc titanate**

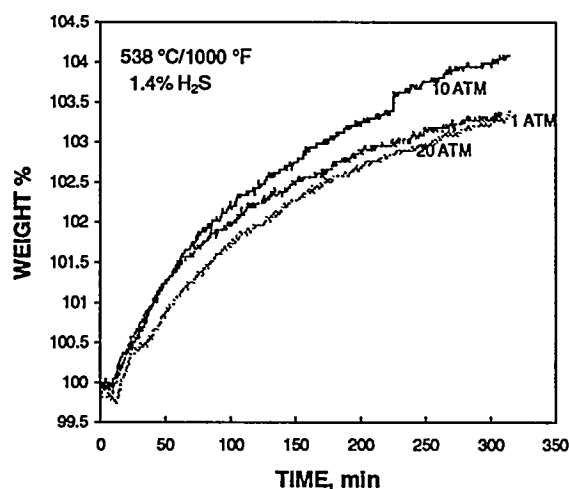


**Figure 6.- TGA reactivity of T-2535M2 zinc titanate as a function of sulfidation pressure**

of bed used (800 ml), the dimensionless time at breakthrough is about 0.25 of the theoretical, or 25% average sulfur loading on the bed, which is the design target (i.e., 6 lb sulfur/ft<sup>3</sup> of bed) for pilot plant and large scale operation.

TGA reactivity tests at pressure on zinc titanate were conducted at RTI. Figure 6 shows the pellet performance as a function of pressure at constant 1.4% H<sub>2</sub>S in the feed gas. Note that this H<sub>2</sub>S concentration is less than the concentration used in standard screening at GE under atmospheric conditions. If the curves are adjusted to the same starting point in the vertical axis, there is no significant difference in performance between 1 atm and 20 atm; furthermore, performance for all three pressures falls within the variation in reactivity from pellet to pellet. Hence, no significant trends from pressure effects are seen in this sorbent.

For regeneration, two additional TGA reactivity tests were performed. One in which sulfate was allowed to form during regeneration at 5 atm pressure, and the other in which sulfate was inhibited from forming, also at pressure. In Figure 7 (left), fresh pellets were sulfided during the first 300 minutes according to the procedure shown in Figure 6. Then, by switching between regeneration condition A (10% SO<sub>2</sub>, 2% O<sub>2</sub>, 88% N<sub>2</sub> at 650 °C) and regeneration condition B (100% N<sub>2</sub> at 730 °C), zinc sulfate was allowed to form and decompose, as given by the weight gain/loss during transition from A to B to A condition. In Figure 7 (right), the same process was performed, except that condition A did not contain any O<sub>2</sub>. The result is a lack of sulfate formation. This experiment demonstrates that the conditions that control the level of sulfate formation and decomposition during regeneration can be adjusted to prevent pellet decrepitation.

## CONCLUSIONS

Tests performed on Z-Sorb<sup>TM</sup> III sorbent showed that the sorbent is capable of reducing H<sub>2</sub>S levels below a target of 20 ppm during desulfurization of simulated coal gases meeting the requirements for desulfurization in commercial operation. During regeneration, sulfate can be decomposed by adjusting the process conditions that lead to thermodynamic instability and thermal decomposition of zinc sulfates. However, the ability to maintain desulfurization of Z-Sorb<sup>TM</sup> III sorbent under cyclic operation is a concern in view of the losses in reactivity and capacity observed in the gas outlet location under dry regeneration conditions in the laboratory. Future evaluation is necessary.

Zinc titanate operation was reinitiated with a bench test also at pressurized conditions in the laboratory. Desulfurization below 20 ppmv was also achieved. Evaluation of regeneration conditions that lead to minimization of sulfate formation and maximization of sulfate decomposition (and hence leading to low

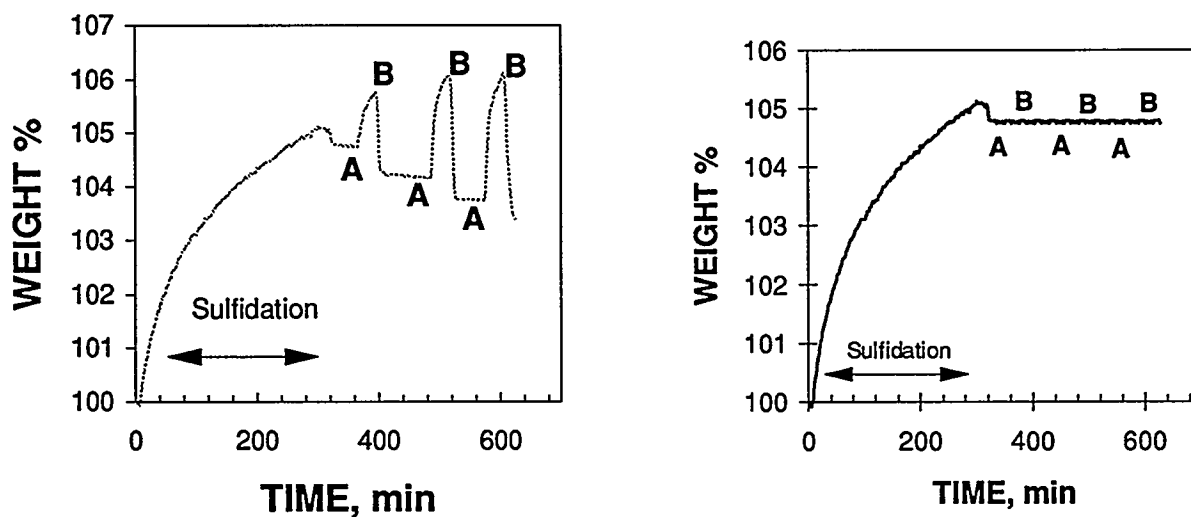


Figure 7.- TGA regeneration of T-2535M2 in the presence (left) or absence (right) of O<sub>2</sub>

attrition losses) were evaluated.

## FUTURE WORK

The results of the cyclic testing of sorbents are being summarized in a topical report to be submitted to DOE in the near future. Many of the ideas under consideration for future testing will be pursued under another current contract with DOE, Advanced Sorbent Development (Contract DE-AC21-94MC31089).

## REFERENCES

- Ayala, R.E. 1991. Enhanced Durability of High Temperature Desulfurization Sorbents for Moving-Bed Applications. Base Program: Development and Testing of Zinc Ferrite Sorbents. Topical Report. DOE/MC/25003-3045. NTIS/DE92001121. Springfield, Va.: National technical Information Service.
- Ayala, R.E. 1993. Enhanced Durability of High-Temperature Desulfurization Sorbents for Moving-Bed Applications. Option 2 Program: Development and Testing of Zinc Titanate Sorbents. Contract DE-AC21-88MC25003. Topical Report submitted to DOE/Morgantown Energy Technology Center. April 1993.
- Ayala, T. Chuck, E. Gal, and R.P. Gupta. 1994. Development of High Temperature Desulfurization Sorbents for Moving-Bed Systems. In *Proceedings of the Coal-Fired Power Systems 94 – Advances in IGCC and PFBC Review Meeting*, p. 637. DOE/METC-94/1008. NTIS/DE94012252. Springfield, Va.: National Technical Information Service.
- Bevan, S., D.J. Najewicz, E. Gal, A.H. Furman, R. Ayala, and A. Feitelberg. 1994. Integrated Operation of a Pressurized Gasifier, Hot Gas Desulfurization System and Turbine Simulator. In *Proceedings of the Coal-Fired Power Systems 94 – Advances in IGCC and PFBC Review Meeting*, p. 222. DOE/METC-94/1008. NTIS/DE94012252. Springfield, Va.: National Technical Information Service.
- Everitt, C.E., and S.J. Monaco. 1994. Data Summary Report for M.W. Kellogg Z-Sorb Sorbent Tests (Z-Sorb-01, Z-Sorb-02, Z-Sorb-03). Final Topical Report. Contract DE-AC21-90MC26328. Report No. 33FF-R93-003.
- Gangwal, S.K., and R.P. Gupta, 1993. Enhanced Durability of Desulfurization Sorbents for Fluidized-Bed Applications. In *Proceedings of the Coal-Fired Power Systems 93 – Advances in IGCC and PFBC Review Meeting*, p. 146-157. DOE/METC-93/6131. NTIS/DE93000289. Springfield, Va.: National Technical Information Service.
- Gangwal, S.K., R.P. Gupta, G.P. Khare, G.A. Delzer, and D.H. Kubicek. 1994. Fluidization Studies using Phillips Z-SORB Sorbent. In *Proceedings of the Coal-Fired Power Systems 94 – Advances in IGCC and PFBC Review Meeting*, p. 654. DOE/METC-94/1008. NTIS/DE94012252. Springfield, Va.: National Technical Information Service.
- Gasper-Galvin, L.D., J.H. Swisher, and K. Hammerbeck. 1994. Characterization and Fixed-Bed Testing of a Nickel-Based Hot Gas Desulfurization Sorbent. In *Proceedings of the Coal-Fired Power Systems 94 – Advances in IGCC and PFBC Review Meeting*, p. 308. DOE/METC-94/1008.

NTIS/DE94012252. Springfield, Va.:  
National Technical Information Service.

Hepworth, M.T., and R. Ben-Slimane. 1994.  
Hot Gas Desulfurization with Manganese-  
Based Sorbents. In *Proceedings of the Coal-  
Fired Power Systems 94 – Advances in  
IGCC and PFBC Review Meeting*, p. 337.  
DOE/METC-94/1008. NTIS/DE94012252.  
Springfield, Va.: National Technical  
Information Service.

Karpuk, M.E, R.J. Copeland, D. Feinber, D.  
Wickham, B. Windecker, and J. Yu. 1994.  
High Temperature Hydrogen Sulfide Removal  
with Stannic Oxide. In *Proceedings of the  
Coal-Fired Power Systems 94 – Advances in  
IGCC and PFBC Review Meeting*, p. 444.

DOE/METC-94/1008. NTIS/DE94012252.  
Springfield, Va.: National Technical  
Information Service.

Siriwardane, R.V., U.Grimm, J. Poston, and S.  
Monaco. 1994. Desulfurization Sorbent  
Development at the Morgantown Energy  
Technology Center. In *Proceedings of the  
Coal-Fired Power Systems 94 – Advances in  
IGCC and PFBC Review Meeting*, p. 662.  
DOE/METC-94/1008. NTIS/DE94012252.  
Springfield, Va.: National Technical  
Information Service.

Westerterp, K.R., W.P.M van Swaaij, and  
A.A.C.M. Beenackers. 1984. Chemical  
Reactor Design and Operation. Wiley, New  
York.



**CONTRACT INFORMATION**

**Contract Number** DE-AC21-88MC25006

**Contractor** Research Triangle Institute  
PO Box 12194  
Research Triangle Park, NC 27709-2194  
Telephone: (919) 541-8023  
Facsimile: (919) 541-8000

**Contractor Project Manager** Santosh K. Gangwal

**Principal Investigator** Raghubir P. Gupta

**METC Project Manager** Daniel C. Cicero

**Period of Performance** September 1, 1993 to September 30, 1995

**Schedule and Milestones**

**FY95 Program Schedule**

	S	O	N	D	J	F	M	A	M	J	J	A	S
Sorbent Characterization	_____												
Sorbent Testing					_____								
Sorbent Production								_____					
TRTU Testing at M.W. Kellogg										_____			
Topical Report												_____	

**OBJECTIVES**

The objective of this study is to determine the feasibility of manufacturing highly reactive and attrition-resistant zinc titanate sorbents by spray drying, suitable for bubbling (conventional) as well as transport-type fluidized-bed reactor systems.

**BACKGROUND INFORMATION**

RTI has been pursuing the sorbent development work with the objective of producing highly reactive and attrition-resistant sorbent particles for fluidized-bed applications since 1988. A number of techniques have been investigated in this program, including granulation and spray drying, to produce fluidizable particles. Earlier efforts in

this project were focused on the development of the reactive and durable sorbents using a granulation technique as described in various RTI publications (Gupta and Gangwal, 1992; Gupta et al., 1993; Gupta and Gangwal, 1994). This effort has led to the development of the ZT-4 sorbent which has been tested in both laboratory and bench-scale reactors with simulated coal gas as well as in pilot-scale semicommercial systems employing real coal gas in the United States as well as in various European countries (Gupta and Gangwal, 1995).

Alternatively, a spray-drying process is extensively employed in the production of various catalysts, particularly fluid catalytic cracking (FCC) catalysts, for use in fluidized-bed reactors. Spray drying offers a number of advantages over a granulation process. For example, spray drying is a commercial process that can be readily scaled to industrial production scale using existing technology to produce large quantities of a product. Spray drying facilitates the addition of other additives and reagents to the composition since additional reagents can simply be added to a slurry prior to spray drying. Furthermore, spray drying provides particles of highly uniform size and shape.

During earlier stages of this contract (FY 1991-1992), attempts were made to prepare reactive and attrition-resistant zinc titanate sorbents by spray drying. United Catalysts, Inc. (UCI) prepared four preliminary formulations by spray drying with and without addition of a silica binder. Testing of these formulations at RTI indicated that the formulations that contained the silica binder had good attrition resistance, but essentially no chemical reactivity. Consequently, the formulations that did not contain the silica binder had reasonable chemical reactivity, but extremely poor attrition resistance (Gupta and Gangwal, 1992). Joint efforts between RTI and DuPont to prepare attrition-resistant particles using DuPont's polysilicic acid technology were not suc-

cessful, primarily due to the presence of free silica in the sorbent (Gupta and Gangwal, 1992).

Despite these unsuccessful attempts, the knowledge gained in these trials was useful and led to the successful development of the CMP-5 sorbent, which is the subject of investigation in this paper.

## PROJECT DESCRIPTION

This project is a collaborative effort with the Contracts Materials Processing (CMP), Inc., a small specialty catalyst manufacturing company in Baltimore, MD. CMP, a subcontractor to RTI in this project, is responsible for preparing various zinc titanate formulations using a pilot-scale spray drier. As noted previously, the zinc titanate sorbents suitable for fluidized-bed applications must demonstrate high chemical reactivity, as measured by the rate of sulfur absorption and the sulfur loading capacity, as well as good fluidizing characteristics and mechanical strength characterized by low attrition losses.

### Sorbent Preparation and Characterization

In the beginning of this program, CMP prepared 14 zinc titanate formulations designated by CMP-X series (CMP-1 to CMP-14). These formulations were prepared by varying the binders, binder amount, Zn-to-Ti atomic ratio, and spray-drier operating conditions. The particle size range of these formulations varied between 40 and 150  $\mu\text{m}$ —typical for commercial FCC catalysts used in the petroleum industry. All of these 14 formulations were characterized for their chemical reactivity and regenerability in a thermogravimetric analyzer (TGA), pore size distribution, particle size distribution, bulk density, BET surface area, and the attrition-resistance (in RTI's three-hole airjet attrition tester). Based on these physical and chemical characterization tests, two superior formulations (CMP-1 and CMP-5) were identified for further testing.

Table 1 shows a comparison of the physical and chemical properties of CMP-1 and CMP-5 formulations. Also included in this table are the properties of the ZT-4L sorbent (a benchmark fluidized-bed sorbent prepared using a granulation technique as noted previously). The properties of CMP-1 and CMP-5 formulations are comparable with the exception of the attrition resistance. The attrition resistance of the CMP-5 formulation is far superior compared to that of the CMP-1 formulation. It is to be noted here that the average particle size (APS) of ZT-4 and CMP formulations is 180 and 80  $\mu\text{m}$ , respectively, primarily due to the different methods of manufacturing. The superior attrition properties of the CMP-5 formulation are attributed to the presence of additional proprietary additives and know-how to spray-dry and impart unusually high attrition resistance to the sorbent. A patent application is pending on the method of manufacturing these spray-dried zinc titanate formulations.

### Bench-Scale Testing

Following the physical and chemical characterization, the CMP-5 formulation was tested in RTI's high-temperature, high-pressure (HTHP) bench-scale test facility. A detailed description of RTI's HTHP test facility is provided elsewhere

**Table 1. Physical and Chemical Properties of Spray-Dried Formulations**

	ZT-4L	CMP-1	CMP-5
Average particle size ( $\mu\text{m}$ )	180	80	80
Attrition resistance			
5-h loss (%)	17	86.6	13.4
20-h loss (%)	71	94.0	14.2
Surface area ( $\text{m}^2/\text{g}$ )	3.53	3.24	2.83
Chemical composition			
ZnO/TiO <sub>2</sub> (molar)	1.5	1.5	1.5
% Binder	5	5	5
TGA sulfur capacity (wt.%)	22	22.5	22.5

(Gupta and Gangwal, 1992; Gupta and Gangwal, 1993). Two HTHP tests, each consisting of 10 sulfidation-regeneration cycles, were performed on the CMP-5 sorbent. The first 10-cycle test was conducted similar to RTI's previous multicycle tests with the ZT-4 sorbent in which the sorbent was sulfided until the breakthrough followed by complete regeneration. In the second 10-cycle test, sulfidation-regeneration cycles were carried out to operate the system in a window of sulfur loading, mimicking the operation of a commercial hot-gas desulfurization system employing a fluidized-bed reactor.

### First 10-Cycle HTHP Testing

Table 2 lists the operating conditions for this run. The sorbent was prescreened in the 80- to 150- $\mu\text{m}$  particle size range. A charge of 200 g of the sorbent was loaded in the 2-in. I.D. cage. Because the bench unit was not equipped with a gas-particle separation device (such as a cyclone), the superficial gas velocity was kept below the terminal velocity for the smallest particle. The sulfidation was carried out at 600 °C (1,112 °F) and at a pressure of 250 psig (18 atm). The coal gas composition used in this test simulated the fuel gas produced from an air-blown fluidized-bed gasifier (as shown in Table 2) and had a reducing power of about 3.0 [determined as a ratio of  $(\text{CO} + \text{H}_2)$  to  $(\text{CO}_2 + \text{H}_2\text{O})$ ]. The regeneration of the sulfided sorbent was initiated at 600 to 650 °C (1,112 to 1,202 °F) with 3 to 4 percent O<sub>2</sub> in N<sub>2</sub>. Regeneration was continued until the SO<sub>2</sub> concentration in the regeneration off-gas fell below 500 ppm.

Figure 1 shows the breakthrough data for the 10 cycles. As can be seen, following initial activation in Cycles 1 and 2, the breakthrough curves for Cycles 3 to 10 were essentially the same, indicating a stable performance of the sorbent. From these breakthrough data, sulfur capacity values at breakthrough (500 ppm of H<sub>2</sub>S in the outlet gas) were estimated and are shown as a function of the

**Table 2. Operating Conditions for First 10-Cycle Run**

Sorbent particle size	80 to 150 $\mu\text{m}$
Sorbent charge	200 g
Reactor diameter	5.08 cm (2 in.)
Reactor L/D	4
Gas flow rate	25 std L/min (53 std ft <sup>3</sup> /h)
Operating pressure	18 atm (250 psig)
Superficial gas velocity	4.4 cm/s (0.15 ft/scc)
Terminal velocity for 80- $\mu\text{m}$ particle	9.6 cm/s (0.3 ft/scc)
Minimum fluidization velocity	0.20 cm/s
$U/U_{mf}$	22
<b>Sulfidation</b>	
Temperature = 600 °C (1,112 °F)	
<b>Gas Composition</b>	
CO	24.0
H <sub>2</sub>	14.0
CO <sub>2</sub>	5.0
N <sub>2</sub>	48.0
H <sub>2</sub> S	1.0
H <sub>2</sub> O	8.0
Reducing power = 3.0 (severely reducing coal gas)	
Breakthrough ppm = 500 ppm H <sub>2</sub> S in outlet gas	
<b>Regeneration</b>	
Temperature	600 to 650 °C (1,112 to 1,202 °F)
Regeneration gas	3 to 4% O <sub>2</sub> in N <sub>2</sub>
End point	500 ppm SO <sub>2</sub> in outlet gas

cycle number in Figure 2. The sulfur capacity was essentially constant from Cycles 3 to 10 at a value of about 24 g S/100 g fresh sorbent. This indicates greater than 95 percent utilization of the sorbent's sulfur capture capacity. The theoretical sulfur capacity of the CMP-5 sorbent was 24.9 g S/100 g sorbent.

Regenerability of this sorbent was found to be extremely good. Figure 3 shows the temperature and SO<sub>2</sub> and O<sub>2</sub> concentration profiles for Cycle 2 (arbitrarily chosen for illustration purposes). In

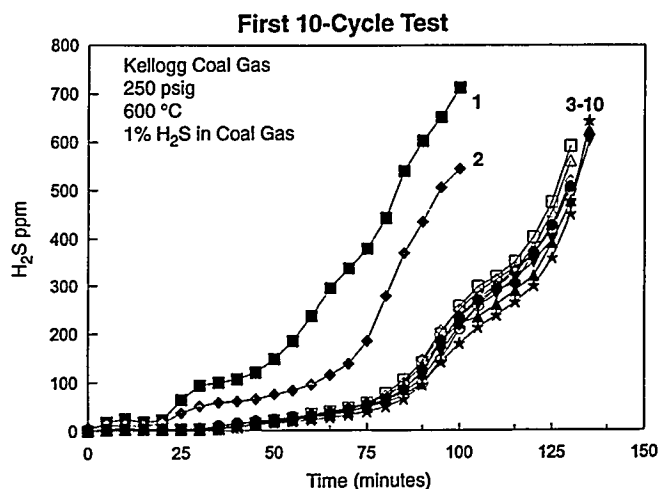


**Figure 1. Breakthrough data for CMP-5 sorbent.**

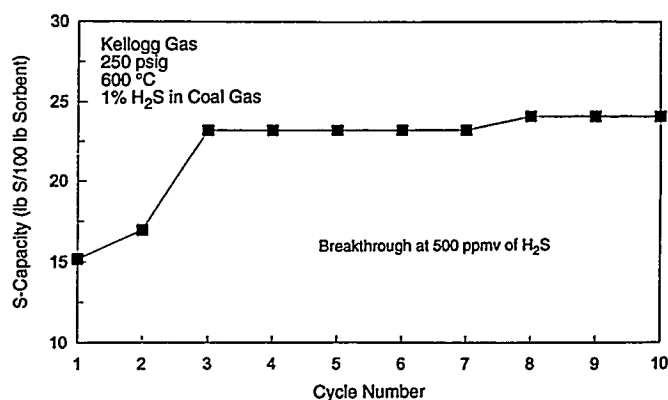


**Figure 2. S-capacity for CMP-5 sorbent at breakthrough.**

this case, the regeneration was initiated at 640 °C (1,184 °F) using 3 percent O<sub>2</sub> in N<sub>2</sub>. As expected, in the beginning the SO<sub>2</sub> concentration and the sorbent bed temperature increased rapidly to a steady-state value of about 20,000 ppmv (2% v/v) for SO<sub>2</sub> concentration and about 690 °C (1,275 °F) for temperature. This SO<sub>2</sub> concentration corresponds to the stoichiometric value for 3 percent O<sub>2</sub> used (it will be two-thirds of the O<sub>2</sub> concentration). As shown in Figure 3, the O<sub>2</sub> con-

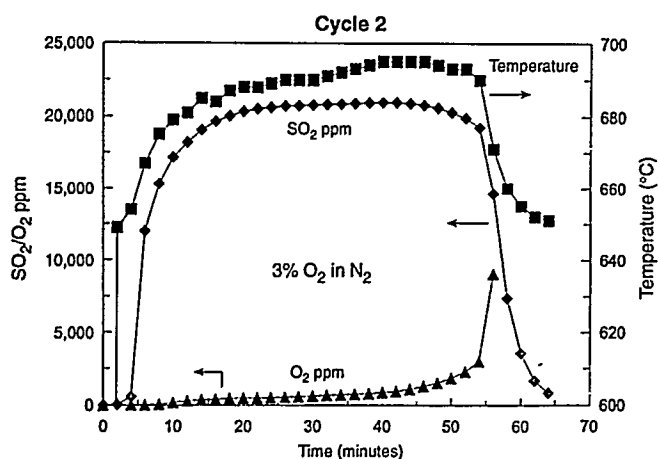


Figure 3. Regeneration of CMP-5 sorbent.

centration during the steady-state  $\text{SO}_2$  evolution is essentially zero and it exhibited a breakthrough when regeneration was nearly complete. The sulfur capacity values obtained from  $\text{H}_2\text{S}$  breakthrough data were also compared with the  $\text{SO}_2$  evolution data obtained during the subsequent regeneration and they matched within  $\pm 2$  percent, indicating that this sorbent can be easily regenerated without any sulfate formation.

At the end of the 10-cycle run, the reactor was opened and the sorbent was removed. Out of 200 g of the sorbent loaded, 1.8 g of the sorbent elutriated during initial heating. Out of the remaining 198.2 g, 197.8 g were collected from the cage after 10 cycles of testing, resulting in a net loss of 0.4 g (0.2 percent). No deposits were found on the sulfidation and regeneration filters.

A sample of the reacted sorbent was characterized for its physical and chemical properties to determine any changes in the sorbent structure. Table 3 compares the properties of fresh and reacted sorbents. As can be seen, about 7 percent increase is observed in the APS, which can be within the error of experimental measurement. No changes are evident in either the mercury pore volume or x-ray diffraction phases. Despite the severely reducing nature of the coal gas, the Zn-

Table 3. Comparison of Physical and Chemical Properties of Fresh and 10-Cycle Regenerated Sorbent in the First 10-Cycle Test

	Fresh	10-cycle reacted
Particle size distribution (wt.%)		
Mesh		
+100	6.2	11.6
-100 + 140	33.6	43.7
-140 + 170	34.1	23.2
-170 + 230	24.9	21.5
-230 + 270	1.2	0.0
Total	100.0	100.0
Average particle size ( $\mu\text{m}$ )	99.6	106.9
Mercury pore volume ( $\text{cm}^3/\text{g}$ )	0.4061	0.3930
Attrition resistance		
5-h loss (wt.%)	12.0	52.8
20-h loss (wt.%)	13.6	76.2
Bulk density ( $\text{lb}/\text{ft}^3$ )	38.3	42.8
XRD <sup>a</sup> phases	$\text{Zn}_2\text{TiO}_4$ , traces of $\text{ZnTiO}_3$	$\text{Zn}_2\text{TiO}_4$ , traces of $\text{ZnTiO}_3$
ICP <sup>b</sup> analysis		
Zn	42.8	42.4
Ti	19.4	20.0

<sup>a</sup> XRD = x-ray diffraction.

<sup>b</sup> ICP = inductively coupled plasma.

to-Ti ratio remained essentially unchanged. However, a decline in the sorbent attrition resistance as measured in a three-hole air-jet attrition tester was noticed due to cycling. The causes for this decline are currently being investigated.

To summarize the pertinent findings of this 10-cycle test, the CMP-5 sorbent exhibited excellent chemical reactivity and sulfur capacity. Nearly complete ( $>95\%$ ) capacity utilization was obtained with this sorbent. The sulfur capacity remained constant over 10 cycles at about 24 g S/100 g of the fresh sorbent. Sorbent was found to have excellent regenerability as evidenced by nearly stoi-

chiometric  $\text{SO}_2$  formation at steady state. No sorbent loss was observed from the reactor. No significant changes were evident in the physical and chemical properties of the sorbent, except for a decline, as yet unexplained, in the attrition resistance.

## Second 10-Cycle HTHP Testing

Following the excellent desulfurization performance of the CMP-5 sorbent in the first 10-cycle run, the second 10-cycle run was carried out to determine the sorbent performance when operated in a window of sulfur loading. Table 4 shows the test conditions for this run, which was made at a pressure of 20 atm (294 psi) and at a sulfidation temperature of 550 °C (1,022 °F) with a simulated air-blown gasifier gas. As indicated in Table 4, in Cycle 1, the sorbent was sulfided until breakthrough followed by a complete regeneration, similar to the first 10-cycle run.

**Table 4. Test Conditions for the Second 10-Cycle Test**

Sulfidation temperature	= 550 °C (1,022 °F)
Pressure	= 20 atm (294 psi)
Coal gas composition	
CO	: 21%
H <sub>2</sub>	: 15%
CO <sub>2</sub>	: 7%
H <sub>2</sub> O	: 9%
H <sub>2</sub> S	: 1%
N <sub>2</sub>	: 47%
Operation Mode	
Cycle 1:	Sulfidation until breakthrough followed by complete regeneration
Cycles 2-10:	Sulfidation up to 7.5 wt.% S-capacity and regeneration until S-level reaches 1 wt.%
Regenerations	
1-5:	5 to 6% O <sub>2</sub> in N <sub>2</sub>
6-10:	5% O <sub>2</sub> , 45% N <sub>2</sub> and 50% steam

However, during Cycles 2 to 10, the sorbent was sulfided to a sulfur loading of 7.5 wt.% and regenerated until the sulfur level of the regenerated sorbent reached 1 wt.%. These sulfur loading values for sulfidation were estimated from the inlet  $\text{H}_2\text{S}$  concentration and the breakthrough data obtained in Cycle 1, while during regeneration this estimation was based on the  $\text{SO}_2$  evolution data. Also in this test, the effect of  $\text{O}_2$  concentration and the presence of steam in the regeneration gas were investigated.

Figure 4 shows the breakthrough behavior of the sorbent for this 10-cycle run. As shown, following the activation of the sorbent in Cycle 1, no change in the chemical reactivity is evident during Cycles 2 to 7. However, when 50 percent (v/v) steam was present in the coal gas, some degradation in the sorbent performance, as indicated by higher prebreakthrough  $\text{H}_2\text{S}$  levels shown in Figure 4, was noticed in the subsequent sulfidation cycles. Previous testing at RTI with ZT-4 sorbent did not exhibit performance degradation due to the presence of steam in the regeneration gas. More tests are necessary to understand this degradation.

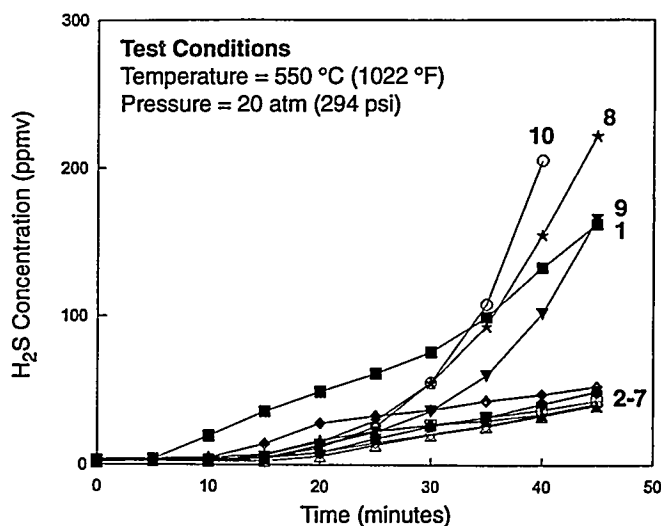


**Figure 4. Breakthrough behavior for the second 10-cycle run.**

Table 5 shows a comparison of physical and chemical properties of the fresh and 10-cycle reacted sorbents. Except for the attrition resistance, hardly any change is observed in particle size distribution, APS, pore volume, and bulk density of fresh and reacted sorbent samples.

### Production of Sorbent with Larger Particle Size

As noted previously, the APS of the CMP-5 sorbent tested in this study was about 80  $\mu\text{m}$  with a particle size range of 40 to 150  $\mu\text{m}$ . This particle size distribution may be suitable for a riser type reactor; however, for a conventional bubbling-bed reactor, the desired particle size of the sorbent is slated to be between 100 and 300  $\mu\text{m}$  (with an APS of 180  $\mu\text{m}$ ). Incidentally, the transport reactor system contemplated by M.W. Kellogg for the hot-gas desulfurization for the Pinón Pine Clean Coal Technology Demonstration plant will use 100- to 300- $\mu\text{m}$  particle size for the sorbent.

**Table 5. Comparison of Physical and Chemical Properties of Fresh and 10-Cycle Regenerated Sorbent in the Second 10-Cycle Test**

	Fresh	10-cycle reacted
Particle size distribution (wt.%)		
Mesh		
+100	6.2	0.0
-100 + 140	33.6	31.9
-140 + 170	34.1	31.3
-170 + 230	24.9	34.7
-230 + 270	1.2	1.4
-270	0.0	0.7
Total	100.0	100.0
Average particle size ( $\mu\text{m}$ )	99.6	93.4
Mercury pore volume ( $\text{cm}^3/\text{g}$ )	0.4061	0.4120
Attrition resistance		
5-h loss (wt.%)	12.0	53.0
20-h loss (wt.%)	13.6	55.4
Bulk density ( $\text{lb}/\text{ft}^3$ )	38.3	38.1

With a subcontract from RTI, CMP modified their pilot-scale spray drier to produce larger particle size of the sorbent. Recently, after a series of trials, CMP successfully produced large particles by spray drying. This formulation designated as CMP-107 and prepared using the recipe of CMP-5 had a particle size distribution in the 80- to 250- $\mu\text{m}$  range with an APS of 165  $\mu\text{m}$ . The yield in the 100- to 300- $\mu\text{m}$  range varied between 70 and 90 percent. Preliminary screening of this sorbent indicated good TGA reactivity and attrition resistance of this sorbent.

A 200-lb batch of this sorbent was produced to demonstrate the scaleup. Out of this, 100 lb sorbent was shipped to M.W. Kellogg for testing in their transport reactor test unit (TRTU). A 20-lb batch was shipped to the U.S. Department of Energy/Morgantown Energy Technology Center (DOE/METC) for testing in METC's Modular Gas Cleanup Rig (MGCR).

### FUTURE WORK

Future work in this project includes testing of the CMP-107 sorbent in M.W. Kellogg's TRTU system and 10-cycle HTHP testing at RTI.

### REFERENCES

- Gupta, R., and S.K. Gangwal. 1992. "Enhanced Durability of Desulfurization Sorbents for Fluidized-Bed Applications—Development and Testing of Zinc Titanate Sorbents." Topical Report to DOE/METC. Report No. DOE/MC/25006-3271. U.S. Department of Energy/Morgantown Energy Technology Center. Morgantown, WV. November.
- Gupta, R., and S.K. Gangwal. 1993. "High-Temperature, High-Pressure Testing of Zinc Titanate in a Bench-Scale Fluidized-Bed Reactor for 100 Cycles." Topical Report to DOE/METC. Contract No. DE-AC21-88MC25006. June.

Gupta, R., and S.K. Gangwal 1994. "Fluidized-Bed Sorbets" in Proceedings of the Coal-Fired Power System 94—Advances in OGCC and PFBC Review Meeting, Report No. DOE/METC 94/1008, Vol. 2, pp. 646-653.

Gupta, R., and S.K. Gangwal. 1995. "Multicycle Testing of ZT-4L Sorbent." Topical Report to DOE/METC. Contract No. DE-AC21-88MC

25006. U.S. Department of Energy/Morgantown Energy Technology Center. Morgantown, WV. June.

Gupta, R., et al. 1993. Fluidizable Zinc Titanate Materials with High Chemical Reactivity and Attrition Resistance." U.S. Patent No. 5,254,516, October 19.



## **7A.3 Desulfurization Sorbent Development Activities at METC**

Ranjani V. Siriwardane  
Morgantown Energy Technology Center

### **ABSTRACT**

Development of a suitable regenerable sorbent is a major barrier issue in the hot gas cleanup program for integrated gasification combined-cycle (IGCC) systems. This has been a challenging problem during the last 20 years, since many of the sorbents developed in the program could not retain their reactivity and physical integrity during repeated cycles of sulfidation and regeneration reactions. A series of promising sorbents (METC 2-10), which were capable of sustaining their reactivity and physical integrity during repeated sulfidation/regeneration cycles, have been developed at the Morgantown Energy Technology Center (METC). These sorbents were tested both in low-pressure (260 KPa/23 psig) and high-pressure (520 KPa/60.7 psig) fixed-bed reactors at 538 °C (1000 °F) with simulated coal gas. High-pressure testing was continued for 20 cycles with steam regeneration. A major research goal during the last year was to lower the cost of materials utilized during the sorbent preparation. The METC 9 sorbent was prepared by substituting low-cost materials for some of the materials in METC 6 sorbent. The sulfur capacity of the two sorbents were similar during the 20-cycle testing. METC 2 sorbent was exposed to coal gas in the Modular Gas Cleanup Rig and it was later tested in the high-pressure fixed-bed reactor. The reactivity of the METC 2 sorbent was unaffected by the exposure to the coal gas. Development of these sorbents will be continued for both fluid-bed and moving-bed applications.

**CONTRACT INFORMATION**

<b>Contract Number</b>	DE-AC21-94MC30012
<b>Contractor</b>	Louisiana State University Department of Chemical Engineering Baton Rouge, Louisiana 70803 (504) 388-1426 (telephone) (504) 388-1476 (telefax)
<b>Contract Project Manager</b>	Douglas P. Harrison
<b>Principal Investigators</b>	Douglas P. Harrison Alejandro Lopez-Ortiz Julie D. White Frank R. Groves, Jr.
<b>METC Project Manager</b>	Tom Dorchak
<b>Period of Performance</b>	April 1994 to April 1997

**ABSTRACT**

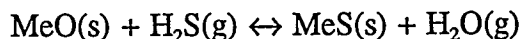
The primary objective of this study is the direct production of elemental sulfur during the regeneration of high temperature desulfurization sorbents. Three possible regeneration concepts were identified as a result of a literature search. The potential for elemental sulfur production from a number of candidate metal oxide sorbents using each regeneration concept was evaluated on the basis of a thermodynamic analysis. Two candidate sorbents,  $\text{Fe}_2\text{O}_3$  and  $\text{CeO}_2$ , were chosen for experimental testing.

The experimental test program using both electrobalance and fixed-bed reactors is now getting underway. The objective is to determine reaction conditions - temperature, pressure, space velocity, and regeneration feed gas composition--which will maximize the yield of elemental sulfur in the regeneration product gas.

Experimental results are to be used to define a conceptual desulfurization-regeneration process and to provide a preliminary economic evaluation.

**BACKGROUND INFORMATION**

High temperature desulfurization of coal-derived gas is an important component in the integrated gasification combined cycle (IGCC) process for electric power generation. A number of metal oxide sorbents which are capable of reacting with  $\text{H}_2\text{S}$  and reducing the outlet  $\text{H}_2\text{S}$  concentration to acceptable levels have been studied. The generic desulfurization reaction may be represented by the following:



For the process to be economical, the sorbent must be regenerable and must maintain activity through many sulfidation-regeneration cycles. Most regeneration studies to date have used total oxidation in which the metal sulfide is reacted with oxygen to regenerate the metal oxide and liberate the sulfur as SO<sub>2</sub>. In addition to the problem of controlling SO<sub>2</sub> in the regenerator off-gas, the highly exothermic total oxidation reaction creates reactor temperature control problems which may accelerate the deterioration of the high surface area, porous sorbent. Decreasing the oxygen concentration of the regeneration gas to assist in temperature control reduces the SO<sub>2</sub> concentration in the regeneration product and complicates the SO<sub>2</sub> control.

Direct production of elemental sulfur during sorbent regeneration would alleviate both problems. Elemental sulfur is a marketable by-product which can be separated by condensation and safely stored and transported.

## PROJECT DESCRIPTION

Three concepts for the possible formation of elemental sulfur were identified from the literature. Thermodynamic analysis showed that sorbents having the strongest affinity for H<sub>2</sub>S removal, e.g., ZnO, would be less conducive to elemental sulfur production than oxides which are less effective for H<sub>2</sub>S removal. Other factors considered during the thermodynamic analysis were carbon deposition from the coal gas, the stability of the metal oxide in the reducing coal gas, the tendency for metal sulfate to be formed during regeneration, and the possible production of volatile reactants or products during both the reduction/desulfurization and regeneration cycles.

Experimental studies using the oxides of iron and cerium for high temperature desulfurization are getting underway. The objective of these studies is to determine reaction conditions--temperature, pressure, regeneration gas composition and space velocity, and sorbent

composition and properties--which maximize the production of elemental sulfur during regeneration. One unique feature involves the development of an analytical system to permit real-time analysis of the sulfur species in the regeneration gas product.

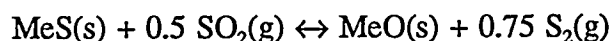
The experimental results will be used to define a conceptual desulfurization-regeneration process suitable for IGCC application. Material and energy balance calculations will be carried out and a preliminary economic evaluation will be performed. This paper summarizes the results of the literature search and thermodynamic analysis, and briefly describes the experimental plans.

## RESULTS--REGENERATION CONCEPTS

Three possible elemental sulfur production concepts were identified from the literature. The general chemistry of each as well as a brief summary of the literature is presented below.

### Reaction With SO<sub>2</sub>

The generic reaction between metal sulfide and SO<sub>2</sub> to yield elemental sulfur is:

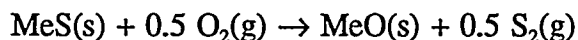


Copeland et al. (1994) have studied the regeneration of SnS(s) while Anderson and Berry (1987) have reported on the regeneration of a sulfided cobalt titanate sorbent. Several studies (Schrodt and Best, 1978; Tseng et al., 1981; Patrick et al., 1993) have examined the regeneration of sulfided iron oxide. Primary questions concern the rate of reaction between metal sulfide and SO<sub>2</sub> and thermodynamic limitations on the maximum partial pressure of S<sub>2</sub>(g) in the regeneration product.

### Partial Oxidation

The formation of elemental sulfur when metal sulfide is reacted with oxygen and steam

under "O<sub>2</sub>-starved" conditions is referred to as partial oxidation. The general stoichiometric reaction is:

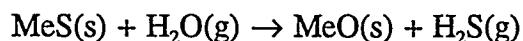


In reality, this stoichiometry represents the net result of a number of simultaneous reactions. In the presence of excess oxygen, total oxidation would occur with MeO(s) and SO<sub>2</sub>(g) as the primary products.

Several references suggest that partial oxidation to produce elemental sulfur may be possible. Joshi et al. (1979), Grindley and Steinfeld (1981), and Van der Waal (1987) have studied the partial oxidation of sulfided iron-based sorbents. As much as 75% of the sulfur released during regeneration was in elemental form, with most of the remainder as H<sub>2</sub>S. Kay and Wilson (1989) and Kay et al. (1993) have reported that elemental sulfur is formed during the regeneration of cerium oxysulfide, Ce<sub>2</sub>O<sub>2</sub>S, at conditions similar to those used for FeS regeneration.

### Reaction With H<sub>2</sub>O/Claus

By reversing the primary desulfurization reaction, regeneration to H<sub>2</sub>S is possible according to the generic reaction:



Although elemental sulfur is not a direct product, H<sub>2</sub>S may be converted to elemental sulfur by the Claus reaction if the H<sub>2</sub>S concentration is sufficiently high. Since regeneration with steam is the reverse of the desulfurization reaction, it is obvious that sorbents having the greatest affinity for H<sub>2</sub>S will be the most difficult to regenerate.

Nielsen et al. (1991) report H<sub>2</sub>S mol fractions in the regeneration product as high as 0.25 when SnS(s) was reacted with H<sub>2</sub>O. H<sub>2</sub> is also produced by this reaction and a separation step is required to recover H<sub>2</sub>S from the excess steam and H<sub>2</sub> by-product. Tamhankar et al.

(1985) and Wakker et al. (1993) have studied the regeneration of sulfided iron-based sorbents with steam while Sohn and Kim (1987) have studied the steam regeneration of ZnS.

## RESULTS--THERMODYNAMIC ANALYSIS

Thermodynamic analysis was used to evaluate the potential of selected metal oxide sorbents to remove H<sub>2</sub>S from Texaco and KRW coal gases, and the feasibility of producing elemental sulfur during regeneration using the concepts previously described.

The free-energy minimization program CHEMQ was used (Kirkpatrick and Pike, 1994). Implementation of CHEMQ requires that the composition of the initial mixture (which may include gaseous, liquid, and solid species) and the temperature and pressure be specified. The CHEMQ data base is searched and all species whose elements are present in the initial mixture are considered as possible components of the equilibrium mixture. The number of mols of each component which minimizes the free energy of the system subject to the elemental material balance constraint established by the initial mixture is then calculated.

Although the initial CHEMQ data base contained 1322 species, several species of interest were not included. Therefore, free energy data from Barin et al. (1993) for 52 compounds including a number of the gaseous sulfur allotropes, and metal compounds of cerium, cobalt, manganese, and molybdenum were added to the data base. Data for a single compound of interest, Ce<sub>2</sub>O<sub>2</sub>S(s), were taken from Kay et al. (1993) since that compound was missing from the compilation of Barin et al.

### Reduction/Desulfurization Cycle Analysis

Coal gas compositions representing a Texaco oxygen-blown gasifier and a KRW air-blown gasifier were considered (see Table 1). The

**Table 1.**  
**Composition of the Texaco Oxygen-Blown**  
**and KRW Air-Blown Gasifier Products**

	Composition, mol%	
	Texaco	KRW
H <sub>2</sub>	31.06	10.0
CO	39.87	15.0
H <sub>2</sub> O	16.81	15.0
CO <sub>2</sub>	10.62	5.0
H <sub>2</sub> S	1.04	1.0
N <sub>2</sub>	-----	54.0
NH <sub>3</sub>	0.21	-----
CH <sub>4</sub>	0.31	-----
$\frac{H_2 + CO}{H_2O + CO_2}$	2.59	1.25
$\frac{C}{O + H}$	0.29	0.22

ratios of  $[(H_2 + CO)/(H_2O + CO_2)]$  and  $[C/(O + H)]$  found at the bottom of Table 1 show that the Texaco gas is more highly reducing and exhibits a greater tendency for carbon deposition, which implies that the operating window for a particular sorbent will be different in different coal gases.

The reduction/desulfurization analysis was carried out by determining the composition resulting from "equilibrating" one mol of metal oxide sorbent in its highest oxidation state with 10 mol of coal gas at selected temperatures and pressures. This initial mixture provided a large excess of metal oxide to H<sub>2</sub>S and of reducing gas to metal oxide. This approach permitted the simultaneous determination of the oxidation state of the excess sorbent, the nature of the sulfided species, and the possible formation of molten or volatile metal species, as well as the potential of the sorbent for removing H<sub>2</sub>S. Eight metal oxide sorbents were examined over a temperature range

of 600 to 1150 K (620 to 1610°F) and pressure range of 1 to 25 atmospheres.

Results of the reduction/desulfurization analysis are summarized in Table 2. The first column identifies the eight sorbents by defining the highest oxidation state metal oxide. Column 2 identifies the chemical nature of the sulfided product; metal sulfide formation is favored from all sorbents except cerium where the favored product is the oxysulfide, Ce<sub>2</sub>O<sub>2</sub>S. In three of the systems -- iron, manganese, and molybdenum -- reduction of excess metal oxide to a lower oxidation state, or, in the case of copper and cobalt, to the elemental form is favored (column 3). At some conditions, ZnO may be reduced to gaseous metallic zinc (column 4) and SnO<sub>2</sub> may be reduced to the low melting metal. SnS(s) has an appreciable vapor pressure, and SnS(g) may be formed at appropriate conditions. Only CeO<sub>2</sub> is not subject to reduction over the range of conditions studied.

The maximum fractional H<sub>2</sub>S removal at conditions outside the region of equilibrium carbon deposition and/or the formation of molten or volatile species is shown in the last column of Table 2. The values range from a low of 0.88 for CeO<sub>2</sub> to 1.00 for both Co(s) and ZnO(s). Equilibrium fractional H<sub>2</sub>S removal is only a weak function of pressure, particularly at temperatures above the carbon deposition region. Three types of temperature effect on H<sub>2</sub>S removal were found. With most sorbents, equilibrium fractional sulfur removal decreased monotonically with increasing temperature. However, with SnO<sub>2</sub> the maximum H<sub>2</sub>S removal occurred at an intermediate temperature, and the equilibrium H<sub>2</sub>S removal with CeO<sub>2</sub> increased with increasing temperature. These effects are illustrated in Figure 1 for MnO, SnO<sub>2</sub>, and CeO<sub>2</sub> sorbents using a Texaco gas at 5 atmospheres.

Cobalt and copper were eliminated from the regeneration analysis because of the tendency for reduction to the metal. The remaining sorbents were analyzed for their potential to form elemental sulfur using the regeneration concepts.

**Table 2.**  
**Reduction/Desulfurization Analysis Summary**  
**600K < T < 1150K**  
**1 atm < P < 25 atm**

Sorbent in Highest Oxidation State	Sulfided Product	Excess Metal	Molten/ Volatile Species	Maximum Fractional H <sub>2</sub> S Removal*
CeO <sub>2</sub>	Ce <sub>2</sub> O <sub>2</sub> S	CeO <sub>2</sub>	None	0.88
Co <sub>3</sub> O <sub>4</sub>	Co <sub>3</sub> S <sub>4</sub>	Co(s)	None	1.00
CuO	Cu <sub>2</sub> S	Cu(s)	None	0.99
Fe <sub>2</sub> O <sub>3</sub>	FeS	FeO, Fe <sub>3</sub> O <sub>4</sub>	None	0.96
MnO <sub>2</sub>	MnS	MnO	None	0.99
MoO <sub>3</sub>	MoS <sub>2</sub>	MoO <sub>2</sub>	None	1.00
SnO <sub>2</sub>	SnS	SnO <sub>2</sub>	SnS(g), Sn(l)	0.98
ZnO	ZnS	ZnO	Zn(g)	1.00

\*at conditions where carbon is not deposited and molten/volatile species are not formed

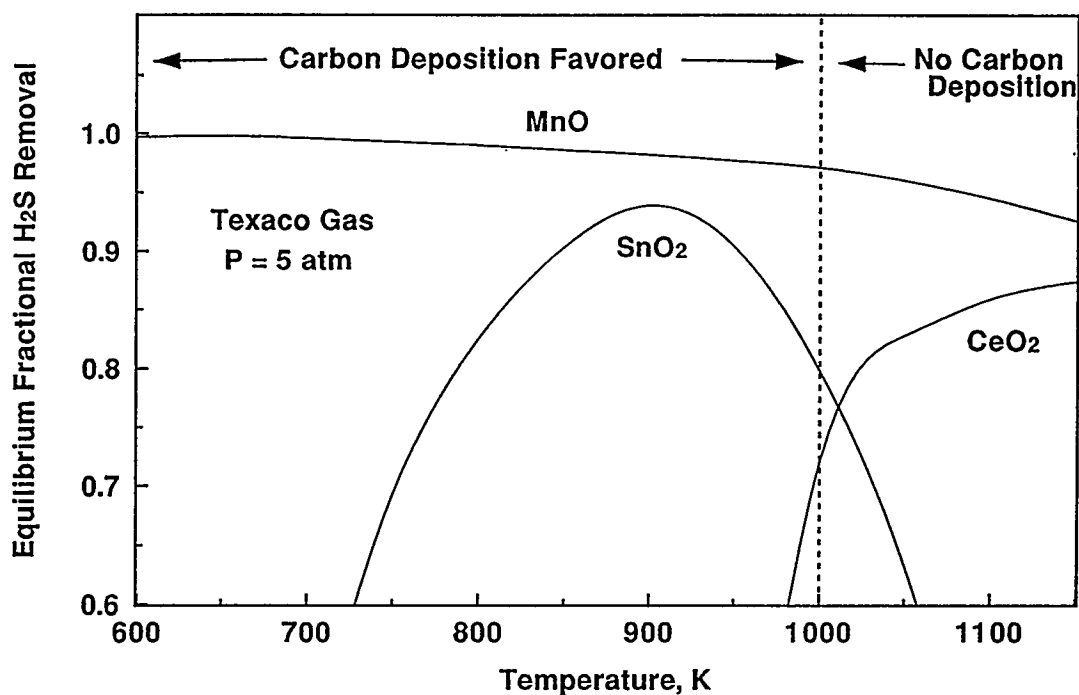


**Figure 1. The Effect of Temperature on Equilibrium H<sub>2</sub>S Removal**

## Regeneration Analysis

The thermodynamic analysis addressed a number of questions. Can the metal sulfide be regenerated under the specified conditions, and, if so, does the regeneration gas contain substantial quantities of elemental sulfur? Is metal sulfate likely to be formed? What is the oxidation state of the regenerated oxide, and are molten or volatile regeneration products likely to be formed?

**Concept 1: Reaction With  $\text{SO}_2$ :** The thermodynamic analysis was carried out by "mixing" one mol of sulfided sorbent with three mols of  $\text{SO}_2$  and determining the equilibrium product composition as a function of temperature and pressure. With excess  $\text{SO}_2$ , complete regeneration would be possible if

thermodynamically favored. Ideal performance would correspond to complete regeneration, i.e., complete transfer of solid phase sulfur to the gas phase, with the gas phase sulfur consisting of equal quantities in the oxidized ( $\text{SO}_2$ ) and elemental ( $\text{S}_x$ ) forms. While the conditions of this analysis do not match actual regeneration conditions, the results provide a valid comparison of the potential of the different sorbents.

$\text{MnS}$ ,  $\text{MoS}_2$ , and  $\text{ZnS}$  were effectively nonreactive with  $\text{SO}_2$  over the temperature and pressure ranges considered, 600 to 1150 K and 1 to 25 atm.  $\text{FeS}$  exhibited moderate reactivity while both  $\text{SnS}$  and  $\text{Ce}_2\text{O}_2\text{S}$  were quite reactive. Results of the equilibrium calculation at 25 atmospheres and 900 and 1050 K for  $\text{SnS}$ ,  $\text{Ce}_2\text{O}_2\text{S}$ , and  $\text{MnS}$  are summarized in Table 3. With  $\text{SnS}$  at 900 K and 25 atmospheres, sulfur is

**Table 3.**  
**Results of Equilibrium Analysis for the**  
**Regeneration of  $\text{SnS}$ ,  $\text{Ce}_2\text{O}_2\text{S}$ , and  $\text{MnS}$**   
**With  $\text{SO}_2$  (1 mol metal sulfide : 3 mols  $\text{SO}_2$ )**  
**P = 25 atm**

System	$\text{SnS}$		$\text{Ce}_2\text{O}_2\text{S}$		$\text{MnS}$	
Temperature, K	900	1050	900	1050	900	1050
Condensed Phase Composition, mol fraction						
Oxide	0.00	1.00	1.00	1.00	trace	trace
Sulfide	0.00	trace	0.00	0.00	1.00	1.00
Sulfate	0.77	0.00	0.00	0.00	0.00	0.00
Sulfur (liq)	0.23	0.00	0.00	0.00	0.00	0.00
Sulfur Distribution (as S), fraction						
Condensed	0.33	trace	0.00	0.00	0.25	0.25
Gas	0.67	1.00	1.00	1.00	0.75	0.75
Sulfur Distribution (as S) Within Gas Phase, fraction						
Elemental ( $\text{S}_x$ )	0.62	0.47	0.49	0.47	trace	trace
Oxide ( $\text{SO}_x$ )	0.38	0.53	0.51	0.53	1.00	1.00
Sulfide ( $\text{H}_2\text{S}$ )	0.00	0.00	0.00	0.00	0.00	0.00

added to the condensed phase, either as  $\text{SnSO}_4(\text{s})$  or  $\text{S}(\text{l})$ , meaning that fractional regeneration is actually negative. At higher temperature  $\text{SnSO}_4(\text{s})$  is unstable and  $\text{S}(\text{l})$  vaporizes so that complete regeneration is possible at 1050 K and 25 atmospheres. The equilibrium distribution of sulfur in the gas phase of 47% elemental and 53% oxide is reasonably close to the ideal 50 - 50 split between the two forms.

Complete regeneration of  $\text{Ce}_2\text{O}_2\text{S}$  is possible at both 900 and 1050 K with the solid product returning to the original  $\text{CeO}_2$  form. The gas phase sulfur distribution is reasonably close to the ideal split between elemental and oxide forms, with the distribution slightly improved at the low temperature. In contrast to  $\text{SnS}$  and  $\text{Ce}_2\text{O}_2\text{S}$ ,  $\text{MnS}$  is almost totally unreactive even at the higher temperature.

#### **Concept 2: Partial Oxidation:**

Duplication of the actual conditions in a regeneration reactor operated in an  $\text{O}_2$ -starved condition with large quantities of steam in the feed gas is impossible because of the inherent batch nature of the thermodynamic calculations. However, a legitimate comparison of sorbent performance was obtained by "mixing" one mol of sulfided sorbent with one mol of  $\text{O}_2(\text{g})$  and one mol of  $\text{H}_2\text{O}(\text{g})$ , and determining the equilibrium composition. The temperature and pressure ranges were 650 to 1100 K and 1 to 25 atmospheres.

Each of the six sulfided sorbents will react, at least to some extent, in the  $\text{O}_2$  -  $\text{H}_2\text{O}$  atmosphere. However, effectively no elemental sulfur can be formed from either  $\text{ZnS}$  or  $\text{MoS}_2$ . A small amount of elemental sulfur may be produced from  $\text{MnS}$ , and a somewhat larger amount from  $\text{FeS}$ . Once again,  $\text{SnS}$  and  $\text{Ce}_2\text{O}_2\text{S}$  are quite reactive and the quantities of elemental sulfur which may be formed are significant.

Selected results of the partial oxidation regeneration analysis for  $\text{FeS}$ ,  $\text{ZnS}$ , and  $\text{Ce}_2\text{O}_2\text{S}$  are presented in Table 4 at 25 atmospheres and 900 and 1050 K. Regeneration of  $\text{FeS}$  is

incomplete at both temperatures with the fraction of sulfur transferred to the gas phase increasing from 0.52 at 900 K to 0.65 at 1050 K. At 950K, the condensed phase sulfur is present as the disulfide,  $\text{FeS}_2$ ; at 1050 K all condensed phase sulfur is  $\text{FeS}$ . The stable oxide is  $\text{Fe}_3\text{O}_4$  at both temperatures. A large majority of the gas phase sulfur is in form of  $\text{SO}_2$  at both temperatures, but both the elemental ( $\text{S}_x$ ) and reduced ( $\text{H}_2\text{S}$ ) sulfur contents increase at higher temperature. The fact that the maximum concentration of elemental sulfur at equilibrium is far below concentration levels which have been reported experimentally is to be expected for two reasons. First, as previously stated, it is not possible to duplicate the experimental conditions corresponding to  $\text{O}_2$ -starved flow in the thermodynamic analysis. In addition, partial oxidation experimental conditions are not expected to closely approach equilibrium.

The reaction of  $\text{ZnS}$  in the  $\text{O}_2$  -  $\text{H}_2\text{O}$  atmosphere is essentially that of oxidation by  $\text{O}_2$  with the formation of  $\text{ZnO}$  and  $\text{SO}_2$ . The amount of  $\text{O}_2$  in the thermodynamic mixture is two-thirds of the stoichiometric requirement, and two-thirds of the  $\text{ZnS}$  is converted to  $\text{ZnO}$ .

$\text{Ce}_2\text{O}_2\text{S}$  is quite reactive. Complete regeneration to  $\text{CeO}_2$  is favored at both temperatures, and significant fractions of the gas phase sulfur should be in elemental form. The gas phase distribution of sulfur species is a relatively strong function of temperature with elemental sulfur formation increasing at lower temperature.

#### **Concept 3: Reaction With Steam/Claus:**

This regeneration concept is a direct reversal of the desulfurization reaction and the expected sulfur product is  $\text{H}_2\text{S}$  instead of elemental sulfur. The concept is of interest, however, if sufficiently high concentrations of  $\text{H}_2\text{S}$  to permit direct feed to a Claus reactor can be produced. It is obvious that sorbents having the greatest affinity for  $\text{H}_2\text{S}$  will be the least amenable to regeneration with steam. For this reason, only the  $\text{SnS}$  and  $\text{Ce}_2\text{O}_2\text{S}$  systems were considered.

Both systems should react with steam, and



**Table 4.**  
**Results of Equilibrium Analysis for the Regeneration**  
**of FeS, ZnS, and Ce<sub>2</sub>O<sub>2</sub>S With O<sub>2</sub> and H<sub>2</sub>O**  
**(1 mol sulfided sorbent : 1 mol O<sub>2</sub> : 1 mol H<sub>2</sub>O)**  
**P = 25 atm**

System	FeS		ZnS		Ce <sub>2</sub> O <sub>2</sub> S	
Temperature, K	900	1050	900	1050	900	1050
Condensed Phase Composition, mol fraction						
Oxide	0.52	0.38	0.67	0.67	1.00	1.00
Sulfide	0.00	0.72	0.33	0.33	0.00	0.00
Disulfide	0.48	0.00	0.00	0.00	0.00	0.00
Sulfate	0.00	0.00	0.00	0.00	0.00	0.00
Sulfur (liq)	0.00	0.00	0.00	0.00	0.00	0.00
Sulfur Distribution (as S), fraction						
Condensed	0.48	0.35	0.33	0.33	0.00	0.00
Gas	0.52	0.65	0.67	0.67	1.00	1.00
Sulfur Distribution Within Gas Phase (as S), fraction						
Elemental	0.01	0.03	trace	0.00	0.58	0.49
Oxide	0.96	0.91	1.00	1.00	0.14	0.18
Sulfide	0.03	0.06	trace	trace	0.28	0.32

both reactions should proceed essentially according to stoichiometry. Only negligible quantities of SO<sub>2</sub> or S<sub>x</sub> should be formed. However, both regeneration reactions produce H<sub>2</sub> and H<sub>2</sub>S in equimolar quantities, so that a H<sub>2</sub> separation step will be required. In order to achieve complete regeneration, it will only be necessary to supply sufficient excess steam to satisfy the thermodynamics.

Figure 2 shows the minimum steam to sorbent ratio required for complete regeneration as a function of temperature at 15 atm. For SnS, the ratio is in the 20 to 25 range and is almost independent of temperature. It is interesting to note that the experimental work on SnS regeneration with steam described by Nielsen et al. (1991) used a ratio of H<sub>2</sub>O to SnS of 30 to 1,

only slightly above the thermodynamic minimum. Ce<sub>2</sub>O<sub>2</sub>S is even more amenable to regeneration with steam. As shown in Figure 2, the minimum steam to Ce<sub>2</sub>O<sub>2</sub>S ratio is in the range of 5 to 10, and increases slightly with increasing temperature. These results are independent of pressure since the reactions do not result in a change in the number of gas phase mols.

## Discussion

The thermodynamic analysis has shown that sorbents having the greatest affinity for H<sub>2</sub>S in the reduction/desulfurization cycle will be the most difficult to regenerate with elemental sulfur (or H<sub>2</sub>S) as a direct product. For practical purposes, this eliminates zinc, manganese,

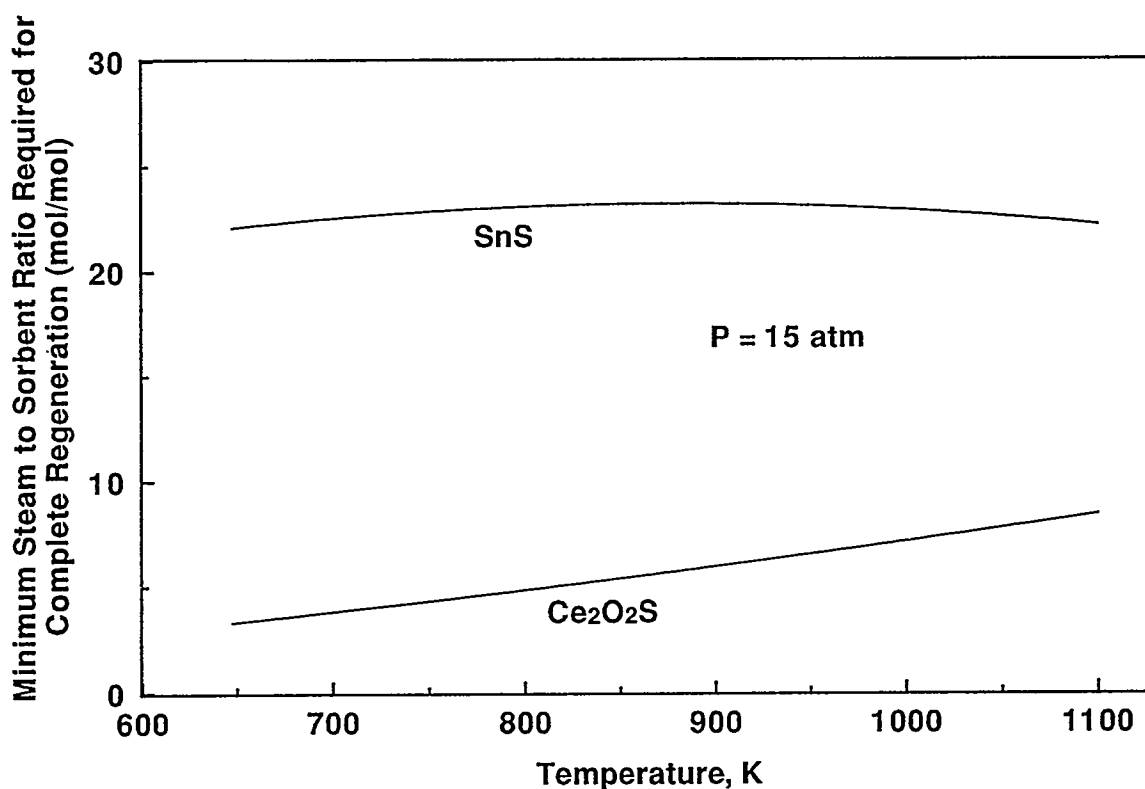


Figure 2. Minimum Steam to Sorbent Ratio for the Complete Steam Regeneration of SnS(s) and Ce<sub>2</sub>O<sub>2</sub>S(s) Sorbents

and molybdenum sorbents, each of which is thermodynamically capable of desulfurization efficiencies which approach 100%. Iron oxide sorbents are less effective for H<sub>2</sub>S removal, and are somewhat more amenable to elemental sulfur production. The most promising regeneration concept for FeS appears to be partial oxidation in which the regeneration atmosphere is deficient in O<sub>2</sub> and contains excess steam. Numerous simultaneous reactions such as listed in Table 5 are expected to occur. Hence, the objective of the experimental study will be to determine conditions which maximize the rate of those reactions producing elemental sulfur to the rate of reactions which produce SO<sub>2</sub>. Regeneration of FeS with SO<sub>2</sub> or H<sub>2</sub>O, while feasible, would require such large quantities of reactant that the concept would not be practical.

The thermodynamic properties of SnS and Ce<sub>2</sub>O<sub>2</sub>S make these systems uniquely suitable to elemental sulfur production. All three of the regeneration concepts show promise with both SnS and Ce<sub>2</sub>O<sub>2</sub>S. Although the thermodynamic characteristics of SnS and Ce<sub>2</sub>O<sub>2</sub>S are similar with respect to elemental sulfur production, there are significant differences in other respects. Under appropriate conditions, either SnS<sub>2</sub> or Sn<sub>2</sub>S<sub>3</sub> may be produced during regeneration. SnSO<sub>4</sub> is moderately stable and high temperatures are required to prevent its formation, particularly at high pressure. The reduction of SnO<sub>2</sub> to liquid metallic Sn may occur in a highly reducing coal gas. Finally, SnS(s) may vaporize at appropriate conditions, a potential problem in both desulfurization and regeneration cycles. The condensed phase of the cerium system is less

**Table 5.**  
**Simultaneous Reactions Involved**  
**in the Partial Oxidation of FeS to Produce**  
**Elemental Sulfur**

**Gas - Solid Reactions**

1.  $2\text{FeS(s)} + 1.5 \text{ O}_2\text{(g)} \rightarrow \text{Fe}_2\text{O}_3\text{(s)} + \text{S}_2\text{(g)}$
2.  $2\text{FeS(s)} + 3.5 \text{ O}_2\text{(g)} \rightarrow \text{Fe}_2\text{O}_3\text{(s)} + 2\text{SO}_2\text{(g)}$
3.  $3\text{FeS(s)} + 4\text{H}_2\text{O(g)} \rightarrow \text{Fe}_3\text{O}_4\text{(s)} + 3\text{H}_2\text{S(g)} + \text{H}_2\text{(g)}$
4.  $3\text{FeS(s)} + 2\text{SO}_2\text{(g)} \rightarrow \text{Fe}_3\text{O}_4\text{(s)} + 2.5 \text{ S}_2\text{(g)}$
5.  $2\text{Fe}_3\text{O}_4\text{(s)} + 0.5 \text{ O}_2\text{(g)} \rightarrow 3\text{Fe}_2\text{O}_3\text{(s)}$

**Gas-Phase Reactions**

6.  $\text{SO}_2\text{(g)} + 2\text{H}_2\text{S(g)} \rightarrow 2\text{H}_2\text{O(g)} + 1.5 \text{ S}_2\text{(g)}$
7.  $\text{H}_2\text{S(g)} \rightarrow \text{H}_2\text{(g)} + 0.5 \text{ S}_2\text{(g)}$
8.  $\text{SO}_2\text{(g)} + 2\text{H}_2\text{(g)} \rightarrow 2\text{H}_2\text{O(g)} + 0.5 \text{ S}_2\text{(g)}$
9.  $\text{S}_2\text{(g)} + 2\text{O}_2\text{(g)} \rightarrow 2\text{SO}_2\text{(g)}$

complex.  $\text{CeO}_2$  is nonvolatile and there is no danger of it being reduced.  $\text{Ce}_2\text{O}_2\text{S}$ , also nonvolatile, is the only sulfided product. As an added advantage, the desulfurization potential of  $\text{CeO}_2$  increases with increasing temperature and in more highly reducing coal gas.

Because of the reduced desulfurization capability of the sorbents of interest, a two-step desulfurization process such as shown in Figure 3 may be required. A primary desulfurization reactor containing an oxide such as iron, tin, or cerium would be followed by a secondary desulfurization reactor containing a high efficiency sorbent such as  $\text{ZnO}$ . Regeneration of  $\text{ZnS}$  would be accomplished in the traditional manner and product gas containing  $\text{SO}_2$  would be recycled to the gasifier. By removing the majority of  $\text{H}_2\text{S}$  in the primary desulfurization step, the secondary

reactor would be smaller and/or require less frequent regeneration. Regeneration of the sorbent in the primary desulfurization reactor would be accomplished using one of the three concepts previously described. Elemental sulfur would be condensed, and the remaining product gas would be recycled to the regeneration reactor or to the gasifier.

## **FUTURE WORK**

In the experimental phase of the project, we are studying the regeneration of  $\text{FeS}$  using the partial oxidation concept, and the sulfidation and regeneration of  $\text{CeO}_2$  using all three regeneration concepts. Both atmospheric and high pressure electrobalance reactors are now being used and a

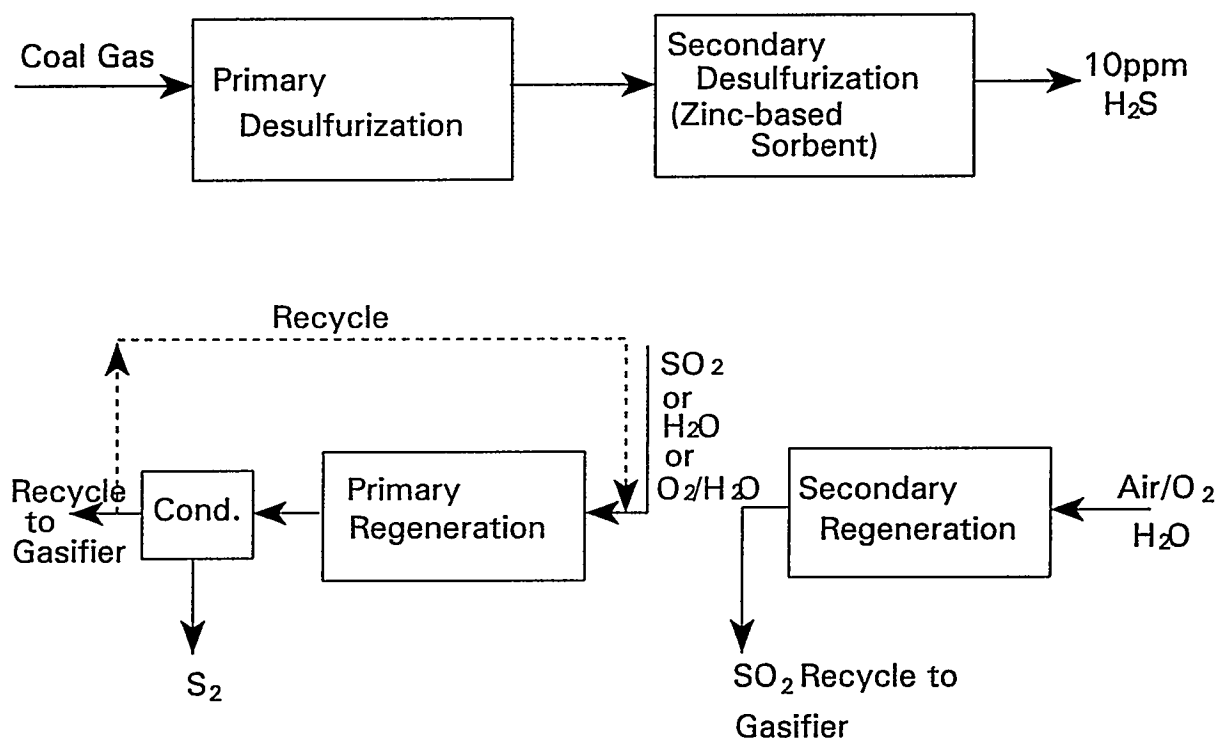


**Figure 3. Two-Step Desulfurization-Regeneration Process**

high-pressure laboratory-scale fixed-bed reactor is being constructed.

The flow rates and the distribution of sulfur species in the reactor product gas will vary with time because of the inherent unsteady state behavior of the fixed-bed reactor. An analytical system is being developed to permit real-time analysis of the distribution of sulfur species in the regeneration product gas. A slip stream of the product gas will be expanded from reaction to atmospheric pressure through a specially designed quartz capillary tube into an oxidizer where all sulfur species will be converted to  $\text{SO}_2$  for total sulfur analysis. The remainder of the product gas will pass through condensers where elemental sulfur and  $\text{H}_2\text{O}$  will be removed.  $\text{SO}_2$  and  $\text{H}_2\text{S}$  concentrations will then be determined using gas chromatography. This will permit elemental sulfur to be determined by difference. Although analysis

by difference is not generally desirable, no alternative has been identified. In addition, the results should be acceptable if we are able to achieve the goal of producing high concentrations of elemental sulfur.

The experimental studies, which will receive primary emphasis during the next year, will be followed by simulation studies, including material and energy balances and a preliminary economic evaluation.

## REFERENCES

Anderson, G.L., and Berry, F.O., 1987, Development of a Hot Gas Cleanup System, Proceedings of the 7th Annual Gasification and Gas Stream Cleanup Systems Review Meeting, DOE/METC-87/6079 (DE87006496), Vol. II.

Barin, I., et al., 1993, Thermochemical Data of Pure Substances, VCH Verlagsgesellschaft, Weinheim, Germany.

Copeland, R.J., et al., 1994, High Temperature Hydrogen Sulfide Removal With Stannic Oxide, Proceedings of the Coal-Fired Power Systems 94 -- Advances in IGCC and PFBC Review Meeting, DOE/METC-94/1008 (DE94012252), Vol. I, p. 444.

Grindley, T., and Steinfeld, G., 1981, Development and Testing of Regenerable Gas Desulfurization Sorbents, DOE/MC/16545-1125.

Joshi, D.K., et al., 1979, Hot Low-Btu Producer Gas Desulfurization in Fixed-Bed of Iron Oxide-Fly Ash, DOE/FE-2257-3.

Kay, D.A.R., and Wilson, W.G., 1989, Method for the Regeneration of Sulfided Cerium Oxide Back to a Form That is Again Capable of Removing Sulfur From Fluid Materials, U.S. Patent 4,857,280.

Kay, D.A.R., et al., 1993, High Temperature Thermodynamics and Application of Rare Earth Compounds Containing Oxygen and Sulfur in Fuel Gas Desulfurization and SO<sub>x</sub> and NO<sub>x</sub> Removal, J. of Alloys and Compounds, 192, 11.

Kirkpatrick, M.O., and Pike, R.W., 1994, Linking Database Management Systems and Chemical Engineering Application Programs - Prediction of Chemical Equilibrium, AIChE Symposium Series, C.C. Chen and S. Watansiri, eds., Vol. 90, No. 298, pp. 174-187, AIChE, New York. (The CHEMQ program is available on the CACHE CD-ROM, Cache Corporation, Austin, Texas, 1994.)

Nielsen, P.E.H., et al., 1991, Steam Regenerable Sulfur Absorption Masses and Their Application in IGCC Plants, paper presented at EPRI Coal Gasification Conference, San Francisco.

Nielsen, P.E.H., and Rudbeck, P., 1993, Hot Gas Cleaning in IGCC Power Plants, Power Generation Technology, Sterling Publications, London.

Patrick, V. and Gavalas, G.R., 1993, Reduction, Sulfidation and Regeneration of Mixed Iron-Aluminum Oxide Sorbent, Industrial and Engineering Chemistry Research, 32, 519.

Schrodt, J.T., and Best, J.E., 1978, Sulfur Recovery from Fuel Gas Desulfurization Sorbent, AIChE Symposium Series, 74, No. 175, p. 189.

Sohn, H.Y., and Kim, D., 1987, Intrinsic Kinetics of the Reaction Between Zinc Sulfide and Water Vapor, Metall. Trans. B, 18B, 451.

Tamhankar, S.S., et al., 1985, Kinetic Study of the Reactions Involved in Hot Gas Desulfurization Using a Regenerable Iron Oxide Sorbent III. Reaction of the Sulfided Sorbent With Steam and Steam-Air Mixtures, Chemical Engineering Science, 40, 1019.

Tseng, S.C., et al., 1981, Kinetic Studies on the Reactions Involved in Hot Gas Desulfurization Using a Regenerable Iron Oxide Sorbent II. Reactions of Iron Sulfide With Oxygen and Sulfur Dioxide, Chemical Engineering Science, 36, 1287.

Van der Waal, W.J.J., 1987, Desulfurization of Process Gas by Means of Iron Oxide on Silica Sorbents, Ph.D. Dissertation, University of Utrecht.

Wakker, J.P., et al., 1993, High Temperature H<sub>2</sub>S and COS Removal With MnO and FeO on  $\gamma$ -Al<sub>2</sub>O<sub>3</sub> Acceptors, Industrial and Engineering Chemistry Research, 32, 139.

**CONTRACT INFORMATION**

**Contract Number** DE-AC21-94MC31258

**Contractor** Research Triangle Institute  
P.O. Box 12194  
Research Triangle Park, NC 27709-2194  
Telephone: (919) 541-8033  
Facsimile: (919) 541-8000

**Other Funding Sources** None

**Contractor Project Manager** Santosh K. Gangwal

**Principal Investigators** Brian S. Turk  
Raghubir P. Gupta

**METC Project Manager** Thomas P. Dorchak

**Period of Performance** March 21, 1994 to March 20, 1997

**Schedule and Milestones**

**FY94-96 Program Schedule**


---

	J	A	S	O	N	D	J	F	M	A	M	J	J	A	S	O	N	D
Concept Assessment	_____																	
Laboratory Development							_____											
Feasibility Demonstration																	_____	

---

**OBJECTIVES**

Regenerable metal oxide sorbents, such as zinc titanate, are being developed to efficiently remove hydrogen sulfide (H<sub>2</sub>S) from coal gas in advanced power systems. Dilute air regeneration of the sorbents produces a tailgas containing a

few percent sulfur dioxide (SO<sub>2</sub>). Catalytic reduction of the SO<sub>2</sub> to elemental sulfur with a coal gas slipstream using the Direct Sulfur Recovery Process (DSRP) is a leading first-generation technology. Currently the DSRP is undergoing field testing at gasifier sites. The objective of this study is to develop

second-generation processes that produce elemental sulfur without coal gas or with limited use.

Novel approaches that were evaluated to produce elemental sulfur from sulfided sorbents include (1) sulfur dioxide (SO<sub>2</sub>) regeneration, (2) substoichiometric (partial) oxidation, (3) steam regeneration followed by H<sub>2</sub>S oxidation, and (4) steam-air regeneration. Preliminary assessment of these approaches indicated that developing SO<sub>2</sub> regeneration faced the fewest technical and economic problems among the four process options. Elemental sulfur is the only likely product of SO<sub>2</sub> regeneration and the SO<sub>2</sub> required for the regeneration can be obtained by burning a portion of the sulfur produced. Experimental efforts have thus been concentrated on SO<sub>2</sub>-based regeneration processes.

## BACKGROUND INFORMATION

### Leading Hot-Gas Desulfurization Technologies

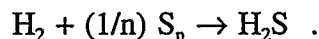
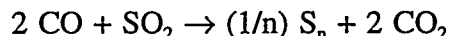
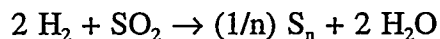
Hot-gas desulfurization research has focused on air-regenerable mixed-metal oxide sorbents such as zinc titanate and zinc ferrite that can reduce the sulfur in coal gas, present primarily as H<sub>2</sub>S, to <20 ppmv and that can be regenerated in a cyclic manner with air for multicycle operation.

The sulfidation/regeneration cycle can be carried out in fixed-, moving-, and fluidized-bed reactor configurations. The regeneration reaction is highly exothermic, requiring the use of large volumes of diluent to control the temperature and results in a dilute SO<sub>2</sub>-containing tailgas that must be further treated. Under contracts with the U.S. Department of Energy/Morgantown Energy Technology Center (DOE/METC), many approaches have been evaluated for treatment of the tailgas. These include adsorption of SO<sub>2</sub> using calcium-based sorbents followed by land-filling of calcium sulfate as well as conventional

methods such as Wellman-Lord coupled with high-temperature syngas reduction and augmented Claus for converting the SO<sub>2</sub> to elemental sulfur. There are two leading advanced approaches that DOE/METC is currently sponsoring to convert the SO<sub>2</sub> tailgas to useful byproducts. These include the General Electric (GE) moving-bed process and the DSRP.

In the GE moving-bed process (Cook et al., 1992), the H<sub>2</sub>S in coal gas is removed by moving a bed of sorbent countercurrent to the upward gas flow. The sulfided sorbent is transferred to a moving-bed regenerator below the moving-bed absorber using a lock-hopper arrangement. In the regenerator, SO<sub>2</sub> recycle and limited air are used to control the temperature of the exothermic reactions, producing a tailgas containing 10- to 13-vol% SO<sub>2</sub>. The regenerated sorbent is lifted back to the absorber using a bucket elevator arrangement. The 10- to 13-vol% SO<sub>2</sub> is a suitable feed for a sulfuric acid plant. The GE moving-bed process has undergone a series of pilot-scale tests and has been selected for demonstration in a Clean Coal Technology project.

In the DSRP (Dorchak et al., 1991; Gangwal et al., 1993), the SO<sub>2</sub> tailgas is reacted with a slipstream of coal gas over a fixed bed of a selective catalyst to directly produce elemental sulfur at the high-temperature, high-pressure (HTHP) conditions of the tailgas and coal gas. Major reactions involved are shown below:



The DSRP was originally envisioned as a two-stage process. Recent results, however, indicate that sufficient selectivity (>99 percent or better) to elemental sulfur can be achieved in a single stage by careful control of the inlet

stoichiometry to maintain a reducing gas ( $H_2 + CO$ ) to  $SO_2$  mole ratio of 2.0. The DSRP integrates well with zinc titanate fluidized-bed desulfurization (ZTFBD) (Gupta et al., 1992), as opposed to fixed- or moving-bed desulfurization because of the relative ease of achieving a constant concentration of  $SO_2$  in the tailgas using the fluidized-bed desulfurization-regeneration system. Both ZTFBD and DSRP have been demonstrated at bench scale using simulated gases and are being demonstrated in an integrated manner using a slipstream of actual coal gasifier gas under another contract awarded to the Research Triangle Institute (RTI) by DOE/METC.

Economic evaluations of the GE moving-bed process coupled to a sulfuric acid plant and fluidized-bed desulfurization coupled to DSRP have been conducted by Gilbert Commonwealth for DOE. These evaluations show that the two approaches are closely competitive, with costs within 1 percent of each other, cost of electricity basis.

### Need for Simpler Processing

Production of a sulfuric acid byproduct, e.g., using the GE moving-bed process, is site specific, requiring a nearby sulfuric acid plant and a ready market because sulfuric acid cannot be stored in bulk for long periods of time and cannot be transported over long distances. Another inherent problem with the GE moving-bed process has been that, in spite of several attempts, a steady (constant) level of  $SO_2$  has not been achieved in the tailgas, which could present operation problems for converting to sulfuric acid in the downstream sulfuric acid plant. A number of other problems have been encountered in the operation of the GE moving-bed process, e.g., control of temperature in the regenerator and corrosion in the  $SO_2$  recycle system.

Elemental sulfur is the desired sulfur byproduct because it is easily stored, transported, or sold. It is also the preferred choice of utilities. DSRP has the advantage that it produces elemental sulfur and is also significantly cheaper than conventional processes to reduce  $SO_2$  to elemental sulfur.

Nevertheless, simpler processes that can be more fully and economically integrated with regenerable sorbents are needed because the DSRP requires a small portion of the fuel gas (i.e., coal gas) to reduce  $SO_2$  to elemental sulfur and, thus, imposes an inherent efficiency and economic penalty on the overall system. For every mole of  $SO_2$  converted to elemental sulfur in DSRP, approximately 2 mols of reducing gas ( $H_2 + CO$ ) are consumed. As the sulfur content of the coal fed to the gasifier increases, obviously the proportion of the reducing gas required in the DSRP will increase as will the cost associated with it. A greater incentive thus exists for developing alternative processing schemes for higher sulfur coals that eliminate or minimize the use of coal gas.

### PROJECT DESCRIPTION

This project seeks to recover sulfur (as elemental sulfur) from sulfided sorbents using alternative regeneration reactions/process schemes that do not result in the production of a dilute  $SO_2$ -containing tailgas requiring coal gas for reduction to sulfur (as in DSRP). The project is divided into three tasks shown in the Schedule and Milestones. Task 1, Concept Assessment, is complete; Task 2, Laboratory Development, is currently ongoing; and Task 3, Feasibility Demonstration, will not begin until 1996.

Based on a concept assessment, the alternative regeneration techniques listed in order of increasing potential are partial oxidation, simultaneous



steam and air regeneration, steam regeneration with direct oxidation of  $\text{H}_2\text{S}$ , and  $\text{SO}_2$  regeneration.

Partial oxidation is attractive due to lack of thermodynamic limitations, thereby allowing the choice of sorbent purely on its ability to remove  $\text{H}_2\text{S}$ . The challenge, however, is to inhibit subsequent oxidation of elemental sulfur to  $\text{SO}_2$  which is rapidly catalyzed by the sorbent as the sulfur attempts to escape its pores. Possible remedies include reducing reaction rates by reducing temperature, limiting the oxygen supply, and reducing sorbent and sulfur contact. However, none of these are complete solutions or achievable in practice without a great deal of difficulty. Lower temperatures would reduce the rate of sulfur vapor diffusions out of the sorbent. Oxygen concentrations at all points in the reactor must be at a level to control the sequential reaction, sorbent  $\rightarrow$  sulfur  $\rightarrow$   $\text{SO}_2$ , to make sulfur but prevent  $\text{SO}_2$  formation. This would require highly complex reactor designs. Reducing contact between sorbent and sulfur will require modifying sorbents to have a wide pore structure without altering attrition resistance. Thus, significant barriers exist to development of partial oxidation for direct sulfur production during regeneration.

The use of steam for regeneration involves the reaction that is simply the reverse of the sulfidation reaction. Thus, an immediate barrier to steam regeneration is that any sorbent capable of removing  $\text{H}_2\text{S}$  down to ppm levels will only release ppm levels of  $\text{H}_2\text{S}$  during steam regeneration. The ppm  $\text{H}_2\text{S}$  release will increase with steam concentration but only weakly (e.g., linearly, depending on sorbent stoichiometry). Higher steam concentrations and temperatures assist the regeneration but could result in severe sorbent sintering. Both steam regeneration followed by  $\text{H}_2\text{S}$  oxidation to sulfur and simultaneous steam and air regeneration followed by Claus reaction face additional technical problems. Mixtures of steam and  $\text{SO}_2$  are corrosive.

Effective condensation of sulfur occurs at a lower temperature than steam at HTHP conditions. A large heat duty is required to generate steam from condensed process steam or fresh water.

Based on detailed thermodynamic calculations and the barriers presented above, all alternative regeneration concepts, other than dry- $\text{SO}_2$  regeneration, were eliminated from further immediate consideration. Assessment and laboratory results of  $\text{SO}_2$  regeneration are described in the Results section. Laboratory experiments to test the  $\text{SO}_2$  regeneration concept were carried out using an atmospheric pressure thermogravimetric analyzer (TGA), a high-pressure TGA, and a high-pressure lab-scale reactor. The high-pressure lab-scale reactor system is shown in Figure 1. The reactor is made of a 1/2-in. stainless steel tube capable of operation at 750 °C and 200 psig. Provision is made for sulfiding the sorbent with simulated coal gas, or regenerating the sorbent with up to 15 vol%  $\text{SO}_2$ . The gas exiting the reactor passes through heated tubing into a 130 °C convective oven where a 0.1-micron filter is used to collect sulfur. A sample of the exit gas is analyzed by gas chromatography (GC) to measure  $\text{H}_2\text{S}$  breakthrough. The gas finally vents through a back-pressure regulator.

Zinc and iron containing sorbents have been the primary candidates that have been tested. The atmospheric pressure and high-pressure TGA experiments have involved cyclic tests using simulated coal gas for sulfidation and up to 15 vol%  $\text{SO}_2$  for regeneration. The concept of  $\text{SO}_2$  regeneration followed by air regeneration has also been evaluated.

## RESULTS

### Assessment of $\text{SO}_2$ Regeneration

Like steam regeneration,  $\text{SO}_2$  regeneration has thermodynamic constraints as the thermodynamic calculations presented later show. However,

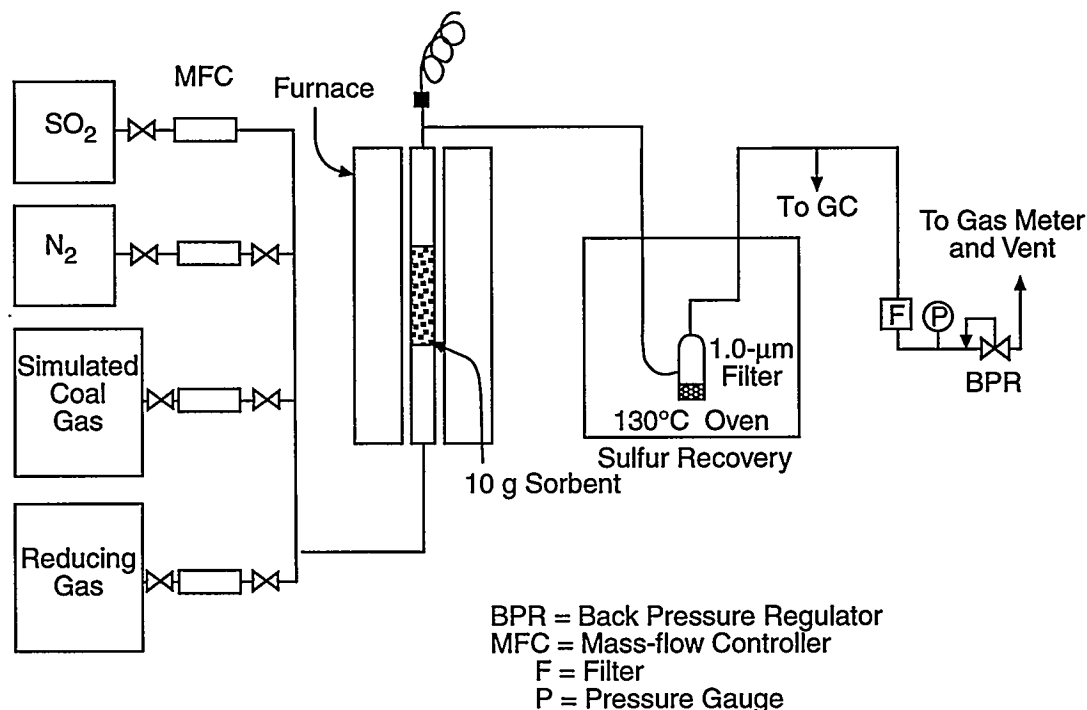


**Figure 1. Laboratory-Scale SO<sub>2</sub> Regeneration Test System**

high-pressure conditions are anticipated to enhance elemental sulfur formation. Based on Le Chatelier's principle, high pressure favors formation of fewer gaseous products. Since formation of sulfur oligomers larger than S<sub>3</sub> result in few moles of gaseous products, high pressure should favor formation of higher oligomers. Also, non-ideal behavior of sulfur oligomers could lead to increased yield at higher pressures.

Unlike thermodynamic limitations for steam regeneration, development of sorbents for SO<sub>2</sub> regeneration may benefit from the thermodynamic limitations. Regeneration with SO<sub>2</sub> will require SO<sub>2</sub> and heat because SO<sub>2</sub> regeneration is endothermic. Oxygen regeneration, which is rapid and extremely exothermic, produces SO<sub>2</sub> and heat. By balancing the amounts of SO<sub>2</sub> and O<sub>2</sub> regeneration, it may be possible to achieve complete regeneration, convert all sulfur species into elemental sulfur, and balance heat requirements. Since SO<sub>2</sub> regeneration is slow,

achieving this balance requires increasing SO<sub>2</sub> regeneration rates. Increasing temperature will increase reaction rates, but the maximum temperature is limited by sorbent sintering and materials of construction available for reactor and process heat integration. Any temperature effects on the thermodynamic equilibrium constant will be further augmented by the increase in reaction rate. Although pressure effects on reaction rate constants are generally assumed insignificant, research with DSRP found rate constants, specifically for the H<sub>2</sub>-SO<sub>2</sub> reaction, increased with pressure while all other conditions were kept constant. Thus HTHP conditions offer considerable potential for effective SO<sub>2</sub> regeneration.

With SO<sub>2</sub> regeneration, sulfate formation, a major cause of sorbent decrepitation, does not occur. Absence of sulfate formation during SO<sub>2</sub> regeneration should increase mechanical stability and extend life expectancy for sorbents. Sulfur dioxide regeneration allows simple separation of

SO<sub>2</sub> and elemental sulfur and dry SO<sub>2</sub> is much less corrosive than a SO<sub>2</sub> and steam mixture. The endothermic nature of SO<sub>2</sub> regeneration may require additional heat in spite of extensive heat recovery from the sulfidation unit and O<sub>2</sub> regenerator. Although a certain amount of sorbent optimization will be needed, SO<sub>2</sub> regeneration has a much greater potential for rapid process development than any of the other alternative regeneration techniques.

### Sorbent Metal-Oxide Selection

A number of sorbent metal-oxide formulations were assessed on the basis of literature information and thermodynamic calculations. A review of the literature indicated regenerable sorbents based on oxides of cerium, copper, cobalt, iron, manganese, molybdenum, tin, and zinc individually and in combinations. These metal or mixed-metal oxides have been investigated both without as well as combined with a secondary oxide, typically silica, alumina, titania, and chromia. The roles of these secondary oxides include support for strengthening mechanical structure, as stabilizers against reduction of the metal oxide to metal in a reducing environment, and/or as modifiers of thermodynamic properties of the metal oxide to enhance elemental sulfur formation during regeneration.

Based on the evaluations, sorbents based on cerium, cobalt, cobalt, molybdenum and tin were found to be poor desulfurizing agents, costly, or not easily regenerated with SO<sub>2</sub>. Some had a combination of these deficiencies. Thus, they were eliminated from further consideration. Of the remaining metal oxides, namely oxides of manganese, iron, and zinc, due to the similarity of reduction and desulfurizing properties of manganese and iron, iron was chosen for further consideration because more is known about iron. Also zinc remained a candidate for further consideration due to its very high desulfurization efficiency even though it showed very poor

thermodynamics for SO<sub>2</sub> regeneration. In combination with iron, zinc could act as a polishing agent for H<sub>2</sub>S which could be regenerated using air to produce SO<sub>2</sub> needed for SO<sub>2</sub> regeneration. Thus, the laboratory work concentrated on iron and zinc-based sorbents.

### Thermodynamic and Process Evaluation of SO<sub>2</sub> Regeneration

As stated earlier, SO<sub>2</sub> regeneration also shows thermodynamic constraints as seen from thermodynamic calculations shown in Table 1. Results are relevant only for zinc- and iron-based sorbents and thus Table 1 is limited to these sorbents. It is noted that, as the sorbent becomes less effective for H<sub>2</sub>S removal, it becomes thermodynamically more easily regenerated by SO<sub>2</sub>. This suggests that a sorbent combination from the top and bottom parts of the table may be necessary for an effective SO<sub>2</sub> regeneration process.

The SO<sub>2</sub> regeneration could be followed by air or O<sub>2</sub> regeneration to complete the regeneration before returning the sorbent to the sulfider as shown conceptually in Figure 2. Of course, alternative process schemes employing various combinations of SO<sub>2</sub> and O<sub>2</sub> regeneration are also possible but are not discussed here in the interest of space.

### Test Results

A number of sorbents based on iron and zinc oxides were prepared and tested for SO<sub>2</sub> regeneration using the TGAs and the laboratory reactor system. The benchmark zinc titanate and zinc ferrite sorbents were ZT-4 and L-7. These sorbents have been developed for fluidized-bed desulfurization incorporating air regeneration under a previous DOE contract. The ZT-4 sorbent (based purely on ZnO as the active sorbent) and other ZnO-only-based sorbents showed essentially no regeneration with 3.3 percent SO<sub>2</sub> in N<sub>2</sub> at up to 800 °C and 10 atm. However, iron- and

**Table 1. Thermodynamic Calculations for Sulfidation and SO<sub>2</sub> Regeneration**

Sorbent	Sulfidation Equilibrium H <sub>2</sub> S Concentration with 20% Steam at 800 K (ppm)	Equilibrium Constants for SO <sub>2</sub> Regeneration			
		800 K		1,000 K	
		S <sub>2</sub> (×10 <sup>-4</sup> )	S <sub>8</sub> (×10 <sup>-4</sup> )	S <sub>2</sub> (×10 <sup>-4</sup> )	S <sub>8</sub> (×10 <sup>-4</sup> )
ZnO	3	0.17	0.51	3.3	1.1
ZnO·TiO <sub>2</sub>	3	0.19	0.56	3.7	1.2
FeO	107	6.2	19.0	55.0	18.0
ZnO·Al <sub>2</sub> O <sub>3</sub>	1,055	61.0	183.0	316.0	100.0
FeO·Al <sub>2</sub> O <sub>3</sub>	3,484	202.0	605.0	717.0	227.0

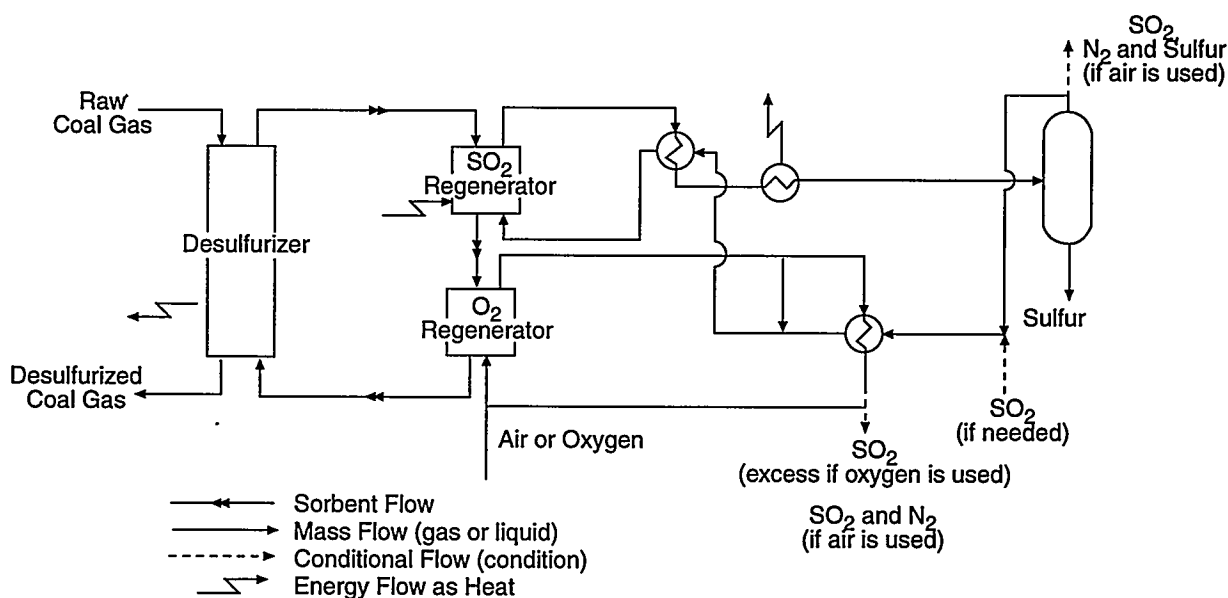


**Figure 2. Three Reactor Systems for SO<sub>2</sub> Regeneration Followed by O<sub>2</sub> Regeneration**

zinc-iron-based sorbents showed good regeneration with SO<sub>2</sub>. The rates of regeneration of the various sorbents depended on how they were prepared. Due to the proprietary nature of the preparations, no data related to the sorbent's preparation or pore structure are presented. Average regeneration rates (expressed in terms of

sulfur production rate) are presented in Table 2 along with average sulfidation rates and conditions. The sulfidations were conducted using a 0.5 vol% H<sub>2</sub>S containing simulated coal gas. The results suggest that SO<sub>2</sub> regeneration is a feasible approach for iron-based sorbents. Significant potential for increased SO<sub>2</sub>-regeneration rates is

**Table 2. Comparison of Sulfidation and SO<sub>2</sub> Regeneration for Several Sorbents  
(3.3 percent SO<sub>2</sub>, 10 atm)**

Sorbent Designation	Sorbent Type (P = proprietary additive)	Sulfidation Temperature (°C)	Regeneration Temperature (°C)	Sulfidation Rate (×10 <sup>-4</sup> ) (g sulfur/g sorbent/min)	Regeneration Rate (×10 <sup>-4</sup> ) (g sulfur/g sorbent/min)
L-7	Zn+Fe	550	800	10.8	2.0
RTI-3	Fe+P	450	800	19.2	18.2
FE-90	Fe	400	800	34.0	4.6
R-2	Zn+Fe	550	700	24.0	2.2
R-3	Fe+P	500	700	3.8	5.8
R-4	Fe+P	500	700	2.0	4.4
R-5	Zn+Fe+P	460	700	13.4	4.4

possible by increasing the SO<sub>2</sub> concentration and pressure and by modifying sorbent properties.

The L-7, R-2, and R-5 sorbents did not show complete regeneration in SO<sub>2</sub> because the zinc portion of the sorbent did not regenerate. The iron-only-based sorbents completely regenerated in SO<sub>2</sub>. To test the potential of SO<sub>2</sub> regeneration (with higher SO<sub>2</sub> concentrations) followed by air regeneration for zinc-iron-based sorbents, the R-5 sorbent was subjected to three cycles at 10 atm, each consisting of a sulfidation at 460 °C, a SO<sub>2</sub> regeneration with 3.3 to 15 percent SO<sub>2</sub> at 650 to 700 °C, and finally an air regeneration with 2 percent O<sub>2</sub> at 700 °C.

The sorbent showed consistent behavior over the three cycles of operation. The rates of sulfidation, SO<sub>2</sub> regeneration, and air regeneration are compared in Table 3. Results show that as SO<sub>2</sub> concentration is increased, regeneration can be carried out effectively at lower temperatures. Also, the various rates are not widely different and thus system design difficulty would not be very formidable.

**Table 3. Comparison of Sulfidation, SO<sub>2</sub>-Regeneration and Air-Regeneration Rates for R-5 Sorbent (Pressure = 10 atm)**

Reactant	Temperature (°C)	Rate g sulfur/ (g sorbent/min)
Simulated Coal Gas (0.5% H <sub>2</sub> S)	460	13.4
SO <sub>2</sub>		
3.3%	700	4.4
3.3%	650	0.22
15%	650	3.7
2% O <sub>2</sub> in N <sub>2</sub>	700	5 <sup>a</sup>

<sup>a</sup> Result probably limited by mass transfer.

Laboratory-scale tests of SO<sub>2</sub> regeneration were carried out with the R-5 sorbent. About 5 g of the sorbent was loaded in the reactor and fully sulfided using simulated coal gas. SO<sub>2</sub> regeneration was then started at 7.8 atm and 700 °C with 15 percent SO<sub>2</sub> in N<sub>2</sub>. Samples were withdrawn after 5.5 h and 10 h of regeneration for TGA analysis. The TGA analysis showed, as expected, that the zinc portion of the sorbent was not regenerated. However, the iron portion of the sorbent regenerated at a rate of 2.1×10<sup>-4</sup> g sulfur/(g sorbent/min). This result is the same order of

magnitude as most TGA results presented in Table 3 at 10 atm. After 10 h of operation, sulfur plugging downstream of the reactor occurred. The sulfur was removed and examined. It was found to be yellow without any kind of odor.

Based on the results, the concept of SO<sub>2</sub> regeneration processes shows significant promise for development as an effective hot-gas desulfurization system with sulfur recovery.

## FUTURE WORK

Laboratory scale tests and TGA experiments will continue to narrow the choices for sorbents for the SO<sub>2</sub> regeneration concept. Feasibility demonstration with a larger reactor system will begin in the next fiscal year. Process evaluations will be carried out using the lab-scale and larger-scale data.

## REFERENCES

- Cook, C.S., et al. 1992. "Integrated Operation of a Pressurized Fixed Bed Gasifier and Hot Gas Desulfurization System." In *Proceedings of the 12th Annual Gasification Gas Stream Cleanup Systems Contractors' Review Meeting*. Vol. 1, DE93000228, p. 84.
- Dorchak, T.P., S.K. Gangwal, and W.J. McMichael. 1991. "The Direct Sulfur Recovery Process." *Environmental Progress* 10(2):68.
- Gangwal, S.K., W.J. McMichael, and T.P. Dorchak. 1992. "The Direct Sulfur Recovery Process for Refinery Gas Processing." AIChE Meeting, New Orleans, March.
- Gangwal, S.K., et al. 1993. "DSRP, Direct Sulfur Production." In *Proceedings of the Coal-Fired Power Systems 93—Advances in IGCC and PFCB Review Meeting*. DOE/METC, Morgantown, WV. June.
- Gupta, R., and S.K. Gangwal. 1992. "Enhanced Durability of Desulfurization Sorbents for Fluidized-Bed Applications—Development and Testing of Zinc Titanate Sorbents." Topical Report to DOE/METC. Report No. DOE/MC/25006-3271. DOE/METC, Morgantown, WV.

## 7A.6 Development of Disposable Sorbents for Chloride Removal From High-Temperature Coal-Derived Gases

### CONTRACT INFORMATION

**Contract Number** DE-AC21-93MC30005

**Contractor** SRI International  
333 Ravenswood Avenue  
Menlo Park, CA 94025  
(415) 326-6200

**Contract Project Manager** Gopala N. Krishnan

**Principal Investigators** G. N. Krishnan, B. J. Wood, and A. Canizales (SRI International)  
R. Gupta and S. D. Shelukar (Research Triangle Institute)  
R. Ayala (GE Corporate Research and Development)

**METC Project Manager** Ronald K. Staubly

**Period of Performance** September 30, 1993 to September 29, 1995

**Schedule and Milestones**

### FY95 Program Schedule

Task	S	O	N	D	J	F	M	A	M	J	J	A	S
Sorbent Preparation and Characterization													
Provision of a Bench-Scale Unit													
Bench Scale Testing													
Parametric Testing													
Data Analysis													
Final Report													

### OBJECTIVE

The objective of this program is to develop alkali-based disposable sorbents capable of

reducing HCl vapor concentrations to less than 1 ppmv in coal gas streams at temperatures in the range 400° to 750°C and pressures in the range 1 to 20 atm. The primary areas of focus of this

program are investigation of different processes for fabricating the sorbents, testing their suitability for different reactor configurations, obtaining kinetic data for commercial reactor design, and updating the economics of the process.

## BACKGROUND INFORMATION

The integrated gasification combined cycle (IGCC) process produces electricity from coal with high efficiency by converting the fuel to coal gas that drives a combustion gas turbine or feeds molten carbonate fuel cells. Both generating methods require relatively contaminant-free gas. Hence, methods must be incorporated between the gasifier and the electricity generator to remove impurities that are formed during gasification from the sulfur, chlorine, nitrogen, and heavy metal constituents indigenous to the coal. One highly undesirable impurity is hydrogen chloride (HCl), a reactive, corrosive, and toxic gas.

The concentration of HCl in coal gas has not been documented extensively, but estimates suggest that it varies widely in the range 1 to 500 ppmv [TRW, 1981]. Bakker and Perkins [1991] noted that concentrations of HCl in coal gas are likely to be about five times greater than those in a coal-fired boiler flue gas stream because of the low specific volumetric flow rate of the coal gas stream. The actual concentration of HCl vapor in a coal gas stream will depend on the chlorine content of the coal, the gasification temperature, and the type of gasifier. Recently, the concentration of HCl vapor was found to be about 300 ppmv in the gas stream from a fixed-bed gasifier using a coal containing 0.24 wt% Cl [Gal et al., 1994].

The effect of impurity HCl in coal gas that fuels a gas turbine is not well defined, and currently no concentration limit standards exist. Nevertheless, the removal of HCl vapor from the gas can only be beneficial in any generating plant, because of the great corrosion potential of the vapor in contact with metal components. Perkins et al. [1990] report that chloride deposits on syngas coolers accelerated the rate of corrosion of the heat exchanger material. HCl reacts with the deposited slags forming low-melting iron chlorides, and thereby accelerates the corrosion rate.

Although high-temperature molten carbonate fuel cells (MCFC) for IGCC power generation

plants are still in the developmental stage, they require a feedgas free of contaminants such as particulate matter, sulfur, and chloride species. During sustained operation, chlorides are deleterious to MCFCs because they can lead to severe corrosion of hardware [Kinoshita et al., 1988]. HCl also can react with the molten carbonate electrolyte to form halides such as LiCl and KCl. The high vapor pressures of these compounds enhance electrolyte loss. An increase in the cell resistance and a corresponding decrease in the cell voltage were observed in feed gas containing 1 ppmv HCl vapor [Pigeaud and Wilemski, 1992]. Hence, the allowable HCl concentration in a MCFC feedgas is estimated to be less than 0.1 ppmv.

Available processes for removing HCl vapor from industrial and incinerator waste gases scavenge HCl by adsorption on activated carbon or alumina, or by reaction with alkali or alkaline earth carbonates or oxides. Typically, commercial sorbents called chloride guards are used for HCl vapor removal from chemical plant process feed stocks. These sorbents reduce chloride contaminant levels to less than 1 ppmv, but they must operate at temperatures less than 450°C. They are also relatively expensive, and cannot be economically regenerated. Hence, they are not suitable for chloride removal from hot coal-derived gas streams. Inexpensive, efficient, and disposable sorbents are needed for these applications.

Equilibrium thermodynamic calculations showed that only Na- and K-based sorbents are capable of reducing HCl levels to less than 1 ppmv at 500°C. Because NaCl has a lower vapor pressure than KCl and sodium minerals are more abundant than potassium minerals, Na-based sorbents were selected as candidate materials [Krishnan et al., 1986].

In a previous program, laboratory- and bench-scale experiments were performed by SRI International [Krishnan et al., 1986] to evaluate three natural carbonate minerals—nahcolite ( $\text{NaHCO}_3$ ), shortite ( $\text{Na}_2\text{CO}_3 \cdot 2\text{CaCO}_3$ ), and dawsonite ( $\text{NaAl}(\text{OH})_2\text{CO}_3$ )—as HCl scavengers for simulated coal gas. All the tested sorbents reacted rapidly with HCl vapor and reduced the HCl vapor concentration from about 300 ppmv to about 1 ppmv. The performance of nahcolite was



superior in its adsorption capacity; the spent sorbent contained up to 54 wt% chloride. Furthermore, the presence of H<sub>2</sub>S and trace metal impurities in the coal gas did not significantly affect the performance of the bed for HCl sorption. An economic evaluation for HCl cleanup costs in a 100 MW<sub>e</sub> plant indicated that the use of nahcolite to remove HCl vapor would add only about \$0.002/kWh (2 mills/kWh) to the cost of the generated electric power.

Thus, alkali-based naturally occurring minerals have been shown in bench-scale experiments to be capable of reducing HCl vapor levels to about 1 ppmv in simulated coal gas streams.

## PROJECT DESCRIPTION

The current program aims to develop alkali-based disposable sorbents capable of reducing HCl vapor in high-temperature coal gas streams to less than 1 ppmv in the temperature range 400° to 750°C and the pressure range 1 to 20 atm. Investigating different processes for fabricating the sorbents, testing their suitability for different reactor configurations, and updating the economics of the process are the primary areas of focus of this program. This project is a collaborative effort between SRI, the prime contractor, and subcontractors Research Triangle Institute (RTI) and General Electric Corporate Research and Development (GE-CRD). RTI is developing and testing sorbents for fluidized-bed reactors, while GE-CRD is preparing sorbents for moving-bed reactors. SRI is preparing and testing sorbents for fixed-bed reactors.

The program is divided into the following six tasks: (1) information required for National Environmental Policy Act (NEPA), (2) sorbent preparation and characterization, (3) provision of bench-scale test unit, (4) bench-scale testing, (5) parametric testing, and (6) data analysis.

In the first-year of the project, several sorbent formulations were prepared for both fixed- and fluidized-bed applications [Krishnan et al., 1994]. Based on results of earlier studies, nahcolite, an abundantly available natural mineral, was selected as the primary choice for the sorbent material. About 600 kg of nahcolite powder, obtained by solution mining from deposits near Rifle,

Colorado, has been provided free of charge by NaTec Resources, Inc., Houston, Texas. Sorbent samples were prepared by pelletizing or granulating the powder with binders and texturizing agents, using pilot-scale equipment. Nahcolite sorbent pellets for use in fixed-bed reactors were extruded in sizes varying from 1.5 to 5 mm diameter and they contained either bentonite or sodium silicate as a binder. The physical properties such as surface area and pore volume of the pellets were not significantly affected by the type of binder used. Differential reactor experiments showed that the sorbent pellets and granules are capable of absorbing large quantities of HCl vapor. The spent sorbents contained as high as 55 wt% chloride. These results were confirmed with integral, fixed- and fluidized-bed reactor experiments using simulated coal gas streams.

Two bench-scale stainless steel pressure vessels capable of operating up to 650°C and 20 atm were constructed. The system at SRI was used for fixed-bed reactor studies whereas the system at RTI was used for fluidized-bed experiments. The sorbents were contained in 5-cm ID quartz tubes inside the stainless steel vessels and non-corrosive components of simulated coal gas mixtures were passed through the annulus between the quartz tubes and the stainless steel vessel to minimize corrosion. HCl and H<sub>2</sub>S were added to this gas mixture inside the quartz tube, upstream of the sorbent bed. The pressure inside the reactor was controlled by a servo-controlled valve made of Hastelloy C metal. The gases leaving the reactor were cooled in a water-cooled heat exchanger made of glass. During cooling, the residual HCl vapor dissolved in the steam condensate and the chloride level in the condensate was determined using ion chromatography. The residual HCl vapor level was calculated from the condensate analysis and the procedure is capable of measuring sub-ppm levels of HCl vapor.

## RESULTS

### Fixed-Bed Reactor Studies

Fixed-bed reactor experiments showed that the pelletized nahcolite sorbents are capable of reducing HCl vapor level in simulated coal gas streams to less than 1 ppmv at 400°C (Figure 1). At a space velocity of 3000 h<sup>-1</sup>, the HCl vapor

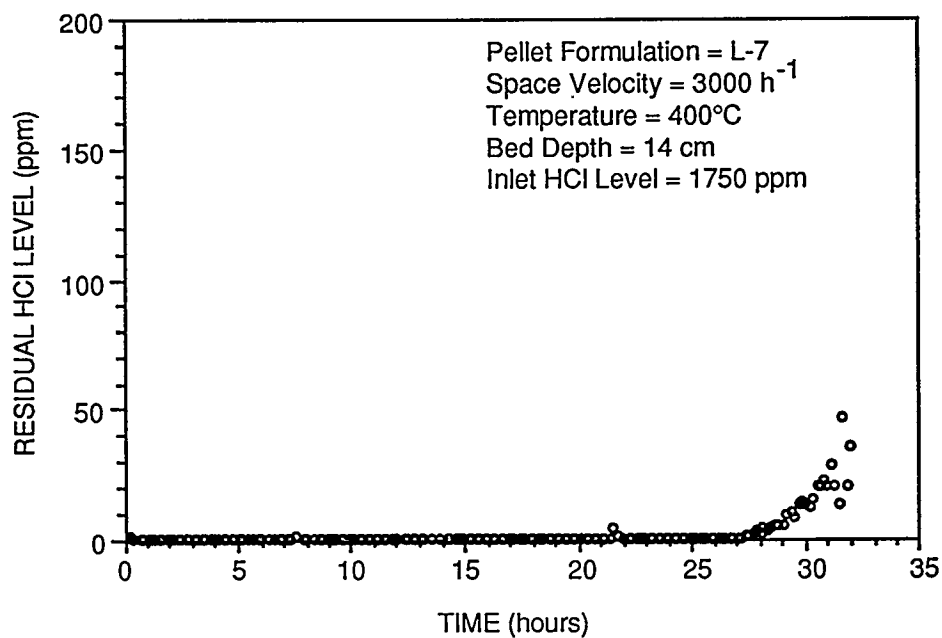


**Figure 1. The HCl Breakthrough Curve of Nahcolite Sorbent Pellets in a Fixed-Bed Reactor**

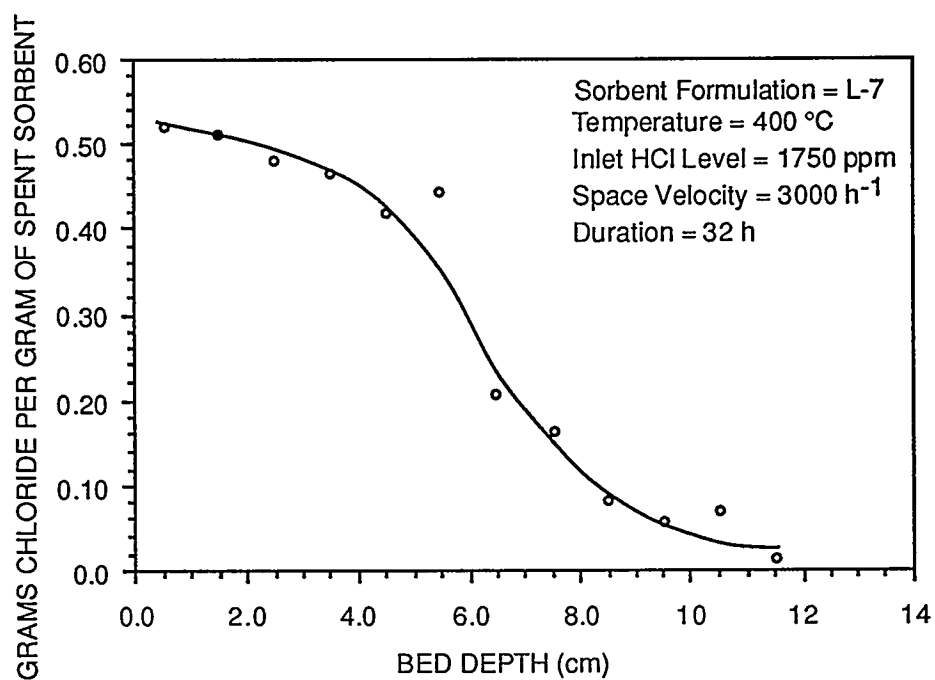


**Figure 2. Distribution of Chloride in the Nahcolite Sorbent Bed**

level was reduced from 1750 ppmv to less than 1 ppmv for nearly 25 h. The experiment was terminated when the residual HCl level reached 50 ppmv. At the end of the experiment, the chloride level in the sorbent pellets was determined as a function of the bed depth. The results showed that the upstream end of the bed was nearly saturated with chloride whereas chloride absorption was beginning to occur at the downstream end of the bed (Figure 2). Similar results were observed at 500° and 600°C.

The kinetics of HCl absorption by a fixed bed of sorbent can be ascertained from the distribution of chloride along the axis of the bed after a period of exposure, or by the rise in outlet HCl concentration with time as breakthrough is reached. A gradual HCl breakthrough and gently sloping profiles of absorbed Cl imply slow absorption kinetics, while a rapid HCl breakthrough and sharp absorbed Cl profiles imply rapid absorption rates. To determine rate constants from integral reactor data, it is necessary to define the rate laws with respect to local HCl concentration and local extent of sorbent conversion. For the present analysis, it is assumed that the rate is proportional to the partial pressure of HCl ( $P_{HCl}$ ) and the local unconverted fraction of sorbent ( $1-X$ ), where  $X = S/S_0$ , the fractional conversion of sorbent.  $S$  and  $S_0$  are the local amount of chloride sorbed and the maximum capacity of the sorbent, respectively, in mol Cl per g sorbent. Thus, the local rate of HCl absorption and NaCl formation can be approximated by equation (1):

Rate ( $z$ ) =

$$\left( \frac{U_0}{RT_0} \right) \frac{dP_{HCl}}{dz} = M_{Cl}^{-1} \rho_s S_0 \frac{dX}{dt} = k P_{HCl} (1-X) \rho_s$$

Equation (1)

$U_0$  = superficial gas velocity  
 $P_0$  = Total Pressure  
 $T_0$  = Temperature  
 $z$  = depth into the bed  
 $\rho_s$  = bed density  
 $M_{Cl}$  = molecular weight of chlorine  
 $P_{HCl}$  = partial pressure of HCl at  $z$   
 $X$  = fractional conversion of sorbent at  $z$   
 $k$  = First order rate constant

If  $Y_{HCl}$  is defined as  $P_{HCl}/P_0$  and equation 1 is solved, equation (2) is obtained:

$$Y_{HCl}(z, t) = Y_0 \left[ \frac{\exp\left(\frac{kP_0 Y_0 t}{S_0 M_{Cl}^{-1}}\right)}{\exp\left(\frac{kP_0 Y_0 t}{S_0 M_{Cl}^{-1}}\right) + \exp\left(\frac{k\rho_s RT_0 z}{U_0}\right) - 1} \right]$$

Equation (2)

Similarly, the amount of chloride absorbed by the solid at a distance  $z$  from the upstream end of the bed and time  $t$  is given by equation (3):

$$S(z, t) = \frac{S_0 \exp(kP_0 Y_0 t / S_0 M_{Cl}^{-1})}{\exp(kP_0 Y_0 t / S_0 M_{Cl}^{-1}) + \exp(k\rho_s RT_0 z / U_0) - 1}$$

Equation (3)

where  $Y_0$  is the inlet concentration of HCl.

By integrating the expression for  $S$  over discrete intervals of bed depth, i.e.,  $\{\ell_i, \Delta\ell_i\}$ , equation (4) is developed:

$$S_i(t) = S_0 - \frac{S_0}{\lambda \Delta\ell_i} \ln \left[ \frac{\exp(\lambda \ell_i) + \exp(\alpha t) - 1}{\exp(\lambda \ell_{i-1}) + \exp(\alpha t) - 1} \right]$$

Equation (4)

$\lambda = k\rho_s RT_0/U_0$  (cm<sup>-1</sup>)  
 $\alpha = kP_0 Y_0/S_0 M_{Cl}^{-1}$  (h<sup>-1</sup>)  
 $\Delta\ell_i$  = bed depth interval (cm)

Equation (4) for  $S_i(t)$  is very similar to equation (3) for  $S(z_i, t)$  with the substitution,  $z_i = (\ell_i + \ell_{i-1})/2$ . Non-linear regression analysis can be used to fit measured values of  $Y_{HCl}(L, t)$  and  $\{S_i(t_f)\}$  where  $L$  is the total bed depth and  $t_f$  is the total elapsed time of the integral fixed-bed isothermal absorption reactor experiments. A two parameter fit to the HCl breakthrough data for  $Y_{HCl}(L, t)$  gives  $\alpha$  and  $(\lambda L)$  while a three parameter fit to the measured chloride content of bed segments gives  $\lambda$ ,  $(\alpha t_f)$ , and  $S_0$ .

The rate constants measured for the nahcolite pellets show little variation with temperature over the range from 400° to 600°C (Table 1). The effectiveness factor for HCl absorption can be estimated as essentially unity, given the measured pore volume distribution before and after chloride

absorption (discussed below). The low apparent activation energy for absorption suggests that gas phase diffusion of HCl, not the chemical reaction or solid-state diffusion of Cl through a NaCl film, governs the absorption rate.

**Table 1. HCl Absorption Rate Constants For Nahcolite Sorbents**

Data Set for Curve-Fit	T (°C)	$\alpha$ (h <sup>-1</sup> )	$\lambda$ (cm <sup>-1</sup> )	$S_o$ (g <sub>Cl</sub> /g <sub>s</sub> )	k (mol <sub>HCl</sub> ·atm <sup>-1</sup> ·g <sup>-1</sup> ·h <sup>-1</sup> )
S <sub>i</sub>	400	0.21	0.61	0.58	2.6
Y <sub>HCl</sub>	400	0.55	1.48	—	5.2
S <sub>i</sub>	500	0.33	1.13	0.58	4.1
S <sub>i</sub>	600	0.13	0.60	0.51	2.2
Y <sub>HCl</sub>	600	0.39	1.08	—	3.7

Conditions:  $Y_o = 1750$  ppmv;  $U_o = 13.3$  cm/s;  $T_o = 298$  K;  $\rho_s = 0.54$  g<sub>Cl</sub>/g<sub>s</sub>;  $t_f = 30.0$  h (400°C), 13.0 h (500°C), 30.6 h (600°C);  $z_L = 14.0$  cm;  $P_o = 1.0$  atm.

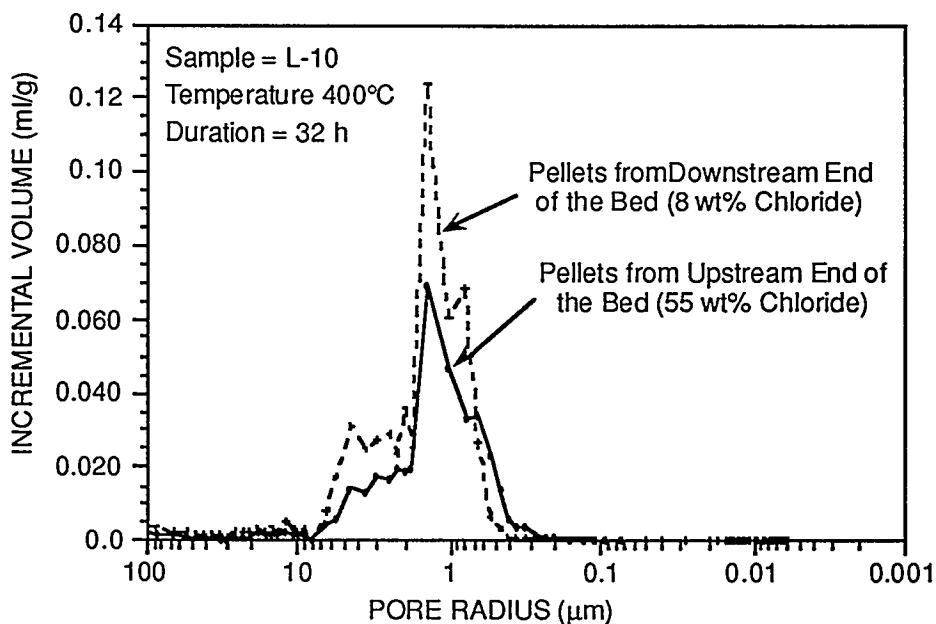


**Figure 3. Pore Size Distribution of Nahcolite Sorbent Pellets**

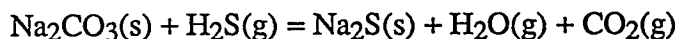
Nahcolite ( $\text{NaHCO}_3$ ) decomposes at temperatures above  $200^\circ\text{C}$  to form  $\text{Na}_2\text{CO}_3$  and  $\text{CO}_2$ :



In the presence of  $\text{HCl}$  vapor, the  $\text{Na}_2\text{CO}_3$  is converted to  $\text{NaCl}$ :



The reaction rate will be hindered if the product  $\text{NaCl}$  obstructs the pores inside the sorbent, reducing the passage of gas molecules. However, mercury porosimetry showed that the pore size distribution is not altered significantly during chlorination of the sorbent (Figure 3). Experiments were also carried out to determine the sorption of  $\text{H}_2\text{S}$  by the nahcolite sorbent according to the following reaction:



A simulated coal gas containing 1700 ppmv  $\text{HCl}$  and 3000 ppmv  $\text{H}_2\text{S}$  was passed through the nahcolite sorbent pellets at  $400^\circ$  and  $600^\circ\text{C}$ . At both temperatures the residual  $\text{HCl}$  level was less than 1 ppmv initially and no significant change in the 1-ppmv breakthrough time was observed. At the end of the runs, the sorbent pellets were analyzed for their chloride and sulfide contents (Table 2). At  $400^\circ\text{C}$ , the absorption of  $\text{H}_2\text{S}$  by the sorbent was negligibly small. The amount of sulfide retained on the sorbent was higher at  $600^\circ\text{C}$  than at  $400^\circ\text{C}$ , but even at  $600^\circ\text{C}$  less than 1% of the total  $\text{H}_2\text{S}$  in the gas phase was absorbed on the pellets. The above results indicate that presence of  $\text{H}_2\text{S}$  does not have a significant impact on the  $\text{HCl}$  removal performance of nahcolite pellets.

**Table 2. Chloride And Sulfide Content Of Spent Nahcolite Pellets**

Temperature ( $^\circ\text{C}$ )	Location	Chloride Level (wt%)	Sulfide Level (wt%)
400	Upstream end	58.0	0.08
400	Downstream end	3.20	0.01
600	Upstream end	50.5	0.57
600	Downstream end	0.57	0.15

Fixed-bed reactor experiments indicated no significant differences in the  $\text{HCl}$  reactivity between pellets made with sodium silicate and bentonite binders. The maximum chloride capacity of the pellets with sodium silicate binder was 10% higher than that of the pellets with bentonite binder, but the rate of initial reaction did not depend strongly on the nature of the binder. Pellets containing sodium silicate binder agglomerated when the reaction temperature was higher than  $500^\circ\text{C}$ . No such agglomeration was observed when bentonite was used as the binder. The crush

strength of the pellets did not change significantly with the extent of chlorination.

### Fluidized-Bed Reactor Experiments

Nahcolite granules (NS-01) suitable for fluidized-bed reactor applications were prepared by slurring the powder in water with 10 wt% kaolinite and 5 wt% bentonite as binders and spray-drying the slurry to obtain granules in the size range 40 to  $120\ \mu\text{m}$ . The fluidization characteristics of this sorbent was found to be excellent as shown in Figure 4.

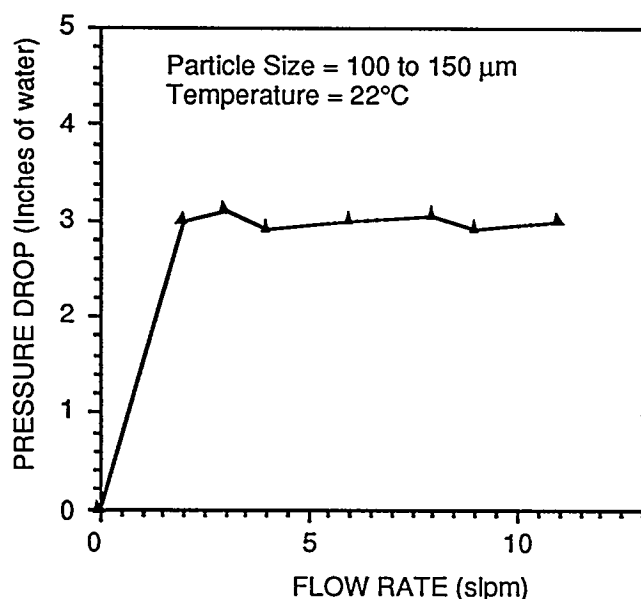


**Figure 4. Fluidization Behavior of NS-01 Sorbent**

In this cold-flow experiment, the pressure drop increased linearly with increasing gas velocity initially and then remained nearly constant over a wide range of gas velocities. This behavior indicated that the spray-dried sorbent could be fluidized easily.

A fluidized-bed sorbent is likely to be fed into the reactor from a hopper using a screw feeder or other feeding device. The angle of repose gives an indication of the flowability of the powder. The flowability is considered to be excellent if the angle of repose is less than 30° and is poor if the angle is more than 45°. The angle of repose measured for NS-01 in the size range 90 to 150 μm was 34° indicating that the powder will flow smoothly.

The attrition resistance of this material was also tested using a standard 3-hole air-jet attrition tester. The NS-01 formulation exhibited a higher attrition resistance than the raw nahcolite powder and a commercial FCC catalyst (Table 3).

The reactivity of the spray-dried sorbent was initially determined in a thermogravimetric apparatus. The HCl absorption of NS-01 sorbent was superior to that of the raw nahcolite powder and commercially available grade #2 baking soda (Figure 5).

**Table 3. Attrition Resistance of Nahcolite Sorbents**

Sorbent	5-h Loss (wt%)	20-h Loss (wt%)
Raw Powder	12.8	37.6
Grade #2 Baking Soda	4.4	13.2
NS-01	5.4	5.8
FCC Catalyst	16.0	14.2

The rate constant and chloride capacity of the spray-dried sorbent (45 to 90 μm in size) were determined as a function of temperature using a gas stream containing 2.1% HCl flowing at less than the minimum fluidization velocity. The rate constants at 450°, 550°, and 650°C were found to be 0.2, 3.0, and 3.0 mole gas·atm<sup>-1</sup>·g<sup>-1</sup>·h<sup>-1</sup> respectively. These values are comparable to those found with 3-mm sorbent pellets. However, the rate constant calculated for the raw nahcolite powder under similar conditions was about 5 times lower than that for the spray-dried sorbent. The chloride capacities of the NS-01 sorbent at 1-ppmv breakthrough time were 32.4, 51.2, and 52.7 wt% respectively at 450°, 550°, and 650°C. The capacities at 550° and 650°C represent near complete utilization of the sorbent.

The high reactivity of the spray-dried sorbent was also confirmed in tests conducted in a 2.5-cm ID fluidized-bed reactor. A series of experiments were conducted with three different nahcolite formulations at 550°C with simulated Texaco coal gas containing 12.5% v/v steam and 1750 ppmv of HCl vapor. The superficial gas velocity was 3.2 times that of the minimum fluidization velocity. As shown in Figure 6, the spray-dried (NS-02) sorbent had the best overall breakthrough performance among these three formulations. The N-01 formulation is a raw powder without any further processing while N-23 was prepared using a granulation technique. The chloride capture capacity of these sorbents were 26.8 (NS-02), 21.0 (N-23) and 9.8 (N-01) wt.% at 1-ppm breakthrough time.

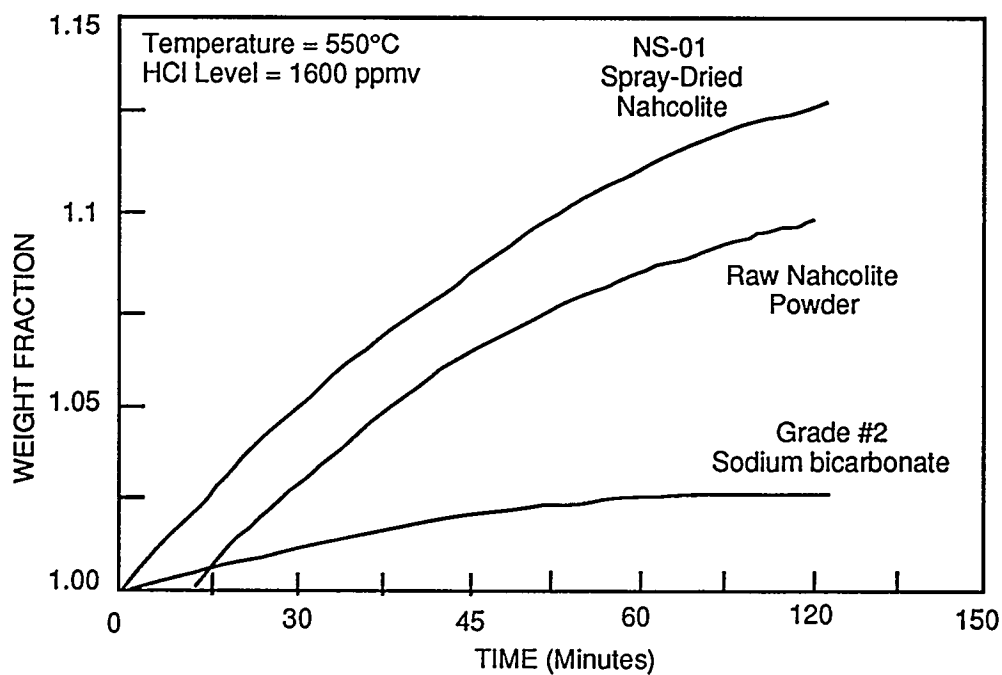


Figure 5. The HCl Reactivity of Various Fluidized-Bed Sorbents

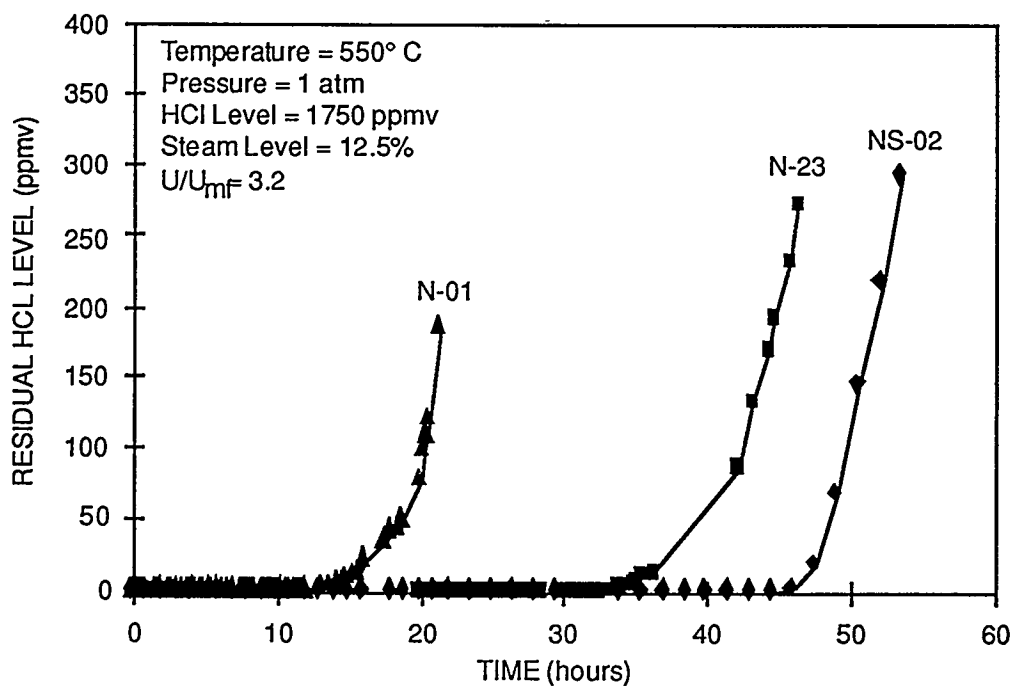


Figure 6. The HCl-Breakthrough Curves for Various Nahcolite Sorbents in a Bubbling Fluidized Reactor

At low fluidization velocities ( $u/u_{mf}=3$ ), especially at elevated pressures, some amount of caking of the NS-01 sorbent was observed. But the cake was not mechanically strong and it was broken easily. The caking problem may be less severe at high gas velocities.

The effect of steam level in the coal gas was also evaluated in the fluidized-bed reactor experiments. The initial residual HCl level was

< 1 ppmv in experiments conducted at 480°C with a simulated coal gas containing 13 or 26% v/v steam. The 1-ppmv breakthrough occurred at the same time in both cases (Figure 7). But the breakthrough profile was sharp at the high steam level compared with the case for low steam level. In the gas containing 13% v/v steam, the residual HCl level remained at about 3 ppmv for an additional 300 minutes, after which it increased sharply.

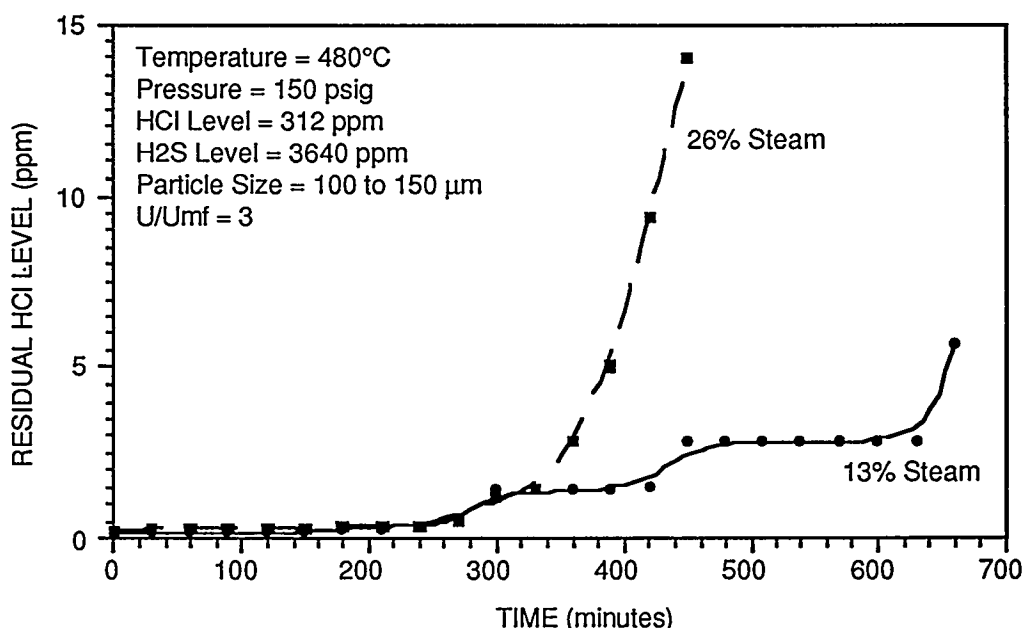


Figure 7. The HCl-Breakthrough Curve in a Fluidized-Bed Reactor in simulated coal gases containing two different steam levels

A limited number of fluidized-bed reactor tests were also conducted with a Grade #2 baking soda in the size range 90 to 150  $\mu\text{m}$ . After calcination at 550°C, the surface area of this powder was less than 0.1  $\text{m}^2/\text{g}$ . In a fluidized bed reactor test at 550°C and 1 atm pressure, severe caking of the powder was encountered which prevented an accurate determination of the rate of HCl uptake.

#### Circulating Fluidization Bed Reactor Test

The HCl vapor removal capability of the spray-dried sorbent was determined at a fixed-bed

gasifier facility located at the General Electric Corporate Research and Development site. During this 100 h test, conducted at about 500°C and 280 psig, the HCl level in the hot coal gas was estimated to be about 580 ppmv. During the first 95 h of testing, a grade #2 baking soda was fed into a circulating fluidized-bed (CFB) reactor. Although the residual HCl level was in the range 50 to 150 ppmv initially, it decreased to less than 15 ppmv as the inventory of the sorbent accumulated. During the last 5 h, the spray-dried nahcolite sorbent (NS-02) was fed into the reactor and the residual HCl level remained at a level less than



15 ppmv. The NS-02 sorbent was fed into the reactor using a screw feeder with out any problem. The material withdrawn from the CFB cyclone contained mainly the spent sorbent and a small amount of fly ash (1.5 wt%).

The chemical analysis of the spent NS-02 sorbent showed that its sodium and chloride contents are about 33.5 and 37.6 wt% respectively. Material balance calculations indicated that the sorbent utilization was about 71%. This pilot-scale test demonstrates that nahcolite sorbent is efficient in reducing the HCl vapor level to very low values in actual coal gasifier conditions.

## FUTURE WORK

Future activities in the program include parametric testing of nahcolite sorbents by varying space velocity (2,000 to 5,000 h<sup>-1</sup>), temperature (400° to 650°C), and pressure (1 to 20 atm). The experimental data will be analyzed to determine the effectiveness of the various sorbent formulations for removal of hydrogen chloride vapor using various types of reactors. A preliminary economic assessment is planned to determine the suitability of the sorbents for removing HCl vapor from hot coal-derived gas streams on an industrial scale.

## REFERENCES

- Bakker, W.T., and R.A. Perkins (1991). "The Effect of Coal Bound Chlorine on Corrosion of Coal Gasification Plant." In *Proceedings of International Conference on Chlorine in Coal*, J. Stringer and D.D. Banerjee, Eds., Elsevier.
- Gal, E., A. Najewicz, A. H. Furman, R. Ayala, and A. Feitelberg (1994). Integrated Operation of a Pressurized Gasifier, Hot Gas Desulfurization System and Turbine Simulator, *In Proceedings of the Coal-fired Power Systems 94 - Advances in IGCC and PFBC Review Meeting*, H. McDaniel, R. K. Staubly, and V. Venkataraman, Eds., Report No.: DOE/METC-94/1008, Morgantown Energy Technology Center, U.S. Department of Energy, Morgantown, WV.
- Kinoshita, K., F. R. McLarnon and E. J. Cairns (1988). *Fuel Cells: A Handbook*, Report No. DOE/METC-88/6096, Morgantown Energy Technology Center, U.S. Department of Energy, Morgantown, WV.
- Krishnan, G.N., G.T. Tong, B.J. Wood, and N. Korens (1986). "High-Temperature Coal-Gas Chloride Cleanup for MCFC Applications." Report No. DOE/MC/21167-2080, Morgantown Energy Technology Center, U.S. Department of Energy, Morgantown, WV.
- Krishnan, G. N., B. J. Wood, A. Canizales, R. Gupta, S. D. Sheluker, and R. Ayala (1994). "Development of Disposable Sorbents for Chloride Removal from High-Temperature Coal-Derived Gases." *In Proceedings of the Coal-fired Power Systems 94 - Advances in IGCC and PFBC Review Meeting*, H. McDaniel, R. K. Staubly, and V. Venkataraman, Eds., Report No.: DOE/METC-94/1008, Morgantown Energy Technology Center, U.S. Department of Energy, Morgantown, WV.
- Perkins, R.A., D.L. Marsh, and P.R. Clark (1990). "Corrosion in Syngas Coolers of Entrained Slagging Gasifiers." Report No. EPRI GS-6971, Electric Power Research Institute, Palo Alto, CA.
- Pigeaud, A. and G. Wilemski (1992). "Effects of Coal-Derived Trace Species on the Performance of Carbonate Fuel Cells." *In Proceedings of the Fourth Annual Fuel Cells Contractors Review Meeting*, W. J. Huber, Ed., Report No.: DOE/METC-92/6127, Morgantown Energy Technology Center, U.S. Department of Energy, Morgantown, WV.
- TRW (1981). "Monitoring Contaminants in Coal Derived Gas for Molten Carbonate Fuel Cells," Final Report to Argonne National Laboratory under contract No. 31-109-38-6108.

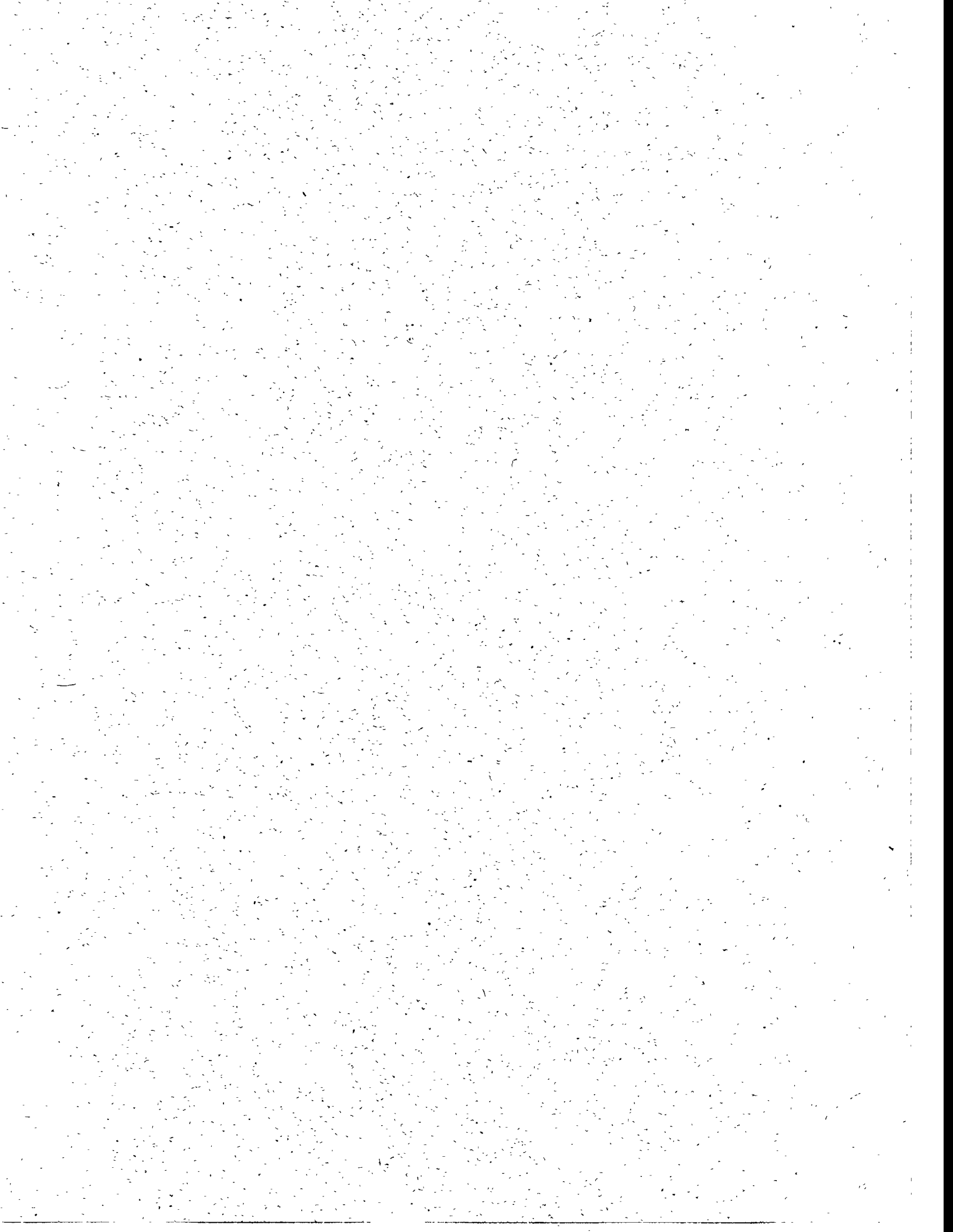


---

## Session 7B

### *Separation Technologies*

---



## 7B.1

# Advanced Metal-Membrane Technology - Commercialization

### CONTRACT INFORMATION

<b>Contract No.</b>	DE-FG03-91ER81229
<b>Contractor</b>	Bend Research, Inc. 64550 Research Road Bend, OR 97701-8599 (503) 382-4100
<b>Other Funding Sources</b>	Teledyne Wah Chang Ballard Power Systems
<b>Contract Project Manager</b>	David J. Edlund
<b>Principal Investigator</b>	David J. Edlund
<b>METC Project Manager</b>	Venkat K. Venkataraman
<b>Period of Performance</b>	March 31, 1992, to March 30, 1995

### ABSTRACT

The gasification of coal offers a potentially significant source of hydrogen for use in clean power generation and as a primary chemical feedstock. However, hydrogen derived from coal continues to be more expensive than hydrogen derived from natural gas or petroleum, due in large part to the expense of separating hydrogen from the mixture of gases produced during gasification. At Bend Research, we have been developing a novel hydrogen-permeable metal membrane that promises to be economical for hydrogen separation and purification, including the purification of hydrogen derived from gasifying coal. Furthermore, the membrane is ideally suited for use at high temperatures (200° to 500°C), making it feasible to produce pure hydrogen directly from hot gas streams.

Through a partnership with Teledyne Wah Chang, we are proceeding with scale-up of prototype membrane modules and field tests to demonstrate the technology to potential users. Additionally, we are working with potential customers to estimate capital savings and operating costs for integrated systems.

In this paper, we present some of the operating characteristics of the metal membrane, including its use to drive equilibrium-limited reactions toward complete conversion (e.g., the water-gas-shift reaction). We also describe our activities for commercializing this technology for a variety of applications.

## **7B.2 Separation of Hydrogen Using Thin Film Palladium-Ceramic Composite Membrane**

### **CONTRACT INFORMATION**

<b>Contract Number</b>	DE-FG22-93MT93008
<b>Contractor</b>	North Carolina A&T State University Office of Research Administration Suite 305, Dowdy Administration Building Greensboro, NC 27411 (910) 334-7995
<b>Contractor Project Manager</b>	Shamsuddin Ilias
<b>Principal Investigators</b>	Shamsuddin Ilias Franklin G. King Nan Su Uduak I. Udo-Aka
<b>METC Project Manager</b>	Venkat K. Venkataraman
<b>Period of Performance</b>	September 01, 1993 to August 31, 1996

---

### **OBJECTIVES**

The primary objective of this study was to prepare and characterize a hydrogen permselective palladium-ceramic composite membrane for high temperature gas separations and catalytic membrane reactors. Electroless plating method was used as a potential route to deposit a thin palladium film on microporous ceramic substrate. The objectives of the work presented here were to characterize the new Pd-ceramic composite membrane by SEM and EDX analysis and to carry out fundamental permeability measurements of the membrane at elevated temperatures and pressures.

### **BACKGROUND INFORMATION**

From environmental and energy considerations, it is generally recognized that membrane separation processes could become wide spread in industrial applications. In recent years, considerable attention has focused on combining the unit operations of separation and reaction to provide purer products by shifting of thermodynamic equilibria [1-3]. The use of membranes to remove products from the reaction zone has obvious industrial interest since it provides lower reaction temperatures, smaller reactors, and reduced downstream separation costs.

The potential application of membranes in high temperature gas separation and reactor technology have been recognized by many investigators. For example, in the coal gasification process, the exit gases are normally hydrogen, carbon monoxide, carbon dioxide, hydrogen sulfide, and water vapor. The objective is to obtain hydrogen from this gas mixture. Currently, it is uneconomical to recover hydrogen because no suitable recovery method exists that can be implemented at high temperatures and pressures. This process' economics is improved if hydrogen can be recovered at a lower cost.

Many heterogeneous catalytic reactions can not reach high conversions because of the limits imposed by the reaction equilibrium. For example, the dehydrogenation reaction of cyclohexane, catalyzed with platinum/alumina at 215°C in a conventional reactor, is limited to 33% conversion [3]. If, however, the product hydrogen is continuously removed from the reaction mixture through an inorganic membrane, the equilibrium is displaced towards the product side and the conversion has been shown to increase to nearly 80%. Since, this reaction is favored by an increase in temperature, it can also be said that the temperature needed for desired conversion can be lowered. This principle can be applied to several other industrially significant reactions. The efficiency of the process depends on the effectiveness of hydrogen removal. Hence, the conversion of reactants can be enhanced dramatically if a method can be developed for recovering hydrogen at higher temperatures.

Recently, there has been increased interest in developing inorganic and composite membranes for in-situ separation of product hydrogen to achieve equilibrium shift in catalytic reactor [4-7]. However, the

productivity of these membrane reactors are severely limited by the poor permeability of currently available membranes. Commercially available non-porous membranes are either thick film or thick walled tubes. Since, permeability is inversely proportional to film thickness, a thick film membrane acts as a poor permseparator. Thus, a major challenge lies in developing a permselective thin film, without compromising the integrity of the film. The success of membranes in these applications will largely depend on the availability of membranes with acceptable permselectivity and thermal stability [5]. The availability of such a membrane for high temperature application could open new areas of research in membrane reactor technology and gas separation.

The development of a process for producing ultra-thin, defect-free composite membranes is important. If such a process is to be developed in a generally applicable form for use with most advanced materials, a high-productivity, high-selectivity coating must be applied on an inexpensive support. To develop a new class of permselective inorganic membranes, we have used electroless plating to deposit a palladium thin-film on a microporous ceramic substrate [8]. Electroless plating is a controlled autocatalytic deposition of continuous film on the surface of a substrate by the interactions of a metal salt and a chemical reducing agent. This method can be used to make thin films of metals, alloys and composites on both conducting and nonconducting surfaces.

## PROJECT DESCRIPTION

### Electroless Plating of Ceramic Substrate

Microporous ceramic alumina

membranes ( $\alpha$ -alumina,  $\phi$  39 mm  $\times$  2 mm thickness, nominal pore size 150 nm and open porosity  $\approx$  42%) were coated with a thin palladium film by electroless plating. Electroless plating is explained by a combination of the cathodic deposition of metal and the anodic oxidation of reductant at the immersion potential.

Electroless plating is a three step process involving pretreatment of the substrate, sensitization and activation of the substrate surface, and electroless plating. The procedure developed in this work for electroless deposition of palladium thin film on microporous ceramic substrate has been reported elsewhere [8].

### Membrane Characterization

The characterization of the membrane included the physical property study as well as the diffusion measurements. The membranes were studied by taking SEM micrograph, EDX analysis and measuring the thickness of the coated film. A steady state counter diffusion method, using gas chromatographic analysis, was used to evaluate the permeability and selectivity of the composite palladium membrane for hydrogen separation. A schematic of the permeability measurement system is shown in Figure 1.

## RESULTS

In this work, thin-film Pd-ceramic composite membrane was developed by electroless deposition of palladium on planar ceramic substrate. The new membrane was characterized and evaluated for hydrogen separation at high temperatures.

The composition of the palladium-ceramic composite membrane surface was

evaluated by EDX analysis. The EDX analysis of the membrane specimen is shown in Figure 2. The analysis showed that the palladium film deposited on the ceramic substrate is highly pure. The film thickness was estimated by weight gain method.

In Figure 3, the SEM micrographs of a composite membrane specimen are shown for the ceramic substrate, sensitized and activated substrate surface and the electroless deposited palladium film on ceramic substrate. From SEM micrographs, no significant surface modifications were observed after the substrate was activated and sensitized. The pore size remained more or less the same. However, after the coating, the surface structure changed dramatically. Pores were fully covered by solid palladium film and no pin holes were detected.

Steady state method was used to measure the effective diffusivity of hydrogen through the ceramic substrate. Experiments were conducted at an operating pressure of 5 psig with zero transmembrane pressure and temperatures ranging from 28°C to 225°C. Figure 4 suggests that the relationship between diffusivity and temperature can be correlated as following:

$$D_e = D_{\infty} \exp\left(\frac{-E_D}{RT}\right) \quad (1)$$

where  $R$  is the universal gas constant ( $J \cdot \text{mole}^{-1} \cdot K^{-1}$ ),  $T$  is the absolute temperature (K),  $D_{\infty}$  is the pre-exponential factor in the Arrhenius relationship for hydrogen diffusivity ( $\text{cm}^2 \cdot \text{sec}^{-1}$ ) and  $E_D$  is the apparent diffusivity activation energy of the substrate ( $J \cdot \text{mole}^{-1}$ ). The effective diffusion coefficient,  $D_e$ , at other temperatures can be calculated using the



above equation once the  $D_{\infty}$  and  $-E_D/R$  are known from the linear plot of Figure 4.

Effect of temperatures at various transmembrane pressure drop on hydrogen transport through the substrate was also investigated in this work. For a porous membrane, one would expect the flux to obey the following relationship with  $n=1$ :

$$N_{H_2} = \frac{D_e}{RT} \left( \frac{(P_{H_2})_{H_2}^n - (P_{H_2})_{Ar}^n}{d} \right) \quad (2)$$

For the experimental hydrogen flux data, the value of  $n$  was estimated by using the Marquardt-Levenberg non-linear least square analysis and was found to be 1.0003. A value of  $n$  equal to 1 implies that the transport of hydrogen through the substrate is not solubility dependent. Given the experimental uncertainty, it will be fair to say that in our case the transport of hydrogen through the substrate is solubility independent and  $n$  is taken as 1. With increasing pressure drop at a given temperature, the hydrogen flux through the substrate is seen to increase. However, with increasing temperature, the flux was observed to decrease. The results are shown in Figure 5.

Two thin-film palladium-ceramic membrane specimens were fabricated by electroless deposition method as discussed in the previous section. By weight-gain method, the palladium film thicknesses were estimated to be 8.5  $\mu\text{m}$  and 12  $\mu\text{m}$ . The permeability experiments were conducted at temperatures of 373K, 473K and 573K. The pressure on the high pressure side ranged from 10 psig to 20 psig and the low pressure side was maintained at 5 psig in all permeability measurement experiments.

The hydrogen flux through metallic dense film may be described by [9]:

$$N_{H_2} = \frac{P_H}{h} [(P_{H_2})_{H_2}^n - (P_{H_2})_{Ar}^n] \quad (3)$$

where  $P_H$  is the permeability coefficient and  $h$  is film thickness. When diffusion through the bulk metal is the rate limiting step, and hydrogen atoms form ideal solution in the metal, then according to Sievert's law hydrogen solubility dependence  $n$  equals to 0.5. However, a value of  $n$  greater than 0.5 may result when surface processes influence the permeation rate or when the Sievert's law is not followed.

Based on Eqn. (3), the hydrogen flux data were analyzed to estimate the value of  $n$  by using the Marquardt-Levenberg non-linear least square method. For the 8.5  $\mu\text{m}$  and 12  $\mu\text{m}$  films, the average values of  $n$  were estimated as 0.778 and 0.5006, respectively. From this analysis, it appears that a palladium film of 12  $\mu\text{m}$  thickness approaches the limiting definition of dense Pd-film according to Sievert's law.

With average values of  $n$  equal to 0.778 and 0.5006 for 8.5  $\mu\text{m}$  and 12  $\mu\text{m}$  Pd-film composite membranes, the hydrogen fluxes are plotted against driving force  $((P_{H_2})_{H_2}^n - (P_{H_2})_{Ar}^n)$  in Figures 6 and 7, respectively. At a given temperature, the slope of the line provides value of  $P_H/h$ . Since the membrane film thickness is known, one may calculate the membrane permeability from the known slopes of the lines at various temperatures as shown in Figures 6 and 7. From these Figures, it can be seen that the hydrogen fluxes increase with increasing temperature at a given driving force  $((P_{H_2})_{H_2}^n - (P_{H_2})_{Ar}^n)$ . This flux behavior is exactly opposite to what we observed in the case of substrate

(Figure 5). This is not an unexpected results. It suggests that a substrate coated with a selective separating layer, the flux of the selective gas component can be increased by increasing the temperature. Therefore, the new membrane will be suitable for separation of hydrogen at high temperatures.

## FUTURE WORK

During the next fifteen months of the project, we plan to work on the following tasks:

- Evaluate the fabricated membrane for permeability and selectivity of hydrogen in presence of other gases such as argon, methane, nitrogen and carbon dioxide.
- Evaluate the economics of recovery of hydrogen from coal gasification process using the new thin film palladium-ceramic composite membrane.
- Extend this membrane development work to palladium-alloy ceramic composite membrane for hydrogen separation.

## ACKNOWLEDGEMENT

The authors wish to thank Drs. Carl Udovich, Gary P. Hagen and Vasu Kulkarni, Amoco Chemical Company - R&D Center, Naperville, for many of their invaluable suggestions and discussions.

## REFERENCES

1. Itoh, N., Xu, W-C., and Haraya, K., "Basic Experimental Study on Palladium Membrane Reactors," *J. Mem. Sci.*, **66**, 149 (1992).
2. Edmund, D.J., and Pledger, W.A., "Thermolysis of Hydrogen Sulfide in a Metal-Membrane Reactor," *J. Mem. Sci.*, **77**, 255 (1993).
3. Itoh N., and Govind R., "Development of a Novel Oxidative Palladium Membrane Reactor," *AIChE Symposium Series 268*, **85**, 10 (1989).
4. Sun, Y.M., and Khang, S.J., "Catalytic Membrane for Simultaneous Chemical Reaction and Separation Applied to a Dehydrogenation Reaction," *Ind. Chem. Eng. Res.*, **27**(7), 1136 (1988).
5. Itoh, N., "Development of a One-side Uniform Model for Palladium Membrane Reactors," *J. Chem. Eng. Japan*, **25**(3), 336 (1992).
6. Ohata, Y., Gondaira M., Kobayashi K., Fujimoto, Y., and Kuroda, K., "Study on the Performance of a Stream Reformer of Town Gas Equipped with Palladium Membranes," *1994 AIChE Annual Meeting*, San Francisco, Paper No. 76i (1994).
7. Ilias, S., and Govind, R., "Development of High Temperature Membrane for Membrane Reactor: an Overview," *AIChE Symposium Series 268*, **85**, 18 (1989).
8. Ilias, S., King, F.G., and Su, N., "Preparation and Characterization of Composite Membrane for High Temperature Gas Separation," *Proc. Coal-Fired Power Systems 94 - Advances in IGCC and PFBC Review Meeting*, Morgantown, WV, vol. II, pp. 721-26 (1994).
9. Uemiya, S., Sato, N., Ando, H., and Kikuchi, E., "The Water Gas Shift Reaction Assisted by a Palladium Membrane Reactor," *Ind. Eng. Chem. Res.*, **30**(3), 585-589 (1991).

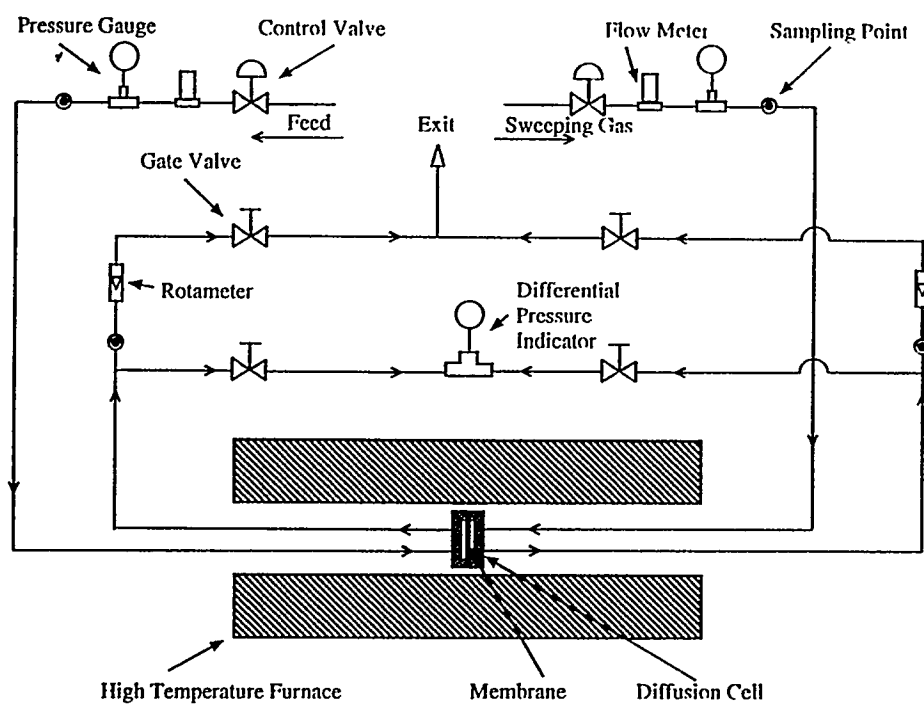


**Figure 1. Schematic of Permeability Measurement Setup**

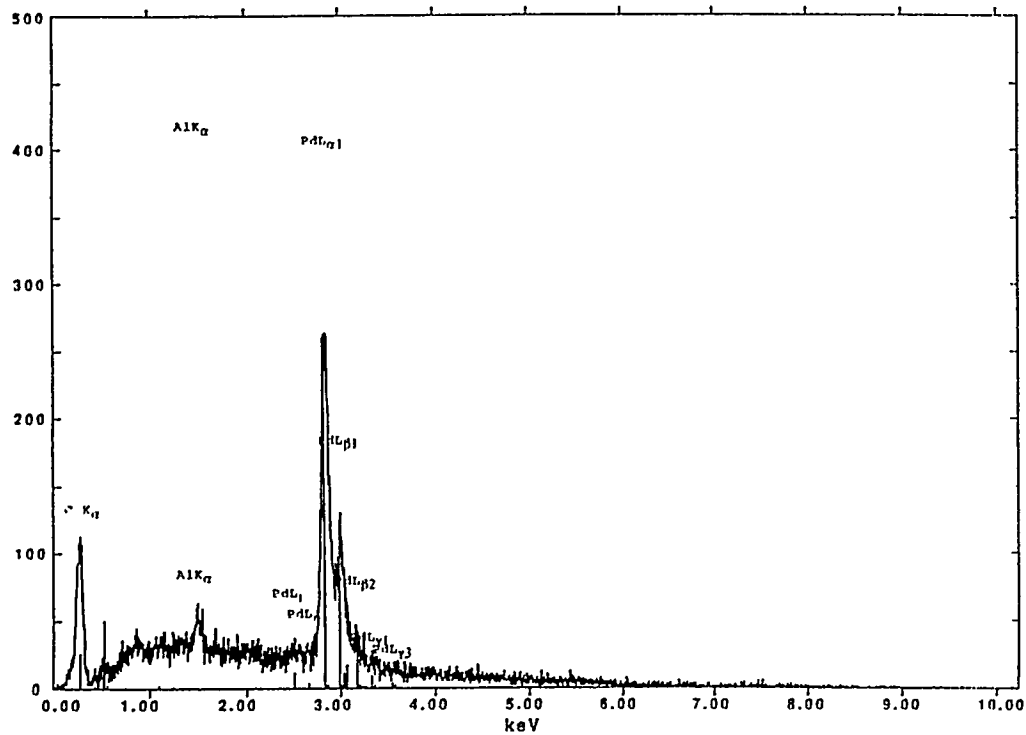
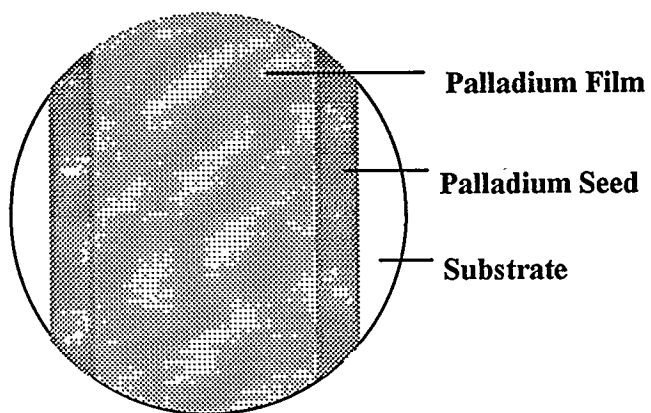
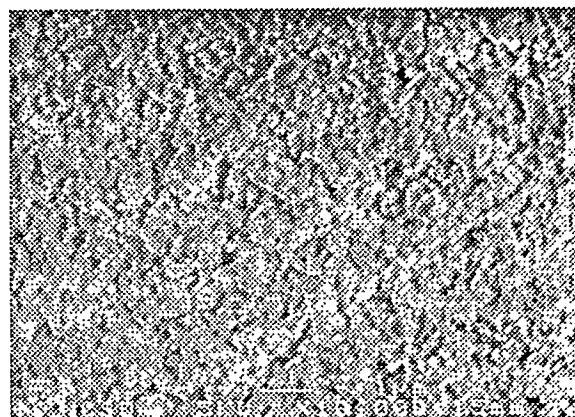


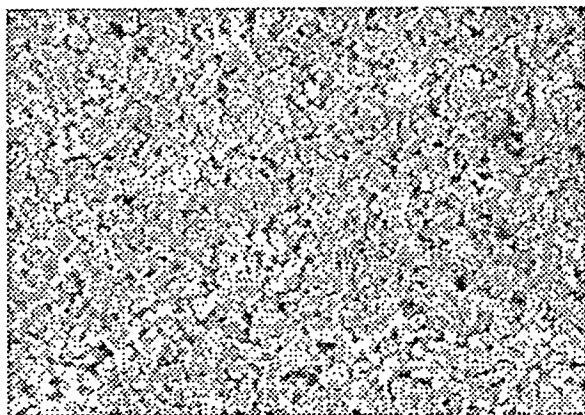
**Figure 2. EDX Analysis of Electroless Deposited Palladium Film on Ceramic Substrate**



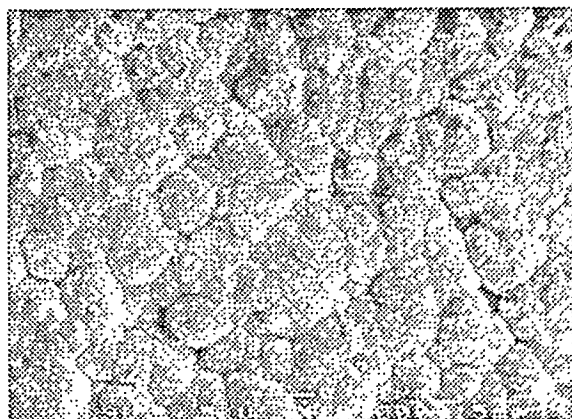
(a)



(b)



(c)



(d)

**Figure 3. SEM Micrographs of Palladium-Ceramic Composite Membrane: (a) Sample Specimen, (b) SEM of Substrate, (c) SEM of Sensitized and Activated Substrate Surface, and (d) SEM of Electroless Deposited Palladium Film on Ceramic Substrate**

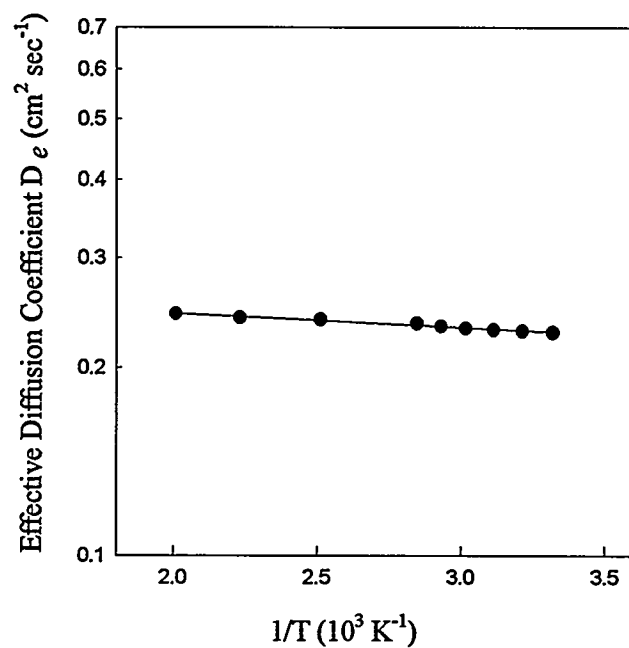


**Figure 4. Correlation of Effective Diffusivity of Hydrogen with Temperature for the Ceramic Substrate**

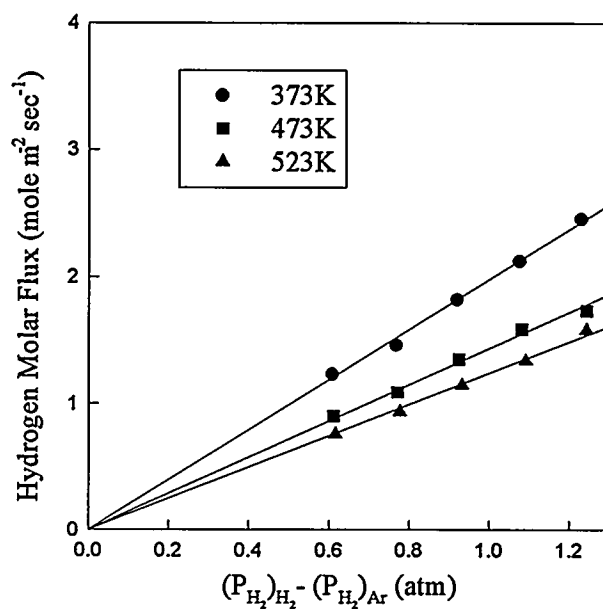


**Figure 5. Effect of Transmembrane Hydrogen Partial Pressure Difference on Fluxes at various Temperatures Through Ceramic Substrate**

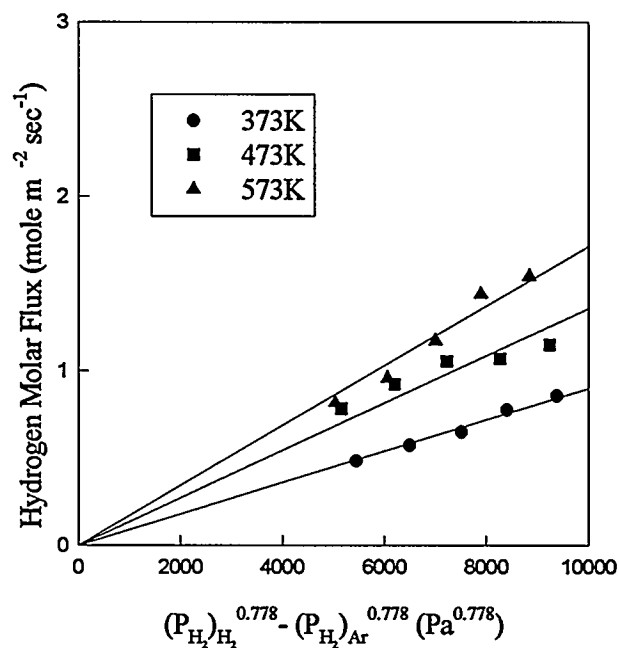


Figure 6. Effect of Driving Force  $((P_{H_2})_{H_2}^n - (P_{H_2})_{Ar}^n)$  on Fluxes at various Temperatures Through Palladium-Ceramic Composite Membrane with Film Thickness of 8.5  $\mu\text{m}$  ( $n=0.778$ )

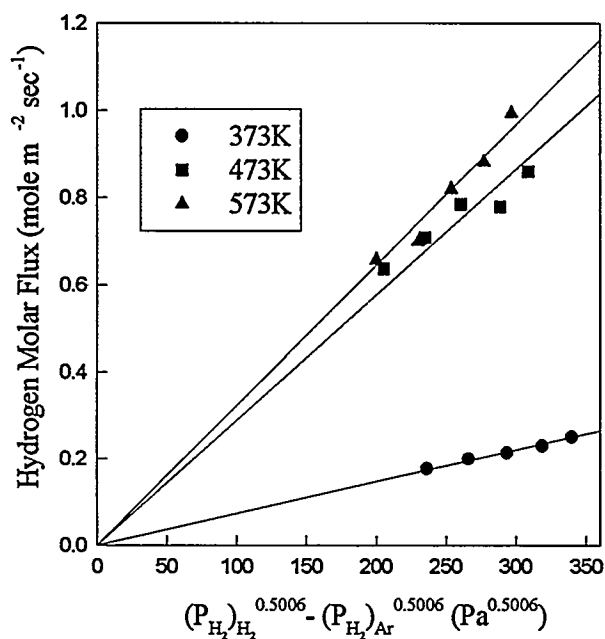


Figure 7. Effect of Driving Force  $((P_{H_2})_{H_2}^n - (P_{H_2})_{Ar}^n)$  on Fluxes at various Temperatures Through Palladium-Ceramic Composite Membrane with Film Thickness of 12  $\mu\text{m}$  ( $n=0.5006$ )

### 7B.3

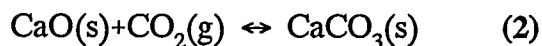
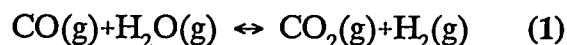
## A Calcium Oxide Sorbent Process for Bulk Separation of Carbon Dioxide

### CONTRACT INFORMATION

Contract Number	DE-AC21-89MC26366
Contractor	Louisiana State University Department of Chemical Engineering Baton Rouge, Louisiana 70803 (504) 388-1426 (telephone) (504) 388-1476 (telefax)
Contract Project Manager	Douglas P. Harrison
Principal Investigators	Douglas P. Harrison (LSU) Chun Han (LSU) George Lee (METC)
METC Project Manager	Venkat K. Venkataraman
Period of Performance	September 1989 to December 1994

### OBJECTIVES

This project began as an experimental investigation of the removal of CO<sub>2</sub> from coal-derived gas at moderate to high temperature using a calcium oxide sorbent. The project evolved into a study of the simultaneous water-gas shift reaction and CO<sub>2</sub> removal to prove the technical feasibility of an alternate process for the production of H<sub>2</sub> from coal-derived gas. The important stoichiometric reactions are:



Favorable results from the experimental tests prompted METC to undertake an Aspen simulation study to carry out the material and energy balance calculations on a conceptual process based upon the above chemistry. This paper summarizes the most relevant of the experimental data and the Aspen simulation results.

### BACKGROUND INFORMATION

Hydrogen is key raw material for many of the most important chemical products such as ammonia and methanol (Shreve and Brink, 1977). It is also becoming increasingly important in

petroleum refining as the rising demand for gasoline coupled with the use of heavier feedstocks result in increased reliance on the various hydropressing operations (Abrardo and Khurana, 1995). The majority of hydrogen is produced by the steam reforming or partial oxidation of gaseous or liquid hydrocarbons. In the future, coal gasification may become an important raw material for  $H_2$  manufacture. The primary products from steam reforming, partial oxidation, and coal gasification -  $CO$ ,  $CO_2$ ,  $H_2$  and  $H_2O$  - are the same.

Synthesis gas is normally upgraded to high purity hydrogen using the water-gas shift reaction followed by  $CO_2$  removal. Multiple catalytic reaction steps are required to achieve the required fractional conversion of  $CO$  and the maximum  $H_2$  production.  $CO_2$  removal is accomplished using wet scrubbing or pressure swing adsorption. Extensive heat exchange networks are required since various steps in the process operate at different temperature.

In contrast, the combined shift-carbonation process accomplishes shift reaction and  $CO_2$  separation in a single processing vessel. No shift catalyst is required because of the higher operating temperature, and heat exchange requirements are reduced because the alternate process operates under more nearly isothermal conditions.

## PROJECT DESCRIPTION

A laboratory-scale fixed-bed reactor having a capacity of 10 to 15 grams of calcium-based  $CO_2$  acceptor was used in the experimental study. Dolomite was found to be superior to limestone as a sorbent precursor and all experimental results and Aspen simulations presented in this paper are based upon dolomite. Gaseous feed components --  $CO$ ,  $CO_2$ ,  $H_2$ , and  $N_2$  -- were obtained from high pressure cylinders with flow rate controlled using high pressure mass flow controllers. Water was added using a high pressure syringe pump. The water was vaporized as it mixed with the

permanent gases by heat tracing the feed lines, and the combined feed was preheated to reaction temperature prior to contacting the sorbent. Reactor feed or product was sampled periodically and analyzed using gas chromatography. A complete description of the reactor and analytical system has been published (Harrison et al., 1993).

Reaction parameters studied included calcination and carbonation temperature and pressure, feed gas composition, reactor space velocity, and sorbent composition and properties. Only a brief summary of the most relevant experimental test results is presented in this paper; more detailed results are available elsewhere (Han and Harrison, 1994; Harrison and Han, 1994; Harrison, et al. 1994).

The final phases of the experimental study were carried out concurrently with the Aspen simulation work performed at METC. Key assumptions involved in the Aspen simulation were that the rates of the shift and carbonation reactions were sufficiently fast to permit equilibrium to be achieved, that 80% conversion of  $CaO$  to  $CaCO_3$  was possible in the carbonation step, and that the average sorbent lifetime was 20 cycles. Each of these assumptions was justified by the experimental results.

## SUMMARY OF EXPERIMENTAL RESULTS

A typical reactor response curve showing concentrations of  $H_2$ ,  $CO_2$ , and  $CO$  in the reactor product gas as a function of dimensionless time,  $t^*$ , is shown in Figure 1. During the early stages of the reaction, referred to as the prebreakthrough period, the  $CO$  and  $CO_2$  concentrations were approximately constant in the range of 80 and 300 ppmv(dry basis), respectively, and the  $H_2$  concentration was a maximum at about 15% (vol). Both the shift and carbonation reactions were fully effective during this period, and these concentrations correspond to 0.998 fractional removal of total carbon oxides. Equilibrium concentrations at these reaction conditions are 20



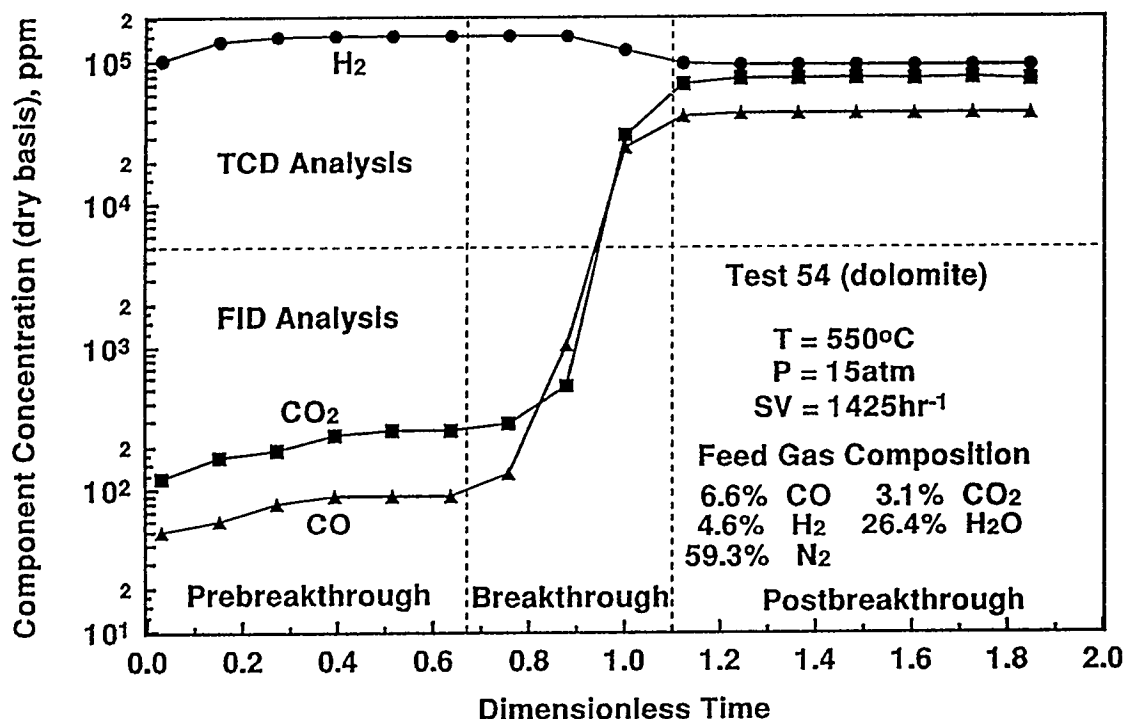


Figure 1. Typical Fixed-Bed Reactor Breakthrough Curves

ppm CO and 110 ppm CO<sub>2</sub>, which correspond to 0.999 equilibrium carbon oxide removal. CO and CO<sub>2</sub> concentrations began to increase rapidly at  $t^* \sim 0.7$  and continued to climb until a second steady-state was reached at  $t^* \sim 1.1$ . During this active breakthrough period the H<sub>2</sub> content decreased from about 15% to 9.4% (dry basis). The beginning of breakthrough corresponded to the time at which the leading edge of the carbonation reaction front reached the exit of the packed bed. During the postbreakthrough period, effectively all of the CaO had been converted to CaCO<sub>3</sub>, and the water-gas shift was the only reaction occurring to any significant extent.

Fractional carbon oxide removal, FCOX, and fractional conversion of CaO,  $X^*$ , as a function of  $t^*$  for this test are shown in Figure 2. Both parameters were calculated directly from the measured concentration-time data of Figure 1. The prebreakthrough value of FCOX remained

above 0.99 for  $t^* \leq 0.85$ . The definition of the dimensionless time is such that  $t^* = X^*$  whenever the fractional removal of carbon oxides is complete, i.e., as long as FCOX = 1. Thus,  $X^*$  was effectively equal to  $t^*$  during the prebreakthrough period. The fractional conversion of CaO increased linearly with time until breakthrough began; thereafter the rate of conversion decreased quickly and reached a final value of  $X^* = 0.93$ .

The results illustrated in Figures 1 and 2 were typical. FCOX values in excess of 0.99 and final  $X^*$  values greater than 0.9 were achieved over a wide range of shift-carbonation temperatures, space velocities, and feed gas compositions. Single-cycle tests proved the feasibility of combining the shift and carbonation reactions to produce a product gas rich in hydrogen with carbon oxide removals closely approaching theoretical equilibrium limits. The

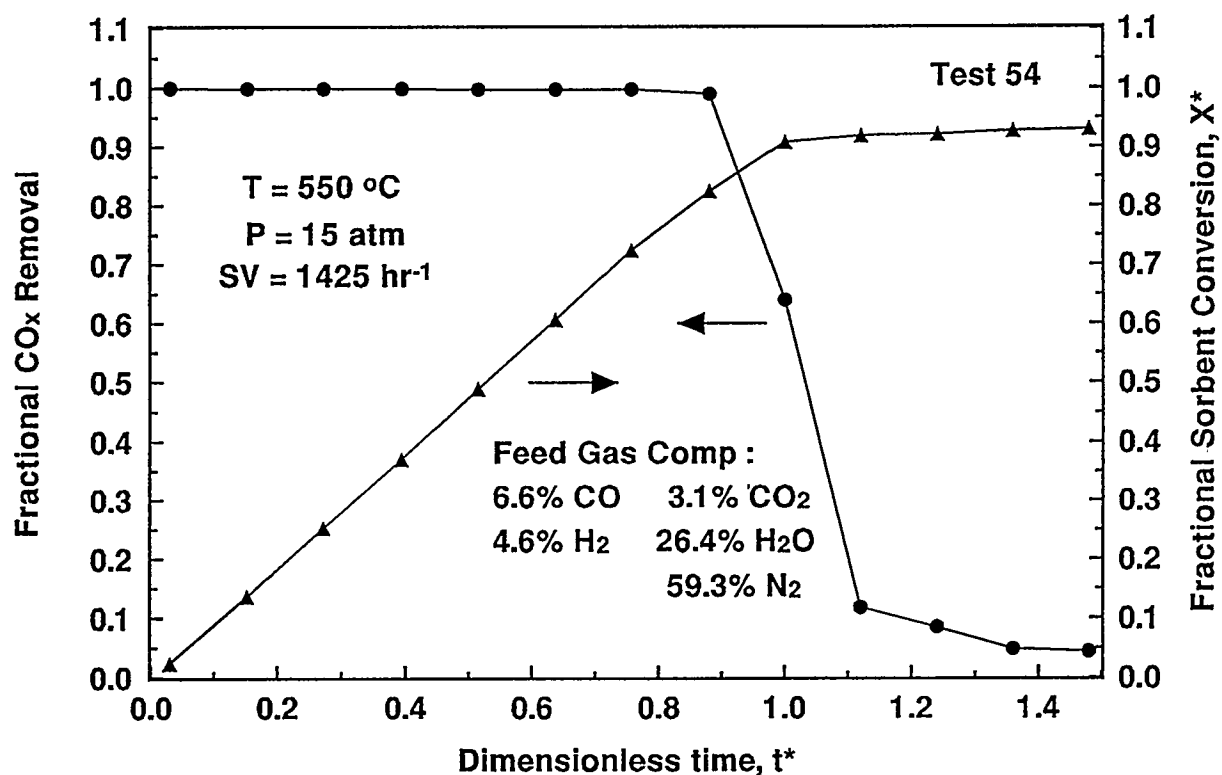


Figure 2. Carbon Oxide Removal and Sorbent Conversion in Fixed-Bed Reactor Test

second major question addressed in the experimental effort was that of sorbent multicycle durability. Although dolomite is widely available and inexpensive, it must maintain the favorable reaction properties through a number of calcination-carbonation cycles if the process is to be commercially attractive. A number of multicycle tests consisting of five, and in two cases eleven, complete cycles were conducted to obtain preliminary information on dolomite durability.

Figure 3 compares the CO and CO<sub>2</sub> concentrations and the fractional removal of total carbon oxides during the prebreakthrough period of an eleven-cycle and a five-cycle test at the same reaction conditions. CO concentrations were typically in the 20 to 30 ppmv range and CO<sub>2</sub> concentrations, although somewhat more variable, were generally in the 180 to 250 ppmv range.

These concentrations correspond to fractional removal of total carbon oxides of either 0.996 or 0.997 in each of the 16 cycles.

Although prebreakthrough concentrations did not increase with increasing number of cycles, sorbent deterioration did occur as shown by the decrease in both the duration of the prebreakthrough period and the slope of the breakthrough curve. These factors are illustrated in Figure 4 where CO<sub>2</sub> breakthrough curves for the first, fifth, and eleventh cycles are compared. The duration of the prebreakthrough period decreased from  $t^* \sim 0.8$  in the first cycle to  $t^* \sim 0.6$  in the fifth cycle to  $t^* \sim 0.25$  in the eleventh cycle. It was on the basis of such multicycle tests that the average sorbent lifetime of twenty calcination-carbonation cycles used in the process analysis was established.

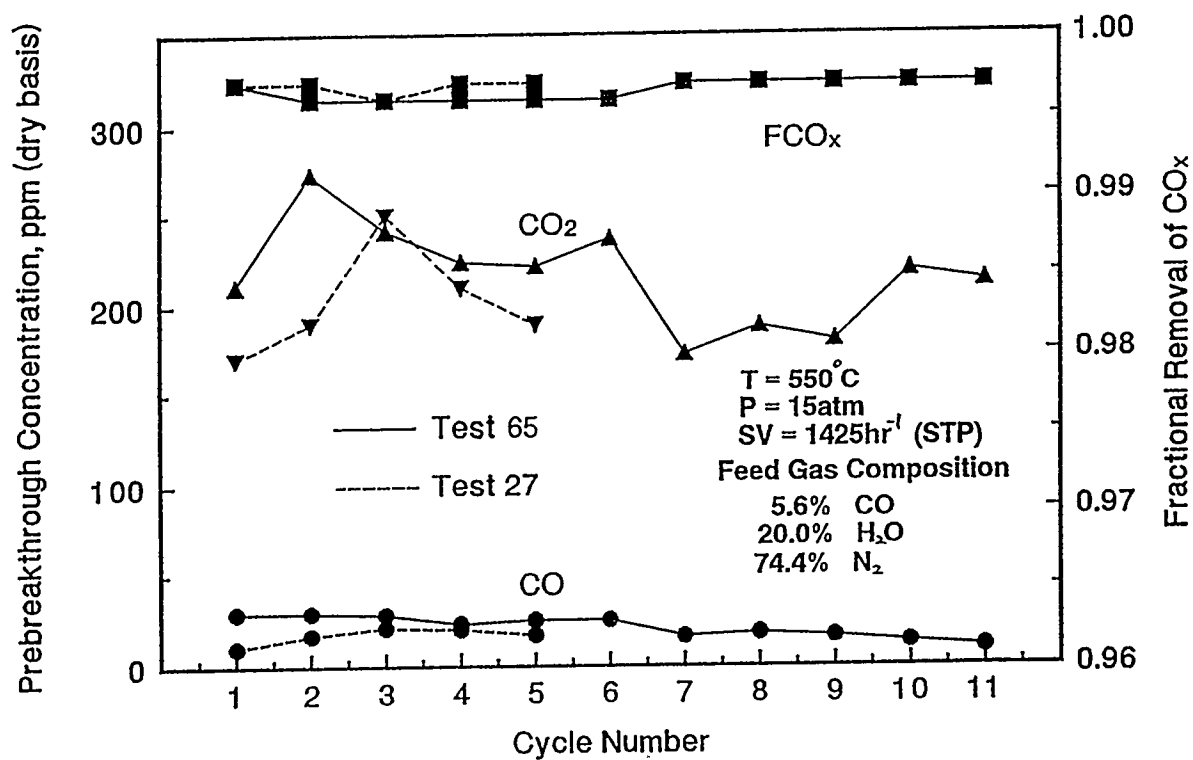


Figure 3. Multicycle Results During the Prebreakthrough Period

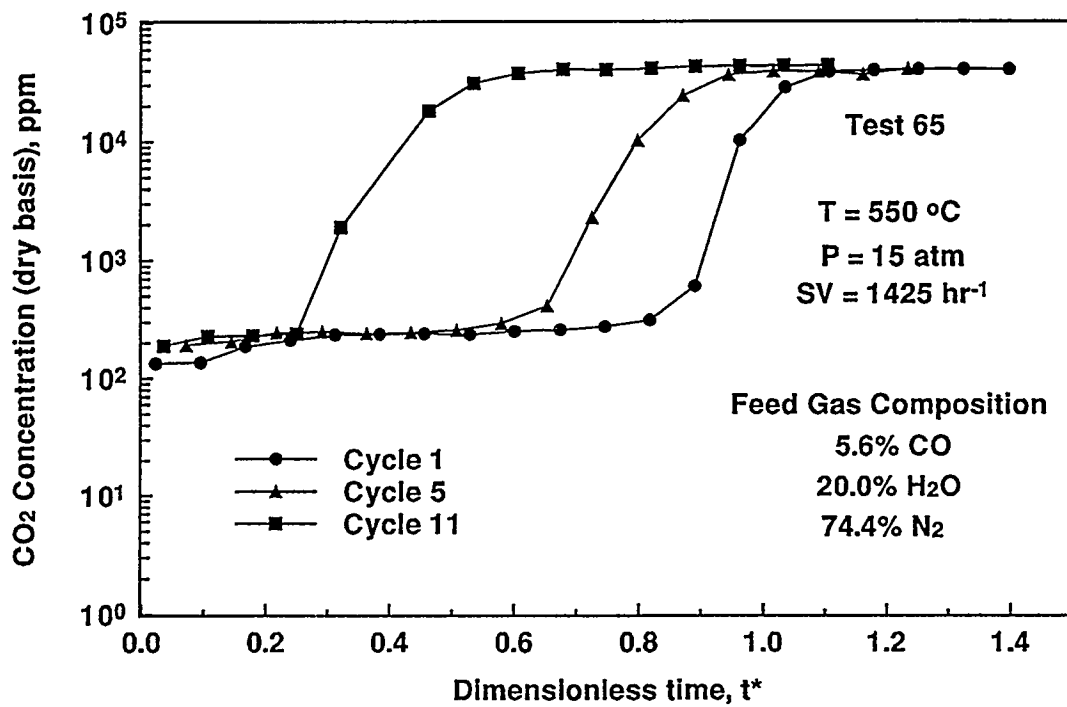


Figure 4. Decreased Duration of the Prebreakthrough Period

## PROCESS SYNTHESIS AND ANALYSIS

METC and LSU researchers collaborated to define the processing steps needed to produce  $H_2$  using the combined shift-carbonation process. METC personnel then used Aspen simulation to carry out material and energy balance calculations.

### The Process

A block flow diagram of the combined shift-carbonation process is shown in Figure 5. A sulfur-free coal gas at 1925°F and 412 psia whose flow rate and composition are shown in the first column of Table 1 passes through a heat recovery steam generator where  $5 \times 10^4$  lb/hr of 400 psia, 1000°F steam is generated by cooling the coal gas to 1100°F. The coal gas stream is then split with approximately one-half fed to the shift-carbonation reactor and the remainder used as fuel to supply

heat required for sorbent regeneration.  $1.6 \times 10^4$  lb/hr of the 400 psia, 1000°F steam is added to the coal gas to produce a 1.3 to 1 molar ratio of steam to carbon monoxide in the reactor feed (see column two of Table 1). This ratio is considerably less than used in a traditional shift reactor. The remainder of the steam is available for power generation or "sale."

The combined coal gas and steam are fed to the shift-carbonation reactor where they contact calcined dolomite. The product gas flow rate and composition, shown in the third column of Table 1, are based upon combined shift-carbonation reaction equilibrium at 1022°F and 340 psia. As shown previously, the experimental results suggest that equilibrium should be closely approached at these conditions. CO and CO<sub>2</sub> concentrations in the reactor product gas stream are shown as zero in Table 1 although the actual equilibrium concentrations are approximately 25 ppm CO<sub>2</sub> and

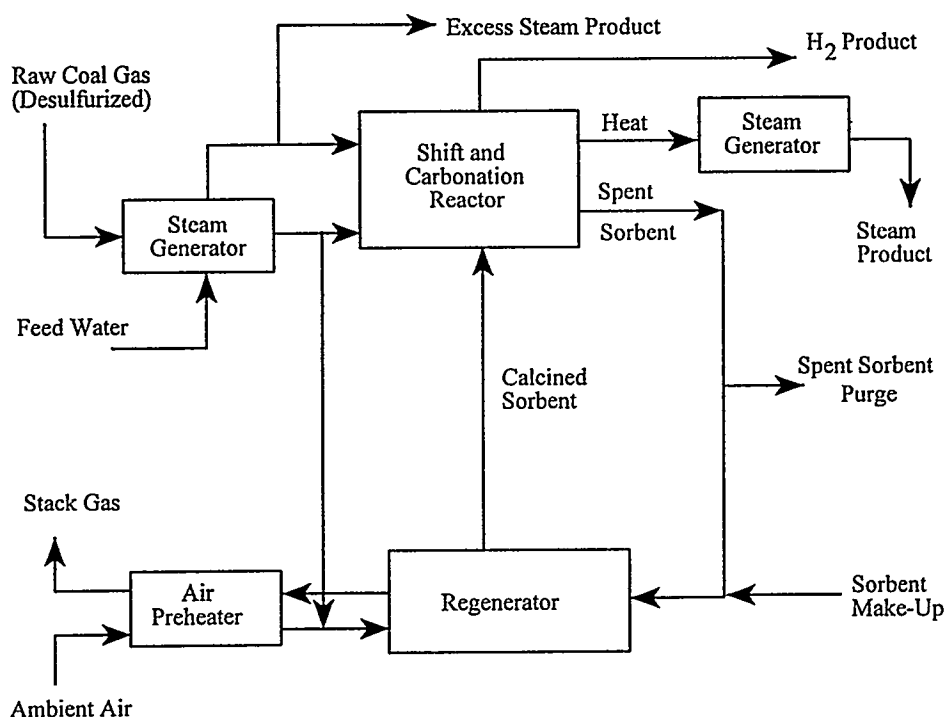


Figure 5. The Combined Shift-Carbonation Process

**Table 1. Flow Rate and Composition of Gas Streams in  
the Shift Carbonation Process**

Stream Description	Desulfurized Coal Gas	Shift-Carbonation Reactor Feed	Shift-Carbonation Reactor Product	Hydrogen Product
Temp., °F	1925	1050	1020	59
Pressure, psia	412	400	340	340
Flow Rate, lb mol/hr lb/hr	1.00x10 <sup>4</sup> 1.99x10 <sup>5</sup>	5.81x10 <sup>3</sup> 1.14x10 <sup>5</sup>	3.69x10 <sup>3</sup> 2.18x10 <sup>4</sup>	3.08x10 <sup>3</sup> 1.09x10 <sup>4</sup>
Composition, mol fraction				
N <sub>2</sub>	0.012	0.010	0.016	0.019
H <sub>2</sub>	0.251	0.213	0.759	0.909
CO	0.336	0.284	0.000	0.000
CO <sub>2</sub>	0.093	0.079	0.000	0.000
H <sub>2</sub> O	0.261	0.374	0.164	0.000
CH <sub>4</sub>	0.042	0.036	0.056	0.067
NH <sub>3</sub>	0.003	0.003	0.004	0.005

30 ppm CO. The mol fraction H<sub>2</sub> in the product stream is 0.759, with the impurities consisting primarily of CH<sub>4</sub>, N<sub>2</sub>, and H<sub>2</sub>O having mol fractions of 0.056, 0.016, and 0.164, respectively. The remaining H<sub>2</sub>O would be removed by cooling and condensation (not shown in Figure 4) to produce a final product containing about 91% H<sub>2</sub> (column 4 in Table 1). CH<sub>4</sub> and N<sub>2</sub> entered with the coal gas and were assumed to be inert in the shift-carbonation simulation. In order to produce a product containing greater than 99% H<sub>2</sub>, the product from the gasifier would have to be essentially CH<sub>4</sub>- and N<sub>2</sub>-free.

Both the shift and carbonation reactions are exothermic, and the energy liberated by the reaction is used to generate an additional 2.3x10<sup>5</sup> lb/hr of 400 psia, 1000°F steam. The total quantity of excess steam produced in the process is about 2.6 x 10<sup>5</sup> lb/hr.

The feed rate of fully calcined dolomite to the shift-carbonation reactor of 2.6x10<sup>5</sup> lb/hr is sufficient to provide 20% excess over the stoichiometric quantity required for complete reaction with the CO and CO<sub>2</sub> present in the coal

gas. Spent sorbent is transferred to the regenerator for decomposition of CaCO<sub>3</sub>. Approximately 5% (1.8x10<sup>4</sup> lb/hr) of the spent sorbent is purged and replaced by an equivalent quantity of make-up dolomite to maintain the required sorbent reactivity.

Regeneration, which takes place at 1650°F and 19 psia, is assumed to be complete, in agreement with experimental results. Heat required for the endothermic regeneration reaction is supplied by the combustion of a portion of the coal gas with preheated air. Because of the large quantity of energy required, about 50% of the coal gas must be used for this purpose, and the production rate of H<sub>2</sub> is reduced proportionally. The total energy required by the endothermic regeneration reaction is almost balanced by the exothermic energy liberated by the shift and carbonation reactions. However, since calcination requires higher temperature, energy exchange is not possible.

Certain heat exchangers, boiler feed water pumps, and a regeneration air blower are not shown in Figure 5. However, the heat duties of

the exchangers were included when calculating the total steam production rate. The total power required by the pumps and blower was estimated to be  $1.7 \times 10^7$  Btu/hr.

A summary of overall process inputs and outputs, including the pumps and blower, is presented in Table 2. The important input streams are the desulfurized coal gas at a rate of  $1.0 \times 10^4$  lb mol/hr ( $1.99 \times 10^5$  lb/hr), and  $2.6 \times 10^5$  lb/hr of make-up dolomite. From these feeds,  $3.1 \times 10^3$  lb mol/hr ( $1.09 \times 10^4$  lb/hr) of 91% H<sub>2</sub> and  $2.63 \times 10^5$  lb/hr of 400 psia, 1000°F steam are produced. Complete results of the material and energy balance calculations for all process streams are available in the final report (Harrison et al., 1994).

## Comparison With Other Processes for H<sub>2</sub> Production

As part of a recent DOE-sponsored study on the production of H<sub>2</sub> from coal gas using a high temperature membrane process, Jungerhans (1992) carried out similar material and energy balance calculations to compare the high temperature membrane process with a conventional process using multiple catalytic shift reactors and pressure swing adsorption (PSA) for H<sub>2</sub> purification. The coal gas feed rate used by Jungerhans was the same as used in this study, and the composition of the coal gases were similar as shown in Table 3. Differences in the

**Table 2. Summary of Process Input and Output Streams**

	lb mol/hr	lb/hr	T, °F	P, psia	Energy, Btu/hr
<b>Inputs</b>					
Desulfurized Coal Gas	$1.0 \times 10^4$	$1.99 \times 10^5$	1925	412	--
Boiler Feed Water	$1.55 \times 10^4$	$2.79 \times 10^5$	59	14.7	--
Dolomite Make-up	$2.82 \times 10^2$	$2.6 \times 10^5$	59	14.7	--
Regeneration Air	$1.5 \times 10^4$	$4.31 \times 10^5$	59	14.7	--
Water Pumps	--	--	--	--	$5.5 \times 10^5$
Air Blower	--	--	--	--	$1.65 \times 10^7$
<b>Outputs</b>					
Hydrogen Product 91% H <sub>2</sub>	$3.08 \times 10^3$	$1.09 \times 10^4$	59	340	--
Steam, 400 psia and 1000°F	$1.46 \times 10^4$	$2.63 \times 10^5$	1000	400	--
Dolomite Purge	$2.82 \times 10^2$	$1.85 \times 10^5$	1000	14.7	--
Stack Gas	$2.09 \times 10^4$	$6.32 \times 10^5$	280	14.7	--

**Table 3. Comparison of the Coal Gas  
Feed Composition Evaluated by  
Jungerhans and This  
Study**

	Jungerhans (1992)	This Study
Flow Rate, lb mol/hr	1.0x10 <sup>4</sup>	1.0x10 <sup>4</sup>
Mol Fraction		
H <sub>2</sub>	0.289	0.251
CH <sub>4</sub>	0.050	0.042
CO	0.386	0.337
CO <sub>2</sub>	0.107	0.093
H <sub>2</sub> S	0.001	0.000
H <sub>2</sub> O	0.150	0.261
N <sub>2</sub>	0.017	0.012
NH <sub>3</sub>	0.000	0.003

composition are important, however. Because of the reduced H<sub>2</sub> and CO content of the coal gas used in the present study, the maximum production rate of H<sub>2</sub> (assuming complete conversion of CO via the shift reaction and complete H<sub>2</sub> recovery) is 13% less. Actual H<sub>2</sub> production rates will, of course, be significantly lower due to incomplete CO conversion, losses during purification, and the necessity to divert a portion of the coal gas for use as fuel. CH<sub>4</sub> and

N<sub>2</sub> impurities were assumed to be totally removed in the PSA unit of the conventional process, and the membrane was considered to be impermeable to CH<sub>4</sub> by Jungerhans.

In spite of these differences, it is instructive to compare the H<sub>2</sub> product from the combined shift-carbonation process to the product from the two processes considered by Jungerhans (see Table 4). The quantity of H<sub>2</sub> produced in the conventional shift and membrane processes is

**Table 4. Comparison of the Products  
from Various Processes for the  
Production of Hydrogen**

	Membrane Separation	Conventional Shift	Combined Shift- Carbonation
H <sub>2</sub> Product lb mol/hr	4637	4490	3080
% H <sub>2</sub>	99.9	100	91.0
% of Theoretical H <sub>2</sub>	68.6	66.5	47.7

larger, both on an absolute basis and as a percentage of the theoretical maximum production rate.  $H_2$  is lost in the membrane process due to incomplete membrane permeation. The nonpermeate stream is used for power generation in a combustion turbine. The small impurity is primarily  $CH_4$  formed by the methanation of CO and  $CO_2$  which permeate the membrane. In the conventional shift process,  $H_2$  losses are associated with diversion of 27% of the coal gas for power generation and from the off-gas of the PSA unit. None of the heavier components escape the PSA separator so that the  $H_2$  content of the product is essentially 100%. The choice of PSA over amine-based wet scrubbing for  $H_2$  purification was dictated by the high  $CH_4$  concentration in the coal gas.  $CH_4$  would not be removed in the wet scrubber and the  $CH_4$  content of the product would be comparable to that produced in the shift-carbonation process.

The lower  $H_2$  production rate in the shift-carbonation process is caused by the need to divert approximately 50% of the coal gas to supply energy for spent sorbent regeneration. The lower  $H_2$  content is due, as previously discussed, to the  $CH_4$  and  $N_2$  content of the coal gas. This problem would not exist if the coal gas was free of  $CH_4$  and  $N_2$ , in which case the  $H_2$  purity would be comparable to that achieved with the other processes.

### Process Improvements

A number of process improvements and/or modifications would be required for the shift-carbonation process to become economically competitive. Three are briefly discussed in the following.

The  $H_2$  product purity is an obvious problem. Increasing the  $H_2$  content could be accomplished by adding an additional purification step, probably a PSA unit. This option would, of course, further reduce the  $H_2$  production rate;  $H_2$  losses in a PSA separator typically are about 20% (Ruthven, 1984). Alternately, use of the shift-

carbonation process could be limited to gasification processes that do not produce significant quantities of  $N_2$  and  $CH_4$ .

The second major problem is the high energy requirement of the endothermic sorbent regeneration reaction. Although the energy released by the exothermic shift and carbonation reactions is approximately equal to the energy required for regeneration, the higher regeneration temperature makes energy exchange impossible. Combustion of approximately 50% of the raw coal gas, which is required to satisfy the regeneration energy requirement, is directly responsible for the reduced  $H_2$  production rate. Alternate energy sources, such as waste gas from nearby processing units, or heat integration with the gasification process are required.

Finally, the pressure difference between the shift-carbonation reactor (340 psia) and the regeneration reactor (19 psia) creates a significant problem. Dual recirculating fluidized-bed reactors, similar to those used in the fluidized-bed catalytic cracking process, are an obvious choice for transporting the large quantities of sorbent between the two reactors. Coupled fluidized beds, however, must operate at approximately equal pressures. Significant reduction in the shift-carbonation reactor pressure is unacceptable since the effectiveness of the carbonation reaction decreases at low pressure. Increasing the regeneration reactor pressure is undesirable because higher regeneration temperature, which would likely accelerate sorbent deterioration, would be required. Innovative thinking will be required to solve the solid transport problem or to identify alternate reactor configurations which can function under the pressure difference and still achieve the desired rapid solid transfer.

### Alternate Applications

There are other applications where the combined reaction-separation process may be applied. One possibility involves carrying out the steam-methane reforming reaction in the presence



of calcined dolomite. This process, which has been suggested previously by Brun-Tsekhovoi et al. (1988), would enable the reforming, shift, and primary  $\text{CO}_2$  separation steps to be accomplished in a single vessel. On the basis of equilibrium calculations, a reactor product containing 95%  $\text{H}_2$  (dry basis) could be produced at 1000 K and 15 atm with a feed consisting of 4 mols of steam per mol of  $\text{CH}_4$ . The equilibrium yield of  $\text{H}_2$  would be 3.5 mols per mol of  $\text{CH}_4$  fed, or 88% of the stoichiometric maximum. Impurities would consist of about 3% unreacted  $\text{CH}_4$  and 1% of both  $\text{CO}$  and  $\text{CO}_2$  not removed in the shift-carbonation step. Further purification to produce essentially pure  $\text{H}_2$  could be accomplished using PSA. In this concept, the endothermic reforming and exothermic shift and carbonation reactions would occur at the same temperature to produce an approximate energy balance. Energy from the combustion of  $\text{CH}_4$  would be required for sorbent regeneration. In the current reforming process, combustion of large quantities of  $\text{CH}_4$  is required to drive the endothermic reforming reaction.

Traditional steam-methane reforming at the same steam to  $\text{CH}_4$  ratio, temperature, and pressure would, at equilibrium, produce a reformer product containing only 71%  $\text{H}_2$  (dry) basis, 61% of the theoretical yield. Subsequent processing including multistage catalytic shift reactors and  $\text{CO}_2$  separators would be required to increase the  $\text{H}_2$  content and yield to the values obtained in the combined reforming-shift-carbonation process.

In another possible application, the combined shift-carbonation process might be coupled with a coal gas-fired molten carbonate fuel cell operating at approximately 1 atm and 650°C. There are two possible locations for the shift-carbonation step. If the coal gas is fed to the shift-carbonation reactor before entering the anode, the  $\text{H}_2$  content would be increased and the  $\text{CO}_2$  content decreased. Both would improve anode operation. Sorbent regeneration would produce the  $\text{CO}_2$  required as cathode feed, which is now produced by combustion of a portion of the coal gas.

Alternately the sorbent process could be located at the anode exit. Only the carbonation reaction would be important since the shift reaction would go essentially to completion within the anode. Selective removal of  $\text{CO}_2$  from the anode exhaust would permit unreacted  $\text{H}_2$  to be recycled to the anode so that 100% of the fuel would be used to generate electricity. Again,  $\text{CO}_2$  obtained during the sorbent regeneration step would be fed to the cathode. The molten carbonate fuel cell application has the advantage of operating near atmospheric pressure, where the dual recirculating fluidized-bed reactor concept could be applied.

## FUTURE WORK

This contract ended in December 1994. The final report has been submitted, and it should soon be published.

## REFERENCES

Abrardo, J.M., and V. Khurana, 1995, Hydrogen Technologies to Meet Refiners' Future Needs, Hydrocarbon Processing, February, 43.

Brun-Tsekhovsi, A.R. et al., 1988, The Process of Catalytic Steam-Reforming of Hydrocarbons in the Presence of Carbon Dioxide Acceptor, Hydrogen Energy Progress VII, Proceedings of the 7th World Hydrogen Energy Conference, Pergamon Press, Vol. 2, 885.

Han, C. and D.P. Harrison, 1994, Simultaneous Shift Reaction and Carbon Dioxide Separation for the Direct Production of Hydrogen, Chemical Engineering Science, 49, 5875.

Harrison, D.P., et al., 1993, A Calcium Oxide Sorbent Process for Bulk Separation of Carbon Dioxide, IV., Proceedings of the Symposium on Coal Fired Power Systems '93,

Morgantown, W.V., June 1993, DOE/METC-93/6131, 335.

Harrison, D.P. and C. Han, 1994, A Calcium Oxide Process for Bulk Separation of Carbon Dioxide, V., 1994, Proceedings of the Coal-Fired Power Systems '94 -- Advances in IGCC and PFBC Review Meeting, Morgantown, WV, June 1994, DOE/METC-94/1008, 351.

Harrison, D.P., et al., 1994, A Calcium Oxide Process for Bulk Separation of Carbon Dioxide, Final Report, DOE Contract DE-AC21-89MC26366, in press.

Jungerhans, R.R., and P. Brandini, 1992, Economic Analysis of Hydrogen Production From Coal By a Membrane-Assisted Process, Final Report, DOE Contract DE-AC-21-90MC26365 (work performed under subcontract to California Institute of Technology).

Ruthven, D.M., 1984, Principles of Adsorption and Adsorption Processes, John Wiley and Sons, New York.

Shreve, R.N. and J.A. Brink, 1977, Chemical Process Industries, McGraw-Hill, New York.

## 7B.4 Thermal/Chemical Degradation of Inorganic Membrane Materials

### CONTRACT INFORMATION

**Contract Number** DE-AC21-92MC28053

**Contractor** SRI International  
333 Ravenswood Avenue  
Menlo Park, CA 94025  
(415) 326-6200

**Contractor Project Manager** Gopala N. Krishnan

**Principal Investigators** Gopala N. Krishnan  
Ashok S. Damle  
Angel Sanjurjo  
Bernard J. Wood  
Kai-Hung Lau

**METC Project Manager** Robert Gross

**Period of Performance** August 24, 1992 to May 19, 1995

**Schedule and Milestones**

### FY95 Program Schedule

Task	S	O	N	D	J	F	M	A	M	J	J	A	S
Experimental Testing													
Final Technical Report (Draft and Approved)													

### OBJECTIVES

The overall objective of this program is to evaluate the long-term thermal and chemical degradation of inorganic membranes that are being developed to separate gaseous products produced by the gasification or combustion of coal in fixed-, fluidized-, and entrained-bed gasifiers, direct coal-fired turbines, and pressurized-fluidized-bed combustors. The evaluation is accomplished by a review of available information in the literature, performing bench-scale experiments, and observing changes developed in membrane samples during exposure to a hot gas stream from an operating coal gasifier.

### BACKGROUND INFORMATION

Coal represents a major source of fossil fuels in the U.S. During gasification of coal, hydrogen is produced as one of the gaseous components in the product gas stream (coal gas). Hydrogen has many uses as a feedstock in the chemical industry and is also the most desirable fuel for fuel cells. The fraction of hydrogen in the coal gas mixture can be enhanced by the water gas shift reaction ( $\text{CO} + \text{H}_2\text{O} = \text{CO}_2 + \text{H}_2$ ). The forward reaction is favored when hydrogen is removed from the gas mixture. Inorganic membranes are capable of separating  $\text{H}_2$  from such gas mixtures at elevated temperatures and pressures. Several impurities, such as  $\text{H}_2\text{S}$ ,  $\text{NH}_3$ , and trace metal compounds,

are also generated during the coal gasification process and they must be removed from the coal gas to protect power generation equipment and meet environmental standards. Inorganic membranes are potentially capable of assisting in the removal of  $H_2S$  and  $NH_3$ . Hence, membrane materials must be identified that possess the required characteristics of permeability, selectivity, and durability for use under conditions expected in hot coal gas streams.

Many studies have examined the performance of ceramic and metal membranes in relatively clean gaseous environments. But, the coal gas at high temperatures can be an aggressive threat not only to the efficient operation but also to the long term survival of inorganic membranes. These gas streams contain several components, such as  $H_2O$ ,  $CO$ ,  $H_2S$ , and alkali vapor, that can react with membranes made of materials such as  $Al_2O_3$ ,  $SiO_2$ ,  $Pd$ , and  $Pt$  in the temperature range of interest ( $450^\circ$  to  $1000^\circ C$ ). Residual fly ash particulate matter, if present after passage through cyclones or filters, contains components such as alkali salts that can react with membrane materials at high temperatures to form different phases. Thus, several thermal and chemical degradation mechanisms could unfavorably alter the properties of inorganic membranes during exposure to high temperature coal gas streams.

## PROJECT DESCRIPTION

The program is divided into the following tasks: (1) development of evaluation methodology, (2) evaluation of potential long-term degradation mechanisms, (3) submission of a topical report and a plan for experimental testing, and (4) experimental testing.

Tasks 1-3 were completed in 1994. The results of the evaluation of potential long-degradation mechanisms were presented at the Coal-Fired Power Systems 94 -- Advances in IGCC and PFBC Review Meeting (Krishnan et al., 1994)

## RESULTS

An evaluation of potential degradation mechanisms, using existing theories and data available in the literature, was published earlier (Krishnan et al., 1993 a; 1993 b; 1994). This evaluation was based on a literature search of computerized data bases that identified several

hundred citations. A critical review of relevant technical articles revealed the following most likely degradation mechanisms in hot coal gas environments:

- Hydrothermal sintering
- Reaction with  $H_2S$
- Reaction with ash particles
- Interaction with alkali components
- Deposition of carbon in the pores of the membrane.

The effects of these mechanisms on the characteristics of several metal and ceramic membranes were experimentally evaluated.

Several candidate membrane materials were selected in consultation with the DOE program manager. Suppliers and manufacturers who were possible sources for different membrane materials were contacted to obtain development status and information regarding demonstrated gas selectivities and permeabilities (at least in the clean laboratory environment). The following membrane materials were selected for testing:

- Alumina membranes (Membralox) with a separation layer pore size of  $40 \text{ \AA}$ , supplied by U.S. Filter Corporation
- Alumina membranes modified by Media and Process Technology, Inc. to form a gas separation layer of amorphous silica
- Vycor porous glass membranes (mainly  $SiO_2$ ) with a pore size of  $40 \text{ \AA}$ , supplied by Corning, Inc.
- Vycor porous glass membranes modified in Professor Gavalas' Laboratory at the California Institute of Technology by depositing an amorphous silica inside the pores
- Platinum foils provided by Bend Research, Inc.
- Palladium foils supplied by Aldrich Chemical Company.

Three different test methods were used to evaluate the degradation of these membrane materials:

- Characterization of changes in physical and chemical properties of the membranes exposed to simulated hot coal gas streams under well-defined conditions in the temperature range 450° to 1000°C and pressures up to 20 atm
- Measurement of the permeation performance of membranes under simulated coal gas conditions
- Determination of changes produced in membrane materials after prolonged exposure to the hot coal gas stream of an operating fixed-bed coal gasifier at the General Electric Corporate Research and Development facility.

Before and after exposure, the membrane samples were characterized by (1) B. E. T. analysis for determination of surface area and pore size distribution, (2) Auger electron spectroscopy for identifying the elemental composition on the surface layers, (3) scanning electron microscopy to indicate changes in morphology, and (4) dynamic flow-weighted pore size distribution analysis. Permeation experiments were also performed to determine pure component permeation as well as mixed-gas permeation rates.

## Results of the Exposure Tests

The pore size of the unmodified Vycor membrane samples increased significantly in simulated coal gas streams at high temperatures and pressures (Table 1). Exposure at 800°C and 1-atm pressure for 76 h increased the mean pore size from 40 to 120 Å, whereas exposure at 1000°C and 1-atm pressure destroyed all microporosity. The loss of microporosity is likely due to the hydrothermal sintering. It can be also attributed to the presence of alkali vapor released from alumina membrane samples that were present in the same test apparatus. At temperatures lower than 650°C, high pressure conditions enlarged the pores significantly. Whereas the increase in the mean pore size was modest at 550°C and 1 atm pressure, it was severe at 20 atm pressure even at 450°C (Figure 1). The effect of gasifier ash at 450° and 550°C was negligible, presumably due to slow reaction kinetics between the two solid phases.

The deleterious effect of coal gas on the relatively large pore Vycor membranes is significant because the pore size needed for good gas separation is less than 10Å. Such a gas separation layer is made by adding or forming an amorphous silica microporous layer. Agglomeration of the amorphous phase is expected to be even more pronounced than observed with the Vycor membrane because of the high surface energy and defect concentration of the microporous layer.

Table 1. Surface Area And Mean Pore Size of Exposed Vycor Membrane Samples

Temperature (°C)	Pressure (psig)	Duration (hours)	Surface Area (m <sup>2</sup> /g)	Mean Pore Size (Å)
As-received	0	0	190	40
1000	0	24	2	1000
800	0	76	33	117
650	0	113	141	45
550	0	410	150	44
550	270	500	103	60
450	300	1000	99	60
550 (ash coat)	0	410	161	44
550 (ash coat)	270	500	110	58
450 (ash coat)	300	1000	105	57

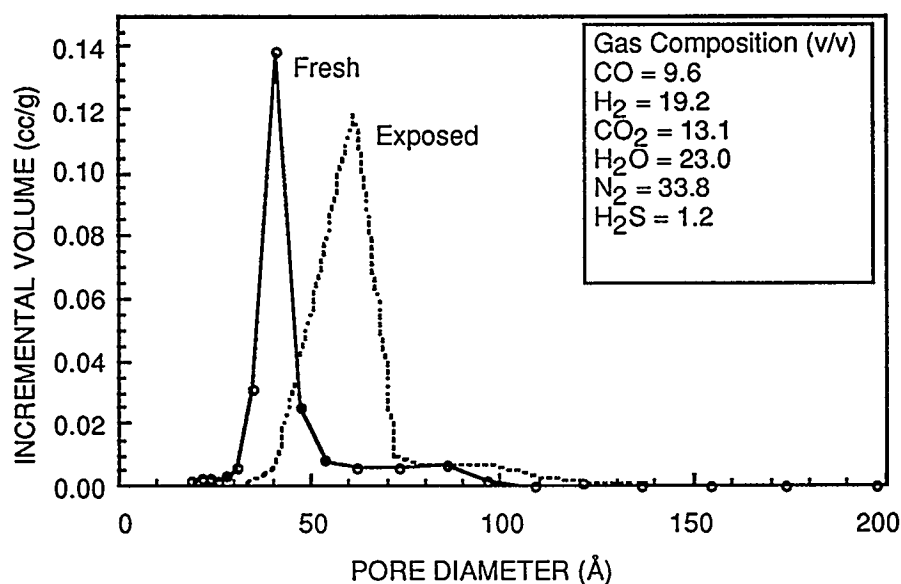


Figure 1. Pore Enlargement in Vycor Membranes During Exposure at 450°C and 20 atm Pressure for 1020 h

The alumina membrane samples are made of several layers of differing pore size (asymmetric) and the pore volume of the microporous layer is only a small fraction of the total pore volume. Hence, the B. E. T. method could not be used to determine its pore size distribution accurately. However, more than 90% of the surface area of the membrane is due to the particles in the microporous layer. Thus, changes in the surface area, as determined by the B. E. T. analysis, would reflect

the changes in the pore size distribution of the microporous layer. The surface area of the alumina samples decreased significantly at the tested conditions, indicating coarsening of the 40 Å layer (Table 2). As with Vycor membranes, the sintering of alumina membranes was not significantly changed at temperatures below 550°C when they were coated with a fixed-bed gasifier ash prior to exposure.

Table 2. Surface Area Of Exposed Alumina Membrane Samples

Temperature (°C)	Pressure (psig)	Duration (hours)	Surface Area (m <sup>2</sup> /gm)
As-received	0	0	2.1
1000	0	24	1.3
800	0	76	0.4
650	0	113	0.9
550	0	410	0.4
550	270	500	0.9
450	300	1000	1.0
550 (ash coat)	0	410	0.8
550 (ash coat)	270	500	1.4
450 (ash coat)	300	1000	1.5

Alumina membrane samples also released a significant amount of sodium vapor ( $\sim 10^{-7}$  atm) at temperatures exceeding 700°C. Evolved sodium vapor actually crystallized the Vycor and quartz materials placed nearby in the same reactor indicating that it is a serious threat to the silica layer in modified-alumina membranes.

In the later stages of the project, a dynamic pore size measurement (DPSM) technique was used to measure the pore size distribution of asymmetric membranes. This technique, originally developed at the Oak Ridge National Laboratory, provides a pore size distribution based on changes in gas permeation rate when membrane pores are blocked with a liquid film (Fain, 1989). The Kelvin equation correlates the pressure at which a vapor will condense as a liquid film in a pore:

$$\ln(P_0/P) = 2\gamma V/(rRT) \text{ or } r = (2\gamma V/RT) \cdot \ln(P/P_0)$$

where,  $P$  and  $P_0$  are, respectively, the partial and saturation pressures of the condensable vapor,  $\gamma$  is the surface tension of the condensate,  $V$  is the molar volume of the condensate,  $r$  is the pore radius where the condensation occurs,  $R$  is the gas constant, and  $T$  is the temperature. At a constant temperature, increasing the partial pressure of the vapor will allow increasingly larger pores to be blocked by the condensate film. The observed changes in the permeate flow as a function of the partial pressure of the vapor can be correlated to a flow-weighted pore size distribution of the membrane. The advantage of this technique is that it could measure accurately the pore size distribution of a thin microporous layer incorporated on supporting thick, macroporous layers. DPSM analysis indicated that the mean size of alumina membrane microporous layer increased from 40 to 65 Å when exposed to a simulated coal gas at 550°C and 20 atm for 500 h (Figure 2).

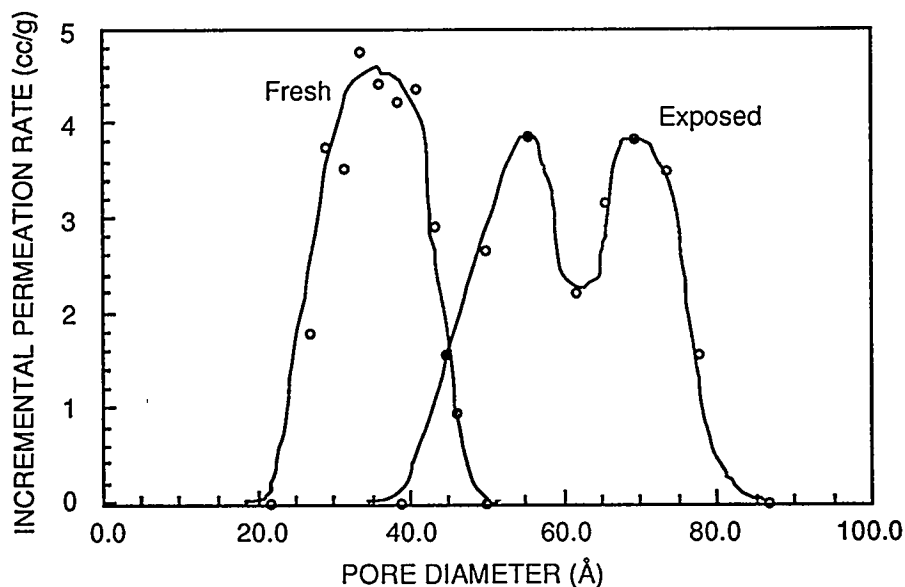


**Figure 2. Pore Size Distribution in Membralox Alumina Membranes during Exposure to a simulated Coal Gas at 550°C and 20 atm pressure for 500 h (Gas Composition was similar to that shown in Figure 1)**

H<sub>2</sub>S present in the hot coal gas could result in the chemisorption of S atoms on Pt and Pd surfaces and possible bulk sulfide formation. Such poisoning could reduce the H<sub>2</sub> permeability of the

metals. The extent of sulfur poisoning on Pt foils exposed to simulated coal gas streams containing 1.2% H<sub>2</sub>S depended on both temperature and pressure. Whereas at 1 atm, the sulfur layer was

less than 10 Å at 1000°C, it increased to 50 Å at 450°C. However, Pt samples exposed at 450°C and 20 atm pressure had extensive surface sulfide coatings, more than 200 Å thick. Thus, the extent of sulfidation increased with decreasing temperature and increasing pressure. Pre-coating of Pt foils by a gasifier ash did not significantly affect the extent of surface sulfidation. Palladium foils melted at temperatures above 650°C and deformed extensively below that temperature due to PdS formation by reaction with H<sub>2</sub>S present in the simulated coal gas. Thus, Pd is not suitable as a membrane material in direct contact with coal gas.

### Membrane Permeation Tests

The permeation performance of several modified-alumina and modified-Vycor membranes (tubular) was evaluated at high temperature and high pressure especially in the presence of steam. Initial experiments with modified membranes produced results different from those reported by the suppliers, possibly as a result of changes that might have occurred during a 3-month storage of the membranes at ambient conditions in the

laboratory prior to testing. In later experiments, two additional modified-alumina membranes and one modified-Vycor membrane were procured and they exhibited permeation characteristics under dry conditions consistent with those reported by the suppliers. All three modified-membrane samples degraded in a few hours in the presence of a feedgas containing about 20% steam in the temperature range 450° to 600°C and at 100 psig total pressure.

Pure component permeation tests with a modified-alumina membrane were first conducted with He and N<sub>2</sub> gases at temperatures up to 600°C. As shown in Table 3, the N<sub>2</sub> permeance decreased with increasing temperature from 0.08 m<sup>3</sup>/(m<sup>2</sup>·h·atm) at 25°C to 0.03 m<sup>3</sup>/(m<sup>2</sup>·h·atm) at 600°C. However, He permeance increased from 0.25 to 7.7 m<sup>3</sup>/(m<sup>2</sup>·h·atm) as temperature was increased from 25° to 600°C. As a result, the pure component He/N<sub>2</sub> selectivity increased from 3 to 227 under dry gas conditions. These results were consistent with those obtained by Media and Process Technologies, Inc. with this membrane.

Table 3. Permeation Results With a Modified-Alumina Membrane

		Permeance m <sup>3</sup> /(m <sup>2</sup> ·h·atm)		Selectivity
Temperature (°C)	Steam (%)	Helium	Nitrogen	P <sub>He</sub> /P <sub>N<sub>2</sub></sub>
Pure Component Tests				
25	—	0.25	0.079	3.2
150	—	1.7	0.049	34.7
300	—	3.8	0.044	86.4
450	—	5.7	0.038	150.0
600	—	7.7	0.034	226.5
Mixed Gas Tests				
300	0	2.3	0.05	45.8
600	0	2.5	0.045	58.3
600 <sup>1</sup>	20	2.2	0.035	63.0
600 <sup>2</sup>	20	2.8	0.34	8.3
Pure Component Permeation Test after Mixed Gas Tests				
25 <sup>3</sup>	—	1.5	0.62	2.4

<sup>1</sup> 1 h after adding steam.

<sup>2</sup> 5 h after adding steam.

<sup>3</sup> After 5 h exposure to 20% steam at 600°C, 100 psig total pressure.



Because of the large stage cut of 80% in this experiment, the calculated permeances and selectivity values during mixed gas tests were significantly lower than the true values.

The effect of steam on the membrane performance was determined at 600°C by adding ~20% steam to the feed gas. The permeate and raffinate gas compositions were monitored for about 5 h. Initially, the results were found to be comparable with those obtained under dry gas conditions. However, both the nitrogen and CO<sub>2</sub> concentrations in the permeate were found to increase steadily in the permeate gas after about 2 h. After about 4 h, the helium and nitrogen permeances increased to 2.8 and 0.34 m<sup>3</sup>/(m<sup>2</sup>·h·atm) respectively with a corresponding He/N<sub>2</sub> selectivity of 8.3. Subsequent pure component permeation measurements at 25°C indicated a substantial increase in permeation rates as compared to the earlier measurements. The helium and nitrogen permeances were found to have increased to 1.5 and 0.62 m<sup>3</sup>/(m<sup>2</sup>·hr·atm) respectively with a pure component selectivity of only 2.4. These results confirmed that the size-selective layer made of silica had been altered during exposure to steam.

The He/N<sub>2</sub> selectivity of another modified-alumina membrane was initially 250, but it also decreased to 4 after less than 30 h exposure to a gas mixture containing 20% steam at 100 psig total pressure in the temperature range 450° to 600°C (Figure 3). During this exposure period, pure-component helium permeance at 450°C decreased from 9.5 to 5.5 cm<sup>3</sup>/(cm<sup>2</sup>·min·atm), whereas nitrogen permeance increased from 0.05 to 1.6 cm<sup>3</sup>/(cm<sup>2</sup>·min·atm).

The DPSM test performed on the modified-alumina membrane before and after exposure showed that the pore diameter of the separation layer in the unexposed membrane was below the detection limit (<15Å) of the technique. Although, the selectivity of the exposed modified-alumina membrane had decreased substantially compared to that of the fresh membrane, the pore size distribution of the exposed membrane was still too small to be measured accurately by the DPSM technique. The present results confirm that for a porous membrane to be used for gas separation in industrial applications, the pore size of the separation layer must be substantially smaller than 15Å.

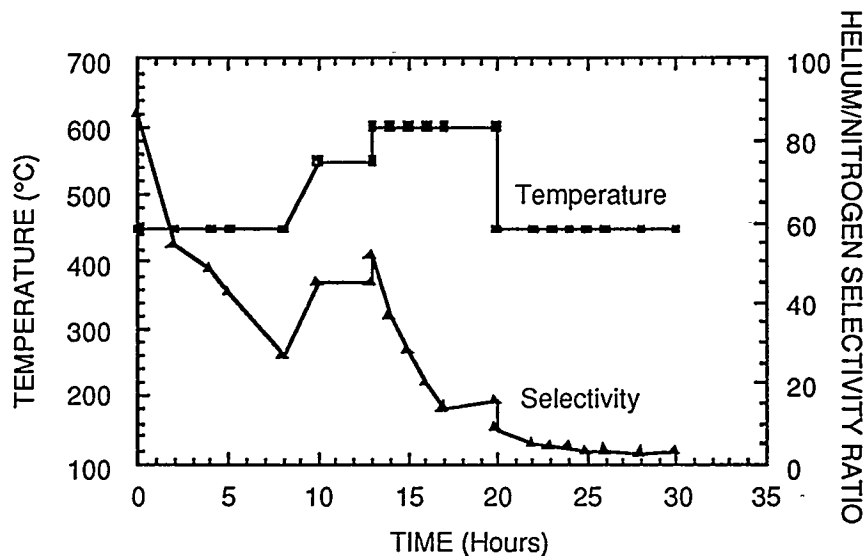


Figure 3. The He/N<sub>2</sub> selectivity of a Modified-Membralox Membrane as a function of Time and Temperature  
(Gas Composition: N<sub>2</sub> = 8.0%; CO<sub>2</sub> = 8.7%; H<sub>2</sub>O = 16.7%; He = Balance)

The He/N<sub>2</sub> permeance ratio of the modified-Vycor membrane also decreased from 160 to 3.5 upon exposure to a gas mixture containing 20% steam at 100 psig total pressure and 450°C for less than 15 hours (Figure 4). During this exposure test, the pure component helium permeance

remained constant at 0.45 cm<sup>3</sup>/(cm<sup>2</sup>·min·atm), whereas, that of nitrogen increased from 0.005 to 0.14 cm<sup>3</sup>/(cm<sup>2</sup>·min·atm). Thus, degradation of both alumina and silica membranes resulted in a substantial increase in nitrogen permeance indicative of coarsening of the size-selective pores.

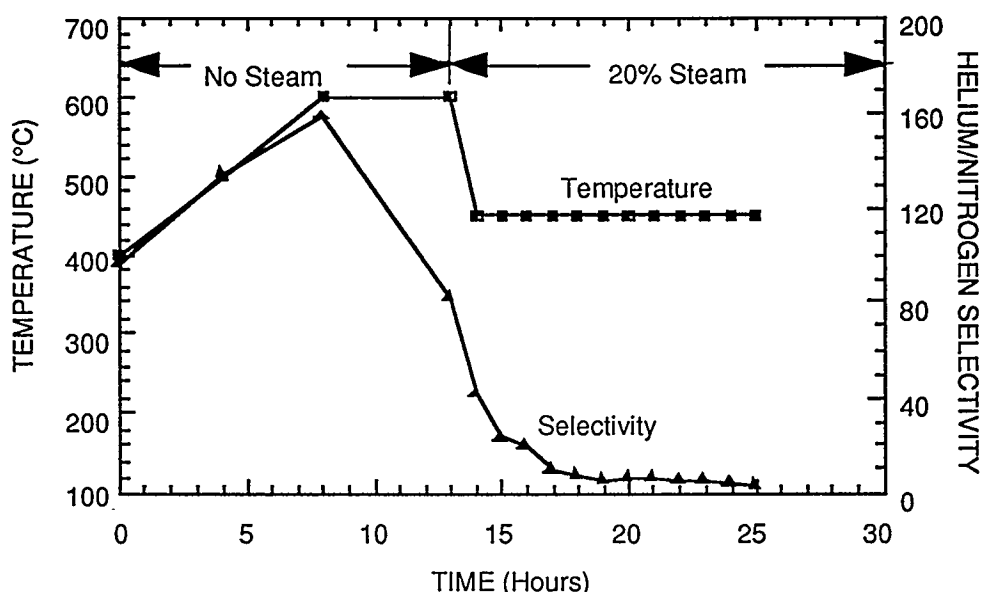


Figure 4. The He/N<sub>2</sub> selectivity of a Modified-Vycor Membrane as a function of Time and Temperature (Gas Composition: N<sub>2</sub> = 40%; He = 40%; H<sub>2</sub>O = 20%)

Both the alumina and Vycor membranes were modified by depositing a thin SiO<sub>2</sub> layer to reduce the pore size. The results indicate that a gas mixture containing ~20% steam at a relatively low total pressure of 100 psig (compared to the typical coal gas pressures of 300 psig) was adequate to increase the pore size of the SiO<sub>2</sub> layer, reducing the gas selectivities to those expected from unmodified alumina and Vycor membranes.

Two different experiments were carried out to determine the permeation characteristics of 25-μm thick Pt foils. In the first experiment, a fresh Pt foil was exposed to a simulated coal gas at 700°C and the permeance of H<sub>2</sub> present in the coal gas was monitored as a function of time. Periodically, the coal gas flow was interrupted and the permeance of H<sub>2</sub> was also determined with pure H<sub>2</sub> as feed gas. Due to burnout of graphite ferrules and seals, the maximum duration of this experi-

ment was 24 h. The H<sub>2</sub> permeance decreased from 0.02 to 0.01 cm<sup>3</sup>/(cm<sup>2</sup>·min·atm) during the initial 4-h exposure to the simulated coal gas (Table 4). At longer exposures, the H<sub>2</sub> permeation rate appeared to remain stable.

In the second experiment, a Pt foil was exposed to a simulated coal gas at 550°C and 270 psig for 500 h and then the H<sub>2</sub> permeance was determined using pure H<sub>2</sub> as feed gas at 115 psig pressure and 700°C. The H<sub>2</sub> permeance increased from an initial value of 0.006 to 0.02 cm<sup>3</sup>/(cm<sup>2</sup>·min·atm), after about 1 h, and then remained stable (Figure 5). This behavior may be explained by the removal of an adsorbed sulfur layer formed at 550°C by reaction with the pure H<sub>2</sub> feed gas at 700°C. Both types of experiments confirm that sulfur atoms are reversibly adsorbed on the surface of a Pt foil at 700°C and they could reduce the H<sub>2</sub> permeability of Pt membranes.

Table 4. Hydrogen Permeation Through Platinum Foil at 700°C

Cumulative Exposure Time (h)	Feed Gas	Feed Pressure (psig)	Hydrogen Permeance $\text{cm}^3/(\text{cm}^2 \cdot \text{min} \cdot \text{atm})$
1	Coal gas	150	0.022
1.5	Hydrogen	80	0.020
2	Hydrogen (dry)	80	0.020
3	Coal gas	250	0.022
18	Coal gas	250	0.016
19	Hydrogen (dry)	80	0.010

Notes: Platinum foil thickness: 25  $\mu\text{m}$   
 Coal gas composition:  $\text{H}_2 = 19.3\%$ ;  $\text{CO} = 9.6\%$ ;  $\text{CO}_2 = 13.1\%$ ;  $\text{N}_2 = 33.8\%$ ;  $\text{H}_2\text{O} = 23.0\%$ ;  $\text{H}_2\text{S} = 1.2\%$   
 Pressure on the permeate side = 0 psig

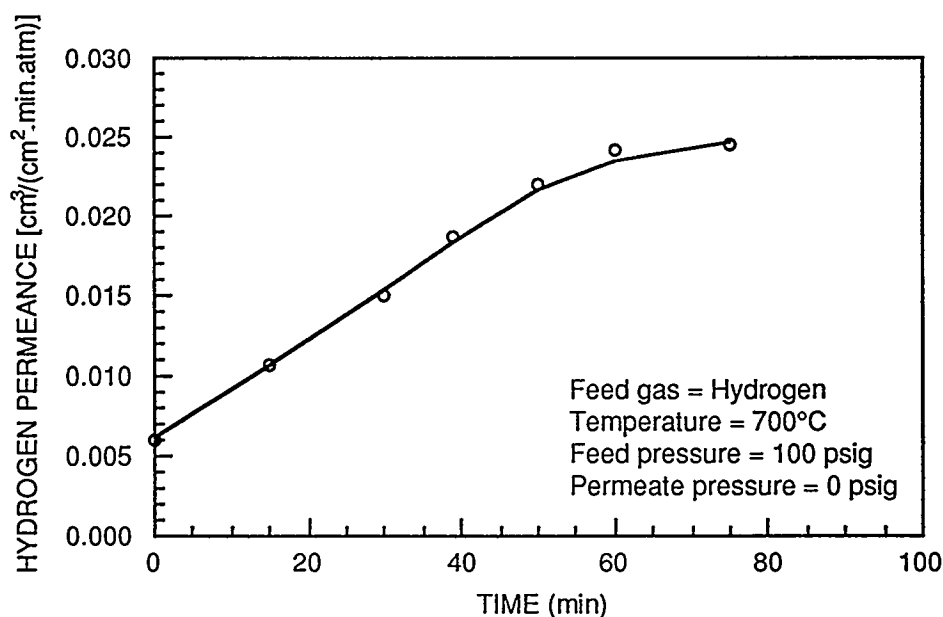


Figure 5. Hydrogen Permeation Through a Platinum Membrane After Exposure to a Simulated Coal Gas at 550°C, 270 psig for 500 h.

#### Exposure to a Coal Gasifier Gas Stream

Alumina, silica, and platinum membrane samples were exposed to hot coal gas stream at about 510°C and 280 psig pressure for 50 h in the General Electric Corporate Research and Development's (GE-CRD) fixed-bed gasifier

facility. The samples were exposed at two locations: (1) downstream of the primary cyclone and (2) downstream of a zinc oxide-based  $\text{H}_2\text{S}$  absorber reactor (which had a secondary cyclone). During the run in which an Illinois #6 coal was gasified, the particulate loadings at locations 1 and 2 were about 100 and 50 ppmw, respectively.

During this exposure testing, all specimens accumulated a substantial amount of a black deposit. The deposit was mainly soot (~98 wt%) with small amount of ash material mixed in it.

All membrane samples suffered some damage during the exposure test. Many of them were broken, apparently due to high gas velocities and normal pressure fluctuations. At the primary cyclone outlet, most of the platinum samples were sheared off the support plates because of the abrasive dust. However, at the secondary cyclone outlet location, fragments of two platinum samples were recovered. All Vycor membrane samples had turned black, apparently due to deposition and absorption of tar vapors. Similarly, the 40 Å microporous layer of the alumina membrane had also turned black. All the recovered samples were washed ultrasonically in distilled water to remove embedded ash particles. The Vycor and alumina samples remained black confirming absorption of organic and tar vapors.

B. E. T. analysis indicated that the mean pore size of the Vycor membrane increased from about 40 Å to about 78 Å with a corresponding decrease in the surface area from 190 to 85 m<sup>2</sup>/g. DPSM test indicated that the modified-alumina membrane tube suffered loss of microporosity and a reduction in permeation rate. These results indicate coarsening of the pores along with pore blockage by absorbed tar or fly ash deposits.

Platinum samples retrieved from the gasifier had sulfur, sodium, and iron impurities on the surface, as determined by Auger-electron spectroscopy measurements. The presence of sulfur atoms was expected due to the H<sub>2</sub>S present in the coal gas. The cause of iron impurity on the sample is not apparent. Discussions with the GE-CRD staff suggested that iron impurity may have come from the erosion of stainless steel pipes through which the coal gas was flowing before contacting the specimens.

The results from this short-term exposure in the product gas stream of an operating coal gasifier confirm that the tested inorganic membranes degrade significantly on exposure to coal gas conditions. The enlargement of pores, even during the relatively short time, raises concern whether porous inorganic membranes could operate effectively as a gas separation device in hot coal gas streams. The observed erosion of the metal

foils indicates that they can be used only in a nearly particle-free gas stream, perhaps downstream of high temperature barrier filters.

## CONCLUSIONS & RECOMMENDATIONS

The experimental tests conducted on the inorganic membrane samples under simulated and actual coal gas conditions indicate that silica- and alumina-based membranes, both modified and unmodified, experience coarsening of their micropores in the high temperature, high pressure, and high steam environment of coal gas streams. The pore coarsening that occurs in the presence of steam at elevated pressures degrades the H<sub>2</sub> selectivity of the modified-membranes quite rapidly. Such membranes are completely unsatisfactory for use in the coal gas environment for an extended period of time. Platinum membranes experience a reduction in the hydrogen permeation rate due to surface sulfidation by H<sub>2</sub>S in the coal gas. The extent of sulfidation increases as the temperature is decreased. Thus, Pt is suitable as an H<sub>2</sub> transfer membrane only at high temperatures (>700°C) because both inherent diffusion rate through the metal and sulfur poisoning of the surface reduce the hydrogen permeation rate at low temperatures. Other major gaseous components of the coal gas stream do not appear to have a significant effect on Pt membranes. Fly ash, if present, may erode the soft metal and hence Pt membranes may be used only downstream of high temperature barrier filters. Palladium membranes are degraded extensively by H<sub>2</sub>S and are not suitable for coal gas applications.

Alternative, chemically and physically stable materials must be identified or methods must be found to improve the resistance of the current membranes if porous inorganic membranes are to be used to separate the gaseous components in the coal gas environment.

## REFERENCES

- Fain, D. E. 1989. A Dynamic Flow-Weighted Pore Size Distribution Analysis. *Proceedings of the First International Conference on Inorganic Membranes (ICIM1)*, Montpellier, France.
- Krishnan, G. N., A. Sanjurjo, A. S. Damle, B. J. Wood, and K. H. Lau. 1994. Thermal/

Chemical Degradation of Inorganic Membranes.  
*Proceedings of the Coal-Fired Power Systems*  
*94 -- Advances in IGCC and PFBC Review*  
*Meeting*, 211-219. DOE/METC-94/1008.  
NTIS/DE94012252. Springfield, Va.: National  
Technical Information Service.

Krishnan, G. N., A. Sanjurjo, B. J. Wood, and  
K. H. Lau. 1993 a. Thermal/ Chemical  
Degradation of Inorganic Membranes.  
*Proceedings of the Coal-Fired Power Systems*  
*93 -- Advances in IGCC and PFBC Review*  
*Meeting*, 211-219. DOE/METC-93/6131.  
NTIS/DE93000289. Springfield, Va.: National  
Technical Information Service.

Krishnan, G. N., A. Sanjurjo, and B. J. Wood,  
1993 b. Thermal/Chemical Degradation of  
Inorganic Membranes. Topical Report. SRI  
International report submitted to U.S.  
Department of Energy under contract DE-AC21-  
92MC28053.

## 7B.5

# Electrochemical Polishing of Hydrogen Sulfide From Coal Synthesis Gas

### CONTRACTOR INFORMATION

**Contractor No.:** DE-FG22-94-PC94207

**Contractor:** Georgia Tech Research Corporation  
School of Chemical Engineering  
778 Atlantic Drive  
Atlanta, GA 30332-0100  
(404) 894-2834 (phone)  
(404) 894-2866 (fax)

**Contractor Project Manager:** E. Faith Gleason

**Principle Investigator:** Dr. Jack Winnick, P.E.

**METC Project Manager:** Dr. Kamal Das

**Period of Performance:** September 1, 1994 to May 31, 1995

### OBJECTIVES

An advanced process has been developed for the separation of  $H_2S$  from coal gasification product streams through an electrochemical membrane. This technology is developed for use in coal gasification facilities providing fuel for co-generation coal fired electrical power facilities and Molten Carbonate Fuel Cell electrical power facilities.

$H_2S$  is removed from the syn-gas by reduction to the sulfide ion and  $H_2$  at the cathode. The sulfide ion migrates to the anode through a molten salt electrolyte suspended in an inert ceramic matrix. Once at the anode it is oxidized to elemental sulfur and swept away for condensation in an inert gas stream. The syn-gas is enriched with the  $H_2$ . Order-of-magnitude reductions in  $H_2S$  have been repeatably recorded

(100 ppm to 10 ppm  $H_2S$ ) on a single pass through the cell.

This process allows removal of  $H_2S$  without cooling the gas stream and with negligible pressure loss through the separator. Since there are no absorbents used, there is no absorption/regeneration step as with conventional technology. Elemental sulfur is produced as a by-product directly, so there is no need for a Claus process for sulfur recovery. This makes the process economically attractive since it is much less equipment intensive than conventional technology.

### BACKGROUND INFORMATION

Use of selective membranes for separating gaseous components from mixtures is a common unit operation. The thermodynamic basis for

separation is very simple: a component will only move down a chemical potential gradient,  $\Delta\mu$ :

$$\Delta\mu_i = \mu_i - \mu_i' = RT \ln\left(\frac{a_i}{a_i'}\right) \quad (1)$$

where the prime ' refers to the extracted phase. Thus, for a separation from a phase with 1% into a pure phase, a minimum pressure ratio of about 100 is needed. In actual practice a higher pressure drop is needed to promote a significant flux. These processes do not produce a high-purity product, nor do they remove one component with perfect selectivity.

The situation is different for a charged species in the presence of an electric potential,  $\Delta\Phi$ . Here, the electrochemical potential,  $\bar{\mu}$ , is the driving force:

$$\Delta\bar{\mu} = \bar{\mu}_i - \bar{\mu}_i' = RT \ln\left(\frac{a_i}{a_i'}\right) + z_i F \Delta\Phi \quad (2)$$

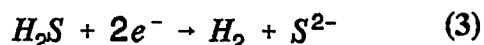
So, for a species with a charge of  $\pm 2$ , a potential difference of 0.06 V can maintain the same concentration difference that requires 100 atm for an uncharged species. The effect is more pronounced as the concentration in the feed drops to levels encountered in contaminant removal, e.g. 10 ppm. Here a pressure driven separation to a pure stream would require more than  $10^5$  atm while an electrochemical separation requires only 0.15 V [1].

This principle has been applied to high temperature gas mixtures including  $H_2S$  in  $N_2$  [2], sour coal gas ( $H_2S$  levels greater than 1000 ppm) [3], and natural gas ( $H_2S$  levels from 1.3% to 100 ppm) [4]. The primary gaseous pollutant in each of these cases has been  $H_2S$  in a fuel gas stream, but removal of  $SO_2$  has also been achieved from flue gas streams [5]. The membrane is exposed to the same pressure on both sides, so there is no theoretical limit to the pressure at which the process can operate. The main thrust of this paper is polishing  $H_2S$  from coal synthesis gas ( $H_2S$  levels of 100 ppm and less).

## PROJECT DESCRIPTION

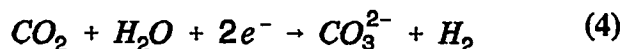
The major gaseous contaminant in raw coal gas is  $H_2S$ . Much of the coal reserves in the United States contain up to 5 wt% sulfur, which is converted to  $H_2S$  during gasification. The  $H_2S$  concentration (and raw coal gas composition) depends on the type of coal and the gasification conditions, but levels from 0.5 to 1.0 volume percent are typical (see Table I for a listing of some representative compositions [6]). Before this gas can be used for power generation, the  $H_2S$  concentration must be reduced to 100 ppm or less (Molten Carbonate Fuel Cell plants require concentrations of no more than 1 ppm  $H_2S$ ). Conventional processes to remove  $H_2S$  rely on low to ambient temperature absorption, followed by sorbent regeneration and Claus treatment for conversion of concentrated  $H_2S$  to elemental sulfur [7].

A hot gas electrochemical membrane process for the removal of  $H_2S$  is illustrated schematically in Figure 2. The process gas is passed by the cathode. Here, the most easily reduced component, that is, the strongest Lewis acid, will be electronated. In many mixtures of sour gas, this is  $H_2S$ :



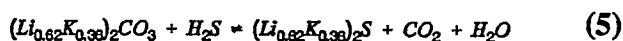
A membrane which contains sulfide ions in a molten state acts to transport sulfide across to the anode where, in the simplest case, hydrogen can be supplied to form  $H_2S$ . If the membrane is capable of preventing the diffusion of hydrogen from the cathode side, an inert sweep gas such as  $N_2$  can be used at the anode to carry away oxidized sulfide ions as vaporous sulfur.

The situation can become complicated when coal gas mixtures are processed. Carbon dioxide and water compete in the reduction reaction by:



The ionic flux through the membrane depends upon the relative mobilities of carbonate and sulfide as well as their concentrations.

From the equilibrium constant for reaction (5) below, it is possible to know the electrolyte composition which would be in equilibrium with a given process gas at a given process temperature. Theoretical membrane electrolyte compositions are calculated by thermodynamic analysis of equilibrium reaction (5). Since membranes similar to those used in the Molten Carbonate Fuel Cell were used in these studies, the cations present were K and Li in a ratio corresponding to the low melting carbonate eutectic ( $\text{Li}_{0.62}\text{K}_{0.38}$ ):



This analysis was performed by finding the Gibbs energy change of reaction (5) at the process temperature and relating this to the equilibrium constant,  $K_a$ , with  $K_a$  defined as:

$$K_a = \frac{(P_{\text{CO}_2} P_{\text{H}_2\text{O}} a_{\text{M}_2\text{S}})}{(P_{\text{H}_2\text{S}} a_{\text{M}_2\text{CO}_3})} \quad (6)$$

If the activity coefficients,  $\gamma$ , of the molten phase constituents (namely the sulfide and carbonate in the electrolyte) are assumed to be equal, then the activities of the molten phase constituents can be replaced by mole fractions ( $X_i$ ):

$$K_a = \frac{(P_{\text{CO}_2} P_{\text{H}_2\text{O}} X_{\text{M}_2\text{S}})}{(P_{\text{H}_2\text{S}} X_{\text{M}_2\text{CO}_3})} \quad (7)$$

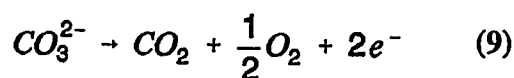
with

$$X_{\text{M}_2\text{S}} + X_{\text{M}_2\text{CO}_3} = 1 \quad (8)$$

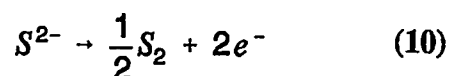
By this analysis, a process gas with a composition of 14.4%  $\text{CO}_2$ , 6.2%  $\text{H}_2\text{O}$ , and 100 ppm  $\text{H}_2\text{S}$  with a run temperature of 973 K will correspond to an electrolyte composition of 0.6% sulfide and 99.4% carbonate. Post-run quantitative chemical analysis of membranes used in these experiments has shown good agreement with predicted electrolyte sulfide levels. Figure 1 shows a comparison of

calculated equilibrium sulfide levels and the corresponding experimentally determined sulfide compositions.

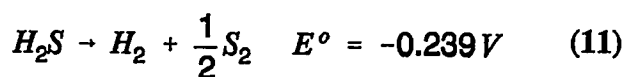
The direct oxidation of carbonate:



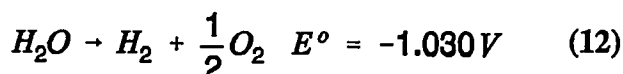
occurs at a standard potential some 0.70 V more positive than that for sulfide:



When the half-cell reactions (3) and (10) are summed, the resulting cell reaction and standard potential at 900 K is:



and when the half-cell reactions (4) and (9) are summed, the resulting cell reaction and standard potential are:



This shows an electrochemical potential 'window of operation' between the two cross cell reactions. If the cross-cell potential (cathode to anode) with current applied to the cell is kept below the level required for the sulfide transport reaction (11) yet above the level required for the carbonate transport reaction (12), then sulfide is preferentially transported across the cell and  $\text{H}_2\text{S}$  is preferentially removed from the process gas stream.

## Theoretical Potentials and Kinetics

The equilibrium potential for combined reactions (3) and (10) is:

$$E = E^\circ - \frac{RT}{nF} \ln \left( \frac{P_{\text{H}_2\text{cathode}} P_{\text{S}_2\text{anode}}^{\frac{1}{2}} a_{\text{S}^{2-}\text{cathode}}}{P_{\text{H}_2\text{S}\text{cathode}} a_{\text{S}^{2-}\text{anode}}} \right) \quad (13)$$

Additional voltage is required to run the



separation cell due to irreversibilities. These losses originate primarily from three sources: ohmic polarization ( $\eta_{ohm}$ ), concentration polarization ( $\eta_{conc}$ ), and activation polarization ( $\eta_{act}$ ) [8].

Ohmic polarization can be described by using Ohm's Law:

$$\eta_{ohm} = IR \quad (14)$$

where  $I$  is the current flowing through the cell and  $R$  is the total cell resistance which includes electronic, ionic and contact resistances.

Several processes contribute to concentration polarization: slow diffusion in the gas phase through the electrode pores, solution/dissolution of reactants/products into/out of the electrolyte, and diffusion of reactants/products through the electrolyte to/from the electrochemical reaction site. For the purposes of our analysis, concentration polarization was estimated by the following equation:

$$\eta_{conc} = \frac{RT}{nF} \ln \left( 1 - \frac{i}{i_L} \right) \quad (15)$$

where  $i$  is the current density applied to the cell and  $i_L$  is the limiting current density dictated by the rate at which reagent can be transported to the electrode surface. The derivation of this equation is beyond the scope of this paper, but the reader is referred to reference [8] for a complete derivation.

Use of equation (15) requires an estimation of the limiting current,  $i_L$ . Since  $i$  is linked to the rate of transport of  $H_2S$  to the electrode surface it can be described by Fick's first law of diffusion:

$$i = \frac{nFD(C_{H_2S_B} - C_{H_2S_S})}{\delta} \quad (16)$$

where  $D$  is the diffusion coefficient of the reacting species,  $C_{H_2S_B}$  is the concentration of  $H_2S$  in the

bulk,  $C_{H_2S_S}$  is the concentration of  $H_2S$  at the electrode surface, and  $\delta$  is the thickness of the diffusion layer. The limiting current,  $i_L$  is the maximum rate at which  $H_2S$  can be supplied to the electrode and occurs when  $C_{H_2S_S} = 0$ :

$$i_L = \frac{nFDC_{H_2S_B}}{\delta} \quad (17)$$

The thickness of the diffusion layer above the electrode surface,  $\delta$ , is not well defined in this system. However, the limiting current density can be estimated using the average mass transfer coefficient,  $k_m$ , for the geometry involved. Thus, the estimation of the limiting current density becomes:

$$i_L = nFk_m\rho \frac{(y_{inlet} - y_{exit})}{\ln \left( \frac{y_{inlet}}{y_{exit}} \right)} \quad (18)$$

where  $\rho$  is the molar density of the gas phase,  $y_{inlet}$  is the mole fraction of  $H_2S$  entering the removal cell, and  $y_{exit}$  is the mole fraction of  $H_2S$  exiting the cell. The average mass transfer coefficient,  $k_m$ , is given by the Sherwood number defined as:

$$N_{Sh} = \frac{k_m D_{eq}}{D} \quad (19)$$

where  $D_{eq}$  is defined as the equivalent channel diameter above the electrode surface:

$$D_{eq} = 4r_H = \frac{4(\text{cross sectional area})}{(\text{wetted perimeter})} \quad (20)$$

The Sherwood number is an empirical term and has been tabulated for a variety of flow channel geometries and physical characteristics of the gas phase [22].

The activation polarization at the cathode and the anode of the cell is tied to the rates of the electrochemical reactions occurring at these

electrodes. There is a close similarity between electrochemical and chemical reactions in that both involve an activation barrier that must be overcome. The standard model to describe the current-overpotential relationship behind these electrochemical kinetics is the Butler-Volmer equation [23]:

$$i = i_0 \left[ \exp\left(\frac{\alpha_a F \eta_{act, electrode}}{RT}\right) - \exp\left(\frac{-\alpha_c F \eta_{act, electrode}}{RT}\right) \right] \quad (21)$$

For specified electrochemical parameters  $\alpha_a$ ,  $\alpha_c$ , and  $i_0$  which must be determined experimentally, the activation overpotential  $\eta_{act, electrode}$  can be solved for at a specified applied current,  $i$ .

The total polarization at each electrode is the sum of activation polarization ( $\eta_{act, electrode}$ ) and the concentration polarization ( $\eta_{conc, electrode}$ ):

$$\eta_{electrode} = \eta_{act, electrode} + \eta_{conc, electrode} \quad (22)$$

The effect of polarization is to shift the Nernstian potential of the electrode ( $E_{electrode}$ ) to a new value ( $V_{electrode}$ ):

$$V_{electrode} = E_{electrode} \pm |\eta_{electrode}| \quad (23)$$

The cross cell voltage includes ohmic polarization and is defined as:

$$V_{cell} = V_{cathode} - V_{anode} - IR \quad (24)$$

The lines presented in Figure 3 were generated analytically using this approach. Figure 3 is presented to demonstrate the relative magnitudes of the different components of the cell potential and is not intended as anything other than an illustration of the expected cell polarizations in a hypothetical laboratory scale removal cell with a perfectly manufactured membrane. The conditions assumed consisted of a cathodic flow rate of a coal synthesis gas equal to the anodic flow rate of  $N_2$  sweep gas (0.0002  $m^3/min$ ), a system pressure of 1 atmosphere, a run

temperature of 898 K, and the polishing of  $H_2S$  from 100 ppm down to 10 ppm. The cathodic and anodic exchange current densities were estimated at 400  $Amp/m^2$  from the results of the free electrolyte studies performed by Banks [9] and White [10]. The exchange coefficients,  $\alpha_a$  and  $\alpha_c$ , were assumed to each be unity. Ohmic resistance across the cell was estimated to be  $1\Omega$  [11]; and the superficial surface area of both the cathode and the anode was  $0.00079 m^2$  ( $7.9 cm^2$ ).

Examination of Figure 3 shows that the calculated activation polarization at both the cathode and the anode is negligible. This shows extremely rapid electrochemical kinetics when compared to diffusion effects in the gas phase and in the electrolyte. All cross-cell potentials are shown to be due primarily to concentration polarization effects. Examination of this illustration shows that at 90% removal (100 ppm  $H_2S$  going to 10 ppm  $H_2S$ ), a total cross-cell potential of only about -0.660 V (cathode to anode) is expected.

Since the carbonate transport reaction (12) is parallel to the sulfide transport reaction (11), some current to the cell will also act to transport  $CO_2$  across the cell. The minimum required potential for this reaction is predicted by the Nernst equation for reaction (12):

$$E = E^\circ - \frac{RT}{nF} \ln \left[ \frac{P_{CO_2, anode} P_{O_2, anode}^{1/2} P_{H_2, cathode} a_{CO_3^{2-}, cathode}}{P_{CO_2, cathode} P_{H_2O, cathode} a_{CO_3^{2-}, anode}} \right] \quad (25)$$

This means that there is a maximum current efficiency with respect to  $H_2S$  removal for any given  $H_2S$  removal, depending on gas composition and the cross-cell potential required for the desired separation of  $H_2S$ . By solving the carbonate transport Nernst equation, (25), at a given cross-cell potential for the  $CO_2$ ,  $H_2$ , and  $H_2O$  levels in the cathode gas and  $CO_2$  and  $O_2$  levels in the anode gas, the extent of this parallel carbonate transport reaction can be determined. This assumes that the electrode kinetics for sulfide and carbonate transport contribute negligible activation overpotential and that concentration overpotential for  $CO_2$  removal is also negligible (a reasonable

assumption since in this case the concentration is some three orders-of-magnitude higher for  $\text{CO}_2$  and  $\text{H}_2\text{O}$  than for  $\text{H}_2\text{S}$ , with approximately 13%  $\text{CO}_2$  and 3.3%  $\text{H}_2\text{O}$  in the cathode gas).

The extent of the anode  $\text{CO}_2$  production with %  $\text{H}_2\text{S}$  removal is presented in Figure 4. Current efficiency is expected to drop to 35% at 90%  $\text{H}_2\text{S}$  removal. This means that, theoretically, applied current to the cell must be increased by a factor of about 3 over stoichiometric current to achieve this removal level. The excess current goes to reduction of  $\text{CO}_2$  and  $\text{H}_2\text{O}$  at the cathode and production of anodic  $\text{CO}_2$ . Even with a current efficiency of only 35%, power costs to perform this removal are negligible, as shown later.

While the above analysis suggested that electrochemical polishing of  $\text{H}_2\text{S}$  from coal gas was possible, experiments were needed to verify that removal of  $\text{H}_2\text{S}$  from very low inlet levels could be attained in the presence of high concentrations of  $\text{CO}_2$  and  $\text{H}_2\text{O}$ . The following is a description of those experiments and a discussion of the results.

## Experimental Methods

**Cell Geometry.** The cell housings were machined from MACOR (machinable ceramic) blocks. The housings were 0.076 m diameter and 0.025 m deep cylinders. Gas flow channels were machined into the large surface faces and gas flow tubes were connected to supply process and sweep gases to the cell (see Figure 5). Once the electrodes and membrane materials were ready for testing, the electrodes were set onto platinum current collectors placed on top of the gas flow channels on one side and contacting the membrane on the other (see Figure 6). The active superficial electrode area was  $0.00079 \text{ m}^2$  ( $7.9 \text{ cm}^2$ ), of which  $0.00064 \text{ m}^2$  ( $6.4 \text{ cm}^2$ ) was exposed to the process gas, the remainder occluded by the flow guides. The full cell was then assembled by placing the membrane between the MACOR

blocks and connecting the gas supply lines to the assembly within a custom designed oven (see Figure 7).

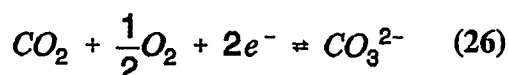
**Electrode Preparation.** Weaver surveyed several possible electrode materials for this system [3,12,13]. Of these, lithiated Ni and NiO electrodes were used for this study. Ni electrodes were donated to this research by the Energy Research Corp. (ERC) as 0.20 m by 0.28 m sheets; average porosity was between 75 and 80%. A die was used to cut 0.032 m diameter electrodes from this sheet. These electrodes were then soaked in 1 M LiOH and then dried. When the Ni electrodes were used, the electrodes were then loaded into the cell and the run was started. If NiO electrodes were to be used, the electrodes were placed between two sintered  $\text{Al}_2\text{O}_3$  sheets and loaded into an oven at 923 K under atmospheric air for at least six hours. Gravimetric analysis of these oxidized electrodes showed that the Ni was at least 96% converted to NiO.

**Membrane Preparation.** The membrane between the two electrodes serves two purposes. First it holds the electrolyte in place between the cathode and the anode by capillary action and prevents the molten salts from completely flooding the porous electrodes; second, the membrane acts to prevent the bulk diffusion of gases between the cathode and the anode side of the cell.

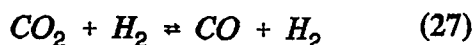
Manufacture of the membrane involved making a composite structure consisting of woven zirconia cloth which was densified with MgO powder. The structure consisted of a single mat of ZYW-30A zirconia cloth (purchased from ZIRCAR Inc.) layered with two tapes of MgO ceramic powder suspended within acrylic binder K565-4 (purchased from Metoramic Sciences, Inc.). An oxygen sweep was applied to both sides of the cell and the cell was loaded into the furnace for heat-up. The binder from the MgO tapes was burned out at 648 K overnight. The temperature was then ramped up to run temperature and the electrolyte was wicked into the MgO powders and

zirconia cloth. Process gas was then supplied to the cell and the electrolyte was allowed to reach the equilibrium described by reaction (5).

**Pre-Run and Analysis.** Once assembled, the cell was loaded into a custom-made furnace and connected to the process and sweep gas supply lines. The exit gas from the cathode was routed to a Beckman IR scanner for reading CO<sub>2</sub> levels and a Teledyne UV scanner for reading H<sub>2</sub>S levels. A Hewlett/Packard gas chromatograph fitted with a flame photometric detector was also used for reading H<sub>2</sub>S levels exiting the cell. A gold reference electrode was placed on the surface of the membrane away from either process electrode and supplied with a flow of 15% CO<sub>2</sub> / 3% O<sub>2</sub> / balance N<sub>2</sub> mixture to maintain a stable thermodynamic reference potential by reaction (26):



Melting of the electrolyte was verified by a sudden improvement in the seals formed by contact of the membrane with the MACOR surfaces along with observed electrical conductivity through the cell. Process gas, consisting of specified levels of CO<sub>2</sub>, CO, H<sub>2</sub>, H<sub>2</sub>O, and H<sub>2</sub>S was then supplied through the cell via a stainless steel shift reactor which allowed the water/gas shift reaction, (27), to go to equilibrium at the process temperature before the gases entered the cell.



**Test Procedure.** Once the cell had reached run temperature, conductivity across the cell was estimated by current interrupt. The equilibrium potentials at the cathode and anode were measured with respect to the reference electrode. Base-line exit cathode gas compositions were also measured at this point. Current was

then applied to the cell in a step-wise fashion and the cell was allowed to equilibrate for at least 15 minutes after each current step. Once stabilized, potentials with respect to the reference electrode and exit gas compositions were measured.

## EXPERIMENTAL RUN RESULTS

This study was primarily concerned with improving H<sub>2</sub>S selectivity and removal efficiency through the development of a gas-impermeable membrane. Removal of H<sub>2</sub>S and CO<sub>2</sub> from the process gas stream at the cathode and evolution of products at the anode was measured over a range of gas compositions representing sour coal gas which had been cleaned of H<sub>2</sub>S to a level of 100 ppm to 10 ppm H<sub>2</sub>S. Process temperature and gas flow-rates were also varied to be representative of conditions likely to be of industrial interest.

The maximum removals reported below are removals of H<sub>2</sub>S and CO<sub>2</sub> on a zero current basis to compensate for the chemical scrubbing effect of the non-equilibrium composition electrolyte in the membrane. H<sub>2</sub>S removal is therefore defined as:

$$\% \text{ Removal} = \left[ \frac{\text{Exit Conc. No Current} - \text{Exit Conc. With Current}}{\text{Exit Conc. No Current}} \right] \times 100 \quad (28)$$

Selectivity is defined by the following equation:

$$\text{Selectivity} = \left[ \frac{\% \text{ Removal}_{\text{H}_2\text{S}}}{\% \text{ Removal}_{\text{CO}_2}} \right] \left[ \frac{\% \text{ CO}_{2\text{Inlet}}}{\% \text{ H}_2\text{S}_{\text{Inlet}}} \right] \quad (29)$$

If selectivity is equal to one, removals of H<sub>2</sub>S and CO<sub>2</sub> are equivalent. If the selectivity is greater than one, H<sub>2</sub>S is preferentially removed.

A total of nine successful experiments were performed. Two of these are presented here. Reproducibility of removal trends was observed in all of these runs.

**Polishing Application with 100 ppm H<sub>2</sub>S in Coal Gas.** This experimental run used a simulated coal gas with a composition of 14.3% CO<sub>2</sub>, 50.8% CO, 4.8% H<sub>2</sub>O, 30.1% H<sub>2</sub>,

and 100 ppm  $\text{H}_2\text{S}$  after shift reaction. It used two tapes of  $\text{MgO}$  and one mat of 0.00076 m thick zirconia cloth as the membrane matrix material. The electrodes were both lithiated  $\text{NiO}$ . The acrylic binders used in the  $\text{MgO}$  tapes (Metoramics K565-4 binder system) were burned out under an  $\text{O}_2$  atmosphere at 623 K and the  $\text{Li/K}$  eutectic-composition electrolyte was added with the cell at run temperature. The inlet gases were passed through a stainless steel shift reactor to allow them to come to their equilibrium composition before passing through the cell.

The cell temperature was 973 K; at this temperature, analysis of the limiting current densities within the system, as outlined earlier, shows that the gas phase limiting current density was  $11.5 \text{ Amp/m}^2$  while the membrane limiting current density was  $32.9 \text{ Amp/m}^2$ . This shows that the maximum flux of material through the membrane is three time greater than the maximum flux of material through the gas phase to the membrane surface.  $\text{H}_2\text{S}$  removal at a variety of flow-rates was observed and is presented here in Figure 8 through Figure 11. Cell polarization is presented in Figure 12. Parametric numbers on this graph are cathodic flowrates in  $\text{m}^3 \times 10^{-6}$ . The measured cross-cell resistance was measured by current-interrupt and was found to be about  $1\Omega$ . With the maximum current applied to the cell of 0.02 Amp, this corresponds to 0.02 V of ohmic loss. This is slight compared to the overall cross-cell potential, which includes concentration effects and other overpotentials.

An  $\text{H}_2\text{S}$  removal level of 89.2% (exit  $\text{H}_2\text{S}$  level brought from 89.5 ppm to 9.7 ppm with applied current) was achieved. Cell current efficiency and species removal for this run are presented in Figure 11. At only slightly above stoichiometric current,  $\text{H}_2\text{S}$  current efficiency is 40%. The remaining 60% of the 0.0012 Amp applied to the cell at this point would remove only 62.9 ppm  $\text{CO}_2$  from the process gas stream with 19.1%  $\text{CO}_2$  entering the cell; such transport of  $\text{CO}_2$  is completely negligible. Even at the highest applied current to the cell the cell at the cathode flow-rate of  $0.000088 \text{ m}^3/\text{min}$ , an  $\text{H}_2\text{S}$  current

efficiency of only 4.6% (see Figure 11). This  $\text{H}_2\text{S}$  current efficiency would correspond to a drop in  $\text{CO}_2$  of only 0.17%. The theoretical maximum current efficiency for this system at 89% removal of  $\text{H}_2\text{S}$  would be approximately 35%.

**Polishing Application to 19 ppm  $\text{H}_2\text{S}$  in Coal Gas.** Several experimental runs using 1 mat of 0.00076 m thick zirconia cloth which was rigidized to 60.8% voids using sub-micron particles of  $\text{ZrO}_2$  within an aqueous slurry (44 wt%) were performed. These were accomplished by cutting a 0.076 m diameter mat of zirconia cloth and soaking it in Zircar brand Rigidizer. The mat soaked the aqueous slurry into its voids and left the  $\text{ZrO}_2$  particles behind after the  $\text{H}_2\text{O}$  was dried out. Two tapes of  $\text{MgO/ZrO}_2$  (4 micron particle size, Aesar) in vinyl binder (B73305 Metoramics binder system) were layered on each side of the rigidized mat to further densify the structure. The electrolyte was eutectic  $\text{Li/K}$  carbonate and was added to the cell as a pressed disk before heat-up. The electrodes were lithiated  $\text{Ni}$ . The housings were MACOR with Al foil gaskets. The run temperature was 923 K. After binder burnout and electrolyte melting, fuel gas of composition 15.2%  $\text{CO}_2$ , 44.2%  $\text{CO}$ , 5.4%  $\text{H}_2\text{O}$ , 35.0%  $\text{H}_2$ , (after shift reaction) with 18.8 ppm  $\text{H}_2\text{S}$  was put through the cell. This gas composition and temperature gives an estimated equilibrium-membrane-sulfide level of 0.06 mole% sulfide. The gas-phase limiting-current density was estimated to be  $1.8 \text{ Amp/m}^2$  and the membrane limiting current density was  $3.4 \text{ Amp/m}^2$ .

$\text{H}_2\text{S}$  removal data was taken at a variety of cathodic flow-rates. Current efficiency and species removal for this run are presented in Figure 13.  $\text{H}_2\text{S}$  levels were brought from 15.8 ppm exiting the cell with no current applied, to 4 ppm  $\text{H}_2\text{S}$  with 0.2 Amp applied. The selectivity of this membrane was high (selectivity of  $2 \times 10^4$ ), but some  $\text{CO}_2$  transport was observed.  $\text{H}_2\text{S}$  current efficiency was low (no higher than 1.2%) because of  $\text{H}_2$  cross-over.

## ECONOMIC PROJECTION

Accurate cost figures for processes early in development are impossible to project. However, it is possible to roughly estimate the power and capital requirements to assess viability. The power consumption has been shown to be overwhelmingly due to cell current, which is near stoichiometric. Cell voltage, as shown earlier, can be estimated with reasonable accuracy. Capital costs can be estimated by analogy with Molten Carbonate Fuel Cell (MCFC) stacks, whose design these cells will mimic.

The proposed Electrochemical Membrane Separator (EMS) design is compared to a Sulfinol process with a Claus plant for sulfur recovery. The base case is provided in a discussion of coal gas processing economics by Oak Ridge National Laboratory (ORNL-5425)[14]. The medium-Btu gas treating facility discussed here treats 590 million kg/hr of coal synthesis gas with composition outlined in Table II. The capital cost for a Sulfinol plant consisting of two parallel units was estimated at 39.4 MM\$ in the first quarter of 1978. This scales to 145 MM\$ in mid-1987 dollars using Marshall-Swift cost indexes[15]. This does not include costs for cooling the gas stream from gasification temperatures (approx. 1023 K) to Sulfinol process temperature (311 K) or the cost of reheating the gas for feed to the turbines of a cogeneration power plant or an MCFC power plant.

The acid gas stream generated by the Sulfinol plant as an  $H_2S$  level of 28.5 vol%. This is fed to a Claus plant capable of handling a load of 247 metric tons/day of sulfur production. The Claus plant for treating this acid gas had an estimated capital cost of 8 MM\$ in 1978 dollars. This scales to 29.4 MM\$ in 1987 dollars by Marshall-Swift indexes. The combined Sulfinol/Claus plant capital cost for treating this coal synthesis gas is therefore 174 MM\$ in 1987 dollars (not including gas cooling and reheating costs).

The capital cost of the EMS is more difficult to estimate than the power consumption.

In the MCFC, current densities greater than 1600 Amp/m<sup>2</sup> are routinely achieved. There are, however, two major differences between the MCFC and the EMS. In the MCFC the gases are relatively rich, as compared with the dilute reactants treated in the EMS. Further, there is no competing reaction to dilute the current carrying anion. Thus, gas-phase diffusion of  $H_2S$  or sulfide migration in the membrane may limit the current density and define the needed active membrane area for a given duty.

Gas-phase transport can be controlled through proper design of the gas channels [16]; pore diffusion in the electrodes has been found not limiting in similar designs for  $CO_2$  removal to very low levels [17]. The limiting step for removal in this analysis is gas diffusion of  $H_2S$  to the cathode of the cell. This was found by comparison of species diffusion through the gas phase to species diffusion through the molten salt electrolyte. The capital cost estimation assumes that the membranes are available as 1.2 m by 1.2 m squares (as used in MCFC units) and are arranged in 'stacks' of parallel removal cells with the process gas equally divided to each cell. Each 'stack' removes approximately 90% of the  $H_2S$  fed to it. There is also assumed to be series of parallel 0.003 m by 0.003 m flow channels directing gas flow across the surface of each electrode. A break-down of the costs associated with the EMS stacks is provided in Table III [18]. For an EMS system operating at a pressure of 42.7 atm at gasification temperatures of 1023 K, the limiting current density for the first stack (which removes  $H_2S$  from 0.9% to 900 ppm) is 1133 Amp/m<sup>2</sup>. The second stack (900 ppm to 90 ppm  $H_2S$ ) has a limiting current density of 113.2 Amp/m<sup>2</sup>. The third stack (90 ppm to the final  $H_2S$  level of 6 ppm) has a limiting current density of 9.986 Amp/m<sup>2</sup>.

Once the limiting current density of the stack is known, the total stack area (or number of cells in the stack) can be calculated by dividing the required stack current by the stack limiting current density. The  $H_2S$  stack current is assumed to be stoichiometric for the moles of  $H_2S$

removed. The total molar flow-rate to be treated by the EMS system is 18.8 kgmole/sec. Thus, the  $\text{H}_2\text{S}$  current applied to the first stack (0.9% to 900 ppm  $\text{H}_2\text{S}$ ) is  $2.82 \times 10^7$  Amps, the second stack (900 ppm to 90 ppm  $\text{H}_2\text{S}$ ) requires  $2.94 \times 10^6$  Amps, and the third stack (90 ppm to 6 ppm  $\text{H}_2\text{S}$ ) requires  $3.05 \times 10^5$  Amps. For the first stack, with  $I_{\text{H}_2\text{S}} = 2.82 \times 10^7$  Amps and  $i_{\text{d,H}_2\text{S}} = 1133$  Amps/ $\text{m}^2$ , the total active membrane area is 24889  $\text{m}^2$ . If 1.2  $\text{m}^2$  by 1.2  $\text{m}^2$  membranes are used in this application, this comes to 17284 electrochemical cells in the first stack. The active membrane area of the second stack is 25971  $\text{m}^2$  (18036 cells), and the active membrane area for the third stack is 30543  $\text{m}^2$  (21210 cells).

Stack power requirements depend on the total current driving the  $\text{H}_2\text{S}$  removal and the cross-cell potential of the removal cell. Because of parallel  $\text{CO}_3^{2-}$  transport, current levels greater than stoichiometric  $\text{H}_2\text{S}$  removal current are required. By the analysis presented earlier in this paper, current efficiency at 90%  $\text{H}_2\text{S}$  removal was found to be 89.1% in the first stack with a cross cell potential of 0.764 Volts. At this current efficiency, the first stack requires 24180 kW. The second stack has a current efficiency of 81.6% with a cross cell potential of 0.665 Volts; at these conditions this translates to 2396 kW required by the stack. The third stack has a current efficiency of 51.6% and a cross cell potential of 0.611 Volts; at these conditions the third stack requires 361 kW. This sums to 26937 kW for the entire system. In these calculations, cell resistivity was estimated to be  $2.5 \times 10^{-5} \Omega \text{ m}^2$  after MCFC results for tape-cast electrolyte membranes of  $5.0 \times 10^{-4}$  m thickness and containing 40 wt% electrolyte [19].

The system costs for the EMS plant are listed in Table III. Note in Figure 14 that there is no need for heating the coal synthesis gas stream since the coal gasification EMS plant operates at gasification temperatures. There is, therefore, no need for a regenerative heat exchanger system to cool for  $\text{H}_2\text{S}$  removal and reheat the gas for use in a cogeneration power plant or MCFC. Since sulfur condenser costs are negligible compared to electrochemical cell stack costs, there are

effectively no heat exchanger costs for this plant. An overall operation cost comparison is shown in Table IV. Note that even with the lower current efficiencies in the polishing steps of the process, the treating cost per 1000 SCM of gas treated are still competitive (in fact, even if the power requirements were doubled, the comparatively low capital investment of the proposed technology compared to the conventional technology still provides favorable economics). The overall operation cost of the two facilities was estimated after the method reported by Maddox in Gas and Liquid Sweetening [20]. The utilities cost and sulfur credit used in this comparison are the same used in a previous natural gas treating plant analysis by Fluor Technology, Inc. [21].

The net treating costs presented in Table IV (\$5.644 / 1000 SCM for conventional technology compared to \$2.192 / 1000 SCM for the proposed EMS technology) refers to the cost associated with sweetening the gas and producing sulfur. The addition of several plant areas would be required to develop a total cost-of-gas-treating. That is, the Net Treating Cost presented here relates only to the systems described and should be used only to establish the relative economic merits of the proposed EMS technology for selective  $\text{H}_2\text{S}$  removal. Once again, the conventional cost of gas treating presented here does not include the cost of cooling the gas for removal of  $\text{H}_2\text{S}$  and reheating the gas to gasification temperatures after treatment. A step which would not be necessary with the proposed EMS technology.

## CONCLUSIONS

Selective removal of  $\text{H}_2\text{S}$  has been demonstrated for polishing application to a coal synthesis gas (100 ppm  $\text{H}_2\text{S}$ ) and for a purification application to coal synthesis gas (10 ppm  $\text{H}_2\text{S}$ ). Electrochemical scrubbing of  $\text{H}_2\text{S}$  from coal synthesis gas at levels higher than 100 ppm has already been shown by Weaver [3,12,13].

The economic study presented in the previous section shows that the proposed technology is economically favorable as a method of coal gas sweetening. The results of the coal gas analysis shows that a  $36.4 \times 10^6$  SCMD coal gas sweetening plant can be operated for \$2.192/1000 SCM using proposed technology, as compared to \$5.644/1000 SCM using conventional technology. The removal results reported here support the design specifications for the last two removal cell stacks in the coal gas plant (more concentrated  $H_2S$  coal gas streams were studied previously by Weaver).

With the development of even more bulk gas-impermeable membranes and the perfection of cell housing passivating techniques, scale up to a pilot facility is imminent.

## ACKNOWLEDGEMENTS

Economic support and additional expertise were provided by the Electric Power Research Institute (EPRI) and the U.S. Dept. of Energy.

## REFERENCES

- [1] J. Winnick, Advances in Electrochemical Science and Engineering, Vol. 1, edited by H. Gerischer and C. Tobias, VCH Publishers, Weinheim, Germany, (1990), 205.
- [2] H. Lim and J. Winnick, *J. Electrochem. Soc.*, **131**, (1984), 562.
- [3] D. Weaver and J. Winnick, *J. Electrochem. Soc.*, **139**, (1992), 492.
- [4] S. Alexander and J. Winnick, *AIChE journal*, **40**, (1994) 613.
- [5] D. McHenry and J. Winnick, *AIChE journal*, **40**, (1994) 143.
- [6] R. Probst and R. Hicks, Synthetic Fuels, McGraw-Hill, New York, (1982) 124.
- [7] A. More, Sulfur, Sulfur Dioxide, and Sulfuric Acid, Verlag Chemie International Inc. Deerfield Beach, FL, (1984) 30.
- [8] U.S. Dept. of Energy, Fuel Cells: A Handbook, DOE/METC-88/6090, Morgantown West VA, (1988) 8.
- [9] E. Banks and J. Winnick, *J. Appl Electrochem.*, **16**, (1986) 583.
- [10] K. White and J. Winnick, *Electrochem Acta*, **30**, (1985) 511.
- [11] S. Alexander and J. Winnick, *J. Sep'n Sci and Tech.*, **25**, (1990) 2057.
- [12] D. Weaver and J. Winnick, *J. Electrochem Soc.*, **134**, (1987) 2451.
- [13] D. Weaver and J. Winnick, *J. Electrochem Soc.*, **136**, (1989) 1679.
- [14] Oak Ridge National Laboratory, ORNL-5425, Coal Gasification Processes: Energy Technology Review No. 70, Noyes Data Corp. Park Ridge, N.J., (1981) 290.
- [15] Marshall and Swift Publ., Co., *Chem. Eng.* **94**, 4, (1987) 7.
- [16] D. Townley and J. Winnick, *I.E.C. Proc Des.*, **20**, (1981) 435.
- [17] M. Kang and J. Winnick, *J. Appl Electrochem.*, **15**, (1985) 431.
- [18] A. Appleby and F. Foulkes, Fuel Cell Handbook, Van Nostrand Reinhold, New York (1989) 574.
- [19] R. Petri and T. Benjamin, *Proceedings of the 21st Intersociety Energy Conversion Engineering Conference*, Vol. 2, ACS Washington, DC, (1986) 1156.
- [20] R. Maddox, Gas and Liquid Sweetening 2nd ed., Campbell Petroleum Series, Norman, OK (1977) 235.



[21] Fluor Technology Inc., *Fluor Contract 342304*, personal communication with D. Borio, ABB/Combustion Engineering, Windsor, CT, (1990).

[22] F. Incropera and D. DeWitt, Fundamentals of Heat and Mass Transfer, 2nd ed., John Wiley and Sons, New York, (1985) 277.

[23] G. Prentice, Electrochemical Engineering Principles, Prentice Hall, Englewood Cliffs, New Jersey, 1991.

**Table I. Representative Coal Gas Composition**

CO:	15 - 30%
CO <sub>2</sub> :	4 - 25%
H <sub>2</sub> :	12 - 59%
N <sub>2</sub> :	0 - 59%
CH <sub>4</sub> :	2 - 19%
H <sub>2</sub> S:	0.5 - 1.5%
	(Dry Basis)

**Table II. Medium Heating Value Coal Synthesis Gas Composition**

Gas	Flow/10 <sup>-3</sup> kg-hr <sup>-1</sup>	Flow/kmole-s <sup>-1</sup>	Vol%
H <sub>2</sub>	92.33	12.9	68.6
N <sub>2</sub>	14.83	0.147	0.781
CO	97.71	0.971	5.16
CO <sub>2</sub>	64.48	0.407	2.16
H <sub>2</sub> O	3.06	0.047	0.250
H <sub>2</sub> S	19.97	0.163	0.866
CH <sub>4</sub>	178.50	3.10	16.5
C <sub>2</sub>	80.21	0.743	3.95
C <sub>3</sub>	36.25	0.230	1.22
C <sub>4</sub>	12.39	0.059	0.313
C <sub>5</sub>	1.60	0.049	0.260
Total	601.33	18.82	100.0
	(36.4x10 <sup>6</sup> SCMD)		

Pressure, 43.2 bar

Temp., 311 K

Heating Value: 19.1 x 10<sup>6</sup> J-m<sup>-3</sup>

**Table III. Break-Down of Capital Investment for CG EMS (1987 US dollars)**

Electrochemical Membrane Separator Cell Stacks/ \$ x 10<sup>6</sup>

Items:	Stack 1	Stack 2	Stack 3
Ion Exchange Area (m <sup>2</sup> x 10 <sup>3</sup> ):	24.9	26.0	30.5
Membranes in Stack:	17284	18036	21210
Anodes:	2.299	2.402	2.824
Cathodes:	0.948	0.991	1.164
Bipolar Hardware:	1.733	1.811	2.129
Membranes:	0.107	0.112	0.131
Auxiliaries:	0.542	0.566	0.666
Assembly:	2.083	2.176	2.558
Stack Cost:	7.712	8.058	9.472
Rectifier:	4.195	4.383	5.153
Controls & Misc.:	5.845	6.107	7.180
Assembly:	4.600	4.807	5.651
Total Stack Cost:	22.35	23.36	27.46

Total EMS Cost:	73.17
Blowers:	0.101
Heat Exchangers:	negligible
Plant Cost:	73.27
Project Contingency (15%):	10.99
Fixed Capital Investment:	84.26

**Table IV. Operation Cost Comparison, CG  
EMS to Sulfinol (1987 US dollars)**

	<u>Sulfinol</u>	<u>EMS</u>
Fixed Capital Investment (US \$ x 10 <sup>6</sup> )	174.4	84.26
<hr/>		
Direct Operations Costs:		
Utilities (\$ x 10 <sup>6</sup> )		
Steam		
(@ \$5.38/1000 kg):	7.379	0.000
Electricity		
(@ \$0.0524/kW-hr):	2.076	12.20
Raw H <sub>2</sub> O		
(@ \$0.198/m <sup>3</sup> ):	8.456	0.610
Gas Losses		
(@ \$77.1/1000 SCM):	0.000	0.000
Chemical Losses	<u>1.307</u>	<u>0.000</u>
	19.22	12.81
<hr/>		
Operating Labor		
(@ \$10.30/hr):	0.180	0.089
Maintenance		
(@ 4% FCI):	6.976	3.370
Plant General		
(@ 40% Labor):	<u>0.072</u>	<u>0.036</u>
	7.228	3.495
<hr/>		
Total Operating Costs:	26.45	16.31
<hr/>		
Indirect Operating Costs:		
Depreciation		
(@ 10% FCI):	17.44	8.426
Tax & Insurance		
(@ 2.5% FCI):	<u>4.360</u>	<u>2.107</u>
Total Indirect Cost	21.80	10.53
<hr/>		
Cost of Profit		
(@ 25% FCI)	43.60	21.07
(Includes income tax, interest on investment, and reasonable profit)		
<hr/>		
Grand Total Treating Cost:	91.85	47.91
<hr/>		
Sulfur Credit		
(@ \$98/metric ton)	-17.89	-17.89
<hr/>		
Net Treating Cost (Grand Total - Credit)	73.96	30.03
<hr/>		
Treating Cost (\$/1000 SCM)	\$5.644	\$2.292

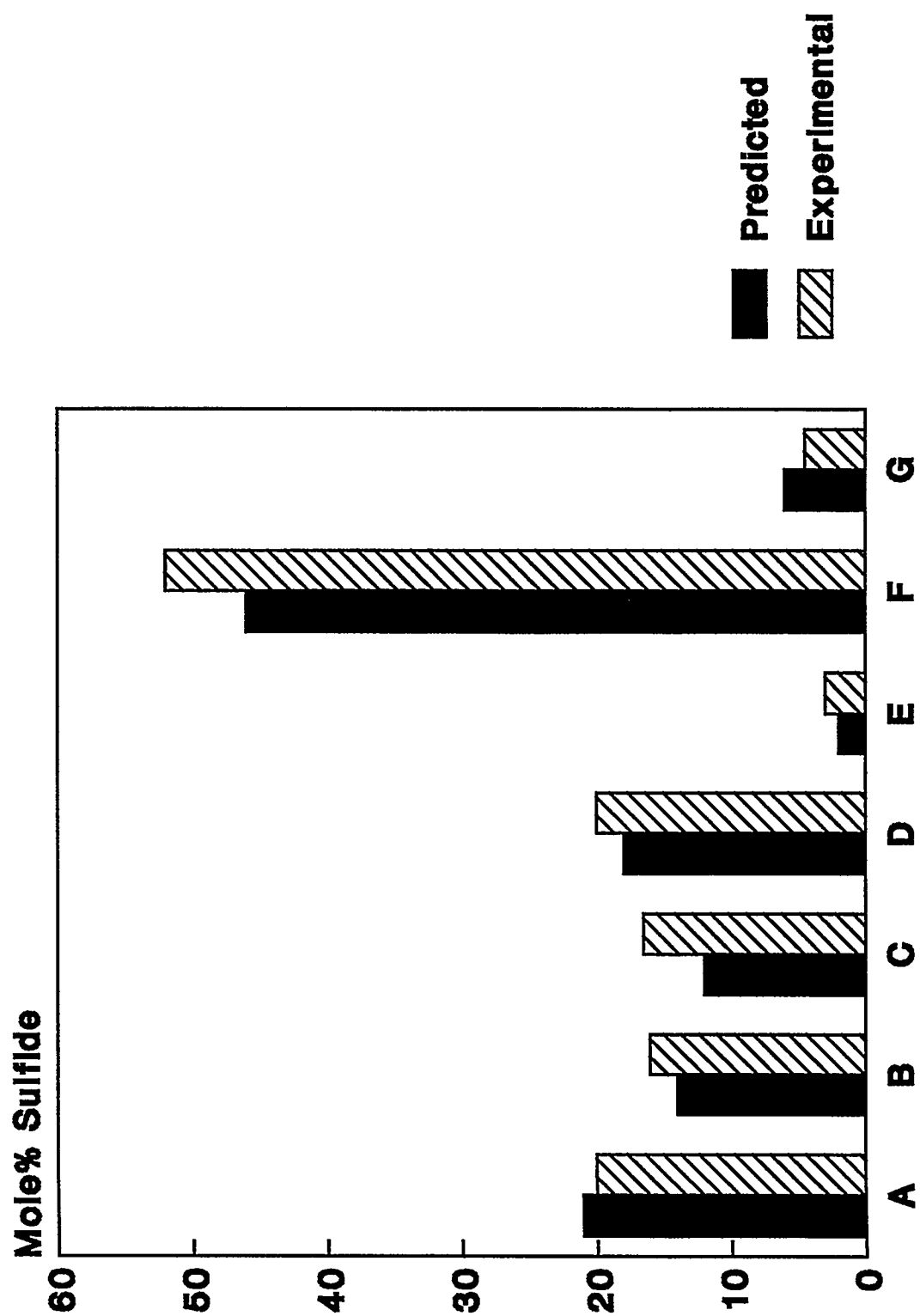


Figure 1. Comparison of Actual Sulfide Levels to Calculated Sulfide Levels in Electrolyte

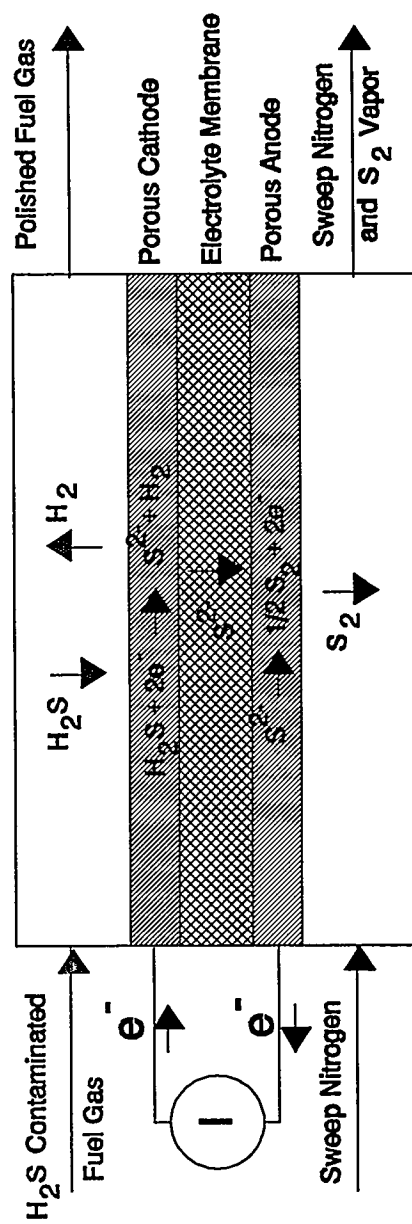


Figure 2. Electrochemical Coal Gas Desulfurization Cell

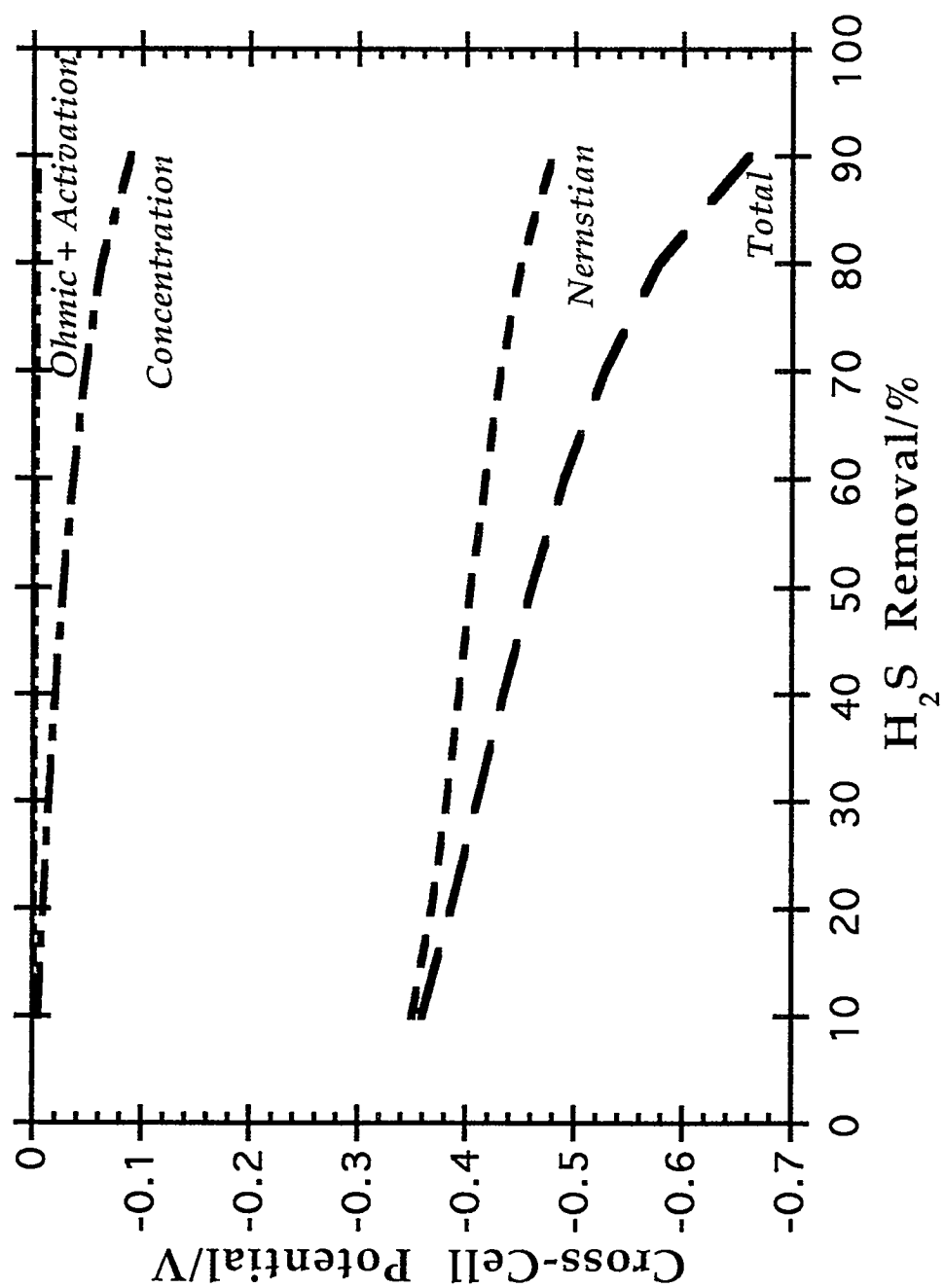


Figure 3. Theoretical Cross Cell Potential vs %  $H_2S$  Removal

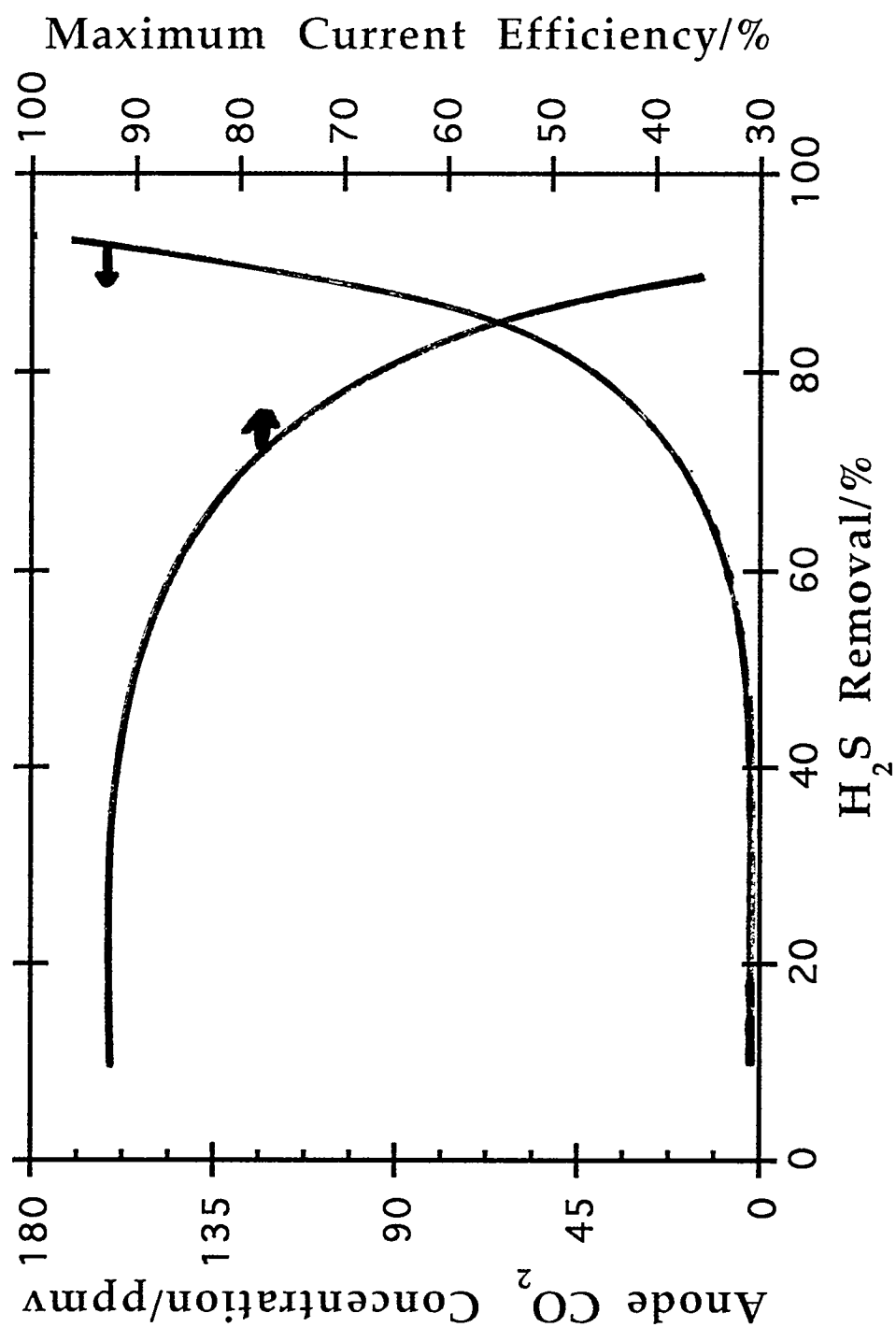
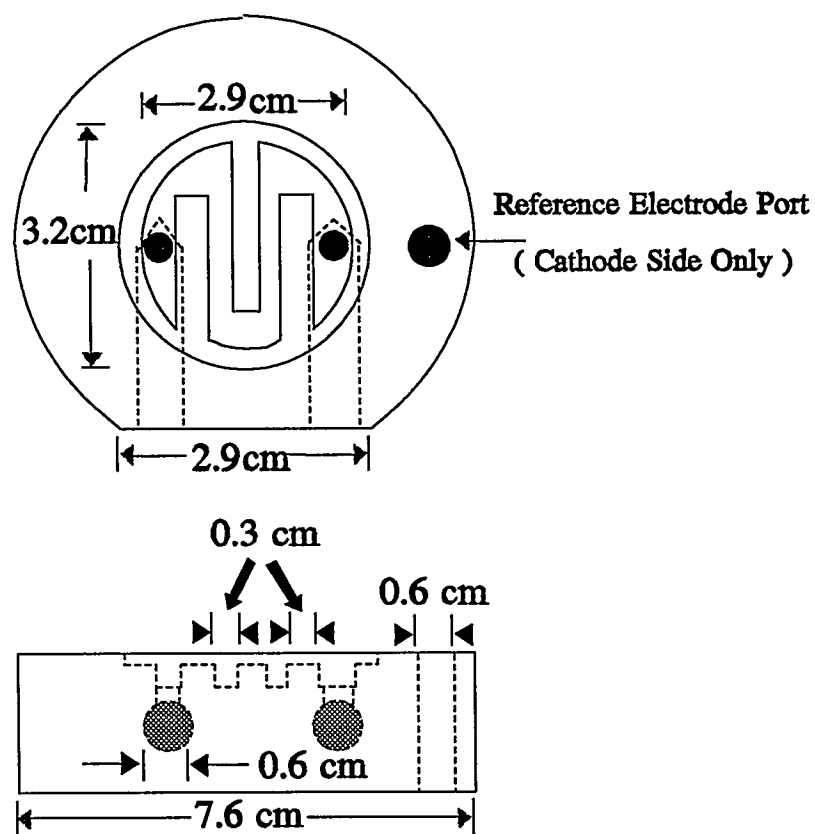
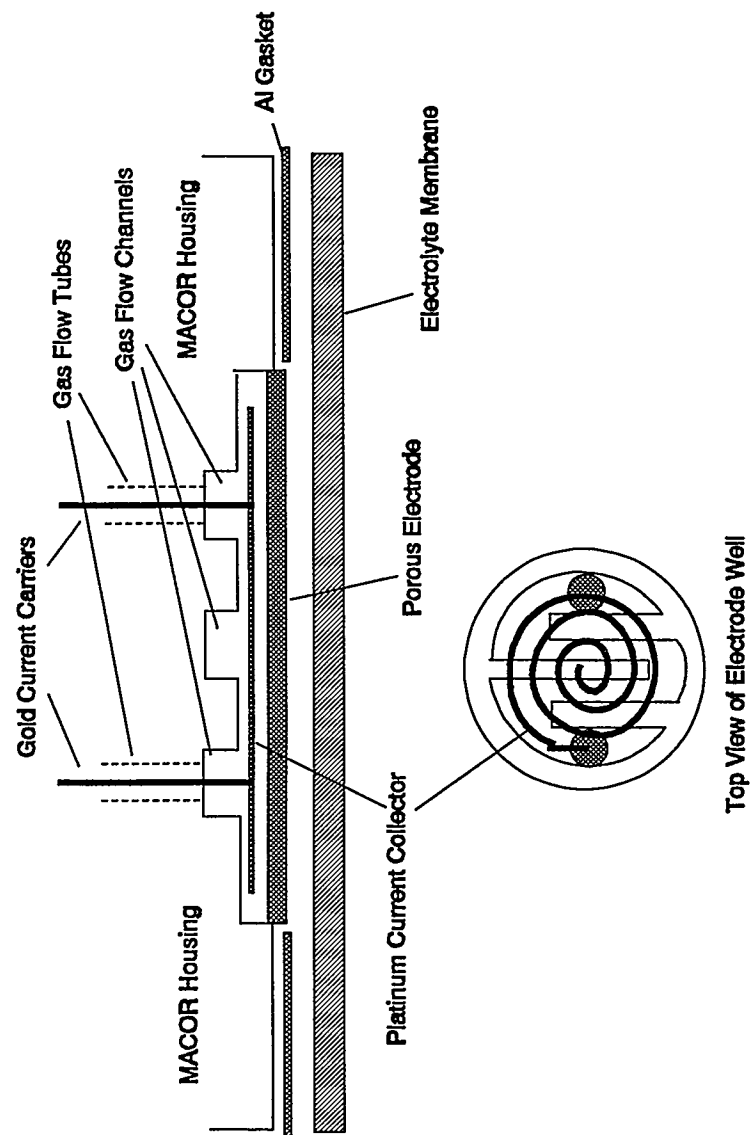


Figure 4. Predicted Anodic  $\text{CO}_2$  Production and Maximum Current Efficiency vs  $\text{H}_2\text{S}$  Removal



**Figure 5. Cell Housing Configuration**





**Figure 6. Housing/Current Collector / Electrode / Gasket / Membrane Configuration**

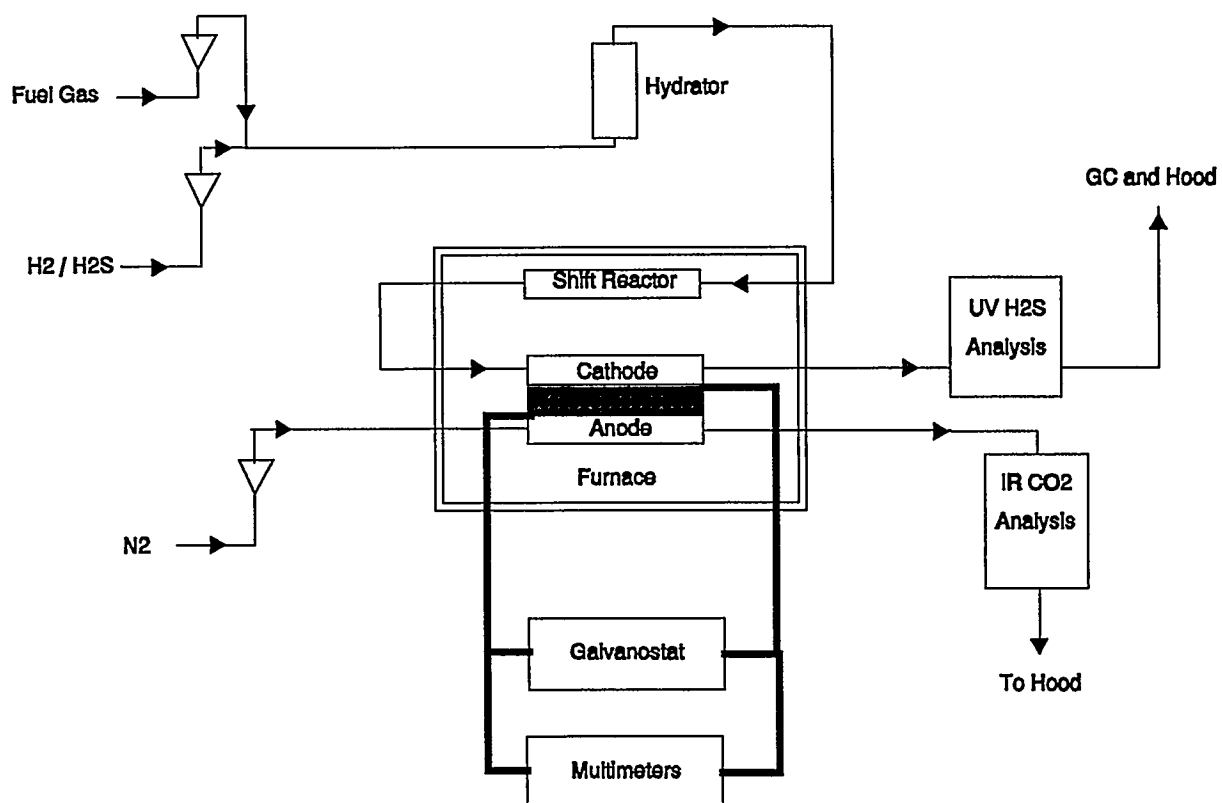


**Figure 7. Experimental Apparatus Configuration for Coal Gas Polishing**

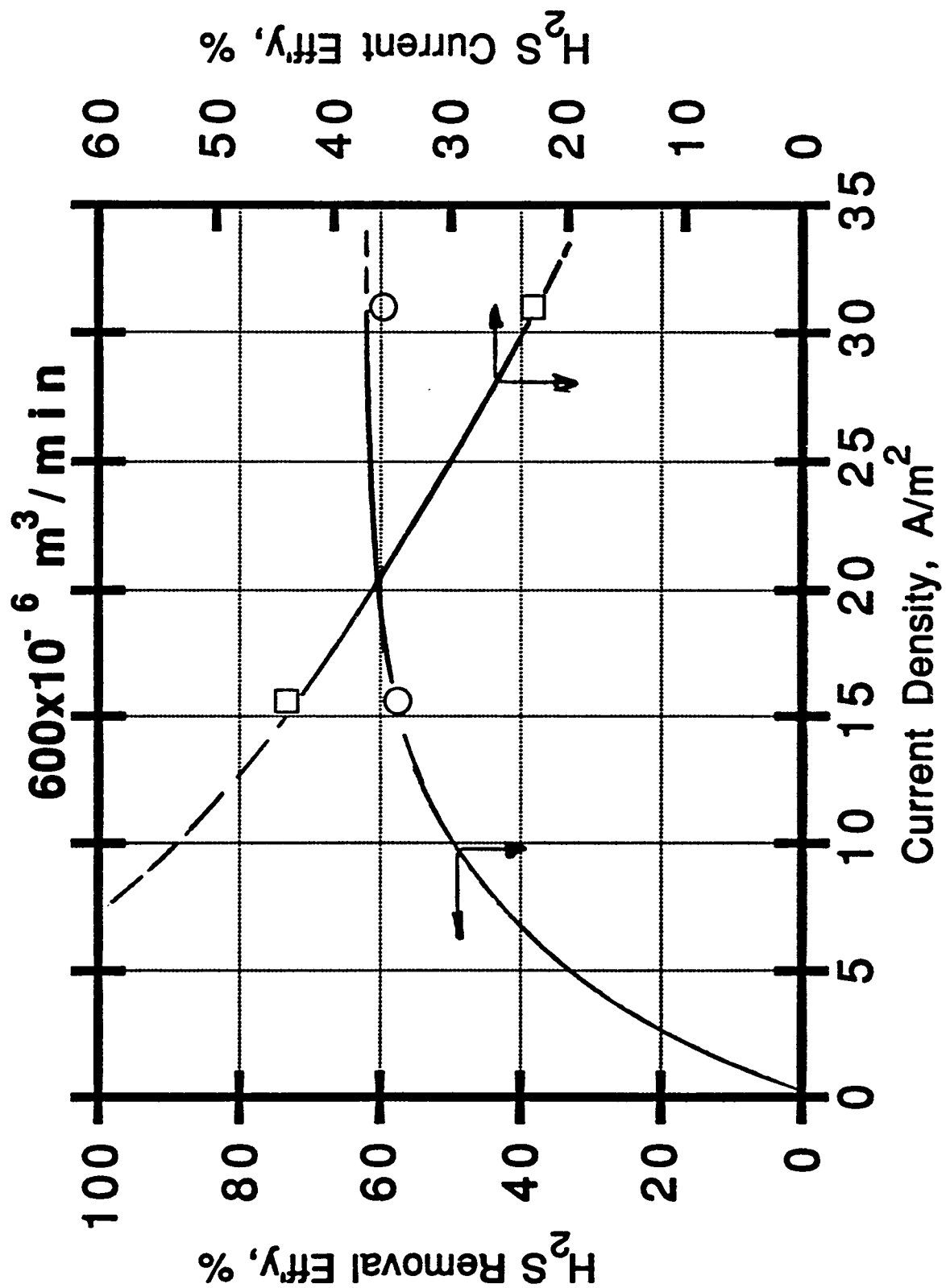


Figure 8. H<sub>2</sub>S Removal and Efficiency vs Applied Current Density, 100 ppm H<sub>2</sub>S, 600 x 10<sup>-6</sup> m<sup>3</sup>·min<sup>-1</sup>

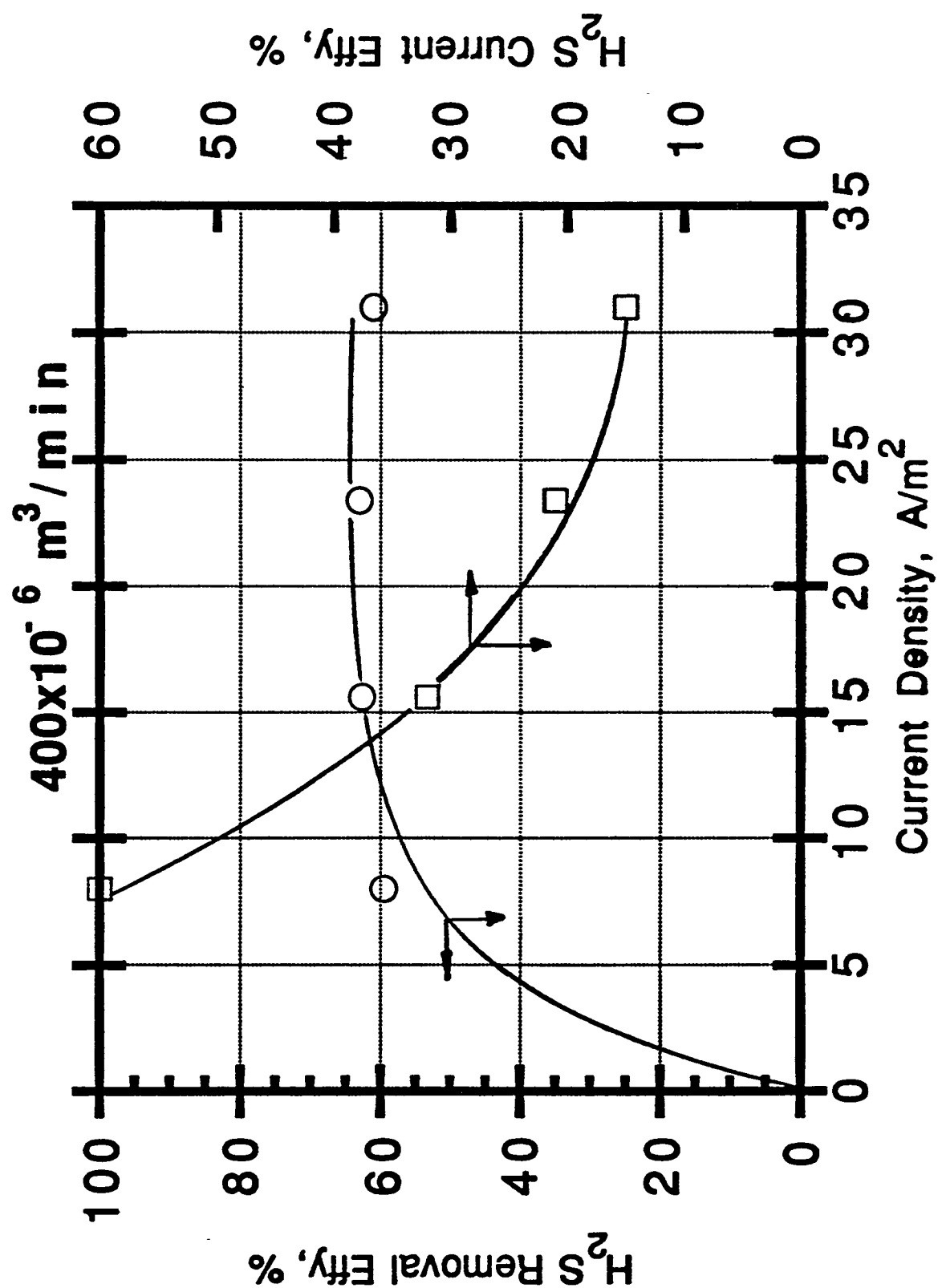


Figure 9.  $\text{H}_2\text{S}$  Removal and Efficiency vs Applied Current Density,  $100 \text{ ppm H}_2\text{S}, 400 \times 10^{-6} \text{ m}^3/\text{min}$

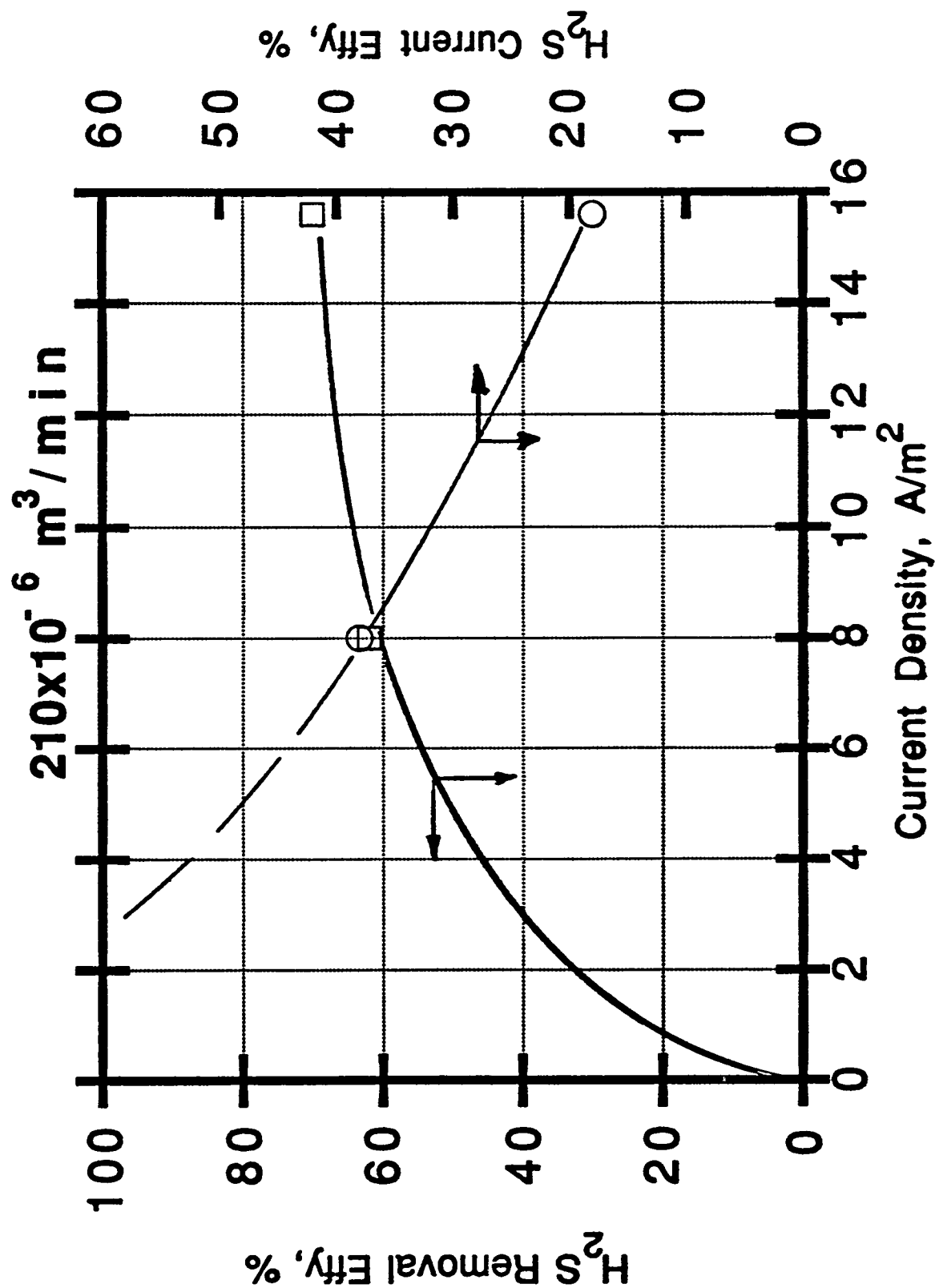


Figure 10. H<sub>2</sub>S Removal and Efficiency vs Applied Current Density, 100 ppm H<sub>2</sub>S, 210 x 10<sup>-6</sup> m<sup>3</sup>·min<sup>-1</sup>

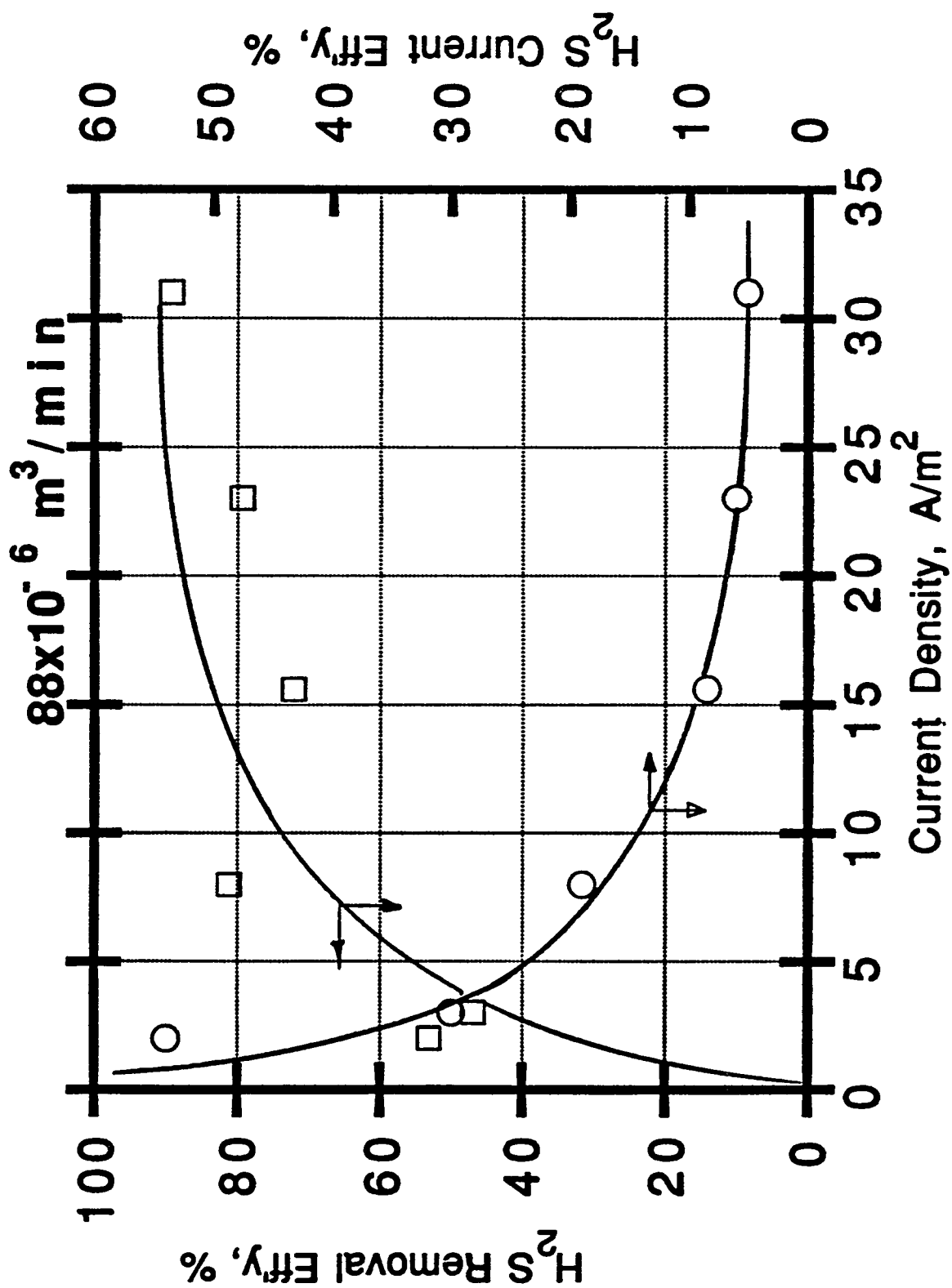


Figure 11. H<sub>2</sub>S Removal and Efficiency vs Applied Current Density, 100 ppm H<sub>2</sub>S, 88 x 10<sup>-6</sup> m<sup>3</sup>·min<sup>-1</sup>

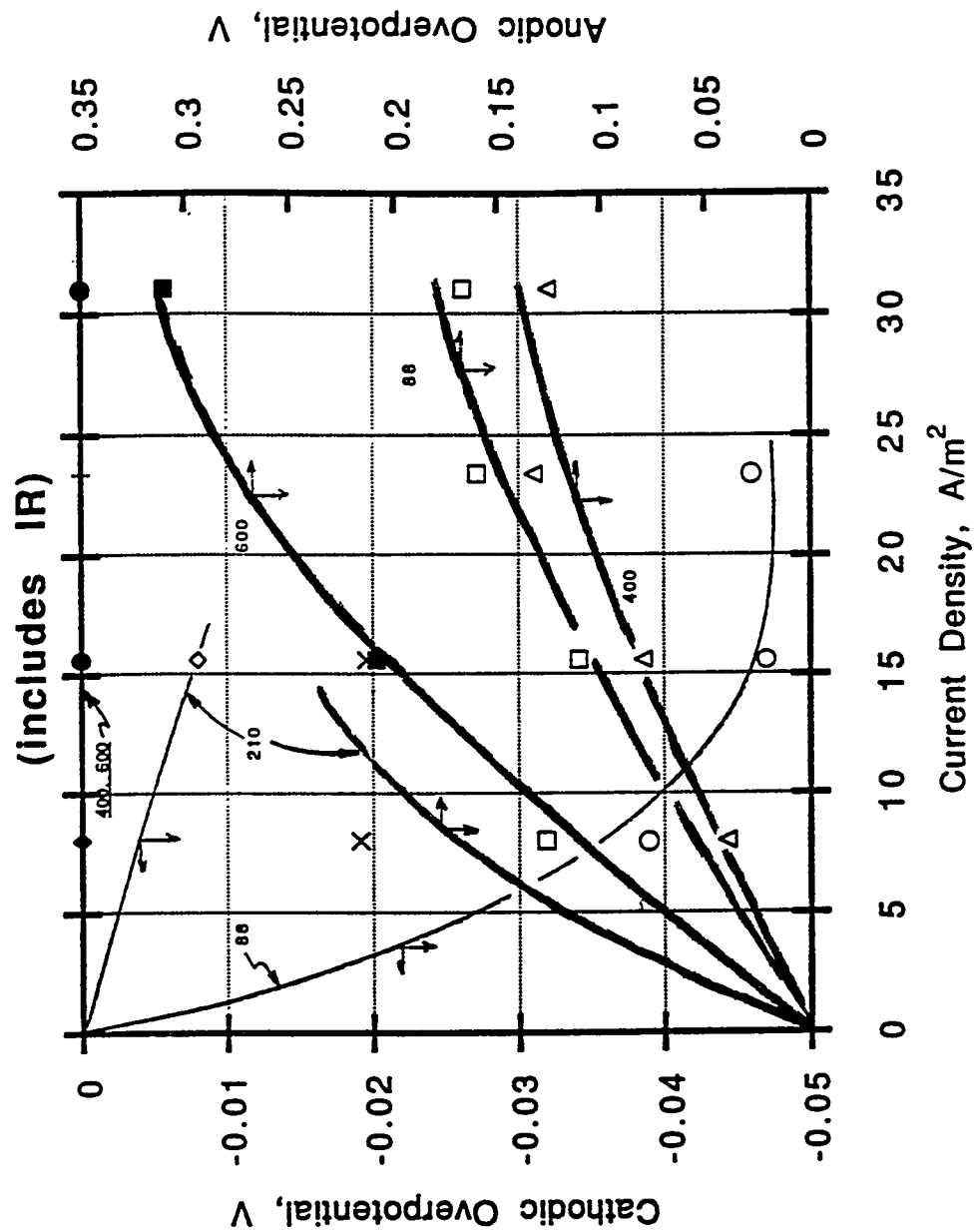


Figure 12. Cell Polarization vs Applied Current, 100 ppm H<sub>2</sub>S, Values are Cathodic Flowrate in m<sup>3</sup>·min<sup>-1</sup> × 10<sup>-6</sup>

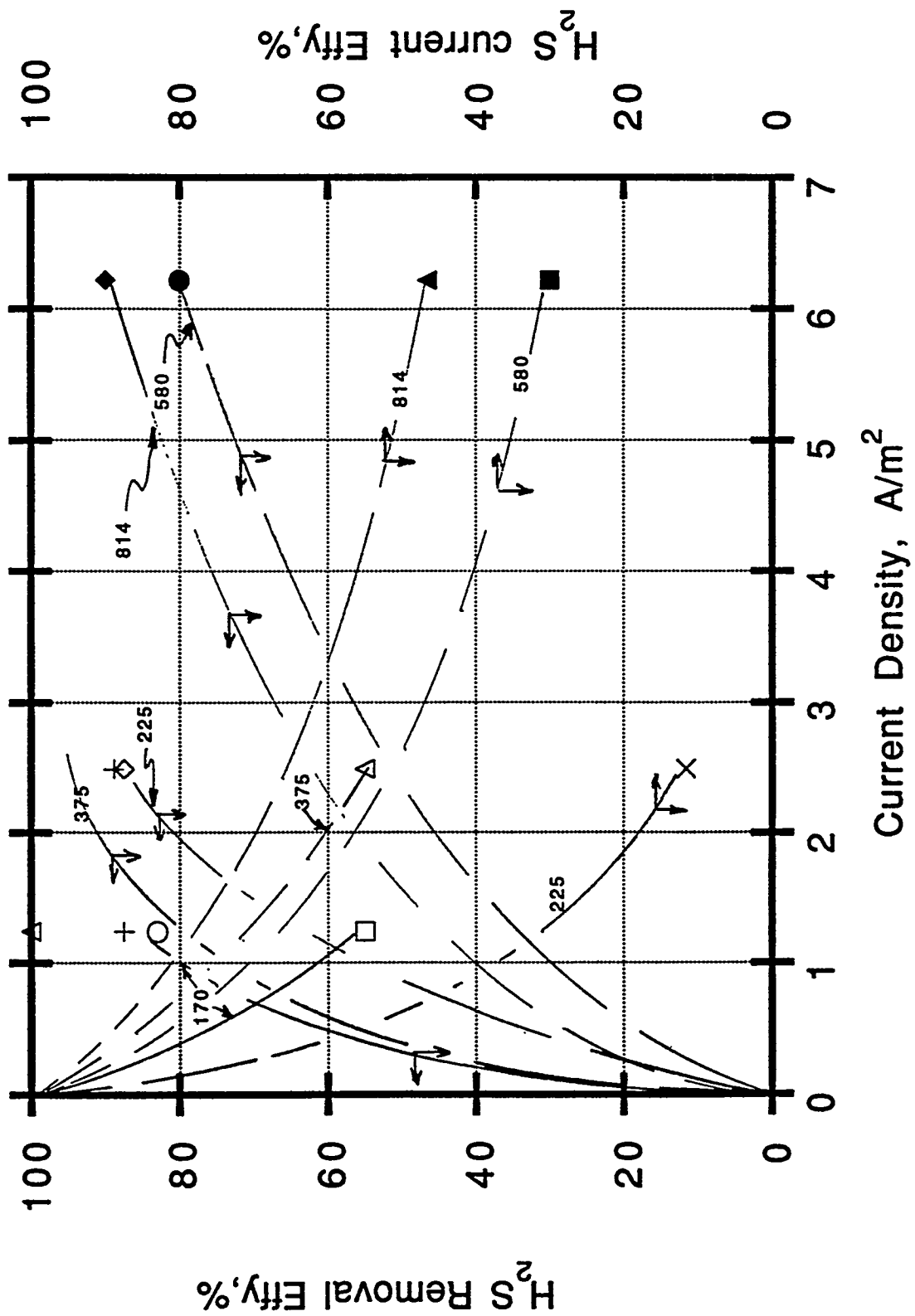


Figure 13.  $\text{H}_2\text{S}$  Removal and Efficiency vs Applied Current Density, 20 ppm  $\text{H}_2\text{S}$ ,  
 Parametric Numbers are Cathodic Flowrate in  $\text{m}^3\text{-min}^{-1} \times 10^{-6}$







---

# Appendices

---



**Advanced Coal-Fired Power Systems '95  
Review Meeting  
June 27-29, 1995**

**Agenda**

**TUESDAY, JUNE 27, 1995**

- 7:30 a.m.           Registration/Continental Breakfast
- 8:15 a.m.           METC Site Tour
- 9:30 a.m.           *Opening Comments*  
Harvey M. Ness  
Morgantown Energy Technology Center
- 9:40 a.m.           *Changing Role of Government R&D*  
Thomas F. Bechtel  
Morgantown Energy Technology Center
- 10:10 a.m.          Keynote Speaker  
*Perspectives of Government Regulations on the Power Industry*  
Jack Motter  
Sierra Pacific Power Company
- 10:50 a.m.          BREAK

**Session 1: PERSPECTIVES ON THE FUTURE OF POWER GENERATION INDUSTRY**

Session Chair: R. Daniel Brdar

- 11:10 a.m.   1.1    *And Deregulation Shall Lead Me to Lie Down In Green Pastures*  
Paul Marley  
U.S. Generating
- 11:40 a.m.   1.2    *World Market: A Survey of Opportunities for Advanced  
Coal-Fired Systems*  
Neville A. Holt  
Electric Power Research Institute
- 12:10 p.m.   1.3    *METC Clean Coal Technology Status — 1995 Update*  
Larry K. Carpenter  
Morgantown Energy Technology Center
- 12:40 p.m.          LUNCH  
METC "Energizer" Cafeteria

## Session 2: ADVANCED POWER SYSTEMS

Session Chair: Robert B. Reuther

- 1:40 p.m. 2.1 *Power Systems Development Facility Progress Report*  
Timothy E. Pinkston  
Southern Company Services
- 2:10 p.m. 2.2 *Second-Generation PFBC Systems Research and Development —  
Pilot Plant Becomes Demonstration Plant Design*  
Jim McClung  
Foster Wheeler Development Corporation
- 2:40 p.m. **Poster Session A — METC CRADA OPPORTUNITIES**  
Assembly Room Lobby
- PA.1 *Dynamic Analysis of Process Reactors*  
Lawrence J. Shadle  
Morgantown Energy Technology Center
- PA.2 *CRADA Opportunities with METC's Gasification  
and Hot Gas Cleanup Facility*  
Edwin N. Galloway  
Morgantown Energy Technology Center
- PA.3 *High Temperature High Pressure Particulate Sampling Probe*  
William P. Chisholm  
Morgantown Energy Technology Center
- PA.4 *CRADA Opportunities in Pressurized Combustion Research*  
Daniel J. Maloney  
Morgantown Energy Technology Center
- PA.5 *Pressure Gain Combustion for Gas Turbines*  
Randall S. Gemmen  
Morgantown Energy Technology Center
- PA.6 *Hot-Gas Filter Testing with the Transport Reactor Development Unit*  
Michael L. Swanson  
University of North Dakota  
Energy & Environmental Research Center
- PA.7 *High Temperature Gas Stream Cleanup Test Facility*  
John S. Ontko  
Morgantown Energy Technology Center

- PA.8    *Cooperative Research and Development Agreements at METC*  
J. Christopher Ludlow  
Morgantown Energy Technology Center
- PA.9    *High Pressure Optical Combustion Probe*  
Steven D. Woodruff  
Morgantown Energy Technology Center
- PA.10   *METC CFD Simulations of Hot Gas Filtration*  
Thomas J. O'Brien  
Morgantown Energy Technology Center
- PA.11   *CRADA Opportunities in the Removal of Particulates from  
Hot-Gas Streams by Filtration*  
Duane H. Smith  
Morgantown Energy Technology Center
- PA.12   *Dynamic Modeling of Power Systems*  
Michael Reed  
Morgantown Energy Technology Center
- 3:40 p.m.   2.3    *Gasification Product Improvement Facility Status*  
Vijay B. Dixit  
DB Riley, Inc.
- 4:10 p.m.   2.4    *Externally Fired Combined Cycle Demonstration*  
Stephen Young  
Hague International
- 4:40 p.m.   2.5    *Advanced Gas Turbine Systems Program*  
Charles M. Zeh  
Morgantown Energy Technology Center
- 5:00 p.m.        ADJOURN
- 5:30 p.m.        SOCIAL  
WVU Erickson Alumni Center
- 6:30 p.m.        BUFFET DINNER  
WVU Erickson Alumni Center

**WEDNESDAY, JUNE 28, 1995**

7:30 a.m. Registration/Continental Breakfast

8:00 a.m. *Opening Comments*  
Richard A. Dennis  
Morgantown Energy Technology Center

**Session 3: HOT GAS PARTICLE CONTROL**

Session Chair: Richard A. Dennis

8:10 a.m. 3.1 *Westinghouse Advanced Particle Filter System*  
Thomas E. Lippert  
Westinghouse Electric Corporation

8:35 a.m. 3.2 *Lightweight Ceramic Filter Components:  
Evaluation and Application*  
Paul M. Eggerstedt  
Industrial Filter & Pump Mfg. Co., Inc.

9:00 a.m. 3.3 *Status of Granular Bed Filter Development Program*  
Keith B. Wilson  
Combustion Power Company

9:25 a.m. 3.4 *Pulsed Combustion and Hot Gas Cleanup Island*  
Ravi R. Chandran  
Manufacturing and Technology Conversion International, Inc.

9:50 a.m. BREAK

10:20 a.m. 3.5 *Filter Component Assessment*  
Mary Anne Alvin  
Westinghouse Electric Corporation

10:45 a.m. 3.6 *Application of CFCC Technology to Hot Gas Filtration Applications*  
Scott Richlen  
U.S. Department of Energy



## Session 4: HOT GAS DESULFURIZATION

Session Chair: Daniel C. Cicero

- 11:10 a.m.      *Introductory Comments*  
Daniel C. Cicero  
Morgantown Energy Technology Center
- 11:20 a.m.    4.1      *Integrated Operation of a Pressurized Fixed Bed Gasifier,  
Hot Gas Desulfurization System and Turbine Simulator*  
Anthony Furman  
GE Corporate Research and Development
- 11:45 a.m.    4.2      *Pilot Scale Experience on IGCC Hot Gas Cleanup*  
Jukka Konttinen  
Enviropower, Inc.
- 12:10 p.m.    4.3      *Zinc Titanate Tests in Transport Reactor*  
William M. Campbell  
The M. W. Kellogg Co.
- 12:35 p.m.      LUNCH  
METC "Energizer" Cafeteria
- 1:35 p.m.    4.4      *Slip-Stream Testing of Hot-Gas Desulfurization  
with Sulfur Recovery*  
Jeffrey W. Portzer  
Research Triangle Institute
- 2:00 p.m.    4.5      *Bench-Scale Testing of Fluid-Bed Sorbent - ZT-4*  
Santosh K. Gangwal  
Research Triangle Institute
- 2:25 p.m.    4.6      *Pilot Plant Tests of Z-Sorb Sorbent*  
Gyanesh Khare  
Phillips Petroleum Company
- 2:50 p.m.      BREAK

## Session 5: FUEL GAS COMBUSTION

Session Chair: Charles M. Zeh

- 3:20 p.m. 5.1 *Fuel Gas Combustion Research at METC*  
Thomas S. Norton  
Morgantown Energy Technology Center
- 3:45 p.m. 5.2 *Performance of Low Btu Fuel Gas Turbine Combustors*  
Alan S. Feitelberg  
GE Corporate Research and Development
- 4:10 p.m. 5.3 *Development of a Topping Combustor for Advanced Concept  
Pressurized Fluidized-Bed Combustion Systems*  
Thomas E. Dowdy  
Westinghouse Electric Corporation
- 4:35 p.m. 5.4 *Development and Demonstration of a Solid Fuel-Fired Gas  
Turbine System*  
Vijay K. Sethi  
Western Research Institute
- 5:00 p.m. **Poster Session B — FILTERS AND SORBENTS**  
Assembly Room Lobby
- PB.1 *Assessment of Ceramic Membrane Filters*  
Rajesh K. Ahluwalia  
Argonne National Laboratory
- PB.2 *Carbon Formation and Metal Dusting in Hot-Gas  
Cleanup Systems of Coal Gasifiers*  
P. F. Tortorelli  
Oak Ridge National Laboratory
- PB.3 *Development of a Monolithic Ceramic Cross Flow Filter*  
David A. Larsen  
Blasch Precision Ceramics, Inc.
- PB.4 *Properties of Ceramic Candle Filters*  
Jack D. Spain  
Southern Research Institute
- PB.5 *Nitride-Bonded Silicon Carbide Composite Filter*  
Bruce N. Thomson  
Textron Specialty Materials

- PB.6 *3-D Woven, Mullite Matrix, Composite Filter*  
Jay E. Lane  
Westinghouse Electric Corporation
- PB.7 *Hot Particulate Removal and Desulfurization Results from the METC Integrated Gasification and Hot Gas Cleanup Facility*  
John M. Rockey  
Morgantown Energy Technology Center
- PB.8 *Simultaneous Hot Desulfurization and Improved Filtration in Coal Utilization Processes*  
Paul M. Eggerstedt  
Industrial Filter & Pump Mfg. Co., Inc.
- PB.9 *Land Application Uses of Dry FGD By-Products*  
Dravo Lime Company
- PB.9a *Liming Efficacy and Transport in Soil of a Dry PFBC By-Product*  
Richard C. Stehouwer  
Ohio State University
- PB.9b *Characterization and Laboratory Weathering Studies of PFBC By-Products*  
Randy K. Fowler  
Ohio State University
- PB.10 *Disposal of Fluidized-Bed Combustion Ash in an Underground Mine to Control Acid Mine Drainage and Subsidence*  
D. Courtney Black  
West Virginia University  
National Research Center for Coal and Energy
- PB.11 *Use of FBC Ash to Stabilize Dairy Barn Feedlots, Minimize Nutrient Pollution, and Develop New Utilization Outlets*  
Ronald F. Korcak  
U.S. Department of Agriculture  
Agricultural Research Service
- PB.12 *Hot Coal Gas Desulfurization with Manganese-Based Sorbents*  
Rachid Ben-Slimane  
University of Minnesota
- PB.13 *High-Temperature H<sub>2</sub>S Removal Using Limestones*  
Scott Lynn  
Lawrence Berkeley Laboratory

- PB.14 *A Long Life ZnO-TiO<sub>2</sub> Sorbent*  
Robert J. Copeland  
TDA Research, Inc.
- PB.15 *Development of Advanced Hot-Gas Desulfurization Sorbents*  
K. Jothimurugesan  
Hampton University
- PB.16 *Advanced Low-Temperature Sorbents*  
Rául E. Ayala  
GE Corporate Research and Development
- PB.17 *Spectral Methods Applied to Fluidized Bed Combustors*  
Thomas S. Raines  
Iowa State University
- PB.18 *Fossil Fuel Conversion - Measurement and Modeling*  
Peter R. Solomon  
Advanced Fuel Research, Inc.
- PB.19 *Development of Methods to Predict Agglomeration and Deposition in FBCs*  
Michael L. Swanson  
University of North Dakota  
Energy & Environmental Research Center
- PB.20 *Evaluation of Options for CO<sub>2</sub> Capture/Utilization/Disposal*  
Richard D. Doctor  
Argonne National Laboratory
- PB.21 *Hot-Gas Filter Ash Characterization*  
Tina M. Strobel  
University of North Dakota  
Energy & Environmental Research Center

6:30 p.m. ADJOURN

#### **THURSDAY, JUNE 29, 1995**

7:30 a.m. Registration/Continental Breakfast

8:00 a.m. *Opening Comments*  
Theodore J. McMahon  
Morgantown Energy Technology Center

**Session 6A: HOT GAS FILTER ISSUES**  
Assembly Room C

Session Chair: Theodore J. McMahon

- 8:10 a.m. 6A.1 *Development and Testing of PRD-66 Hot Gas Filters*  
Jeffrey A. Chambers  
DuPont Lanxide Composites, Inc.
- 8:35 a.m. 6A.2 *Filter Systems for IGCC Applications*  
Robert Gieger  
Pall Corporation
- 9:00 a.m. 6A.3 *Thermal and Chemical Stability of Ceramic Candle Filters*  
Mary Anne Alvin  
Westinghouse Electric Corporation
- 9:25 a.m. 6A.4 *Novel Oxide-Oxide Fiber Reinforced Hot Gas Filter Development*  
Richard A. Wagner  
Babcock & Wilcox
- 9:50 a.m. BREAK
- 10:20 a.m. 6A.5 *Filter Cake Characterization Studies*  
Richard A. Newby  
Westinghouse Electric Corporation
- 10:45 a.m. 6A.6 *Hot Gas Filtration Technical Issues*  
Duane H. Pontius  
Southern Research Institute

**Session 7A: SORBENT DEVELOPMENT AND PROCESSES**  
Assembly Room C

Session Chair: Thomas P. Dorchak

- 11:10 a.m. 7A.1 *Moving-Bed Sorbents*  
Rául E. Ayala  
GE Corporate Research and Development
- 11:35 a.m. 7A.2 *Spray-Dried Fluid-Bed Sorbent Tests - CMP-5*  
Raghubir P. Gupta  
Research Triangle Institute

- 12:00 p.m. 7A.3 *Desulfurization Sorbent Development Activities at METC*  
Ranjani V. Siriwardane  
Morgantown Energy Technology Center
- 12:25 p.m. LUNCH  
METC "Energizer" Cafeteria
- 1:25 p.m. 7A.4 *Advanced Sulfur Control Concepts*  
Douglas P. Harrison  
Louisiana State University
- 1:50 p.m. 7A.5 *Advanced Sulfur Control Concepts*  
Santosh K. Gangwal  
Research Triangle Institute
- 2:15 p.m. 7A.6 *Development of Disposable Sorbents for Chloride Removal  
from High-Temperature Coal-Derived Gases*  
Gopala N. Krishnan  
SRI International
- 2:40 p.m. Closing Remarks  
Harvey M. Ness  
Morgantown Energy Technology Center

**THURSDAY, JUNE 29, 1995**

- 7:30 a.m. Registration/Continental Breakfast
- 8:00 a.m. *Opening Comments*  
Peter E. Botros  
Morgantown Energy Technology Center

**Session 6B: HAZARDOUS AIR POLLUTANTS (HAPS)**  
Assembly Rooms A/B

Session Chair: Peter E. Botros

- 8:10 a.m. 6B.1 *HAPS Utility Data Analysis*  
Richard Hargis  
Pittsburgh Energy Technology Center

- 8:35 a.m. 6B.2 *Comparison of HAPs from Advanced and Conventional Power Systems: Tidd versus Cardinal*  
Thomas A. Erickson  
University of North Dakota  
Energy & Environmental Research Center
- 9:00 a.m. 6B.3 *Trace Metal Transformation in Gasification*  
Steven A. Benson  
University of North Dakota  
Energy & Environmental Research Center
- 9:25 a.m. 6B.4 *Hazardous Air Pollutant Testing of the LGTI Coal Gasification Plant*  
A. Gwen Eklund  
Radian
- 9:50 a.m. BREAK
- 10:20 a.m. 6B.5 *Development of Mercury and Chloride Monitors for Coal Gasifiers*  
Glenn A. Norton  
Ames Laboratory  
Iowa State University
- 10:45 a.m. 6B.6 *On-Line Elemental Analysis of Fossil Fuel Process Streams by Inductively Coupled Plasma Spectrometry*  
William P. Chisholm  
Morgantown Energy Technology Center

### **Session 7B: SEPARATION TECHNOLOGIES**

Assembly Rooms A/B

Session Chair: Venkat K. Venkatraman

- 11:10 a.m. 7B.1 *Advanced Metal-Membrane Technology - Commercialization*  
Roger Peterson  
Teledyne Wah Chang
- 11:35 a.m. 7B.2 *Separation of Hydrogen Using Thin Film Palladium-Ceramic Composite Membrane*  
Shamsuddin Ilias  
North Carolina A&T State University

- 12:00 p.m. 7B.3 *A Calcium Oxide Sorbent Process for Bulk Separation of Carbon Dioxide*  
Douglas P. Harrison  
Louisiana State University
- 12:25 p.m. LUNCH  
METC "Energizer" Cafeteria
- 1:25 p.m. 7B.4 *Thermal/Chemical Degradation of Inorganic Membrane Materials*  
Gopala Krishnan  
SRI International
- 1:50 p.m. 7B.5 *High Temperature Electrochemical Polishing of H<sub>2</sub>S from Coal Gasification Process Streams*  
Jack Winnick  
Georgia Tech. Research Corp.
- 2:15 p.m. *Closing Remarks*  
Venkat K. Venkataraman  
Morgantown Energy Technology Center



# Meeting Participants

---

**Javad Abbasian**

Manager, Gas Cleanup  
Institute of Gas Technology  
1700 S. Mt. Prospect Road  
Des Plaines, IL 60018  
708-768-0611, (FAX) 708-768-0600  
ABBASIAN@IGT.ORG

**Rajesh K. Ahluwalia**

Mechanical Engineer  
Argonne National Laboratory  
9700 South Cass Avenue  
Argonne, IL 60439-4841  
708-252-5979, (FAX) 708-252-4007  
WALIA@TD.ANL.GOV

**G. Ahmadi**

Professor  
Clarkson University  
MAE, Box 5725  
Potsdam, NY 13699-5725  
315-268-2322, (FAX) 315-268-6438

**Mary Anne Alvin**

Senior Engineer  
Westinghouse STC  
1310 Beulah Road  
Pittsburgh, PA 15235-5098  
412-256-2066, (FAX) 412-256-2121

**Gerald L. Anderson**

Project Director  
Benmol Corporation  
1121 King Street  
Alexandria, VA 22314  
703-683-4288, (FAX) 703-683-4635

**Rodney J. Anderson**

Physical Scientist  
Morgantown Energy Technology Center  
U.S. Department of Energy  
P.O. Box 880, M/S A03  
Morgantown, WV 26507-0880  
304-285-4709, (FAX) 304-285-4403  
RANDER@METC.DOE.GOV

**David H. Archer**

Adjunct Professor  
Carnegie Mellon University  
114 Kentzel Road  
Pittsburgh, PA 15237-2816  
412-268-6808, (FAX) 412-268-3348

**Hiromichi Atsumi**

Technical Service  
3M Japan  
8-8 Minami-Hashimoto  
3-Chome  
Sagamihara, Kanagawa 229  
Japan

**Raul Ayala**

Chemical Engineer  
GE Corporate R&D  
P.O. Box 8  
Building K-1, ES103  
Schenectady, NY 12301  
518-387-5850, (FAX) 518-387-7258

**William J. Ayers**

Division Director, Project Engineering  
Morgantown Energy Technology Center  
U.S. Department of Energy  
P.O. Box 880, M/S C03  
Morgantown, WV 26507-0880  
304-285-4125, (FAX) 304-285-4403  
WAYERS@METC.DOE.GOV

**Dennis M. Bachovchin**  
Engineer  
Westinghouse STC  
1310 Beulah Road  
Pittsburgh, PA 15325  
412-256-2250, (FAX) 412-256-2121

**Tiejun (T.J.) Bai**  
Associate Professor  
Clark Atlanta University  
223 J.P. Brawley Drive  
Atlanta, GA 30314  
404-880-6938, (FAX) 404-880-6853  
TBAI@CAU.AUC.EDU

**Richard A. Bajura**  
Director, NRCCE  
West Virginia University  
P.O. Box 6064  
Evansdale Drive  
Morgantown, WV 26506  
304-293-2867, (FAX) 304-293-3749

**Rita A. Bajura**  
Associate Director, PTM  
Morgantown Energy Technology Center  
U.S. Department of Energy  
P.O. Box 880, M/S B06  
Morgantown, WV 26507-0880  
304-285-4109, (FAX) 304-285-4292  
RBAJUR@METC.DOE.GOV

**David L. Baty**  
Section Manager, Composites  
Babcock & Wilcox  
Research and Development Division  
P.O. Box 11165  
Lynchburg, VA 24506-1165  
804-522-5472, (FAX) 804-522-6196

**Thomas F. Bechtel**  
Director  
Morgantown Energy Technology Center  
U.S. Department of Energy  
P.O. Box 880, M/S C02  
Morgantown, WV 26507-0880  
304-285-4511, (FAX) 304-285-4403  
TBECHT@METC.DOE.GOV

**Joel Beeghly**  
Project Manager  
Dravo Lime Company  
3600 Neville Road  
Pittsburgh, PA 15225  
412-777-0711, (FAX) 412-777-0727

**Justin L. Beeson**  
Project Manager  
Morgantown Energy Technology Center  
U.S. Department of Energy  
P.O. Box 880, M/S C04  
Morgantown, WV 26507-0880  
304-285-4671, (FAX) 304-285-4403  
JBES0@METC.DOE.GOV

**Rachid Ben-Slimane**  
Post Doctoral Associate  
University of Minnesota  
500 Pillsbury Drive, S.E.  
Minneapolis, MN 55455-0220  
612-624-7587, (FAX) 612-626-7750  
BENSL002@GOLD.TC.UMN.EDU

**Steven Benson**  
Deputy Associate Director  
Energy and Envir. Research Center  
University of North Dakota  
P.O. Box 9018  
Grand Forks, ND 58202-9018  
701-777-5177, (FAX) 701-777-5181

**Lutz Bergmann**  
President  
Filter Media Consulting, Inc.  
P.O. Box 2189  
La Grange, GA 30241-2189  
706-882-3108, (FAX) 706-882-3039

**Joe Berns**  
Graduate Student  
University of Minnesota  
684 Civil Engineering Building  
500 Pillsburg  
Minneapolis, MN 55455  
612-625-3071, (FAX) 612-626-7750

**Stephen Bevan**  
Program Manager  
GE Environmental Services  
200 North 7th Street  
Lebanon, PA 17046  
717-274-7077, (FAX) 717-274-7060

**Ken Bingaman**  
Senior Engineer, IGCC Tech.  
GE Environmental Services  
200 North 7th Street  
Lebanon, PA 17046-5006  
717-274-7112, (FAX) 717-274-7060

**D. Courtney Black**  
Project Manager  
West Virginia University  
Environmental Technology Division  
P.O. Box 6064, Evansdale Drive  
Morgantown, WV 26506-6064  
304-293-2867, (FAX) 304-293-7822

**Alan E. Bland**  
Program Manager  
Western Research Institute  
365 N. 9th Street  
Laramie, WY 82071  
307-721-2443, (FAX) 307-721-2345

**Mohammad Bodruzzaman**  
Associate Professor  
Tennessee State University  
3500 John Merritt Boulevard  
Nashville, TN 37209  
615-963-5367, (FAX) 615-963-5397  
ZAMAN@HARPOTNSTATE.EDU

**Jeff Bolebruch**  
Market Manager  
Blasch Precision Ceramics  
580 Broadway  
Albany, NY 12204  
518-436-1263, (FAX) 518-436-0098

**Donald L. Bonk**  
Project Manager  
Morgantown Energy Technology Center  
U.S. Department of Energy  
P.O. Box 880, M/S C04  
Morgantown, WV 26507-0880  
304-285-4889, (FAX) 304-285-4403  
DBONK@METC.DOE.GOV

**George S. Booras**  
Manager, Tech. Assessment  
Electric Power Research Institute  
P.O. Box 10412  
Palo Alto, CA 94303-0813  
415-855-2471, (FAX) 415-855-2950  
GBOORAS@MSM.EPRI.COM

**Daniel E. Boss**  
Research Scientist  
BIRL  
1801 Maple Avenue  
Evanston, IL 60201-3135  
708-491-3373, (FAX) 708-467-1022

**Peter E. Botros**  
Project Manager  
Morgantown Energy Technology Center  
U.S. Department of Energy  
P.O. Box 880, M/S C04  
Morgantown, WV 26507-0880  
304-285-4162, (FAX) 304-285-4403  
PBOTRO@METC.DOE.GOV

**R. Daniel Brdar**  
Product Manager, IGCC  
Morgantown Energy Technology Center  
U.S. Department of Energy  
P.O. Box 880, M/S D01  
Morgantown, WV 26507-0880  
304-285-4666, (FAX) 304-285-4403  
RBRDAR@METC.DOE.GOV

**Richard A. Brown**  
Project Manager  
Electric Power Research Institute  
3412 Hillview Avenue  
Palo Alto, CA 94303  
415-855-2216, (FAX) 415-855-8501  
RICBROWN@MSM.EPRI.COM

**William H. Buttermore**  
Director, Fossil Energy Program  
Ames Laboratory  
Iowa State University  
280 Metals Development Building  
Ames, IA 50011-3020  
515-294-3758, (FAX) 515-294-3091  
BUTTERMORE@AMESLAB.GOV

**John W. Byam**  
President  
JB International  
228 Grand Street  
Morgantown, WV 26505-7509  
304-296-0598, (FAX) 304-296-0598  
72134.3545@COMPUSERVE.COM

**Chad Byrd**  
Research Assistant  
West Virginia University  
3103 Chestnut Hill  
Morgantown, WV 26505  
304-599-4710, (FAX) 304-293-4139

**Greg Cammerata**  
Engineer, Engineering Studies  
Allegheny Power Service Corp.  
800 Cabin Hill Drive  
Greensburg, PA 15601  
412-838-6499, (FAX) 412-830-5008

**Barbara L. Campbell**  
Student  
Hampton University  
Department of Engineering  
Hampton, VA 23668  
804-728-6872

**Bill Campbell**  
Manager, Clean Coal Technology  
M.W. Kellogg Company  
601 Jefferson Avenue  
Houston, TX 77002-7990  
713-753-2184, (FAX) 713-753-7836

**Larry Carpenter**  
Division Director, Major Projects  
Morgantown Energy Technology Center  
U.S. Department of Energy  
P.O. Box 880, M/S D04  
Morgantown, WV 26507-0880  
304-285-4161, (FAX) 304-285-4403  
LCARPE@METC.DOE.GOV

**R. Don Carson**  
Project Director  
Jacobs-Sirrine Engineers, Inc.  
P.O. Box 5456  
Greenville, SC 29607  
803-676-5037, (FAX) 803-676-5033

**Jeffrey A. Chambers**  
Project Leader  
Dupont Lanxide Composites  
P.O. Box 6077  
1300 Marrows Road  
Newark, DE 19714-6077  
302-456-6235, (FAX) 302-456-6480  
CHAMBEJA@SOC.DNET.DUPONT.COM

**Ravi Chandran**  
Manager, East Coast Dev. Facility  
MTCI  
6001 Chemical Road  
Baltimore, MD 21226  
410-354-0420, (FAX) 410-354-0471

**Ta-Kuan Chiang**  
Mechanical Engineer  
Morgantown Energy Technology Center  
U.S. Department of Energy  
P.O. Box 880, M/S N05  
Morgantown, WV 26507-0880  
304-285-4406, (FAX) 304-285-4403  
TCHIAN@METC.DOE.GOV

**William P. Chisholm**  
Cluster Leader  
Morgantown Energy Technology Center  
U.S. Department of Energy  
P.O. Box 880, M/S A04  
Morgantown, WV 26507-0880  
304-285-4730, (FAX) 304-285-4403  
WCHISH@METC.DOE.GOV

**Chris D. Chriswell**  
Analytical Chemist  
Ames Laboratory  
U.S. Department of Energy  
Iowa State University  
Ames, IA 50011  
515-294-6776, (FAX) 515-294-3091

**Colin D. Chriswell**  
Analytical Chemist  
Ames Laboratory  
U.S. Department of Energy  
Iowa State University  
Ames, IA 50011  
515-294-6776, (FAX) 515-294-3091

**Suk-Hyun Chun**  
Senior Researcher  
Research Management Center  
935-34, Pangbae-Dong  
Seocho-Ku, Seoul, Korea  
Seoul, Korea 137-060  
822-525-3474, (FAX) 822-522-8093

**Daniel C. Cicero**  
Cluster Leader  
Morgantown Energy Technology Center  
U.S. Department of Energy  
P.O. Box 880, M/S C04  
Morgantown, WV 26507-0880  
304-285-4826, (FAX) 304-285-4403  
DCICER@METC.DOE.GOV

**Nancy C. Cole**  
Manager, Fossil Energy Materials  
Oak Ridge National Laboratory  
P.O. Box 2008  
Oak Ridge, TN 37831-6153  
615-574-4824, (FAX) 615-574-5118  
COLENC@ORNL.GOV

**Robert J. Copeland**  
Principal Engineer  
TDA Research, Inc.  
12345 W. 52nd Avenue  
Wheat Ridge, CO 80033  
303-940-2323, (FAX) 303-422-7763  
MECH@TDA.COM

**Delisa Cox**  
Student  
Hampton University  
Department of Engineering  
Hampton, VA 23668  
804-728-6872

**Ran K. Datta**  
Professor  
Virginia Tech  
VPI and State University  
301 Holden Hall  
Blacksburg, VA 24061-0256  
703-231-3577, (FAX) 703-231-3028

**Robert Dawson**  
Associate Scientist  
Ames Laboratory  
273 Metal Development  
Iowa State University  
Ames, IA 50011  
515-294-1028, (FAX) 515-294-3091  
DAWSON@AMESLAB.GOV

**Paul J. De Wild**  
Netherlands Energy Research  
P.O. Box 1, 1755 ZG Petten  
Westerduinweg 3  
Petten, Netherlands  
022-464-557, (FAX) 022-463-489  
DEWILD@ECN.NL

**Michael R. Delallo**  
DOE Program Manager  
Gilbert/Commonwealth, Inc.  
2675 Morgantown Road  
Reading, PA 19607  
610-855-2675, (FAX) 610-796-1584

**Richard A. Dennis**  
Project Manager  
Morgantown Energy Technology Center  
U.S. Department of Energy  
P.O. Box 880, M/S C04  
Morgantown, WV 26507-0880  
304-285-4515, (FAX) 304-285-4403  
RDENNI@METC.DOE.GOV

**Robert S. Dickens**  
Regional Manager, Power Generation  
Hartford Steam Boiler  
59 Hartford Street  
Westover, WV 26505  
304-291-2442, (FAX) 304-291-5138

**Urmila M. Diwekar**  
Professor  
Carnegie Mellon University  
Baker Hall 129/EPP Department  
Pittsburgh, PA 15213  
412-268-3003, (FAX) 412-268-3757  
URMILA@CMU.EDU

**Vijay B. Dixit**  
Project Manager  
DB Riley, Inc.  
45 McKeon Road  
Worcester, MA 01610  
508-792-4807, (FAX) 508-792-4817

**W. F. Domeracki**  
Program Manager  
Westinghouse Electric Corporation  
4400 Alafaya Trail  
MC 381  
Orlando, FL 32826-2399  
407-281-2715, (FAX) 407-281-5014

**Thomas P. Dorchak**  
Project Manager  
Morgantown Energy Technology Center  
U.S. Department of Energy  
P.O. Box 880, M/S C04  
Morgantown, WV 26507-0880  
304-285-4305, (FAX) 304-285-4403  
TDORCH@METC.DOE.GOV

**Thomas E. Dowdy**  
Senior Project Engineer  
Westinghouse Electric Corporation  
4400 Alafaya Trail  
MC 381  
Orlando, FL 32826  
407-281-3387, (FAX) 407-281-5014

**Dave Eckels**  
Assistant Scientist  
Ames Laboratory  
Iowa State University  
5 Spedding  
Ames, IA 50011  
515-294-7943

**Paul Eggerstedt**  
Executive Vice President/Research  
Director  
Industrial Filter  
5900 Ogden Avenue  
Cicero, IL 60650  
708-656-7800, (FAX) 708-656-7806

**A. Gwen Eklund**  
Principal Project Manager  
Radian Corporation  
8501 N. Mopac Boulevard  
Austin, TX 78759  
512-454-4797, (FAX) 512-454-8807  
GWEN\_EKLUND@RADIAN.COM

**Thomas A. Erickson**  
Research Associate  
Energy and Environmental Research Center  
University of North Dakota  
P.O. Box 9018  
Grand Forks, ND 58202-9018  
701-777-5153, (FAX) 701-777-5181

**Martin Fankhanel**  
Project Manager  
M.W. Kellogg Company  
P.O. Box 4557  
Houston, TX 77210-4557  
713-753-2938, (FAX) 713-753-3800

**Alan S. Feitelberg**  
Chemical Engineer  
GE Corporate R&D  
K-1, ES122  
1 River Road  
Schenectady, NY 12301  
518-387-5737, (FAX) 518-387-7258  
FEITELBERG@CRD.GE.COM

**Ali Feliachi**  
Professor  
West Virginia University  
Department of Elec. and Computer Eng.  
P.O. Box 6101  
Morgantown, WV 26506-6101  
304-293-6375, (FAX) 304-293-8602  
FELIACHI@FACULTY.COE.WVU.EDU

**Martin Ferer**  
Professor  
West Virginia University  
P.O. Box 6315  
Morgantown, WV 26506-6315  
304-293-3422, (FAX) 304-293-5732  
FERER@WVNVMS.WVNET.EDU

**Edward M. Fischer**  
Technical Service Specialist  
3M Company  
3M Center  
Building 207-1S-23  
St. Paul, MN 55144  
612-426-4210, (FAX) 612-733-0221  
EMFISCHER1@MMM.COM

**Randall K. Fowler**  
Graduate Student  
Ohio State University  
Williams Hall  
OARDC-OSU  
Wooster, OH 44691  
614-292-2001

**Gregory C. Franzen**  
Vice President, Operations  
GMRC, Ltd.  
12200 Marion Lane, No. 5225  
Minnetonka, MN 55305  
612-544-4214, (FAX) 612-544-1136

**Chris Frey**  
Assistant Professor  
North Carolina State University  
P.O. Box 7908  
Raleigh, NC 27695-7908  
919-515-1155, (FAX) 919-515-7908  
FREY@EOS.NCSU.EDU

**Jack A. Fuller**  
Chairperson  
West Virginia University  
Department of Management  
Morgantown, WV 26506  
304-293-7935  
FULLER@WVUBEL.BE.WVU.EDU

**Anthony H. Furman**  
Project Engineer  
GE Corporate R&D  
ESB-203, K-1  
Schenectady, NY 12301  
518-387-5849, (FAX) 518-387-7258  
FURMAN@CRD.GE.COM

**Edwin N. Galloway**  
Mechanical Engineer  
Morgantown Energy Technology Center  
U.S. Department of Energy  
P.O. Box 880, M/S C03  
Morgantown, WV 26507-0880  
304-285-5429, (FAX) 304-285-4403  
EGALLO@METC.DOE.GOV

**Santosh K. Gangwal**  
Senior Program Director  
Research Triangle Institute  
P.O. Box 12194  
Research Triangle Park, NC 27709  
919-541-8033, (FAX) 919-541-8000  
SKG@RTI.ORG

**Lee Gasper-Galvin**  
General Engineer  
Morgantown Energy Technology Center  
U.S. Department of Energy  
P.O. Box 880, M/S N04  
Morgantown, WV 26507-0880  
304-285-4832, (FAX) 304-285-4403  
LGASPE@METC.DOE.GOV

**Randall Gemmen**  
Mechanical Engineer  
Morgantown Energy Technology Center  
U.S. Department of Energy  
P.O. Box 880, M/S N05  
Morgantown, WV 26507-0880  
304-285-4536, (FAX) 304-285-4403  
RGEMME@METC.DOE.GOV



**Timm Gennrich**  
Senior Product Development Chemist  
3M Company  
3M Center  
Building 207-1S-23  
St. Paul, MN 55144-1000  
612-733-4013, (FAX) 612-733-0221

**Guido Gentile**

Engineer  
Ansaldo  
C.SO F.M. Perrone 25  
Genoa, 16161  
Italy

**Madhav Ghate**

Division Director, Technology Base Mgmt.  
Morgantown Energy Technology Center  
U.S. Department of Energy  
P.O. Box 880, M/S C05  
Morgantown, WV 26507-0880  
304-285-4135, (FAX) 304-285-4403  
MGHATE@METC.DOE.GOV

**Robert Gieger**

Staff Scientist and Project Manager  
Pall Corporation  
25 Harbor Park Drive  
Portwashington, NY 11050  
516-484-3600, (FAX) 516-484-3628

**Philip Goldberg**

Project Manager  
Pittsburgh Energy Technology Center  
P.O. Box 10940  
MS 922-247  
Pittsburgh, PA 15236  
412-892-5806, (FAX) 412-892-5917  
GOLDBERG@PETC.DOE.GOV

**Thomas Grindley**

Chemical Engineer  
Morgantown Energy Technology Center  
U.S. Department of Energy  
P.O. Box 880, M/S N04  
Morgantown, WV 26507-0880  
304-285-4286, (FAX) 304-285-4403  
TGRIND@METC.DOE.GOV

**Robert W. Gross**

Mechanical Engineer  
Morgantown Energy Technology Center  
U.S. Department of Energy  
P.O. Box 880, M/S N04  
Morgantown, WV 26507-0880  
304-285-4235, (FAX) 304-285-4403  
RGROSS@METC.DOE.GOV

**Raghubir P. Gupta**

Research Chemical Engineer  
Research Triangle Institute  
P.O. Box 12194  
Research Triangle Park, NC 27709  
919-541-8023, (FAX) 919-541-8000  
GUPTA@RTI.ORG

**James A. Hall**

Specialist, Generation Technology  
Tennessee Valley Authority  
1101 Market Street  
LP 50-C  
Chattanooga, TN 37402-2801  
615-751-8816, (FAX) 615-751-7545

**Jack Halow**

Division Director, Combustion/Cleanup  
Morgantown Energy Technology Center  
U.S. Department of Energy  
P.O. Box 880, M/S N06  
Morgantown, WV 26507-0880  
304-285-4114, (FAX) 304-285-4403  
JHALOW@METC.DOE.GOV

**Richard Hargis**

Chemical Engineer  
Pittsburgh Energy Technology Center  
P.O. Box 10940  
Pittsburgh, PA 15236-0940  
412-892-6065, (FAX) 412-892-6204

**Douglas P. Harrison**

Alumni Professor  
Louisiana State University  
Department of Chemical Engineering  
Baton Rouge, LA 70803  
504-388-3066, (FAX) 504-388-1476

**Cynthia Heisey**

Program Specialist  
GE Environmental Services  
200 North 7th Street  
Lebanon, PA 17046  
717-274-7349, (FAX) 717-274-7060

**Howard Hendrix**

Principal Research Engineer  
Southern Company Services  
P.O. Box 1069  
Wilsonville, AL 35186  
205-669-5876, (FAX) 205-669-5843

**Richard Higgins**

Manager, Membrane Development  
Ceramem Corporation  
12 Clematis Avenue  
Waltham, MA 02154  
617-899-0467, (FAX) 617-899-1227

**Norman T. Holcombe**

Project Manager  
Morgantown Energy Technology Center  
U.S. Department of Energy  
P.O. Box 880, M/S C05  
Morgantown, WV 26507-0880  
304-285-4829, (FAX) 304-285-4403  
NHOLCO@METC.DOE.GOV

**Neville Holt**

Manager, New Coal Generation Tech.  
Electric Power Research Institute  
3412 Hillview Avenue  
Palo Alto, CA 94303  
415-855-2503, (FAX) 415-855-8501  
NHOLT@EPRINET.EPRI.COM

**Frank I. Honea**

Project Manager  
Illinois Clean Coal Institute  
P.O. Box 8  
Carterville, IL 62918  
618-985-3500, (FAX) 618-985-6166

**Clayton L. Huber**

Manager, R&C and Tech. Marketing  
Hope Gas, Inc.  
Bank One Center West  
P.O. Box 2868  
Clarksburg, WV 26302  
304-623-8668, (FAX) 304-623-8919

**Ziaul Huque**

Assistant Professor  
Prairie View A&M University  
Mechanical Engineering Department  
Prairie View, TX 77429  
409-857-4023, (FAX) 409-857-2222  
ZHUQUE@ANDREW.CEA.PUAMU.EDU

**John Hurly**

Materials Scientist  
Pall Aeropower Corporation  
6301 49th Street, North  
Pinellas Park, FL 34665  
813-522-3111, (FAX) 813-528-0516

**Shamsuddin Ilias**

North Carolina A&T State University  
Chemical Engineering Department  
Greensboro, NC 27411  
910-334-7564, (FAX) 910-334-7904  
ILIAS@GARFIELD.NCAT.EDU

**Keijo Jaanu**  
Project Manager  
VTT Energy  
P.O. Box 1603  
Jyväskylä 40101  
Finland

**Suresh Jain**  
Program Manager  
U.S. Department of Energy  
FE-231  
Washington, DC 20585  
301-903-0508, (FAX) 301-903-2406  
SURESH.JAIN@HQ.DOE.GOV

**Lisa A. Jarr**  
Patent Advisor  
Morgantown Energy Technology Center  
U.S. Department of Energy  
P.O. Box 880, M/S A03  
Morgantown, WV 26507-0880  
304-285-4555, (FAX) 304-285-4403  
LJARR@METC.DOE.GOV

**Andrew B. Jeffery**  
President  
Specific Surface Corporation  
14 Menfi Way  
Hopedale, MA 01747  
508-473-3200, (FAX) 508-473-3200  
SURFACES@AOL.COM

**Lin Jianxing**  
Senior Engineer  
CDS International, Inc.  
Beijing Research Institute  
Hepingli  
Beijing 10013  
China

**Eric Johnson**  
Professor  
West Virginia University  
P.O. Box 6106  
Morgantown, WV 26506  
304-293-3111

**Richard A. Johnson**  
Project Manager  
Morgantown Energy Technology Center  
U.S. Department of Energy  
P.O. Box 880, M/S D06  
Morgantown, WV 26507-0880  
304-285-4564, (FAX) 304-285-4403  
RJOHNS@METC.DOE.GOV

**K. Jothimurgesan**  
Assistant Professor  
Hampton University  
Department of Engineering  
Hampton, VA 23668  
804-727-5817, (FAX) 804-727-5189

**Roddie R. Judkins**  
Manager  
Lockheed Martin Energy Systems  
P.O. Box 2008  
Oak Ridge, TN 37831-6084  
615-574-4572, (FAX) 615-574-7721

**Kenji Kamei**  
Manager, Technology Development  
Kawasaki Heavy Industries  
World Trade Center, Building 4-1  
Hamamatu-Cho 2-Chome  
Minatoku, Tokyo 105  
Japan  
033-435-2080, (FAX) 033-432-4629

**Joseph P. Kanosky**  
General Engineer  
Morgantown Energy Technology Center  
U.S. Department of Energy  
P.O. Box 880, M/S C03  
Morgantown, WV 26507-0880  
304-285-4649, (FAX) 304-285-4403  
JKANOS@METC.DOE.GOV

**Brian A. Keenan**  
Business Director, Power  
BOC Process Systems  
30 Priestley Road  
Guildford  
Surrey, GU2 5YH  
United Kingdom  
148-330-0900, (FAX) 148-330-2009

**Frank A. Kelleher**  
Director, Government Affairs  
Foster Wheeler USA Corporation  
1701 Pennsylvania Avenue, N.W.  
Washington, DC 20016  
202-298-7750, (FAX) 202-342-0597

**Kent Keys**  
Business Unit Manager  
United Catalysts, Inc.  
P.O. Box 32370  
Louisville, KY 40232  
502-634-7245, (FAX) 502-637-3732

**Gyanesh Khare**  
Senior Research Specialist  
Phillips Petroleum Company  
92-E Building  
Phillips Research Center  
Bartlesville, OK 74004  
918-661-9435, (FAX) 918-662-2007

**Hyung-Taek Kim**  
Assistant Professor  
Ajoy University  
Woncheondong San-5  
Paldal-Gu  
Suwon  
Korea  
331-219-2321, (FAX) 331-212-4951

**Soung S. Kim**  
Project Manager  
Pittsburgh Energy Technology Center  
P.O. Box 10940  
Pittsburgh, PA 15236  
412-892-6007, (FAX) 412-892-5917  
KIM@PETC.DOE.GOV

**David Kinsinger**  
Licensing Specialist  
Phillips Petroleum Company  
261 Patent Library  
Phillips Research Center  
Bartlesville, OK 74004  
918-661-1244, (FAX) 918-662-2007

**John B. Kitto**  
Babcock & Wilcox  
1562 Beeson Street  
Alliance, OH 44601  
216-829-7710, (FAX) 216-829-7293  
COMPUSERVE-76330,1306

**Julianne Klara**  
Chemical Engineer  
Pittsburgh Energy Technology Center  
P.O. Box 10940  
Pittsburgh, PA 15236-0940  
412-892-6289, (FAX) 412-892-4818  
JKLARA@PETC.DOE.GOV

**Michael G. Klett**  
Project Manager  
Gilbert/Commonwealth, Inc.  
P.O. Box 1498  
Reading, PA 19603  
215-775-2600, (FAX) 215-775-2670

**Chuck Komar**  
Staff Engineer  
Morgantown Energy Technology Center  
U.S. Department of Energy  
P.O. Box 880, M/S B05  
Morgantown, WV 26507-0880  
304-285-4107, (FAX) 304-285-4403  
CKOMAR@METC.DOE.GOV

**Jukka Konttinen**  
Research Engineer  
Enviropower, Inc.  
P.O. Box 35  
Osuusmyllynkatu 13  
Fin-33701 Tampere  
Finland  
358-241-3575, (FAX) 358-241-3599

**Ron Korcak**  
Research Leader  
USDA/ARS  
B-010A Fruit Lab  
Barc-West  
Beltsville, MD 20705  
301-504-5650, (FAX) 301-504-5062

**Gopala Krishnan**  
Program Manager  
SRI International  
333 Ravenswood Avenue  
Menlo Park, CA 94025  
415-859-2627, (FAX) 415-859-2111  
GOPALA\_KRISHNAN@QM.SRI.COM

**Radha P. Krishnan**  
International Energy Programs  
Science Applications International  
301 Laboratory Road  
Oak Ridge, TN 37830  
615-481-2370, (FAX) 615-482-6828

**Subha K. Kumpaty**  
Assistant Professor  
Rust College  
150 E. Rust Avenue  
Holly Springs, MS 38635  
601-252-8000, (FAX) 601-252-6107  
MESUBHA@CRAYY.MCSR.OLEMISS.EDU

**K. C. Kwon**  
Professor  
Tuskegee University  
Chemical Engineering Department  
Engineering and Architecture  
Tuskegee, AL 36088  
334-727-8976, (FAX) 334-727-8090  
KWONK@ACD.TUSK.EDU

**Paul G. Lahaye**  
Chairman/CEO  
Hague International  
3 Adams Street  
South Portland, ME 04106  
207-799-7346, (FAX) 207-799-6743

**Jay E. Lane**  
Senior Engineer  
Westinghouse STC  
1310 Beulah Road  
Pittsburgh, PA 15670-5098  
412-256-2195, (FAX) 412-256-1267  
LANE@STC.PGH.WEE.COM

**Jeff L. Larkin**  
Senior Marketing Engineer  
Westinghouse Electric Corporation  
4400 Alafaya Trail  
MC 381  
Orlando, FL 32826-2399  
407-281-2472, (FAX) 407-281-5014

**David A. Larsen**  
Manager, Product Development  
Blasch Precision Ceramics  
580 Broadway  
Albany, NY 12204  
518-436-1263, (FAX) 518-436-0098

**Larry O. Lawson**  
Process Engineer  
Morgantown Energy Technology Center  
U.S. Department of Energy  
P.O. Box 880, M/S A04  
Morgantown, WV 26507-0880  
304-285-4735, (FAX) 304-285-4403  
LLAWSO@METC.DOE.GOV

**William Lawson**  
Division Director, Tech. Base Program  
Morgantown Energy Technology Center  
U.S. Department of Energy  
P.O. Box 880, M/S B05  
Morgantown, WV 26507-0880  
304-285-4173, (FAX) 304-285-4403  
WLAWSO@METC.DOE.GOV

**Jean-Francois Le Costaouec**  
Senior Engineer  
Techniweave, Inc.  
109 Chestnut Hill Road  
Rochester, NH 03868  
603-335-2115, (FAX) 603-335-3200

**George Lee**  
Chemical Engineer  
Morgantown Energy Technology Center  
U.S. Department of Energy  
P.O. Box 880, M/S E01  
Morgantown, WV 26507-0880  
304-285-4824, (FAX) 304-285-4403  
GLEE@METC.DOE.GOV

**Seong W. Lee**  
Professor  
Morgan State University  
Cold Spring Lane and Hillen Road  
Baltimore, MD 21239  
410-319-3137, (FAX) 410-319-3843  
SLEE@MOE.MORGAN.EDU

**Thomas E. Lippert**  
Manager  
Westinghouse Electric Corporation  
1310 Beulah Road  
Pittsburgh, PA 15235-5098  
412-256-2440, (FAX) 412-256-2121

**H. P. Loh**  
Chemical Engineer  
Morgantown Energy Technology Center  
U.S. Department of Energy  
P.O. Box 880, M/S E01  
Morgantown, WV 26507-0880  
304-285-4546, (FAX) 304-285-4403  
HLOH@METC.DOE.GOV

**James Longanbach**  
Project Manager  
Morgantown Energy Technology Center  
U.S. Department of Energy  
P.O. Box 880, M/S C04  
Morgantown, WV 26507-0880  
304-285-4659, (FAX) 304-285-4403  
JLONGA@METC.DOE.GOV

**J. Chris Ludlow**  
General Engineer  
Morgantown Energy Technology Center  
U.S. Department of Energy  
P.O. Box 880, M/S B05  
Morgantown, WV 26507-0880  
304-285-4608, (FAX) 304-285-4403  
JLUDLO@METC.DOE.GOV

**Scott Lynn**  
Professor  
Lawrence Berkeley Laboratory  
University of California  
Department of Chemical Engineering  
Berkeley, CA 94720-1462  
510-642-1634, (FAX) 510-642-4778

**Kanwal Mahajan**  
General Engineer  
Morgantown Energy Technology Center  
U.S. Department of Energy  
P.O. Box 880, M/S E01  
Morgantown, WV 26507-0880  
304-285-4965, (FAX) 304-285-4403  
KMAHAJ@METC.DOE.GOV

**Daniel J. Maloney**  
Physical Scientist  
Morgantown Energy Technology Center  
U.S. Department of Energy  
P.O. Box 880, M/S N05  
Morgantown, WV 26507-0880  
304-285-4629, (FAX) 304-285-4403  
DMALON@METC.DOE.GOV

**Paul Marley**  
U.S. Generating Company  
7500 Old Georgetown Road  
Bethesda, MD 20814  
301-718-6865, (FAX) 301-718-6900

**Tim McClanahan**  
Chemical Engineer  
Tennessee Valley Authority  
P.O. Box 1010  
Muscle Shoals, AL 35660  
205-386-2177, (FAX) 205-386-3799

**Jim McClung**  
Project Manager  
Foster Wheeler Development Corporation  
12 Peach Tree Hill Road  
Livingston, NJ 07039  
201-535-2315, (FAX) 201-535-2242

**Heather M. McDaniel**  
Project Manager  
Morgantown Energy Technology Center  
U.S. Department of Energy  
P.O. Box 880, M/S C04  
Morgantown, WV 26507-0880  
304-285-5430, (FAX) 304-285-4403  
HMCDAN@METC.DOE.GOV

**Ted McMahon**  
General Engineer  
Morgantown Energy Technology Center  
U.S. Department of Energy  
P.O. Box 880, M/S C04  
Morgantown, WV 26507-0880  
304-285-4865, (FAX) 304-285-4403  
TMCMAH@METC.DOE.GOV

**Daniel Mei**  
Associate Professor  
Prairie View A&M University  
P.O. Box 397  
Mechanical Engineering Department  
Prairie View, TX 77446  
409-857-4023, (FAX) 409-857-2222

**Joseph S. Mei**  
Mechanical Engineer  
Morgantown Energy Technology Center  
U.S. Department of Energy  
P.O. Box 880, M/S N05  
Morgantown, WV 26507-0880  
304-285-4409, (FAX) 304-285-4403  
JMEI@METC.DOE.GOV

**Sandra Meischen**  
Tennessee Valley Authority  
Environmental Research Center  
CEB 1C  
Muscle Shoals, AL 35660  
205-386-3539, (FAX) 205-386-2191

**James C. Mercer**  
Petroleum Engineer  
Morgantown Energy Technology Center  
U.S. Department of Energy  
P.O. Box 880, M/S A04  
Morgantown, WV 26507-0880  
304-285-4509, (FAX) 304-285-4403  
JMERCER@METC.DOE.GOV

**Frank Q. Miao**  
Senior Engineer  
Westinghouse Electric Corporation  
4400 Alafaya Trail  
MC 504  
Orlando, FL 32826-2399  
407-281-3228, (FAX) 407-281-5007

**Aubrey L. Miller**  
Professor  
West Virginia University  
435 ESB  
Morgantown, WV 26506  
304-293-2111

**Ken J. Mills**  
Business Manager  
Norton Chem Process Product Corporation  
P.O. Box 350  
Akron, OH 44309-0350  
216-677-3514, (FAX) 216-677-3609

**Kunihiko Minami**  
Manager, Plant No. 4, Sales Section  
Sasakura Engineering Co., Ltd.  
3-8 Yoesu 1-Chome  
Chuo-Ku  
Tokyo, 103  
Japan  
813-327-7771, (FAX) 813-328-1928

**Marek Misztal**  
Engineer  
Inst. Chemical Processing Coal  
Zamkowa 1, PL-41-803 Zabrze  
Zabrze  
Poland  
483-171-5152, (FAX) 483-171-0809

**Darren Molloy**  
Project Manager  
Morgantown Energy Technology Center  
U.S. Department of Energy  
P.O. Box 880, M/S C04  
Morgantown, WV 26507-0880  
304-285-5447, (FAX) 304-285-4403  
DMOLLO@METC.DOE.GOV

**Jack Motter**  
Director, Technology Management Pinon  
Sierra Pacific Power Company  
6100 Neil Road  
P.O. Box 10100  
Reno, NV 89520-0400  
702-689-4013, (FAX) 702-689-3815

**Wang Naiji**  
Associate Engineer  
CDS International, Inc.  
Beijing Research Institute  
Hepingli  
Beijing 10013  
China

**David Najewicz**  
Manager, Energy and Environ. Systems  
GE Corporate R&D  
P.O. Box 8, K-1  
Engineering Systems Building  
Schenectady, NY 12301  
518-387-6427, (FAX) 518-387-7258

**Harvey M. Ness**  
Division Director, Gasification  
Morgantown Energy Technology Center  
U.S. Department of Energy  
P.O. Box 880, M/S C04  
Morgantown, WV 26507-0880  
304-285-4172, (FAX) 304-285-4403  
HNESS@METC.DOE.GOV



**Robert Ness**  
Research Manager  
Energy and Environmental Research Center  
University of North Dakota  
P.O. Box 9018  
Grand Forks, ND 58202  
701-777-5000, (FAX) 701-777-5181

**Richard Newby**  
Fellow Engineer  
Westinghouse STC  
1310 Beulah Road  
Pittsburgh, PA 15235  
412-256-2210, (FAX) 412-256-2121

**Grady B. Nichols**  
Principal Engineer  
Southern Research Institute  
P.O. Box 55305  
Birmingham, AL 35255-5305  
205-581-2361, (FAX) 205-581-2448

**P. E. Hojlund Nielsen**  
Senior Scientist  
Haldor Topsoe A/S  
55 Nymollevej  
Lyngby DK-2800  
Denmark  
454-527-2000, (FAX) 454-527-2999

**Stephen D. Noel**  
Electrical Engineer  
Morgantown Energy Technology Center  
U.S. Department of Energy  
P.O. Box 880, M/S A04  
Morgantown, WV 26507-0880  
304-285-4441, (FAX) 304-285-4403  
SNOEL@METC.DOE.GOV

**Yoshiki Noguchi**  
Chief Engineer  
Hitachi, Ltd.  
Hitachi Works 1-1 Saiwai-Cho  
3 Chome Hitachi-Shi  
Ibarahi-Ken, 317  
Japan  
029-423-5264, (FAX) 029-423-6607

**Victor P. Nokku**  
Research Assistant  
Rust College  
150 E. Rust Avenue  
Holly Springs, MS 38635  
601-252-8000, (FAX) 601-252-6107

**Glenn Norton**  
Chemist  
Ames Laboratory  
Iowa State University  
281 Metals Development Building  
Ames, IA 50011  
515-294-1035, (FAX) 515-294-3091  
NORTON@AMESLAB.GOV

**Thomas S. Norton**  
Mechanical Engineer  
Morgantown Energy Technology Center  
U.S. Department of Energy  
P.O. Box 880, M/S N05  
Morgantown, WV 26507-0880  
304-285-4617, (FAX) 304-285-4403  
TNORTO@METC.DOE.GOV

**John Notestein**  
Chief Engineer  
Morgantown Energy Technology Center  
U.S. Department of Energy  
P.O. Box 880, M/S A05  
Morgantown, WV 26507-0880  
304-285-4232, (FAX) 304-285-4403  
JNOTES@METC.DOE.GOV

**Thomas J. O'Brien**

Physical Scientist  
Morgantown Energy Technology Center  
U.S. Department of Energy  
P.O. Box 880, M/S N05  
Morgantown, WV 26507-0880  
304-285-4571, (FAX) 304-285-4403  
TOBRIE@METC.DOE.GOV

**Kazushi Ono**

Project Leader  
New Energy and Indust. Tech.  
Sunshine 60 30F 1-13-Chome  
Higashi-Ikebururo Toshima-Ku  
Tokyo  
Japan

**John Ontko**

Mechanical Engineer  
Morgantown Energy Technology Center  
U.S. Department of Energy  
P.O. Box 880, M/S N05  
Morgantown, WV 26507-0880  
304-285-4930, (FAX) 304-285-4403  
JONTK@METC.DOE.GOV

**James Osa**

Graduate Student  
Tennessee State University  
3500 John Merritt Boulevard  
Nashville, TN 37209  
615-963-5367, (FAX) 615-963-5397

**Carol J. Painter**

Senior Research Engineer  
Westinghouse STC  
1310 Beulah Road  
Pittsburgh, PA 15235-5098  
412-256-2202, (FAX) 412-256-1267  
PAINTER@CIS.PGH.WEC.COM

**Dale L. Perry**

Lawrence Berkeley Laboratory  
University of California  
Berkeley, CA 94720  
510-486-4819, (FAX) 510-486-5799

**J. Roger Peterson**

Market Development Manager  
Teledyne Wah Chang  
P.O. Box 460  
Albany, OR 97321-0460  
503-967-6904, (FAX) 503-967-6992

**Don W. Pfennig**

Custom Products Specialist  
United Catalysts, Inc.  
P.O. Box 32370  
Louisville, KY 40232  
502-634-7248, (FAX) 502-637-3732

**Timothy E. Pinkston**

Technical Manager  
Power Systems Development Facility  
P.O. Box 1069  
Wilsonville, AL 35186  
205-669-5860, (FAX) 205-669-5843

**William Place**

Manager  
DB Riley, Inc.  
Neponset Street  
Worcester, MA 01606  
508-792-4826, (FAX) 508-792-4817

**Duane Pontius**

Director, Particulate Science  
Southern Research Institute  
P.O. Box 55305  
2000 Ninth Avenue, South  
Birmingham, AL 35255-5305  
205-581-2268, (FAX) 205-581-2448  
DHPSRI@AOL.COM

**Jeffrey W. Portzer**

Research Chemical Engineer  
Research Triangle Institute  
P.O. Box 12194  
Research Triangle Park, NC 27709  
919-541-8025, (FAX) 919-541-8000  
JWP@RTI.ORG

**Victor Powell**

Statistician  
North Carolina A&T State University  
Greensboro, NC 27407

**Thomas S. Raines**

Graduate Student  
Iowa State University  
2942 Eisenhower Circle  
Ames, IA 50010  
515-294-6402, (FAX) 515-294-3261  
TRAINES@IASTATE.EDU

**S. N. Rao**

Assistant Technical Manager  
Burns & Roe Services Corporation  
P.O. Box 18288  
Pittsburgh, PA 15236  
412-892-6488, (FAX) 412-892-4604  
SRAO@ORION.PETC.DOE.GOV

**Lawrence K. Rath**

Division Director, Process and Proj. Eng.  
Morgantown Energy Technology Center  
U.S. Department of Energy  
P.O. Box 880, M/S E01  
Morgantown, WV 26507-0880  
304-285-4094, (FAX) 304-285-4403  
LRATH@METC.DOE.GOV

**Michael E. Reed**

Chemical Engineer  
Morgantown Energy Technology Center  
U.S. Department of Energy  
P.O. Box 880, M/S E01  
Morgantown, WV 26507-0880  
304-285-4860, (FAX) 304-285-4403  
MREED@METC.DOE.GOV

**Bob Reuther**

Product Manager, PFBC  
Morgantown Energy Technology Center  
U.S. Department of Energy  
P.O. Box 880, M/S D01  
Morgantown, WV 26507-0880  
304-285-4578, (FAX) 304-285-4403  
RREUTH@METC.DOE.GOV

**Scott Richlen**

CFCC, Program Manager  
U.S. Department of Energy  
1000 Independence Avenue, S.W.  
Forrestal Building, EE-221  
Washington, DC 20585  
202-586-2078, (FAX) 202-586-8134

**Robert E. Riley**

Pilot Plant Manager  
United Catalysts, Inc.  
P.O. Box 32370  
Louisville, KY 40232  
502-634-7399, (FAX) 502-637-3732

**John M. Rockey**

Chemical Engineer  
Morgantown Energy Technology Center  
U.S. Department of Energy  
P.O. Box 880, M/S N04  
Morgantown, WV 26507-0880  
304-285-4711, (FAX) 304-285-4403  
JROCKE@METC.DOE.GOV

**Paul Rodebaugh**

Supervisor Engineer  
Florida Power and Light  
700 Universe Boulevard  
P.O. Box 14000  
Juno Beach, FL 33408-0420  
407-691-2620, (FAX) 407-691-2695

**Edward S. Rubin**

Professor  
Carnegie Mellon University  
Baker Hall, 128-A/EPP Department  
Pittsburgh, PA 15213  
412-268-5897, (FAX) 412-268-3757  
RUBIN@ANDREW.CMU.EDU

**Rich Sadowski**

Director, Advanced Tech. Gasification  
Jacobs-Sirrine Engineers, Inc.  
1041 East Butler Road  
Greenville, SC 29606  
803-676-5082, (FAX) 803-676-5033

**J. A. Salter**

Staff Research Engineer  
Shell Synthetic Fuels, Inc.  
P.O. Box 2099  
Houston, TX 77252  
713-544-7718, (FAX) 713-544-7705

**Lou Salvador**

Deputy Director  
Morgantown Energy Technology Center  
U.S. Department of Energy  
P.O. Box 880, M/S A05  
Morgantown, WV 26507-0880  
304-285-4147, (FAX) 304-285-4403  
LSALVA@METC.DOE.GOV

**Iwao Sawada**

Manager, R&D Section  
Sasakura Engineering Co., Ltd.  
7-32, Takeshima 4-Chome  
Nishiyodogawa-Ku  
Osaka, 555  
Japan  
816-473-2138, (FAX) 816-473-4290

**Dale Schmidt**

GPIF Site Manager  
Morgantown Energy Technology Center  
U.S. Department of Energy  
P.O. Box 880, M/S D04  
Morgantown, WV 26507-0880  
304-285-4359, (FAX) 304-285-4403  
DSCHMI@METC.DOE.GOV

**John H. Schwartz**

President  
Stanton Energy Industry Consultant  
RD No. 1, Liberty Court  
New Stanton, PA 15672  
412-446-3300, (FAX) 412-446-1266

**Kumar Sellakumar**

Assistant R&D Manager  
Ahlstrom Pyropower  
8970 Crestmar Point  
San Diego, CA 92121-3222  
619-450-2604, (FAX) 619-552-8296  
SELLAKUMAR\_KUMAR@CCMAIL.  
AHLSTRO

**Vijay K. Sethi**

Program Manager  
Western Research Institute  
364 N. 9th Street  
Laramie, WY 82070  
307-721-2376, (FAX) 307-721-2233

**Larry Shadle**

Cluster Leader  
Morgantown Energy Technology Center  
U.S. Department of Energy  
P.O. Box 880, M/S N04  
Morgantown, WV 26507-0880  
304-285-4647, (FAX) 304-285-4403  
LSHADL@METC.DOE.GOV

**Suhas D. Shelukar**

Research Chemical Engineer Associate  
Research Triangle Institute  
P.O. Box 12194  
Research Triangle Park, NC 27709  
919-541-8042, (FAX) 919-541-8000  
SDS@RTI.ORG

**Zhang Shengtao**

Vice President  
Central Coal Mining Research  
Hepingli  
Beijing 100013  
China

**Qu Sijian**

Deputy Director, Carbonization Division  
Central Coal Mining Research  
Beijing Research Institute of Coal  
Ccmri, Hepingli  
Beijing 100013  
China

**Ranjani V. Siriwardane**

Research Chemist  
Morgantown Energy Technology Center  
U.S. Department of Energy  
P.O. Box 880, M/S N04  
Morgantown, WV 26507-0880  
304-285-4513, (FAX) 304-285-4403  
RSIRIW@METC.DOE.GOV

**Duane H. Smith**

Cluster Leader  
Morgantown Energy Technology Center  
U.S. Department of Energy  
P.O. Box 880, M/S A04  
Morgantown, WV 26507-0880  
304-285-4069, (FAX) 304-285-4403  
DSMITH@METC.DOE.GOV

**Robert G. Smith**

Senior Research Specialist  
3M Company  
3M Center  
Building 203-1-01  
St. Paul, MN 55144-1000  
612-733-2564, (FAX) 612-737-5484  
RGSMITH@MMM.COM

**Thomas M. Smith**

Gas R&D Analyst  
Northern Indiana Public Service  
801 E. 86th Avenue  
Merrillville, IN 46410  
219-647-4554, (FAX) 219-647-4321

**L. Douglas Smoot**

Professor  
Brigham Young University  
265L Crabtree Tech. Building  
Provo, UT 84602  
801-378-8930, (FAX) 801-376-6033  
LDS@BYU.EDU

**Nelson Sobel**

Senior Vice President, Tech. Director  
Pall Corporation  
P.O. Box 2030, Route 281  
Cortland, NY 13045  
607-753-6041, (FAX) 607-753-8525

**Peter R. Solomon**

President  
Advanced Fuel Research, Inc.  
87 Church Street  
East Hartford, CT 06108  
203-528-9806, (FAX) 203-528-0648

**Jack D. Spain**

Research Engineer  
Southern Research Institute  
P.O. Box 55305  
Birmingham, AL 35255-5305  
205-581-2323, (FAX) 205-581-2010

**Ron Staubly**  
Project Manager  
Morgantown Energy Technology Center  
U.S. Department of Energy  
P.O. Box 880, M/S C04  
Morgantown, WV 26507-0880  
304-285-4991, (FAX) 304-285-4403  
RSTAUB@METC.DOE.GOV

**Robert Steffen**  
Project Manager  
Stanton Energy Industry Consultant  
RD No. 1, Liberty Court  
New Stanton, PA 15672  
412-446-3300, (FAX) 412-446-1266

**Richard Stehouwer**  
Senior Researcher  
Ohio State University  
OARDC  
Wooster, OH 44691  
216-263-3655  
STEHOUWER.1@OSU.EDU

**David P. Stinton**  
Staff Scientist  
Oak Ridge National Laboratory  
P.O. Box 2008  
Oak Ridge, TN 37831-6063  
615-574-4556, (FAX) 615-574-6918  
STINTONDP@ORNL.GOV

**Larry E. Stoddard**  
Manager, Advanced Technology  
Black & Veatch  
11401 Lamar  
Overland Park, KS 66211  
913-339-7225, (FAX) 913-339-2934  
STODDARDLE@BV.COM

**Warren E. Straszheim**  
Associate Scientist  
Ames Laboratory  
270 Metals Development Building  
Ames, IA 50011-3020  
515-294-8187, (FAX) 515-294-3091  
WES@AMESLAB.GOV

**Larry D. Strickland**  
Division Director, Gas Cleanup  
Morgantown Energy Technology Center  
U.S. Department of Energy  
P.O. Box 880, M/S N04  
Morgantown, WV 26507-0880  
304-285-4494, (FAX) 304-285-4403  
LSTRIC@METC.DOE.GOV

**Tina M. Strobel**  
Research Associate  
Energy and Environment Research Center  
University of North Dakota  
P.O. Box 9018  
Grand Forks, ND 58202  
701-777-5000, (FAX) 701-777-5181

**D. W. Sutherland**  
Senior Design Engineer  
Pall Corporation  
3643 New York State, Route 281  
P.O. Box 2030  
Cortland, NY 13045-0930  
607-753-6041, (FAX) 607-756-1862

**Michael L. Swanson**  
Research Engineer  
Energy and Environment Research Center  
University of North Dakota  
P.O. Box 9018  
Grand Forks, ND 58202  
701-777-5239, (FAX) 701-777-5181

**Yong X. Tao**  
Assistant Professor  
Tennessee State University  
3500 John A. Merritt Boulevard  
Nashville, TN 37209-1561  
615-963-5390, (FAX) 615-963-5397  
TAOY@HARPO.TNSTATE.EDU

**Jerry Temchin**  
Technical Advisor  
U.S. Department of Energy  
FE-232  
Washington, DC 20585  
301-903-4743, (FAX) 301-903-2406  
JEROME.TEMCHIN@HQ.DOE.GOV

**Bruce Thomson**  
Program Manager  
Textron Specialty Materials  
2 Industrial Avenue  
Lowell, MA 01851  
508-934-7519, (FAX) 508-934-7597

**Peter Tortorelli**  
Senior Staff Member  
Oak Ridge National Laboratory  
P.O. Box 2008  
Oak Ridge, TN 37831-6156  
615-574-5119, (FAX) 615-574-5118  
PFT@ORNL.GOV

**Robert Travers**  
PFBC Program Manager  
U.S. Department of Energy  
FE-232/GTN  
Washington, DC 20585  
301-903-6166, (FAX) 301-903-2406

**Brian S. Turk**  
Research Chemical Engineer Associate  
Research Triangle Institute  
P.O. Box 12194  
Research Triangle Park, NC 27709  
919-541-8024, (FAX) 919-541-8000  
BST@RTI.ORG

**John W. Vaklyes, Jr.**  
National Sales Manager  
Ceramem Separations, Inc.  
952 East Fir Street  
Palmyra, PA 17078  
717-838-7911, (FAX) 717-838-7880

**Lawrence E. Van Bibber**  
Project Manager  
Gilbert/Commonwealth, Inc.  
237 Toura Drive  
Pittsburgh, PA 15236  
412-892-4194, (FAX) 412-655-9629

**Vince Vanpelt**  
Tennessee Valley Authority  
Environmental Research Center  
CEB 1C  
Muscle Shoals, AL 35660  
205-386-2489, (FAX) 205-386-2191

**Venkat K. Venkataraman**  
Project Manager  
Morgantown Energy Technology Center  
U.S. Department of Energy  
P.O. Box 880, M/S C05  
Morgantown, WV 26507-0880  
304-285-4105, (FAX) 304-285-4403  
VVENKA@METC.DOE.GOV

**Michael J. Virr**  
President  
Spinheat, Ltd.  
2349 Black Rock Turnpike  
Fairfield, CT 06430  
203-373-0036, (FAX) 203-373-0283

**Lurgi Von Wedel**  
Engineer  
LLB Lungi Lentjes Babcock  
Duisburger Street 375  
Oberhausen, 46041  
Germany  
208-833-4391, (FAX) 49 208 807-448  
100340,2307@COMPUSERVE.COM

**Richard A. Wagner**  
Principal Engineer  
Babcock & Wilcox  
P.O. Box 11165  
Lynchburg, VA 24506-1165  
804-522-5697, (FAX) 804-522-6980  
RICH.A.WAGNER@RDD.MCDERMETT.  
COM

**Robert J. Weber**  
Senior Engineer  
Ames Laboratory  
Iowa State University  
307 Durham  
Ames, IA 50011-2252  
515-294-8723, (FAX) 515-294-1152  
WEBER@IASTATE.EDU

**Robert F. Weimer**  
Chief Engineer, New Technology  
Air Products and Chemicals, Inc.  
7201 Hamilton Boulevard  
Allentown, PA 18195-1501  
610-481-7626, (FAX) 610-481-5084  
WEIMERRF@TTOWN.APCI.COM

**Paul Weitzel**  
Technical Consultant  
Babcock & Wilcox  
20 S. Van Buren Avenue  
Barberton, OH 44203  
216-860-1655, (FAX) 216-860-2348

**Jim Welshimer**  
Manager, Technical Service  
National Lime and Stone Company  
P.O. Box 120  
Findlay, OH 45839  
419-422-4341, (FAX) 419-422-3952

**John M. Wheeldon**  
Process Engineer  
Power Systems Development Facility  
P.O. Box 1069  
Wilsonville, AL 35186  
205-669-5857, (FAX) 205-669-5843

**Gerald F. Wheeler**  
Program Manager  
U.S. Department of Energy  
FE-231  
Washington, DC 20585  
301-903-3511, (FAX) 301-903-2406  
GERALD.WHEELER@HQ.DOE.GOV

**Gary White**  
North Carolina A&T State University  
2609 Pine Lake Drive  
Greensboro, NC 27407  
910-285-4076, (FAX) 910-285-4403

**Jay S. White**  
Process Engineer  
Gilbert/Commonwealth, Inc.  
P.O. Box 1498  
Reading, PA 19603  
215-775-2600, (FAX) 215-775-2670

**Stan Whitney**  
PFBC Marketing Manager  
Babcock & Wilcox  
20 S. Van Buren Avenue  
Barberton, OH 44203  
216-860-1142, (FAX) 216-860-2348

**Paul R. Wieber**  
Associate Director, OID  
Morgantown Energy Technology Center  
U.S. Department of Energy  
P.O. Box 880, M/S A03  
Morgantown, WV 26507-0880  
304-285-4544, (FAX) 304-285-4403  
PWIEBE@METC.DOE.GOV

**James T. Wilbur**  
Manager  
Burns & Roe Services Corporation  
P.O. Box 18288  
Pittsburgh, PA 15236  
412-892-5916, (FAX) 412-892-4736



**Mark Williams**  
Product Manager, Fuel Cells  
Morgantown Energy Technology Center  
U.S. Department of Energy  
P.O. Box 880, M/S D01  
Morgantown, WV 26507-0880  
304-285-4747, (FAX) 304-285-4403  
MWILLI@METC.DOE.GOV

**John S. Wilson**  
Vice President  
Rich-Mar Systems Corporation  
1004 Grand Street  
Morgantown, WV 26505  
304-291-2311, (FAX) 304-291-2312  
71212.3172@COMPUSERVE.COM

**Keith Wilson**  
Project Manager  
Combustion Power Company  
2101 Webster Street  
Suite 1700  
Oakland, CA 94612  
510-286-8820, (FAX) 510-286-8824  
JWATTS@HOOKED.COM

**William G. Wilson**  
President  
Gas Desulfurization Corporation  
820 Harden Drive  
Pittsburgh, PA 15229-1109  
412-364-1822

**Jack Winnick**  
Professor  
Georgia Tech  
Chemical Engineering Department  
Atlanta, GA 30332  
404-894-2839, (FAX) 404-894-2866

**David C. Wolfe**  
Research Manager  
United Catalysts, Inc.  
P.O. Box 32370  
Louisville, KY 40232  
502-634-7349, (FAX) 502-637-3732  
DCW@IGLOU.COM

**Ronald H. Wolk**  
Principal  
Wolk Integrated Tech. Services  
1056 Hyde Avenue  
San Jose, CA 95129  
408-996-7811, (FAX) 408-996-2746  
WOLKINTTS@AOL.COM

**Steven D. Woodruff**  
Research Chemist  
Morgantown Energy Technology Center  
U.S. Department of Energy  
P.O. Box 880, M/S A04  
Morgantown, WV 26507-0880  
304-285-4175, (FAX) 304-285-4403  
SWOODR@METC.DOE.GOV

**I. G. Wright**  
Staff Development Engineer  
Oak Ridge National Laboratory  
P.O. Box 2008  
Building 4500S  
Oak Ridge, TN 37831-6156  
615-574-4451, (FAX) 615-574-5118  
WRIGHTIG@ORNL.GOV

**Robert J. Wright**  
U.S. Department of Energy  
Office of Fossil Energy  
Advanced Research FE-72  
Washington, DC 20585-0002  
301-903-5471, (FAX) 301-903-8350  
ROBERT.WRIGHT@HQ.DOE.GOV

**Steve R. Wright**  
Vice President, R&D  
Micro Composite Materials  
4608-D Industry Lane  
Durham, NC 27713-5414  
919-544-1717, (FAX) 919-361-3535  
SWRIGHT@NANDO.NET

**Ye Xianbin**  
Senior Engineer  
Central Coal Mining Research  
Hepingli  
Beijing 100013  
China

**Xu Xiaodong**  
Engineer  
Central Coal Mining Research  
Beijing Research Institute of Coal  
Ccmri, Hepingli  
Beijing  
China

**Chang-Keun Yi**  
Researcher  
Korea Institute of Energy Research  
71-2 Jang-Deng, Yoosung  
Taejon 305-343  
South Korea  
CKYI@SUN330.KIER.RE.KR

**Stephen B. Young**  
Director, Corporate Planning  
Hague International  
P.O. Box 449  
Kennebunk, ME 04043  
207-985-3540, (FAX) 207-985-4097  
SBYOUNG@HAGUE.COM

**Charles M. Zeh**  
Product Manager, Heat Engines  
Morgantown Energy Technology Center  
U.S. Department of Energy  
P.O. Box 880, M/S D01  
Morgantown, WV 26507-0880  
304-285-4265, (FAX) 304-285-4403  
CZEH@METC.DOE.GOV

**Kenneth B. Zella**  
Marketing Manager  
Pall Aeropower Corporation  
301 49th Street, North  
Pinellas Park, FL 34665  
813-522-3111, (FAX) 813-528-0516

**Claudio Zeppi**  
ENEL  
Via A Pisano 120  
Pisa, SG100  
Italy  
395-085-0139, (FAX) 395-053-5651

**Xu Zhengang**  
Senior Engineer  
CDS International, Inc.  
Beijing Research Institute  
Hepingli  
Beijing 10013  
China

**Jianren Zhou**  
Assistant Professor  
Prairie View A&M University  
Mechanical Engineering Department  
Prairie View, TX 77446  
409-857-4023, (FAX) 409-857-2222

# Author Index

## A

Abbasian, J. . . . . 407  
 Adeyiga, A.A. . . . . 402  
 Ahluwalia, R.K. . . . . 279  
 Allan, S.E. . . . . 559  
 Alvin, M.A. . . . . 160, 485, 517  
 Anderson, R.J. . . . . 104  
 Ayala, R.E. . . . . 187, 407, 591, 631

## B

Bachovchin, D. . . . . 263  
 Beeghly, J.H. . . . . 358  
 Ben-Slimane, R. . . . . 367  
 Benson, S.A. . . . . 549, 559  
 Bevan, S. . . . . 187, 250, 472  
 Bigham, J.M. . . . . 358  
 Black, D.C. . . . . 360  
 Bowen, J.H. . . . . 250  
 Brekke, D.W. . . . . 549  
 Brewster, B.S. . . . . 425  
 Brown, R.C. . . . . 417  
 Bruck, G.J. . . . . 123  
 Burkhard, F. . . . . 32  
 Buttermore, W.H. . . . . 574

## C

Cairns, E.J. . . . . 382  
 Campbell, W.M. . . . . 215  
 Canizales, A. . . . . 631  
 Carli, G. . . . . 32  
 Carpenter, L.K. . . . . 19  
 Carson, R.D. . . . . 47  
 Casleton, K.H. . . . . 71  
 Cesario, M. . . . . 394  
 Chambers, J.A. . . . . 467  
 Chandran, R.R. . . . . 158  
 Chiang, T-K. . . . . 98  
 Chisholm, W.P. . . . . 587  
 Chriswell, C.D. . . . . 574  
 Chuck, T. . . . . 591  
 Conn, R. . . . . 32  
 Copeland, R.J. . . . . 394

Crooker, P. . . . . 32  
 Culberson, H. . . . . 47

## D

Damle, A.S. . . . . 667  
 Delzer, G.A. . . . . 241  
 DeVan, J.H. . . . . 292  
 Diaz, E.S. . . . . 160, 485  
 Dick, W.A. . . . . 356, 358  
 DiPietro, S.G. . . . . 320  
 Dixit, V.B. . . . . 47  
 Dockter, B.A. . . . . 449  
 Doctor, R.D. . . . . 448  
 Domeracki, W.F. . . . . 263  
 Dowdy, T.E. . . . . 263  
 Dubovik, M. . . . . 394

## E

Eckels, D.E. . . . . 574  
 Edlund, D.J. . . . . 645  
 Eggerstedt, P.M. . . . . 140, 342  
 Erickson, T.A. . . . . 440, 549, 559

## F

Feher, G. . . . . 202  
 Feinberg, D. . . . . 394  
 Feitelberg, A.S. . . . . 187, 250  
 Fowler, R.K. . . . . 358  
 Furman, A. . . . . 187

## G

Galloway, E.N. . . . . 70  
 Gangwal, S.K. 215, 220, 229, 402, 601, 622  
 Gemmen, R.S. . . . . 79  
 Geyer, H.K. . . . . 279  
 Ghazanfari, R. . . . . 202  
 Gieger, R. . . . . 472  
 Gleason, E.F. . . . . 678  
 Gray, D.D. . . . . 360  
 Greenwood, G.J. . . . . 241  
 Groves, F.R. . . . . 610  
 Gupta, R.P. 215, 229, 591, 601, 622, 631

## H

Haas, J.C. ....	150
Haley, J.S. ....	87
Hamblen, D.G. ....	425
Han, C. ....	655
Harrison, D.P. ....	610, 655
Hassett, D.J. ....	559
Hauserman, W.B. ....	559
Head, W.J. ....	360
Henderson, A.K. ....	440
Hendrix, H.L. ....	23
Henningsen, G.B. ....	215
Hepworth, M.T. ....	367
Hill, A.H. ....	407
Holt, N.A.H. ....	4
Hung, S.L. ....	250
Hurley, J.P. ....	449

## I

Ilias, S. ....	646
Im, K.H. ....	646

## J

Janus, M.C. ....	79
Jarr, L.A. ....	104
Johnson, D. ....	472
Jothimurugesan, K. ....	402
Judkins, R.R. ....	292

## K

Karpuk, M.E. ....	394
Katrinak, K.A. ....	559
Khare, G.P. ....	241
King, F.G. ....	646
Kinsinger, D.L. ....	241
Konttinen, J. ....	202
Koopmann, G.H. ....	158
Korcak, R.F. ....	362
Krishnan, G.N. ....	631, 667
Kubicek, D.H. ....	241
Kulcsar, D. ....	32

## L

Lacey, M.A. ....	250
LaHaye, P.G. ....	55
Lane, J.E. ....	329

Larsen, D.A. ....	302
Lau, K-H. ....	667
Lawson, L.O. ....	69
LeCostaouec, J-F. ....	329
Lee, G. ....	655
Lehtovaara, A. ....	202
Lippert, T.E. ....	123, 160, 485, 517
Lopez-Ortiz, A. ....	610
Loth, J.L. ....	158
Lu, C. ....	32
Ludlow, J.C. ....	104
Lynn, S. ....	382

## M

Mack, A. ....	32
Maloney, D.J. ....	71
Mann, M.D. ....	87, 440
Mann, R.M. ....	573
Manning, K.S. ....	250
Mansour, M.N. ....	158
Maxwell, D.P. ....	573
Mojtahedi, W. ....	202
Moore, D.L. ....	23

## N

Najewicz, D. ....	187
Nehrozoglu, A. ....	32
Ness, R.O. ....	87
Newby, R.A. ....	123, 517
Noel, S.D. ....	69
Norton, G.A. ....	574
Norton, T.S. ....	71, 249

## O

O'Brien, T.J. ....	107
O'Keefe, C.A. ....	559
Ontko, J.S. ....	98
Orozco, N.J. ....	55

## P

Painter, C.J. ....	329
Peters, R.E. ....	574
Pickup, H. ....	55
Pinkston, T.E. ....	23
Pontius, D.H. ....	318, 531

Portzer, J.W. ....	220
Prudhomme, J. ....	150

## R

Radford, K.C. ....	329
Radulovic, P.T. ....	425
Raines, T.S. ....	417
Reed, M.E. ....	109
Richards, G.A. ....	79, 105
Richlen, S. ....	183
Robertson, A. ....	32
Rockey, J.M. ....	70, 340
Rush, R.E. ....	23

## S

Sack, W.A. ....	360
Sadowski, R.S. ....	47
Sanjana, Z.N. ....	123
Sanjurjo, A. ....	667
Schmalzer, D.K. ....	448
Seger, J.L. ....	55
Serio, M.A. ....	425
Sethi, V.K. ....	275
Shadle, L.J. ....	69
Shelleman, D. ....	279
Shelukar, S.D. ....	631
Siriwardane, H.J. ....	360
Siriwardane, R.V. ....	609
Smeltzer, E.E. ....	160, 485, 517
Smith, D.H. ....	108
Smoot, L.D. ....	425
Sobel, N. ....	472
Solomon, P.R. ....	425
Soto, U.I. ....	358
Speight, J.G. ....	275
Starrett, H.S. ....	318
Stout, W.L. ....	362
Strobel, T.M. ....	449
Strom-Olsen, J. ....	55
Su, N. ....	646
Swanson, M.L. ....	87, 440

## T

Thamaraichelvan, P. ....	47
Thiede, T.D. ....	417
Thomson, B.N. ....	320

Torpey, M. ....	32
Tortorelli, P.F. ....	292
Tressler, R.E. ....	279
Tucker, M.S. ....	70
Turk, B.S. ....	622

## U

Udo-Aka, U.I. ....	646
--------------------	-----

## V

Van Hook, J. ....	32
Venkataramani, V.S. ....	407
Vimalchand, P. ....	23

## W

Wagner, R.A. ....	510
Weidinger, G. ....	3
Wetherold, R.G. ....	573
Wheeldon, J.M. ....	23
White, J.D. ....	610
White, J.S. ....	109
Williams, W.A. ....	573
Wilson, K.B. ....	150
Windecker, B. ....	394
Winnick, J. ....	678
Wood, B.J. ....	631, 667
Woodruff, S.D. ....	105
Wright, I.G. ....	292

## Y

Yavuzkurt, S. ....	158
Young, S. ....	55

## Z

Zeh, C.M. ....	65
Zhu, C. ....	279
Ziemkiewicz, P.F. ....	360
Zoldak, F. ....	32
Zygarlicke, C.J. ....	559

# Organization Index

---

## A

Advanced Fuel Research, Inc. ....	425
Ahlstrom Ash Development Corporation .....	362
Ahlstrom Pyropower, Inc. ....	417,440
American Electric Power Company .....	356
Ames Laboratory .....	574
Anker Energy Corporation .....	360
Argonne National Laboratory .....	279, 448

## B

Babcock and Wilcox .....	510
Ballard Power Systems .....	645
Bend Research, Inc. ....	645
Blasch Precision Ceramics, Inc. ....	302
Brigham Young University .....	425

## C

CRS Serrine Engineers, Inc. ....	47
Combustion Power Company .....	23, 150

## D

DB Riley, Inc. ....	47
Dakota Gasification .....	472
Dravo Lime Company .....	356,358
DuPont Lanxide Composites Inc. ....	467

## E

Electric Power Research Institute .....	4, 23, 356, 440, 449
Enviropower Inc. ....	202

## F

Foster Wheeler .....	23
Foster Wheeler Development Corporation .....	32

## G

GE Corporate Research and Development .....	407, 591, 631
GE Environmental Services, Inc. ....	187, 250, 472
Georgia Tech Research Corporation .....	678
Gilbert/Commonwealth, Inc. ....	109

## H

Hague International .....	55
Hampton University .....	402

## I

Industrial Filter and Pump Manufacturing Co., Inc. ....	23, 140, 342
Institute of Gas Technology .....	407
Iowa State Electric Power Research Institute .....	417
Iowa State University .....	417, 574

## J

Jacobs-Sirrine Engineers, Inc. ....	47
-------------------------------------	----

## L

Lawrence Berkeley Laboratory .....	382
Louisiana State University .....	610, 655

## M

Manufacturing and Technolgy Conversion International, Inc. ....	158
The M.W. Kellogg Company .....	23, 215
Morgantown Energy Technology Center .....	19, 65, 69, 70, 71, 79, 98, 104,
.....	105, 107, 108, 109, 249, 340, 587, 609, 655

## N

Nolan Multimedia .....	23
North Carolina A&T State University .....	646
North Dakota Industrial Commission .....	440
Northern States Power Company , .....	440

## O

Oak Ridge National Laboratory .....	292
Ohio Coal Development Office .....	356
Ohio Edison Company .....	356
Ohio State University .....	358

## **P**

Pall Corporation .....	472
Phillips Petroleum Co. ....	241

## **R**

Radian Corporation .....	573
Research Triangle Institute .....	215, 220, 229, 402, 591, 601, 622, 631

## **S**

Southern Company Services, Inc. ....	23
Southern Research Institute .....	318, 531
SRI International .....	631, 667

## **T**

TDA Research, Inc. ....	394
Techniweave, Inc. ....	329
Teledyne Wah Chang .....	645
Textron Specialty Materials .....	320

## **U**

U.S. Department of Agriculture .....	362
U.S. Department of Energy .....	183
U.S. Generating Company .....	3
University of Minnesota .....	367
University of North Dakota Energy & Environmental Research Center ..	87, 440, 449, 549, 559

## **W**

Western Research Institute .....	275
Westinghouse Electric Corporation .....	23, 123, 160, 263, 329, 485, 517
West Virginia University .....	360





This cover stock is 30% post-consumer waste  
and 30% pre-consumer waste, and is recyclable.

